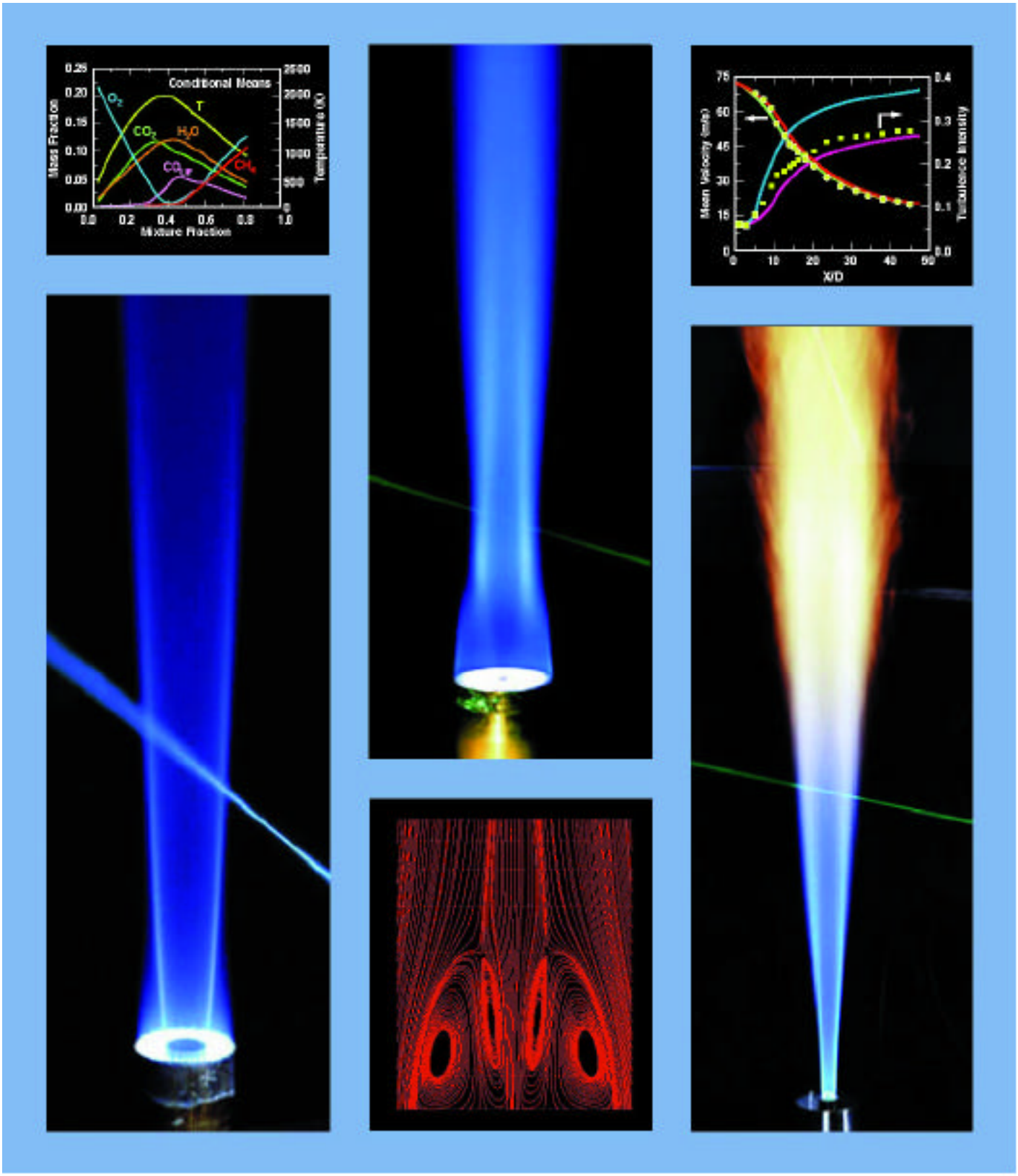

Proceedings of the Third International Workshop on Measurement and Computation of Turbulent Nonpremixed Flames

Boulder, Colorado
July 30 - August 1, 1998

Third International Workshop on Measurement and Computation
of Turbulent Nonpremixed Flames

Boulder, Colorado
July 30 - August 1, 1998

Preface to the TNF3 Workshop Proceedings

The International Workshop on Measurement and Computation of Turbulent Nonpremixed Flames is an ongoing collaboration among experimentalists and modelers interested in fundamental issues of nonpremixed and partially premixed turbulent combustion. The Third Workshop (TNF3) focused on comparisons of measured and modeled results for four target flames of hydrocarbon fuels (CH_4 or natural gas). There were eighty-four registered participants, and each received a notebook containing results on the four target flames. This notebook also contained the two-page abstracts of contributed posters on the target flames and on other related topics. The proceedings of the TNF3 Workshop are provided here in PDF format to allow all interested researchers and students access to the information contained in the workshop notebook.

A few comments from the program co-chairs are included below to highlight some of the major discussion issues and outcomes. However, we have not attempted to distill the many discussions that took place during the workshop or to provide additional explanation of the figures and text that appeared in the notebook. Most of the comparisons are in graphical form, and written commentary is limited. The target flame comparisons have brought up several interesting issues and questions that will require more work to resolve, and it is clear that we are not finished with this set of flames. Accordingly, the information contained here should be viewed as work in progress unless it also appears in a separately published reference. Readers are advised to avoid the error of drawing premature conclusions based upon the information contained in these proceedings alone because the reasons for agreement or disagreement among the experiments and calculations may not be apparent from the graphical comparison. Those who have specific questions regarding target flame results or the posters are encouraged to contact the authors and contributors directly.

Collaborative research on these flames is continuing, and a fourth TNF Workshop is being planned for the summer of 1999. In addition, several of the organizers and contributors are working on a paper that will review progress in measurement and modeling of hydrogen flames and hydrocarbon flames, as addressed by the Second and Third TNF Workshops and by recent publications.

The ongoing workshop process is made possible through the voluntary contributions of many people. We sincerely thank all those who contributed to the success of the Boulder workshop.

This PDF version of the workshop proceedings was assembled by Ken Buch with support from Sandia National Laboratories under funding from the US Department of Energy, Office of Basic Energy Sciences. The PDF files were generated from the original postscript or MS Word files provided by the authors. The translation of MS Word files across various platforms and versions numbers has left minor glitches in some of the graphs. Also, line graphs that came from MS Word files are typically reproduced at lower resolution than the originals. Pages that were generated from postscript files do not view very well on the computer screen, but print quality should be excellent. On the whole the PDF format seems to provide a convenient and effective means of distributing this type of information. Comments on the format and content are welcome.

Further information on TNF Workshop objectives, history, and current activities may be found on the web (**www.ca.sandia.gov/tdf/Workshop.html**).

Third International Workshop on Measurement and Computation
of Turbulent Nonpremixed Flames

Boulder, Colorado
July 30 - August 1, 1998

Comments from the Program Co-Chairs

The following comments highlight some of the major discussion topics and outcomes from the Boulder workshop. They are not intended as a complete summary of the target flame comparisons, and they do not necessarily represent a consensus of opinions of the TNF3 participants and contributors.

The Target Flames

One of the primary objectives of the TNF Workshop is to establish and maintain a library of data sets on turbulent nonpremixed and partially premixed flames that is appropriate for testing various turbulent combustion models. In developing this library we have started from the simplest cases (hydrogen jet flames in coflow) and are gradually increasing the complexity of the flow field and the fuel. Our goal is to provide a sufficient number of reliable and reasonably complete data sets to test a wide range of turbulent combustion models and better understand the capabilities of models to capture important fundamental combustion processes. Flames may be added or deleted from the library based upon the availability of new data and the interests of the modelers participating in the workshop.

These collaborative comparisons provide experimentalists with useful feedback on the completeness and appropriateness of each data set, including documentation of boundary conditions and experimental uncertainty. In some cases the process points to gaps in the documentation or questions that call for additional measurements.

The four TNF3 target flames all include CH_4 as a primary component of the fuel, but they represent a range in flow field complexity. They were presented at the workshop in order of increasing complexity. Each of these flames is at a different stage with regard to the process of comparing measured and modeled results, and so we include here a few comments to outline the status of each flame and place it in the context of the overall workshop process.

Simple $CH_4/H_2/N_2$ Jet Flame (DLR Flame)

The DLR flame was a late addition to the list of target flames that appeared in the first announcement of the Boulder workshop. Scalar measurements were contributed by Wolfgang Meier and coworkers at DLR Stuttgart, while velocity measurements were provided by Egon Hassel and coworkers at TU Darmstadt. Three modelers contributed calculations.

An important attribute of this flame in the context of the data library is that it combines methane kinetics with the simple jet geometry. Thus it provides a logical bridge between the simple H_2 jet flames and the pilot- or bluff-body stabilized methane flames. In fact, the burner is the same as that used for the "H3" hydrogen flame in the library. The inclusion of H_2 in the fuel stream makes differential diffusion a significant issue near the base of the flame. This point was made clear by

results from Heinz Pitsch (not included here) comparing flamelet calculations with Le=1 vs. Le≠1. The differential diffusion effect is believed to be responsible for some of the differences among measured and modeled results in Section 1. Consequently, this flame is not as simple a test case for methane chemistry as one might like. However, the relatively clean boundary conditions at the nozzle make it a useful target, particularly for the few models that include effects of differential diffusion. Also, imaging data on this flame provide information on turbulence structure that are useful in the interpretation of near-field effects.

The figures comparing measured and modeled results for the DLR flame have been revised since the workshop to combine the different calculations onto the same graph wherever possible. In addition to the three calculations represented in these figures, the poster abstract from H. Pitsch includes comparisons of calculations using three different chemical mechanisms.

Additional scalar measurements on this flame would be useful. The available scalar point data do not include simultaneous point measurements of OH or NO. Also, the Raman scattering measurements of CO are affected by fluorescence interferences and may not have sufficient accuracy to really test the details of the reduced chemical kinetic mechanisms and the turbulence-chemistry coupling models. Experiments to fill in these data are planned as a collaboration between DLR Stuttgart and Sandia.

Piloted CH_4/Air Flame (Flame D)

Flame D is one in a series of piloted flames measured recently at Sandia. Velocity measurements were obtained at TU Darmstadt using the piloted burner and a set of calibrated flow controllers loaned from Sandia. While the pilot adds some flow complexity, it does not appear to present a special problem to the turbulence models, and most calculations were conducted using the same model constants as for simple jet flames. The participating modelers generally agreed that one could not expect current RANS models to accurately predict the near field ($x/d<5$) of simple or piloted jet flames, and detailed comparisons in the near field were not carried out. In fact, several of the models required special treatment of the near field in order to produce a stable flame, and some comments on this are included in the model descriptions. Comparisons starting at $x/d=7.5$ show that some models did better than others in calculating the overall velocity and fixture fraction fields. However, these differences were not discussed in detail, and the general view was that all of the models were close enough on the mean axial velocity and mixture fraction profiles to allow comparison of the details of the species results.

The discussions of Flame D focused mainly on issues of chemistry. Plots of conditional means in Section 2 provide the most direct information regarding chemistry in this flame. There is close agreement between measurements and most of the models for fuel-lean conditions. However, the plots of measured and predicted conditional means show wide variations among calculations of species mass fraction in fuel rich conditions. The reasons for these differences are not fully understood at this time, and this is one obvious area for further investigation. All of the calculations, except the PDF/ILDM calculation from TU Darmstadt, were based on the GRI-1.2 or GRI-2.1 mechanisms. Therefore, it appears that differences in the turbulence-chemistry coupling models, rather than differences between the mechanisms, are responsible for the wide variations observed in the results on conditional means. It is quite possible that relatively minor changes in the parameters of the models could improve agreement with the measurements. However, this has yet to be demonstrated.

We note that the ILDM calculation is limited by the fact that the ILDM table used in this calculation was based on a manifold that was only defined for a limited interval in mixture fraction surrounding the stoichiometric condition. Outside of this region the calculated results for H_2 and CO are unrealistic, due to the assumptions used in constructing the table. The same observation is made in the poster by Hinz et al. and also in the discussion of the Delft flame calculations (Section 3), which were based on a similar ILDM implementation. An ILDM approach using different assumptions in constructing the table or an approach using more than two progress variables might well provide better agreement with the measurements, and there is room for further work here.

Piloted Natural Gas Flame (Delft III)

The boundary conditions for this piloted flame are more complicated than for Flame D, and measurement problems caused by interferences from soot precursors and soot are more severe. However, there is now a significant bank of data for this flame using different techniques in different labs. In particular, the poster by Versluis et al. reports recent CARS temperature measurements that are in good agreement with Rayleigh scattering measurements from Sandia. Such redundant measurements are very useful with regard to model validation and the establishment of reliable benchmark data sets. The Delft flames also uses a "practical" fuel, which may be an important consideration, at least politically, when making the connection between fundamental research and industrial applications.

The Delft III flame was used already as a target for the Second Workshop on Aerodynamics of Steady-State Combustion Chambers and Furnaces (A.S.C.F) held in Piza, Italy on November 28-29, 1996, and only one modeler outside of TU Delft contributed results to the TNF3 Workshop. Accordingly, Tim Peeters presented a status report on the Delft flame (Section 3) rather than a comparison of measured and modeled results.

One important aspect of the TU Delft calculations of their own flame is their comparison of three different mixing models. Some comments on this are also included in the poster abstract from Peeter Nooren. This type of study on the effects of changing one submodel at a time are very useful, both for understanding the sensitivity of results to such changes and for evaluating the accuracy, applicability, or efficiency of specific submodels. We encourage more work on this type of parametric investigation.

Bluff-Body Stabilized CH_4/H_2 Flame

The recirculating flow field of this case represents a significant challenge for turbulence models, and the emphasis of the TNF3 round of comparisons on the bluff-body cases was on the flow field calculations. Nonreacting and reacting cases were considered, and relatively simple models for the chemistry were used. Assaad Masri, the coordinator for this flame, has provided a good overview of these comparisons in Section 4.

One area of discussion in Boulder had to do with the apparent qualitative differences between predicted streamline patterns in the recirculation zone (lower center image on the proceedings cover page, for example) and the pattern derived from the measurements (not included in these proceedings). Some people expressed the opinion that such qualitative differences were an indication of an overall deficiency in the RANS models and that large eddy simulation (LES) should be pursued if one wished to improve the accuracy of flow-field calculations for this type of flame. We note that comparisons in a recent paper by Dally et a. (Combust. Theory Modelling

2:193-219) of the measured and computed flow patterns for one of the nonreacting bluff-body cases show reasonably good qualitative agreement.

Experimental Uncertainly

The determination and clear documentation of experimental uncertainty is a critical issue for the process of establishing benchmark data sets and testing models. Norm Laurendeau commented on this in Boulder, and we wish to emphasize some of those comments. First, none of the comparisons of measured and modeled results include error bars on the experimental data. These should be included in the future. Second, confidence levels should be provided as part of any estimates of uncertainty, and the method of establishing the uncertainties and confidence intervals should be documented.

While most of the experimentalist contributing data to the workshop library have included some estimates of uncertainty, it is clear that we can and should do a more complete job in this area. We will continue to try to emphasize the documentation of uncertainties. We will also consider the possibility of providing specific guidelines for the determination and reporting of experimental uncertainties in connection with data sets to be included as TNF target cases. Comments and contributions on this topic are welcome.

In a similar vein, modelers are encouraged to document such things as tests for grid independence, sensitivity to boundary conditions, sensitivity to changes in model constants, and any special procedures used to start a calculation or establish a stable solution.

Some Areas for Further Work on the TNF3 Target Flames

There are several areas where further work is needed in connection with the four target flames. We hope to address some of these over the coming year and at the TNF4 Workshop in Darmstadt, Germany during the summer of 1999. These include:

- additional measurements of minor species in the DLR flame
- investigation of the reasons for the large differences in predicted conditional means for fuel-rich conditions in Flame D
- comparison of results on NO formation (Some calculations of Flame D included NO, but this was not discussed in detail in Boulder.)
- additional measurements and analysis of flame radiation as it influences NO formation in these hydrocarbon flames
- extension of calculations to piloted flames E and F, which have significant localized extinction
- inclusion of more complete chemistry in the calculations of the bluff-body flames
- investigation of the LES models for calculating these target flames, particularly the bluff-body flame

Some Possibilities for Future Target Flames

While the above list may already imply more work than can be accomplished in time for the TNF4 Workshop, there was also discussion in Boulder about the next types of flames that should be addressed. Swirling flames are a prime target for those who have research connections with practical applications. Several groups are already working on swirling flames, as reflected by the posters. A few data sets are already in the literature, other experiments are in progress, and two or

three groups are considering new experiments on "simple" swirling flames. We strongly recommend that the experimental and computational people interested in swirling flames collaborate on: i) the evaluation of existing data sets to determine whether they are appropriate for the sort of model testing that the workshop is doing, ii) the design of new or supplementary experiments to ensure that boundary conditions, flow parameters, measured quantities, and measurement accuracies are consistent with the requirements for model testing, and iii) the acquisition of complete and complementary data on selected flames in different laboratories. Several workshop participant also expressed interest in turbulent counterflow flames as being useful for testing certain aspects of combustion models. Discussions on both types of flames are continuing.

Program Co-Chairs:

Dr. Robert S. Barlow
Reacting Flow Department, MS 9051
Sandia National Laboratories
7011 East Avenue
Livermore, CA 94551-0969, USA
1-925-294-2688
1-925-294-2595 FAX
barlow@ca.sandia.gov

Professor J.-Y. Chen
Department of Mechanical Engineering
University of California
6163 Etcheverry Hall
Berkeley, CA 94720, USA
1-510-642-3286
1-510-642-6163 FAX
jychen@firebug.me.berkeley.edu

Third International Workshop on Measurement and Computation
of Turbulent Nonpremixed Flames

Boulder, Colorado
July 30 - August 1, 1998

Contents

Third International Workshop on Measurement and Computation
of Turbulent Nonpremixed Flames

Boulder, Colorado
July 30 - August 1, 1998

Program Co-Chairs: R. Barlow and J.-Y. Chen

Introduction

Objectives: This workshop is intended to facilitate collaboration and information exchange among experimental and computational researchers in the field of turbulent nonpremixed combustion. The emphasis is on fundamental issues of turbulence-chemistry interactions. Main objectives are to:

- Select a few well-documented flames that can serve as experimental benchmarks covering a progression in geometric and chemical kinetic complexity, attempt to fix any major inconsistencies or gaps in these data sets, and make the data accessible on the internet.

- Provide an effective framework for comparison of different combustion modeling approaches and use the process to better our understanding of turbulent flames.

We emphasize that this is not a competition among models, but rather a means of identifying areas for potential improvements in a variety of modeling approaches. This collaborative process benefits from contributions by participants having different areas of expertise, including velocity measurements, scalar measurements, turbulence modeling, chemical kinetics, reduced mechanisms, mixing models, radiation, and combustion theory. The process also benefits from the rapid time scale of communication that is afforded by the internet. Data sets, computational submodels, and some results of comparisons are being made available on the web to allow convenient access by all interested researchers.

Background: The 1st TNF Workshop was held in Naples, Italy in July 1996, before the 26th Combustion Symposium. Objectives were to identify experimental data sets and establish preliminary guidelines for collaborative comparisons of measured and predicted results. The 2nd Workshop was held in Heppenheim, Germany in June 1997 and focused on comparison of results for hydrogen jet flames, including NO formation.

Scope: The focus of this 3rd Workshop is on jet flames of hydrocarbon fuels. Target flames were selected based upon the availability of detailed scalar and velocity data and the interest expressed by participants at the Heppenheim workshop. Some of the data for these target flames have only become available within the past year as a result of collaborative experiments. In order of complexity, the target flames are:

- Simple jet flame of $CH_4/H_2/N_2$ — DLR Stuttgart/TU Darmstadt
- Piloted CH_4/air jet flame (Flame D) — Sandia/TU Darmstadt
- Piloted natural gas jet flame (Delft III flame) — TU Delft/Sandia
- Bluff-body stabilized flame of CH_4/H_2 — U Sydney/Sandia

In addition to discussions on the target flames, the organizers encourage discussions on several related topics including: comparisons of measurements and predictions of other flames of interest; aspects of computational submodels for turbulent flow, mixing, chemistry, radiation, and turbulence-chemistry interaction; new experimental and computational results; possible target cases for swirling flames and flames within enclosures; progress in LES of reacting flows; and priorities for collaborative research.

Acknowledgments: Administrative support for the TNF Workshop is provided by Sandia National Laboratories with funding from the United States Department of Energy, Office of Basic Energy Sciences. Special thanks to Susan Canon.

Third International Workshop on Measurement and Computation
of Turbulent Nonpremixed Flames

Boulder, Colorado
July 30 - August 1, 1998

Agenda

Thursday Evening Session -- Reception, Introduction, and Poster Session

5:00 - 6:00 p.m.	*Reception in the poster room*
6:00 - 6:20 p.m.	Introductory remarks -- R. Barlow
6:20 - 9:00 p.m.	Poster session continues *with light dinner buffet and no host bar*

Friday Morning Sessions -- Results on Target Flames

7:30 - 8:00	*Continental breakfast in the poster room*
8:00 - 10:15	Presentation of results on target flames: A. Masri, Moderator DLR $CH_4/H_2/N_2$ Jet Flame Piloted CH_4-air Flame Delft III Flame
10:15 - 10:45	*Break (Coffee)*
10:45 - 1:00	Presentation and discussion of target flames: R. Barlow, Moderator CH_4/H_2 Bluff-Body Flame Open discussion of all target flame results
1:00	*Lunch*

Friday Afternoon Break for Recreation and Small Group Discussions

5:00 - 6:00	*Poster hour (refreshments in the poster room)*
6:00	*Dinner*

Friday Evening Session -- Discussion on Issues of Chemistry

7:30 - 9:30	Issues of Chemistry: N. Peters, Moderator Contributors: J. Warnatz, U. Maas, J-Y Chen, S. Pope

Saturday Morning Sessions -- Discussions on Other Key Issues

8:00 - 8:30	*Continental breakfast in the poster room*
8:30 - 10:30	Mixing Models and Relevance of Target Flames: S. Pope, Moderator Contributors: D. Roekaerts, J-Y Chen
10:30 - 11:00	*Break (Coffee)*
11:00 - 1:00	Current and Future Turbulence Models: J. Janicka, Moderator Contributors: S. Menon A. Kerstein,
1:00	*Lunch*

Saturday Afternoon Break for Recreation and Small Group Discussions

5:00 - 6:00	*Poster hour (refreshments in the poster room)*
6:00	*Dinner (Barbecue)*

Saturday Evening Session -- Summary and Planning of Future Activities

7:30 - 9:30	R. Bilger, Moderator

THIRD INTERNATIONAL WORKSHOP ON MEASUREMENT AND COMPUTATION OF TURBULENT NONPREMIXED FLAMES

July 30 – August 1, 1998 Boulder, Colorado

Names and Affiliations of Participants

Xue-Song Bai
Lund Institute of Technology
E-mail: bai@ms.vok.1th.se

Robert Barlow
Sandia National Laboratories
E-mail: barlow@ca.sandia.gov

Benoit Bedat
CERFACS
E-mail: bedat@cerfacs.fr

Robert Bilger
The University of Sydney
E-mail: bilger@mech.eng.usyd.edu.au

Eric Bish
FLUENT
E-mail: esb@fluent.com

Tilmann Blasenbrey
Stuttgart University
E-mail: tilmann@itv.uni-stuttgart.de

Edward Brizuela
University of Buenos Aires
E-mail: ebrizuel@fi.uba.ar

Gilles Cabot
University of Rouen
E-mail: gilles.cabot@univ-rouen.fr

Sebastien Caillat
CORIA
E-mail: sebastien.caillat@coria.fr

Antonio Cavaliere
Universita Federico II
E-mail: antcaval@unina.it

Chong Cha
University of Washington
E-mail: chongcha@u.washington.edu

J.Y. Chen
University of California at Berkeley
E-mail: jychen@euler.me.berkeley.edu

Ruey-Hung Chen
University of Central Florida
E-mail: chenrh@pegasus.cc.ucf.edu

Yungcheng Chen
The University of Sydney
E-mail: ycchen@mech.eng.usyd.edu.au

Bassam Dally
The University of Sydney
E-mail: bassam@chem.eng.usyd.edu.au

Christian Del Taglia
ETH - Zurich
E-mail: det@ltnt.iet.mavt.ethz.ch

Robert Dibble
University of California, Berkeley
E-mail: dibble@newton.berkeley.edu

Friedrich Dinkelacker
University of Erlangen
E-mail: fdi@ltt.uni-erlangen.de

Andreas Dreizler
Stuttgart University
E-mail: dreizler@itv.uni-stuttgart.de

Tarek Echekki
Sandia National Laboratories
E-mail: techekk@ca.sandia.gov

Joseph Fielding
Yale University
E-mail: joseph.fielding@yale.edu

Jonathan Frank
Physical Sciences, Inc.
E-mail: frank@psicorp.com

Robert Gallagher
Sandia National Laboratories
E-mail: rjgalla@ca.sandia.gov

Jüerg Gass
ETH Zurich
E-mail: gass@iet.mavt.ethz.ch

Dirk Geyer
Technical University of Darmstadt
E-mail: geyer@hrz2.tu-darmstadt.de

Jay Gore
Purdue University
E-mail: gore@ecn.purdue.edu

Gerd Grünefeld
University of Bielefeld
E-mail: gruenefe@physik.uni-bielefeld.de

Eva Gutheil
Universitaet Heidelberg
E-mail: gutheil@iwr.uni-heidelberg.de

Egon Hassel
Technical University of Darmstadt
E-mail: hassel@hrz1.hrz.tu-darmstadt.de

Jan Hessler
Argonne National Laboratory
E-Mail: hessler@anl.gov

John Hewson
Lawrence Berkeley National Laboratory
E-mail: jhewson@lbl.gov

Alexander Hinz
Technical University of Darmstadt
E-mail: ahinz@hrzpub.tu-darmstadt.de

Ryoji Homma
University of California at Berkeley
E-mail: homma@fireplace.me.berkeley.edu

Johannes Janicka
Technical University of Darmstadt
E-mail: janicka@hrzl.hrz.th-darmstadt.de

William Jones
Imperial College
E-mail: w.jones@ic.ac.uk

Carolyn Kaplan
Naval Research Laboratory
E-mail: ckaplan@lcp.nrl.navy.mil

Alan Kerstein
Sandia National Laboratories
E-mail: arkerst@ca.sandia.gov

George Kosaly
University of Washington
E-mail: kosaly@u.washington.edu

Andreas Kronenburg
The University of Sydney
E-mail: kronenb@mech.eng.usyd.edu.au

Tilo Landenfeld
Technical University of Darmstadt
E-mail: tlandenf@hrz1.hrz.tu-darmstadt.de

Normand Laurendeau
Purdue University
E-mail: laurende@ecn.purdue.edu

Bernhard Lenze
University of Karlsruhe
E-mail: bernhard.lenze@ciw.uni-karlsruhe.de

Peter Lindstedt
Imperial College
E-mail: p.lindstedt@ic.ac.uk

Mark Linne
Colorado School of Mines
E-mail: mlinne@mines.edu

Sven Linow
Technical University of Darmstadt
E-mail: slinow@hrz2.hrz.tu-darmstadt

Marshall Long
Yale University
E-mail: marshall.long@yale.edu

Ulrich Maas
Stuttgart University
E-mail: maas@itv.uni-stuttgart.de

W. Malalasekera
Loughborough University
E-mail: w.malalasekera@lboro.ac.uk

Mohy S. Mansour
University of Cairo
E-mail: mmansour@alpha1-eng.cairo.eun.eg

Assaad Masri
The University of Sydney
E-mail: masri@mech.eng.usyd.edu.au

Wolfgang Meier
DLR Stuttgart
E-mail: wolfgang.meier@dlt.de

Suresh Menon
Georgia Institute of Technology
E-mail: menon@falcon.ae.gatech.edu

Houston Miller
George Washington University
E-mail: houston@gwu.edu

Christopher Montgomery
Reaction Engineering International
E-mail: montgomery@reaction-eng.com

Gus Nathan
University of Adelaide
E-mail: gnathan@mecheng.adelaide.edu.au

Massimo Nutini
Pirelli Cavi e Sistemi S.p.A.
E-mail: massimo.nutini@pirelli.com

Andreas Obieglo
ETH-Zurich
E-mail: obieglo@iet.mavt.ethz.ch

Tim Peeters
Delft University of Technology
E-mail: t.peeters@tn.tudelft.nl

Norbert Peters
University of Aachen
Fax: 49 241 8888 223

Heinz Pitsch
UC San Diego
E-mail: hpitsch@ames.ucsd.edu

William Pitts
NIST
E-mail: wpitts@nist.gov

Stephen Pope
Cornell University
E-mail: pope@mae.cornell.edu

M. Pourkashanian
University of Leeds
E-mail: fue6lib@sun.leeds.ac.uk

Larry Rahn
Sandia National Laboratories
E-mail: rahn@ca.sandia.gov

Michael Renfro
Purdue University
E-mail: renfro@ecn.purdue.edu

Dirk Roekaerts
Delft University of Technology
E-mail: dirkr@wt.tn.tudelft.nl

Bernd Rogg
Ruhr Universität
E-mail: lstm@lstm.ruhr-uni-bochum.de

Bob Schefer
Sandia National Laboratories
E-mail: rwsche@ca.sandia.gov

Dietmar Schmidt
Stuttgart University
E-mail: schmidt@itv.uni-stuttgart.de

Rodney Schmidt
Sandia National Laboratories
E-mail: rcshmi@cs.sandia.gov

Christof Schulz
University of Heidelberg
E-mail: christof.schulz@urz.uni-heidelberg.de

Thomas Smith
Sandia National Laboratories
E-mail: tmsmith@cs.sandia.gov

N. Swaminathan
The University of Sydney
E-mail: nedunche@cmc1.mech.eng.usyd.edu.au

Fumiaki Takahashi
University of Dayton Research Institute
E-mail: ftakahas@engr.udayton.edu

Tadao Takeno
Nagoya University
E-mail: takeno@mech.nagoya-u.ac.jp

Stefano Traverso
Instituto di Macchine e Sistemi Energetici
E-mail: stefano@imseap.imse.unige.it

Paul Van Slooten
United Technologies Research Center
E-mail: vanslopr@utrc.utc.com

Michel Versluis
Delft University of Technology
E-mail: m.versluis@tn.tudelft.nl

Jürgen Warnatz
Universität Heidelberg
E-Mail: warnatz@iwr.uni-heidelberg.de

Forman Williams
University of California, San Diego
E-mail: faw@ames.ucsd.edu

Kejian Xiao
Universitaet Stuttgart
E-mail: xiao@itv.uni-stuttgart.de

Jun Xu
Cornell University
E-mail: xujun@mae.cornell.edu

Atsushi Yuasa
University of California at Berkeley
E-mail: yuasa@firebug.me.berkeley.edu

Bernard Zamuner
ONERA
E-mail: zamuner@onera.fr

SECTION 1

DLR/Darmstadt $CH_4/H_2/N_2$ Jet Flame

Coordinated by Wolfgang Meier

DLR $CH_4/H_2/N_2$ Jet Diffusion Flame

General Description of the Flame

The **burner** consisted of a 35†cm long straight stainless steel tube (i.d. 8†mm) with a thinned rim at the exit. The tube was surrounded by a contoured nozzle (i.d. 140†mm) supplying the lower part of the flame with co-flowing dry air at an exit velocity of typically 0.3†m/s [1]. It is the same burner as for the standard flame „H3“.

The **fuel** was a mixture of 33.2%†H_2, 22.1%†CH_4, and 44.7%†N_2 (by volume). H_2 was chosen as an additive in order to stabilize the flame without changing the simple flow field of a straight tube. The dilution by N_2 was necessary for a reduction of signal background from laser-induced fluorescence of PAHs and C_2 radicals. Furthermore, this gas composition yielded a nearly constant Rayleigh scattering cross section throughout the flame allowing the application of 2D Rayleigh thermometry. The exit velocity of the cold jet was 42.15†m/s, resulting in a Reynolds number of Re=15200.

Measurements

Raman/Rayleigh measurements of f, T, N_2, O_2, H_2, CH_4, CO, CO_2, H_2O were performed with a spatial resolution of 0.6 mm at the downstream positions x/D=5, 10, 20, 40, 60, and 80. For axial profiles, the positions x/D=2.5, 100, and 120 were also included. At each point, 400 single-pulse measurements were recorded, from which some samples with very high signal background were filtered out. The data set is available in the Internet [2].

Velocity measurements were performed with a two-component LDV apparatus at the TU Darmstadt [3]. Radial profiles of the mean axial velocity U and radial velocity V, as well as the Reynolds-stress tensor components uíuí and uíví have been determined at 7 downstream locations. An axial profile of U and uíuí has also been measured.

2D LIF (qualitative) and **2D Rayleigh** (quantitative) measurements of OH, CH, NO, and T yielded a characterization of the structures and temperature gradients within the flame.

The **precision**, **accuracy**, **bias** due to filtering, as well as other details of the measuring techniques and results, have been documented in a paper concerning the investigations of this flame [4].

Calculations

Model calculations for this flame have been performed by J.-Y. Chen (UC Berkeley), H. Pitsch (UC San Diego), and H. Sanders.

Primary Contact: Wolfgang Meier, Institut für Verbrennungstechnik, DLR Stuttgart, Pfaffenwaldring 38-40, D-70569 Stuttgart, Germany
(Fax:†+49-711/6862-578,†Tel.:†+49-711/6862-397,†E-mail:wolfgang.meier@dlr.de)

References

1. http://www.tu-darmstadt.de/fb/mb/ekt/flamebase.html
2. http://www.st.dlr.de/EN-CV/
3. For details contact Egon Hassel (hassel@hrz1.hrz.tu-darmstadt.de)
4. V. Bergmann, W. Meier, D. Wolff, W. Stricker: Appl. Phys. B 66, 489 (1998)

Calculation Methods

J.-Y. Chen (UC Berkeley)

Turbulence Model: Parabolic code using Reynolds stress with joint scalar PDF approach.

Mixing Model: Modified Curlís mixing model.

Chemistry Model: 10 step reduced chemistry based on GRI 1.2 detailed CH_4 mechanism.

H. Pitsch (UC San Diego)

Turbulence Model: Flowfield calculations based on FLUENT code.

Flamelet Model: Unsteady flamelet model, Le=1.

Chemistry Model: 14 step reduced mechanism (N. Peters).

H. Sanders

Turbulence Model: The turbulence model is based on Launders, Reece, and Rodi.

Flamelet Model: Laminar flamelets including full differential diffusion.

Chemistry Model: GRI 2.11 mechanism.

Axial Profiles of f, U, and T

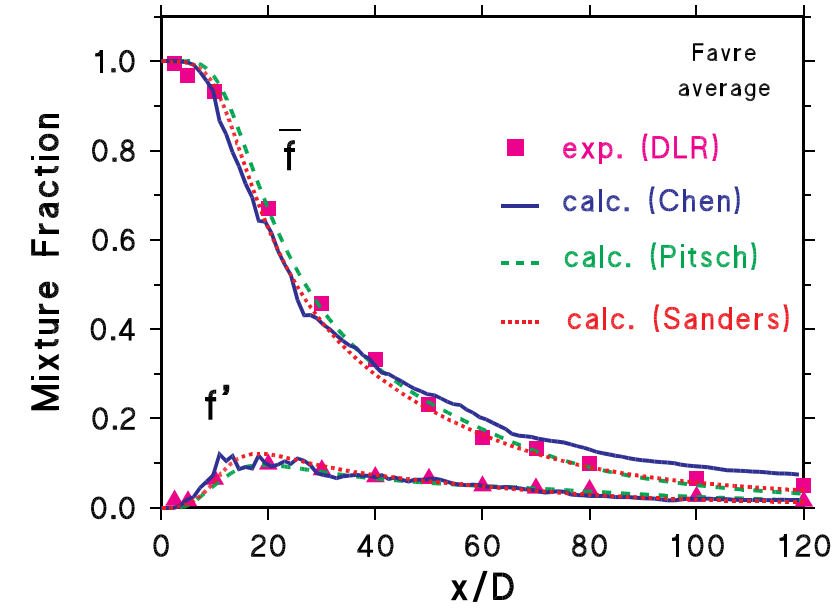

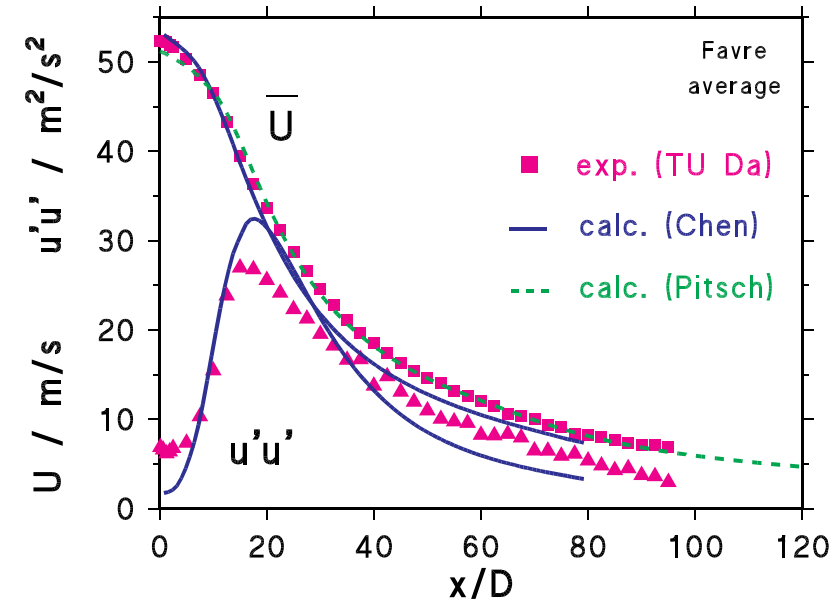

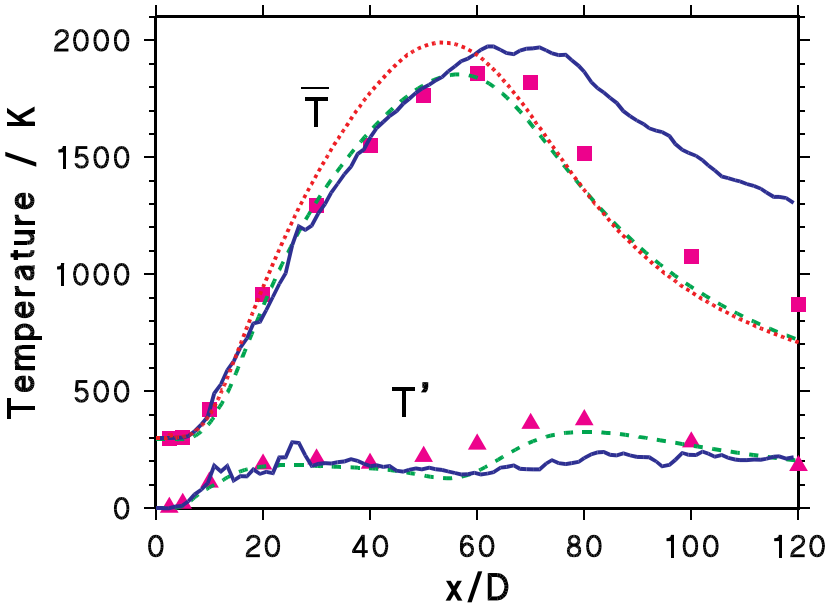

Radial Profiles of f, U, and T at x/D=5 and 40

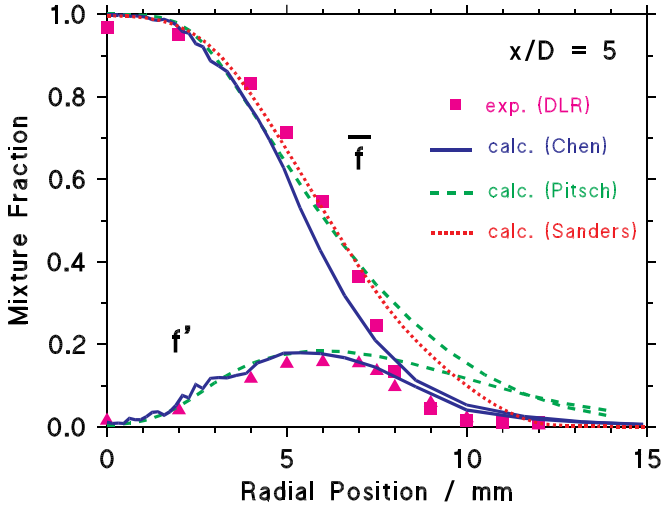

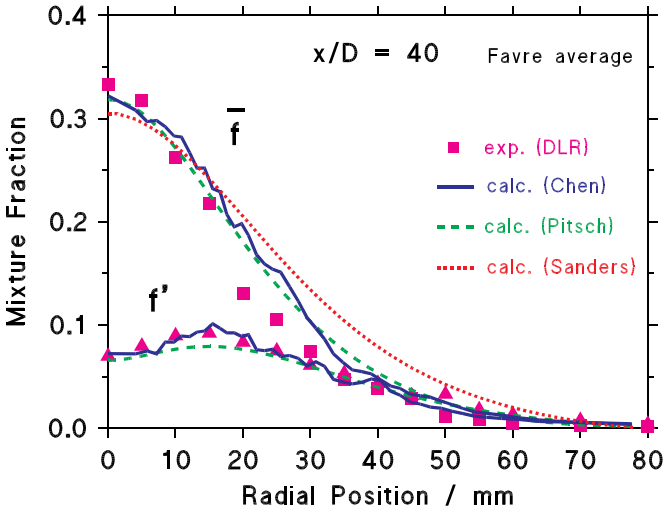

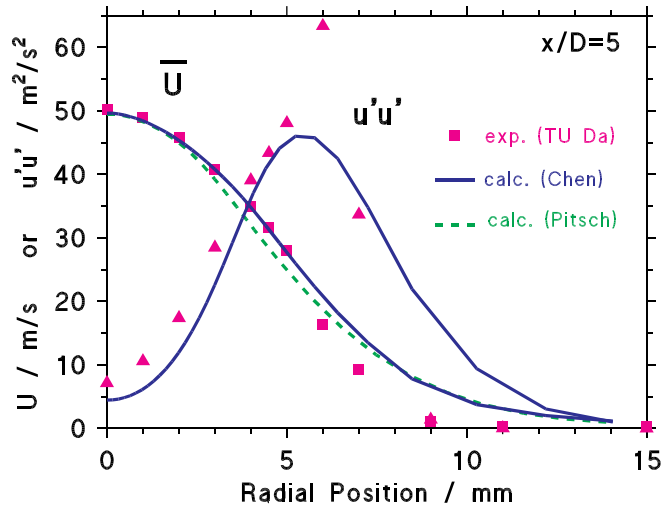

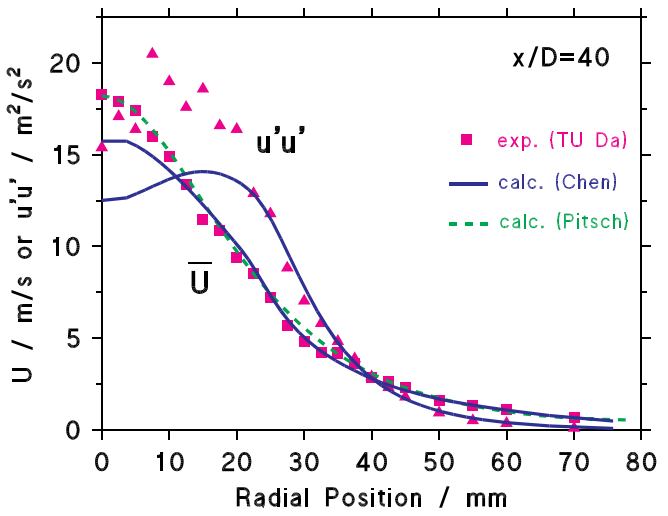

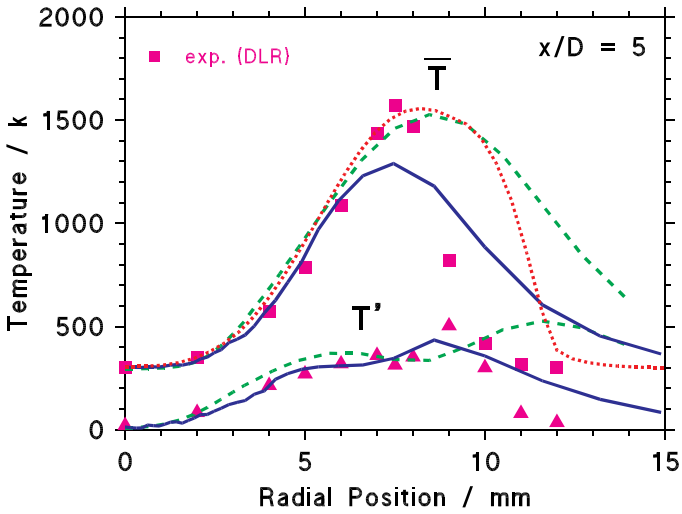

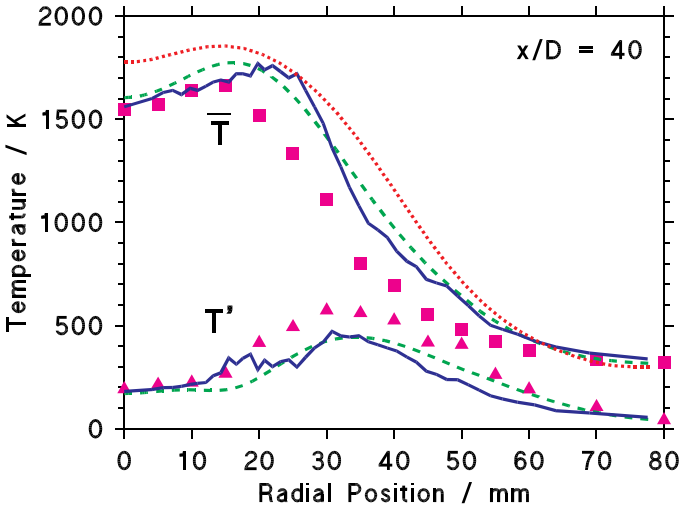

Axial Profiles of Major Species

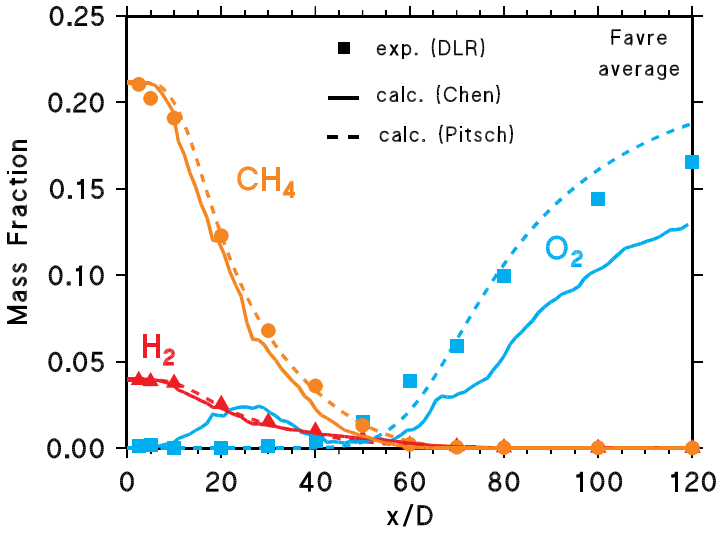

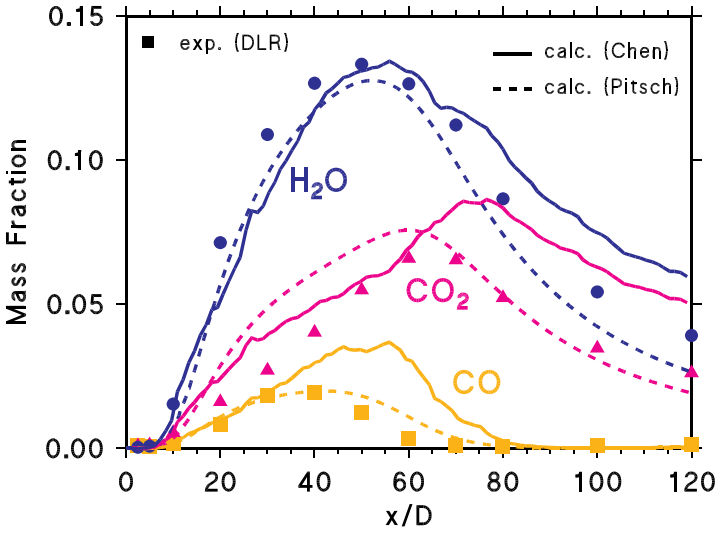

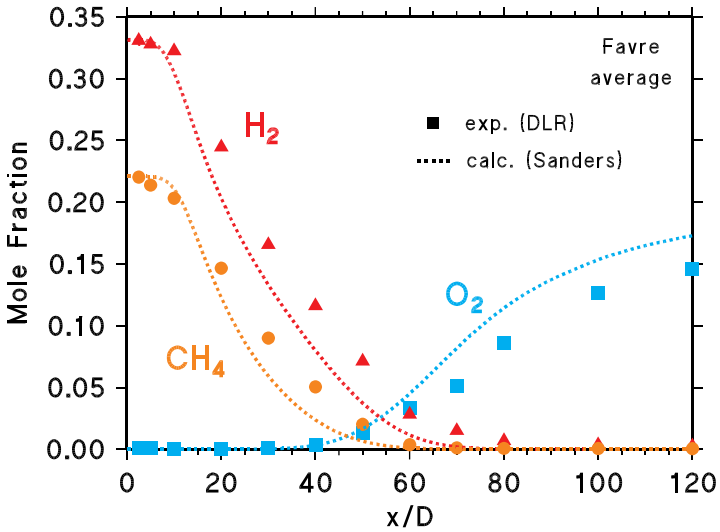

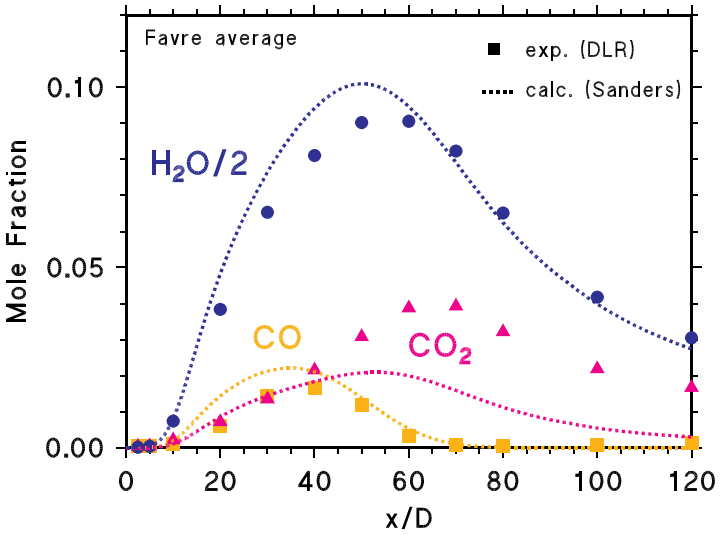

Comparison: Exp. (DLR) – Calc. (Chen) – Calc. (Pitsch)

conditional means of H_2O and CO_2 at x/D=5 and 40

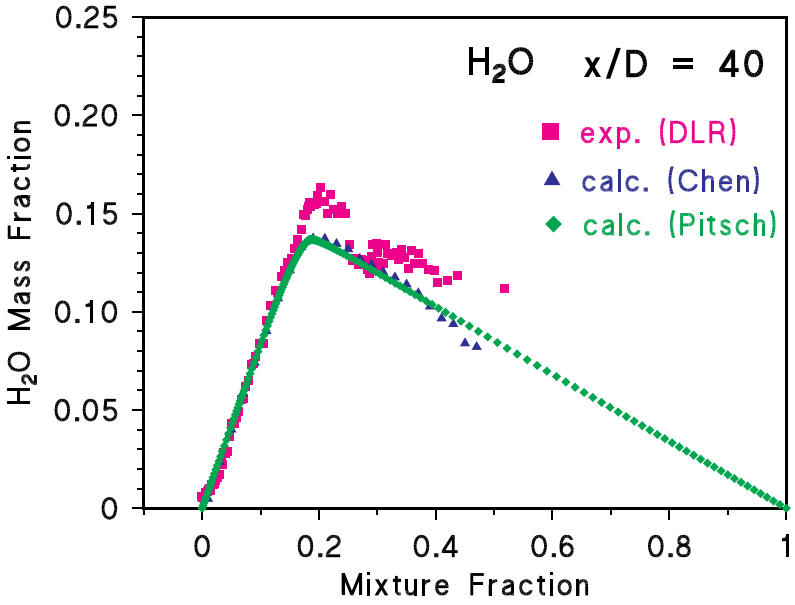

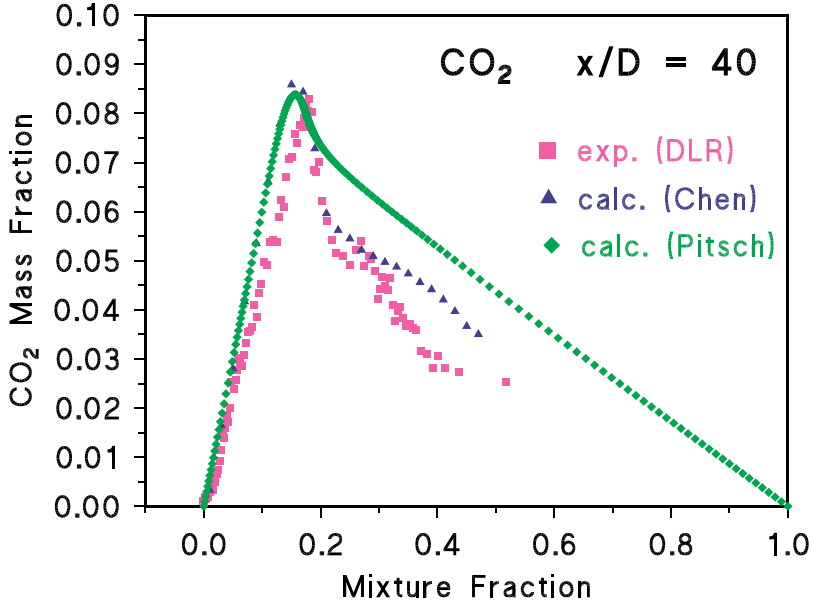

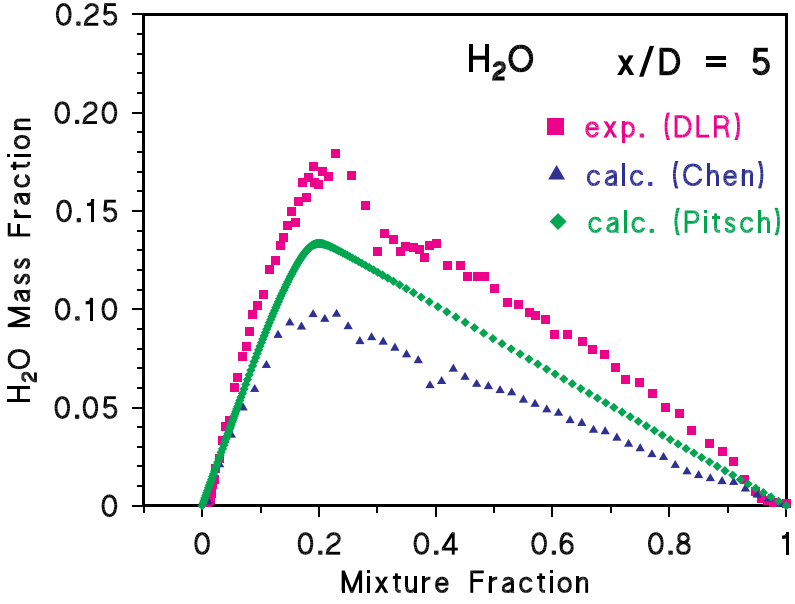

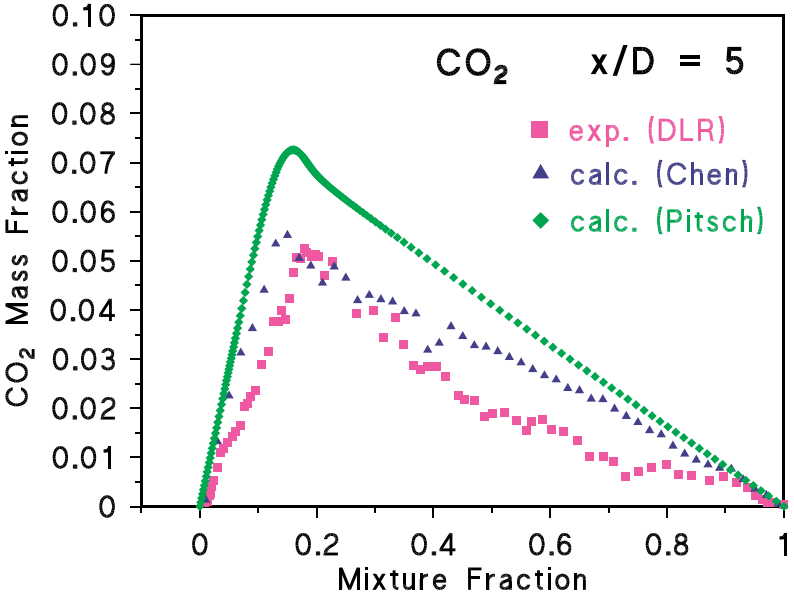

Comparison: Exp. (DLR) – Calc. (Chen) – Calc. (Pitsch)

conditional means of T and CO at x/D=5 and 40

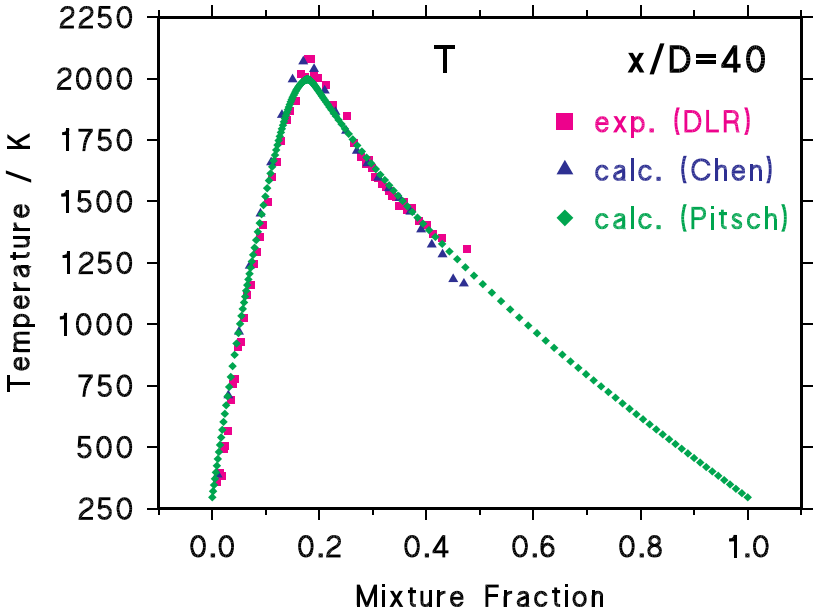

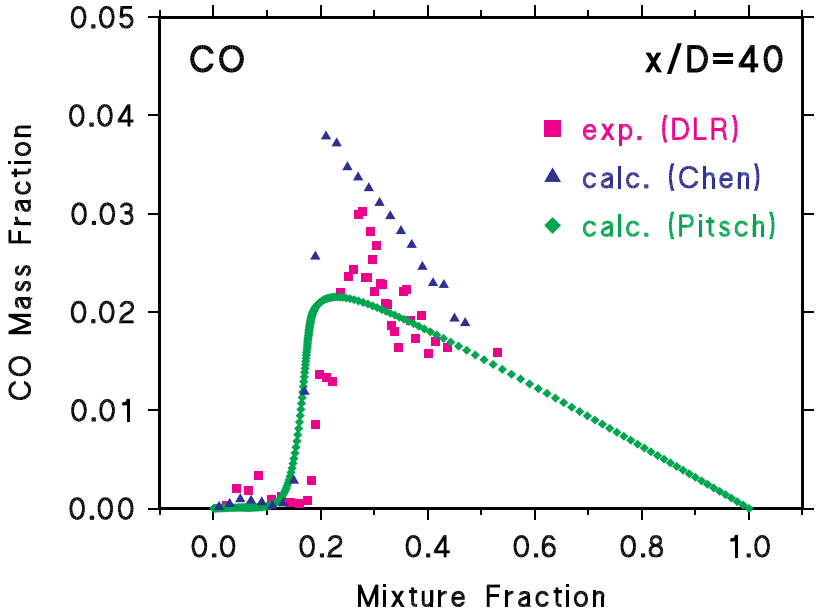

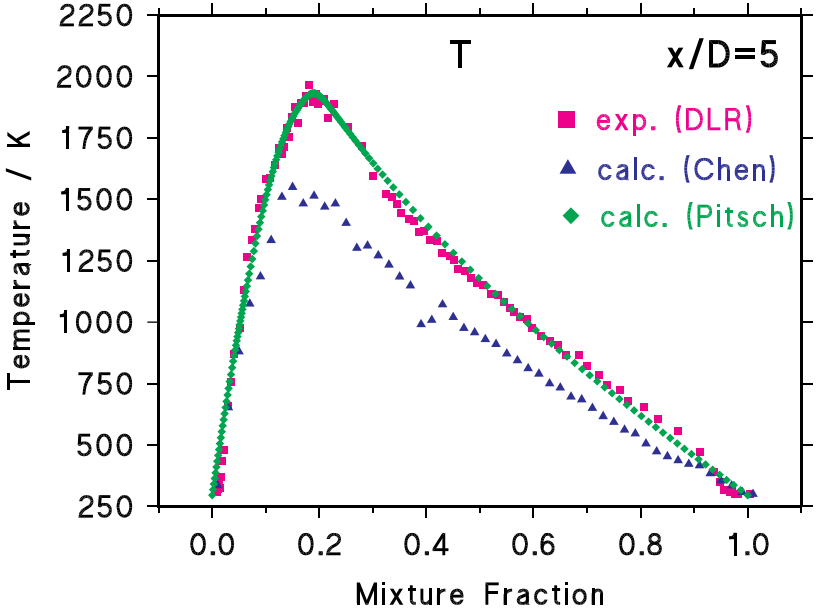

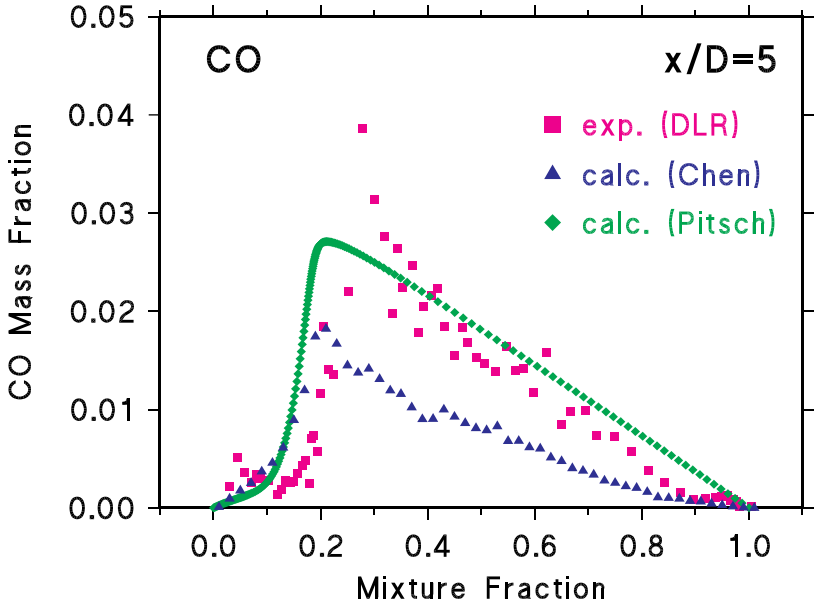

Comparison: Exp. (DLR) – Calc. (Chen)

scatterplots of temperature at x/D=5 and 40

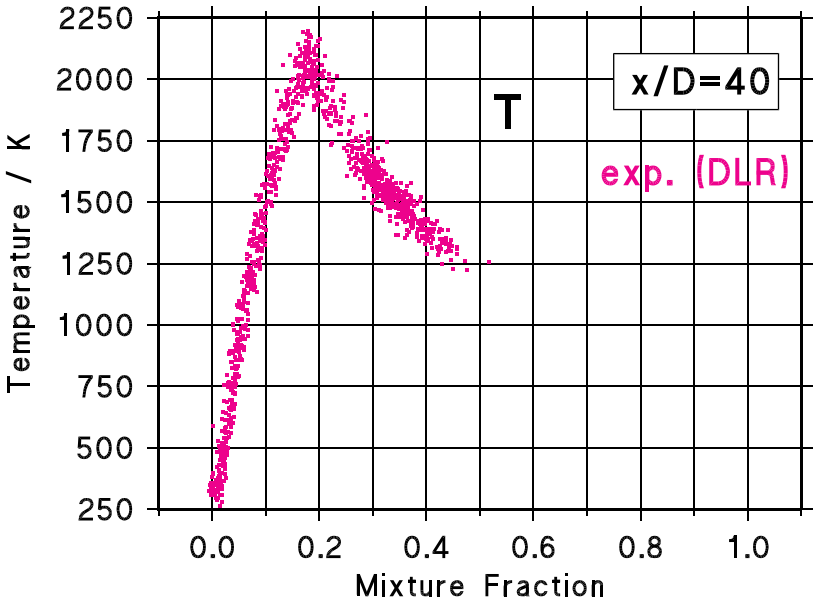

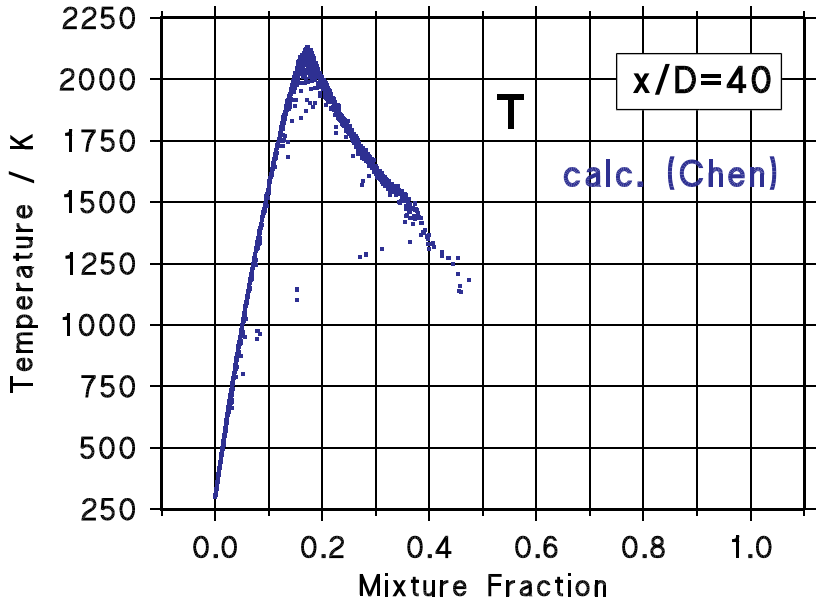

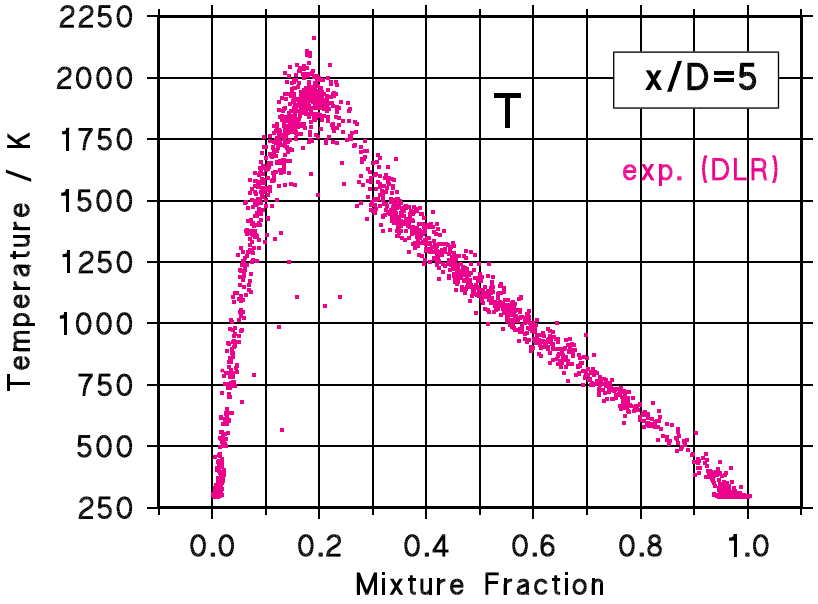

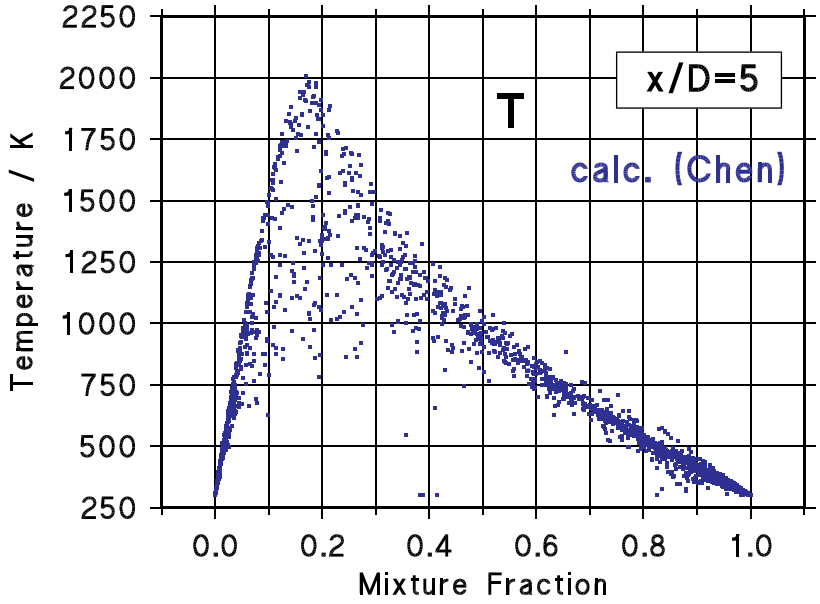

Comparison: Exp. (DLR) – Calc. (Chen)

scatterplots of CO at x/D=5 and 40

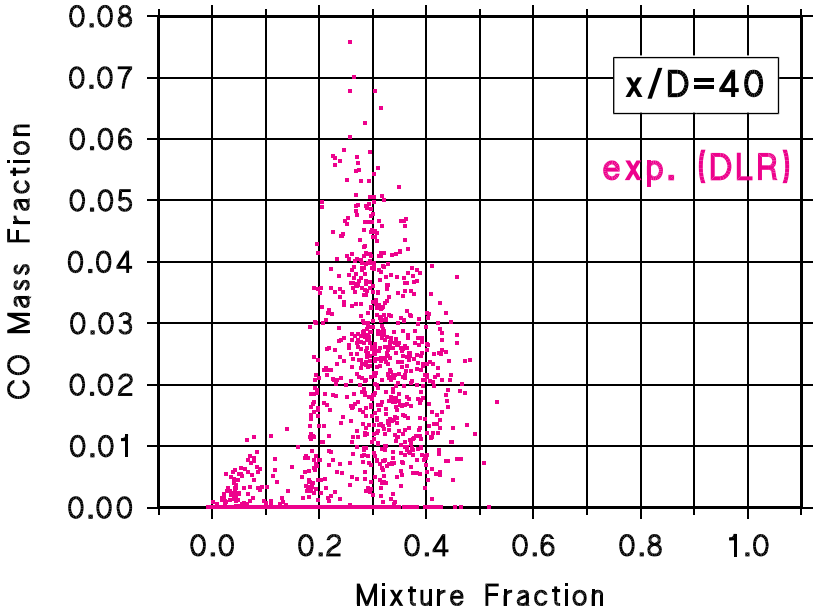

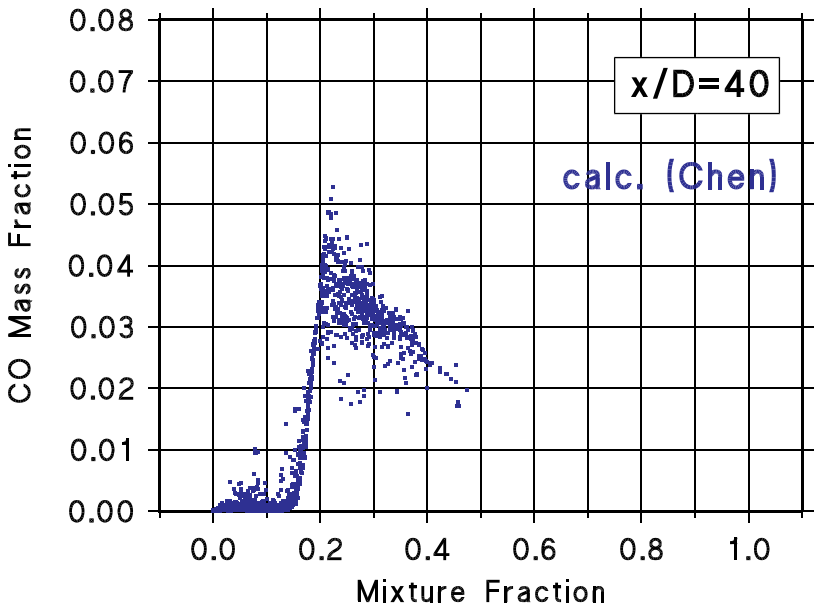

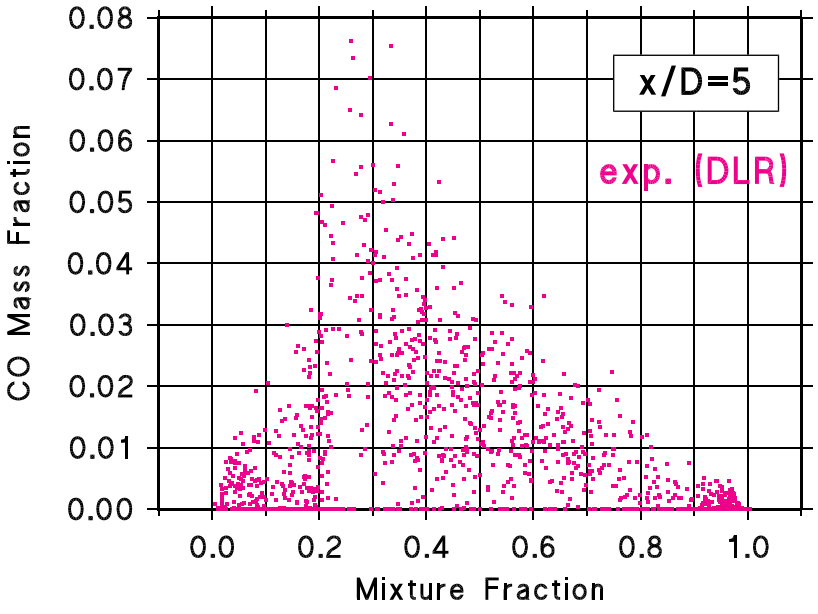

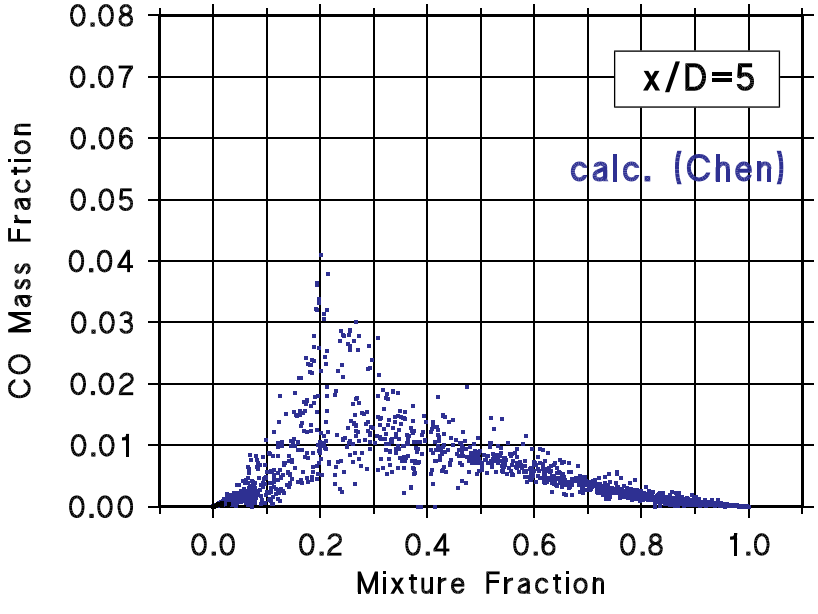

SECTION 2

Sandia/Darmstadt Piloted CH_4/Air Flame D

Coordinated by Robert Barlow

Third International Workshop on Measurement and Computation of Turbulent Nonpremixed Flames

Boulder, Colorado
July 30 - August 1, 1998

Piloted CH4/Air Flame D Comparisons

Coordinator: R. S. Barlow, Sandia National Laboratories

Flame Description: Flame D is one in a series piloted jet flames operated using the Sydney University piloted burner geometry [1,2]. This burner has a nozzle diameter of d=7.2 mm and a premixed pilot that extends to a diameter of 18.2 mm. The main jet composition is 25% CH_4 and 75% air, selected to reduce the level of fluorescence interference from soot precursors. The complete series of six flames spans jet Reynolds numbers from 1,100 (laminar) to 44,800 (turbulent with significant localized extinction). Flame D has a jet Reynolds number of 22,400 and has only a small probability of localized extinction. The stoichiometric value of the mixture fraction is 0.351, and the stoichiometric flame length is ~47d.

Experimental Overview: The data base on Flame D includes simultaneous point measurements of T, N_2, O_2, CH_4, CO_2, H_2O, and H_2 by Rayleigh/Raman scattering and of OH, NO, and CO by laser-induced fluorescence [1,2]. Two-component LDV data where measured during the past year at TU Darmstadt. The burner and a set of calibrated flow controllers were loaned from Sandia in order to insure equivalence of flow conditions.

Contributed Calculations: Results of eight calculations were contributed for comparison with the experiments.

· PDF/Detailed chemistry	J-Y Chen, UC Berkeley
· Monte-Carlo/Flamelet w/ equal diffusivities	J-Y Chen, UC Berkeley
· Monte-Carlo/Flamelet w/ differential diffusion	J-Y Chen, UC Berkeley
· CMC/Detailed chemistry	Roomina, Bilger; U Sydney
· CMC/Detailed chemistry w/ radiation	Roomina, Bilger; U Sydney
· PDF/ILDM	Hinz, Janicka; TU Darmstadt
· PDF/ILDM (subsequently withdrawn)	Xiao, Maas; U Stuttgart
· LFSR based on measured mixture fraction data	Paul, Sivathanu, Gore; Purdue

Contents of this Section:

· Summaries of calculation methods
· Axial profiles of velocity, mixture fraction, temperature, and Favre-average species mass fractions
· Radial profiles of U, u", and u"v" at x/d=45
· Radial profiles of Favre-average F, F", T, Y_{CO}, Y_{H2}, and Y_{OH} at x/d=7.5 15, 30, 45, and 60
· Conditional means of T, Y_{CO2}, Y_{H2O}, Y_{CH4}, Y_{O2}, Y_{CO}, Y_{H2}, and Y_{OH} at x/d=7.5 15, 30, 45, and 60
· Scatter plots of T, Y_{CO2}, Y_{CO}, Y_{H2O}, Y_{H2}, and Y_{OH} and x/d=15 and 30
· Flame D documentation file

Preliminary Observations: A major strength of this data set is in the measurements of combustion intermediates and minor species. Accordingly, the comparisons included here emphasize issues of chemistry more than the details of the flow/mixing fields. Mean axial velocity profiles are in reasonable agreement with the measurements. The calculations tend to yield a stoichiometric flame length that is slightly shorter than measured. However, the differences should not interfere with interpretation of chemistry issues based on conditional means and scatter plots. Radial profiles show some relatively large differences, particularly in the lower portion of the flame. Conditional means show *large* differences among the calculations, particularly in the fuel-rich region. Axial profiles of Y_{NO} are included for the flamelet and CMC calculations and show a strong influence of radiation.

References:

[1] Barlow, R. S. and Frank, J. H., "Effects of Turbulence on Species Mass Fractions in Methane/Air Jet Flames," *Twenty-Seventh Symposium (International) on Combustion,* The Combustion Institute, Paper 4A10 (1998).
[2] www.ca.sandia.gov/tdf/Workshop.html

Joint Scalar PDF Simulation of Turbulent Reacting Flows with Detailed Chemistry on a Parallel Cluster

J.-Y. Chen
Department of Mechanical Engineering
University of California at Berkeley
Berkeley, California 94720
phone: (510)-642-3286 Fax: (510) 642-6163
e-mail: jychen@euler.me.berkeley.edu

C. Yam*, and R. Armstrong
Sandia National Laboratories
* postdoctoral researcher, currently with Aerojet.

Turbulence Model:

K-ε model with $C_{\varepsilon 2}$=1.8 (Standard value=1.94). Turbulent viscosity in the joint scalar pdf $\nu_t=C_\mu/\sigma_f$, where σ_f =0.8.

Chemistry model and kinetic mechanism:

Detailed GRI 1.2 mechanism.

Mixing model and number of pdf particles:

Modified Curl's model with 50 particles/cell.

Coupling model:

Eulerian composition PDF with fractional step. 2-D elliptic time dependent flow solver with projection method. Second-order accuracy in space and time for flow field. The scalar PDF is first order accurate in time.

Solution domain:

Axisymmetric grids of 50x70 nodes clustered around the jet centerline and near field.
Physical domain: 0-70 diameters in axial direction, 0-18 diameters from jet centerline to outer stream.

Boundary conditions (state any differences from those in the documentation file):

Scalar field is prescribed according to experimental data (web). Mean velocity is prescribed to give the same mean values. The exact form differs from the experimentally suggested shape due to difficulty in treating the sharp changes in the boundary layer (noted below).

Location of start of computations:

x=0.

Convergence criteria or length of calculation:

Computations were performed using well-mixed reactor until mean flow field reached steady state (30,000 steps roughly). Finite rate mixing was turned on and the computation proceeded up to 2,000 steps. Time step=1.4E-5 second with CFL=0.2.

Machine used and approximate CPU time required:

Pentium Pro. 200MZ, 256MB, 4 CPU (max. equipped). Operating System: LINUX.
Total number of CPU used: 32 (load balancing is not applied for this run).
Total run time is about 7 days for 2,000 steps with direct stiff solver DVODE.

Comments on modeling issues:

When the inlet velocity is prescribed with sharp boundary layers for the fuel jet and the pilot, the k-ε model blows up, even with a very small CFL number (say, 0.05). Instead of a sharp boundary layer, a smooth profile was used, and the k-e model was run with $C_{\varepsilon 2}$=1.8. If the standard value $C_{\varepsilon 2}$=1.94 is used, the velocity decays too fast in the near field compared to the experimental data.

Steady State Flamelet Modeling of Turbulent Reacting Flows based on Monte Carlo Joint Scalar PDF

J.-Y. Chen
Department of Mechanical Engineering
University of California at Berkeley
Berkeley, California 94720
phone: (510)-642-3286 Fax: (510) 642-6163
e-mail: jychen@euler.me.berkeley.edu

Turbulence Model:

Reynolds stress modeling with C_{cor}=0.025 (details are given in Ref. 1)

Chemistry model and kinetic mechanism:

Steady state flamelets generated with detailed GRI 2.11 mechanism using Sandia's opposed Tsuji burner code. Flamelets computed for multi-component diffusion a=5, 10,25,50,100,200,300,400,600,700 (1/s); for equal diffusivity (setting diffusivity = thermal diffusivity) a=5, 10,25,50,100,200,300,400,600,800,1000 (1/s).
Library generated using mixture fraction and scalar dissipation rate (f,X_f) as two parameters. NO is computed by splitting source into positive and negative parts using a sink time scale, i.e., W_{NO}= SNO- [NO]/τ_{NO} (Ref. 2).

Mixing model and number of pdf particles:

Modified Curl's model with 800 particles/cell. A lognormal distribution is assumed for the scalar dissipation rate. The particle properties are computed from flamelet library (f,X_f) where X_f is sampled from the lognormal distribution with its mean value estimated based scalar fluctuation and mean turbulence time scale (Ref. 2).

Coupling model:

Eulerian composition PDF with parabolic marching downstream code using von Miss transformation.

Solution domain:

Axisymmetric grids of 50 across half of the jet. About 1400 steps to reach x/D=90 with variable step size.

Boundary conditions (state any differences from those in the documentation file):

Scalar field is prescribed according to experimental data (web). Mean velocity and turbulence statistics are prescribed according to experimental data (or estimated) in the Sandia's Workshop Web for Flame D.

Location of start of computations:

x=0.

Convergence criteria or length of calculation:

Up to 90 diameters.

Machine used and approximate CPU time required:

Pentium Pro. 200MZ, 256MB, 90 minutes (1 and 1/2 hours). Operating System: LINUX.

Radiation Model:

Only H_2O and CO_2 are included with absorption coefficients recommended by the workshop. Only SNO is modified with an exponenetial ratio described in Ref. 2.

Comments on modeling issues:

The source splitting is used to compute NO in order to include 'reburning' of NO in rich parts of flame.

Reference:

1) Chen, J.-Y. and Kollmann, W. "Comparison of prediction and measurement in nonpremixed turbulent flames," Chapter 5 in *Turbulent Reactive Flows*, Edited by P. Libby and F.A. Williams, Academic Press, Ltd., 1994.
2) Chen, J.-Y. and Chang, W.-C., *Twenty-Sixth Symposium (International) on Combustion*, The Combustion Institute, 1996, pp. 2207-2214.

Conditional Moment Closure Modeling of Piloted Flame D: Summary Page

M. R. Roomina and R. W. Bilber
Department of Mechanical and Mechatronic Engineering
The University of Sydney, NSW 2006, AUSTRALIA
roomina@mech.eng.usyd.edu.au; biger@mech.

Turbulence model, including values of model constants:

The governing equations for the flow and mixing field are expressed by the Favre-averaged equations in axisymmetric boundary-layer form for continuity, momentum, turbulence kinetic energy, turbulent kinetic dissipation rate and the mean and variance of the mixture fraction. The closure used here for the turbulence is the k-ε-g model of Launder et al. (1972).

Turbulence coefficients for k-ε-g model											
C_μ	C_0	$C_{\varepsilon 1}$	$C_{\varepsilon 2}$	$C_{\varepsilon 3}$	C_{g1}	C_{g2}	σ_k	σ_ε	σ_g	σ_ξ	
$0.09- 0.04f$	0.5	1.43	$1.92-0.0667f$	0.72	2.7	1.79	1.0	1.3	0.7	0.7	$f \equiv \left\lvert \frac{R_\mu}{1.6u_0}\left(\frac{du_c}{dx}\right) - \left\lvert \frac{du_c}{dx} \right\rvert \right\rvert^{0.2}$

Subscript c denotes centreline value, u_0 is the jet exit velocity and R_μ represents the radial width of mixing region.

Chemistry model and kinetic mechanism:

GRI-Mech 2.11, 49species, 279 reactions.

Mixing model and number of pdf particles (if appropriate):

Clipped Gaussian pdf

Coupling model:

Conditional Moment Closure

Solution domain (xmin,xmax,ymin,ymax) and grid structure:

x/D=0 to x/D=100 and y/D=0 to y/D=15.

Boundary conditions (state any differences from those in the documentation file):

The coflow velocity is taken 1.0 m/s

The fuel and air temperatures are assumed 300°K instead of 294°K.

It is also assumed that the pilot is a stoichiometric mixture of the main fuel.

Location of start of computations:

Adiabatic equilibrium compositions are employed for the reactive scalars down to five jet diameters (x/D=5), in order to assure the ignition of the flame in the near-field region due to high mixing rates.

Convergence criteria or length of calculation:

The calculations are carried out down to x/D=100.

Currently absolute tolerance levels of 10^{-8} for major species, 10^{-12} for minor species and 10^{-4} for enthalpy are employed. The relative tolerance level is taken as 10^{-4}.

Machine used and approximate CPU time required:

DEC 3000/400 ALPHA work station. Approximate CPU time is 120 hrs.

Comments on modeling issues:

Check on the adequacy of number of grid points in the cross-stream direction. When the starting profiles are not smooth, the truncation error in the CFD solver may seriously affect the solution if convection is large. This check can be done by examination of flow and mixing field results, in particular radial profiles of velocity and mixture fraction along with conservation of mass and momentum. Additional grid points can be introduced to smooth up the radial profiles.

Check on the unity of integral of pdf over mixture fraction space at various axial locations. Significant deficiency in magnitude of pdf may lead to inaccurate conditional mean scalar dissipation and consequently conditional and unconditional species mass fractions.

Check on initial profiles of species concentration where equilibrium initialisation is employed. High equilibrium concentration levels are inappropriate for some of minor species in particular NO and NO_2. Correct NO and NO_2 levels can be predicted if concentration of these species are suppressed in the initial profiles.

Reference:

Launder, B. E., Morse, A., Rodi, W. and Spalding, D. B.(1972). The prediction of free shear flows—A comparison of six turbulence models. *NASA Free Shear Flows Conference*, Virginia, NASA Report Number SP-311.

Numerical Simulation of a Turbulent Piloted Methane / Air Jet Flame (Flame D) using a Finite-Volume - Monte-Carlo-PDF Code: Models and Boundary Conditions

Alexander Hinz, Egon P. Hassel, Johannes Janicka
FG Energie– u. Kraftwerkstechnik, Technische Universität Darmstadt,
Petersenstr. 30, 64287 Darmstadt, Germany
phone: +49-6151/16 2502, fax: +49-6151/16 6555, e-mail: ekt@hrzpub.tu-darmstadt.de

Overview about models, boundary and initial conditions, and comments on the simulation.

Turbulence Model:

Modified $k-\varepsilon$ model with constants C_μ and $C_{\varepsilon 2}$ according to [Launder72]. Turbulent viscosity in PDF diffusion term $\nu_t = C_\mu/\sigma_f \cdot \tilde{k}^2/\tilde{\varepsilon}$ with $\sigma_f = 0.83$.

Chemistry Model and Kinetic Mechanism:

ILDM table parameterized with mixture fraction and two reaction progress variables x_{CO_2} and x_{H_2O} [Maas90].

Mixing Model, Number of PDF Particles:

Modified Curl's model [Janicka79] for scalar mixing with 100 particles in each cell.

Coupling Model:

Eulerian composition PDF solved via fractional step method in coupling with a CFD code (2D elliptic finite-volume code, staggered grid, SIMPLE method, TDMA-ADI solver) (Hybrid method) [Pope81, Chen96].

Solution Domain:

Assuming axis-symmetry; grid: 120×80 nodes, condensed near the centerline and the inlet boundary, $L_x = 1000$ mm, $L_r = 677$ mm with 11 nodes inside the jet radius, $r(12) = 3.6$ mm, 12 nodes inside the pilot, $r(25) = 9.1$ mm, 55 nodes in the coflow. The expansion factors are $\alpha_x = 1.04$, $\alpha_r = 1.05$ for $r \leq 9.1$ mm and $\alpha_r = 1.09$ for $r > 9.1$ mm.

Boundary Conditions:

At inlet boundary, scalars assigned according to documentation with all particles having the same values in a particular cell (Dirac-PDF). Velocities and turbulent quantities according to measurements for $r \leq 10.43$ mm and to estimations in documentation for $r > 10.43$ mm, linearly interpolated onto the grid. Dissipation according to [Masri90], reduced to get $\partial\tilde{k}/\partial x = 0$ at the nozzle.

Location of Start of Computation:

Computation starts at $x = 0.0$ mm.

Convergence Criteria or Length of Calculation:

PDF procedure takes about 30 000 steps (including fine-tuning of constants) with a time step $dt = 1 \cdot 10^{-5}$ s which corresponds to more than 0.3 s real time ($L_x/U_{bulk} = 1$ m$/49.8$ m/s ≈ 0.02 s).

Machine used and Approx. CPU Time:

About 140 h on an ALPHA lx533, including process of evolving stably burning flame.

Comments:

Problems arise with the IEM model to get the flame stably burning. Evolution of a burning flame is partly successful with increase of decay rate ($C_\phi = 8$) for $x/d < 5$. The standard $k-\varepsilon$ model yields too steep centerline decay. The start profile is a block profile extended axially in the domain according to the inlet conditions. Time scales become large far downstream, thus the evolution of a converged solution takes comparatively long and larger scattering can be observed in the profiles.

References:

Barlow, R., Frank, J.H. (1998), 27^{th} *Symp (Int.) Comb.*, accepted

Chen, J.-Y., Chang, W.-C. (1996), 26^{th} *Symp (Int.) Comb.*, pp. 2207-2214

Janicka, J., Kolbe, W., Kollmann, W. (1979), *J. Non-Equil. Thermodyn.*, 4, pp. 2292-2307

Launder, B.E., Morse, A., Rodi, W., Spalding, D.B. (1972), *Tech. Report, NASA SP-311*

Maas, U., Pope, S.B. (1992), *Comb. Flame*,88 (3), pp. 239-264

Masri, A.R., Pope, S.B. (1990), *Comb. Flame*,81, pp. 13-29

Pope, S.B. (1981), *Combust. Sci. Technol.*, 25, pp. 159-174

Laminar Flamelet State Relationships based calculation for Sandia piloted CH_4-Air Flame D

R. N. Paul, Y. R. Sivathanu and J. P. Gore
Thermal Sciences and Propulsion Center
Purdue University
West Lafayette, IN-47907

Favre averaged mean and RMS (root mean square) of temperature and species mole fractions are calculated using the laminar flamelet concept. Predictions of Favre averaged mean and RMS temperature, N_2, O_2, H_2O, H_2, CH_4, CO, CO_2, OH and NO are compared with the measurements. The laminar flamelet state relationships (LFSR) for density, temperature and species are constructed using the Sandia one-dimensional code OPPDIF in conjunction with the GRI kinetic mechanism, version 2.11. For the LFSR calculations, the fuel is premixed with limited amount of air to yield a stream whose composition is identical to the jet fluid used in Flame D. The opposed oxidizer stream is air. The fuel stream and air stream velocities are varied between 5 – 50 cm/s to parametrically consider the effects of stretch rate. Equal velocities for fuel and air with a separation distance of 2 cm are used for LFSR calculations. Radiation effects are studied using the optically thin emission approximation and the Planck mean absorption coefficients summarized at the TNF web site.

OPPDIF calculations to generate LFSR took most of the computer time for the present calculations. The calculations are performed on IBM 370 UNIX based workstation. The first solution takes around 10 hours of CPU time starting with an initial guess corresponding to the equilibrium composition. However, if a good initial guess is available, state relationships can be obtained in typically half an hour of CPU time. A mixture fraction is calculated from the OPPDIF solutions by adding the local carbon and hydrogen mass and multiplying it by the ratio of the total mass to the mass of carbon and hydrogen in the fuel stream.

Given the state relationships, the Favre averaged mean and RMS of scalar flow properties are found using a clipped Gaussian, Favre averaged probability function (PDF) of mixture fraction. The parameters of the mixture fraction PDF are obtained from the Favre mean and RMS of the mixture fractions from the experimental data provided at the TNF Workshop web site. Calculations of Favre averaged scalars are performed individually for each locations where measurements are available.

A comparison between mean and RMS values of temperatures and major species concentrations shows that the laminar flamelet concept is applicable for the operating conditions of Sandia flame D. The temperature and major species mole fractions predictions based on the state relationships involving an order of magnitude variation in stretch rates are in agreement with each other and with the data within the experimental uncertainty. For CO, H_2, and NO mole fractions, consideration of radiative heat loss improves the agreement between measurements and predictions significantly. However, for these species, the effects of higher stretch rates and those of radiative heat loss are qualitatively similar. Therefore, in spite of the encouraging agreement between measurements and predictions for major species concentrations, laminar flamelet state relationships with radiation heat loss and stretch-rate as parameters appear necessary, for minor species predictions.

Piloted Flame D: Axial Profiles of U, F, and T

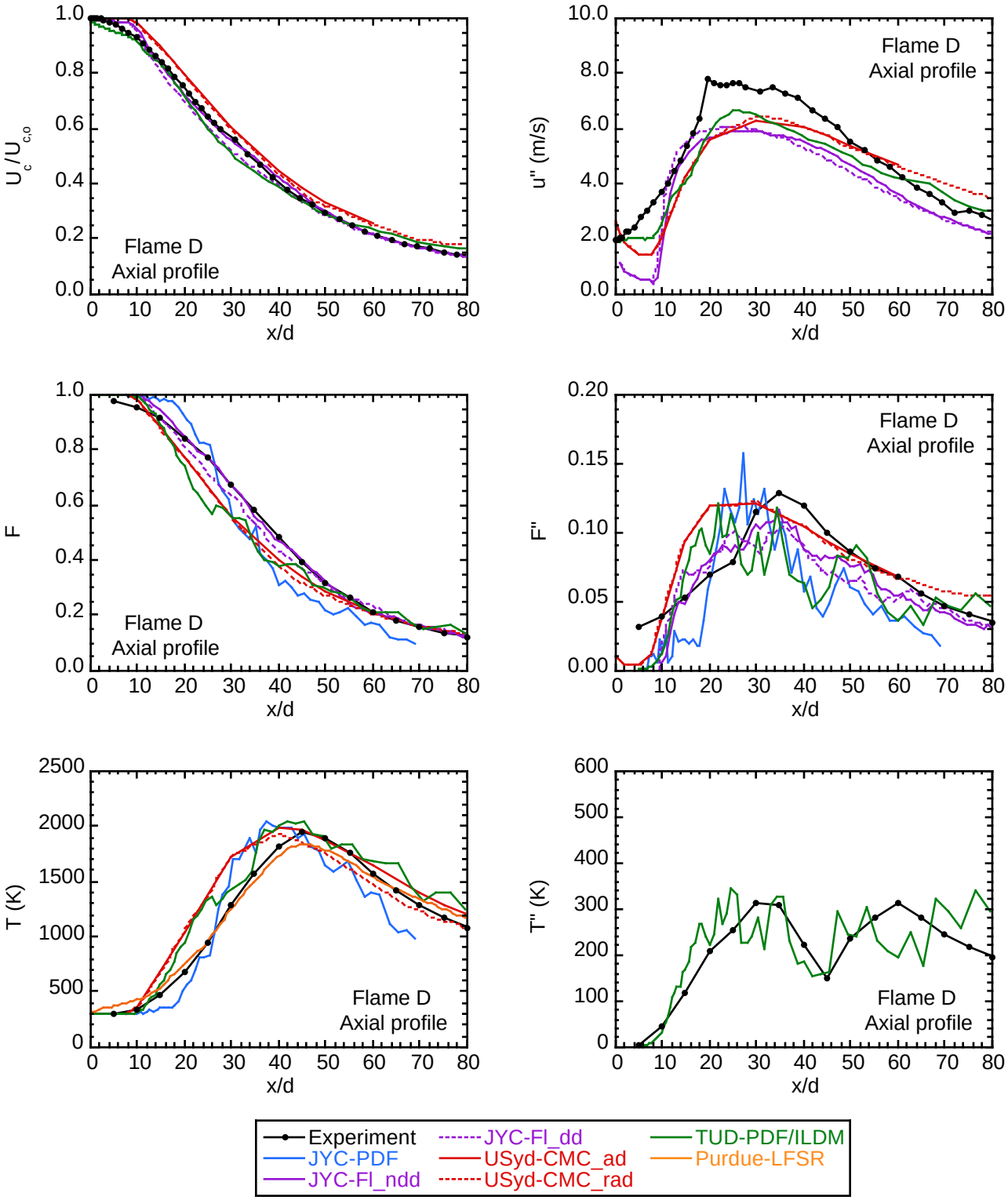

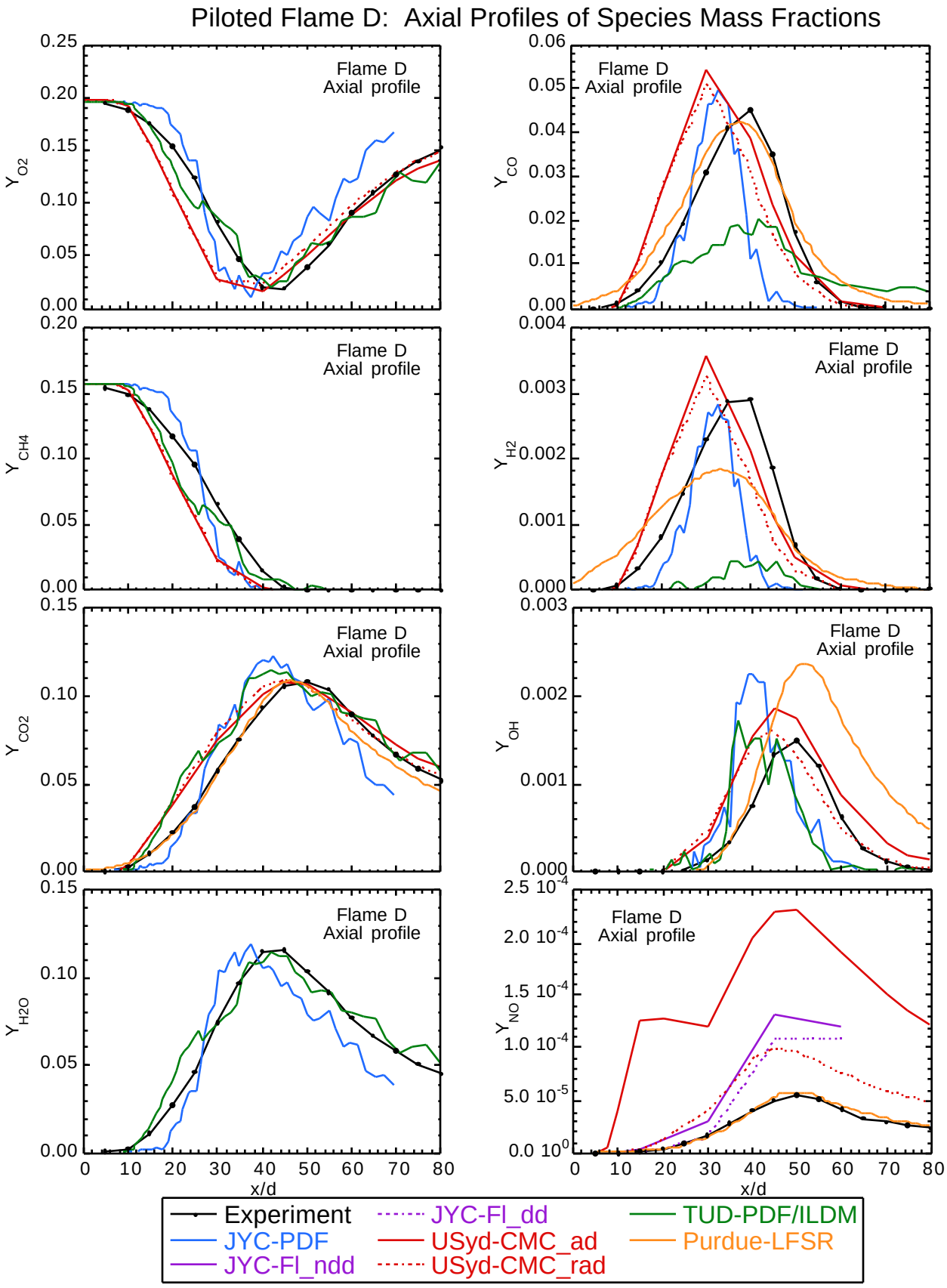
Piloted Flame D: Axial Profiles of Species Mass Fractions
Flame D
Axial profile
Y_{O2}
Y_{CO}
Y_{CH4}
Y_{H2}
Y_{CO2}
Y_{OH}
Y_{H2O}
Y_{NO}
x/d
Experiment
JYC-PDF
JYC-Fl_ndd
JYC-Fl_dd
USyd-CMC_ad
USyd-CMC_rad
TUD-PDF/ILDM
Purdue-LFSR

Piloted Flame D: Radial Profiles of U, u'', u''v'' at x/d=45

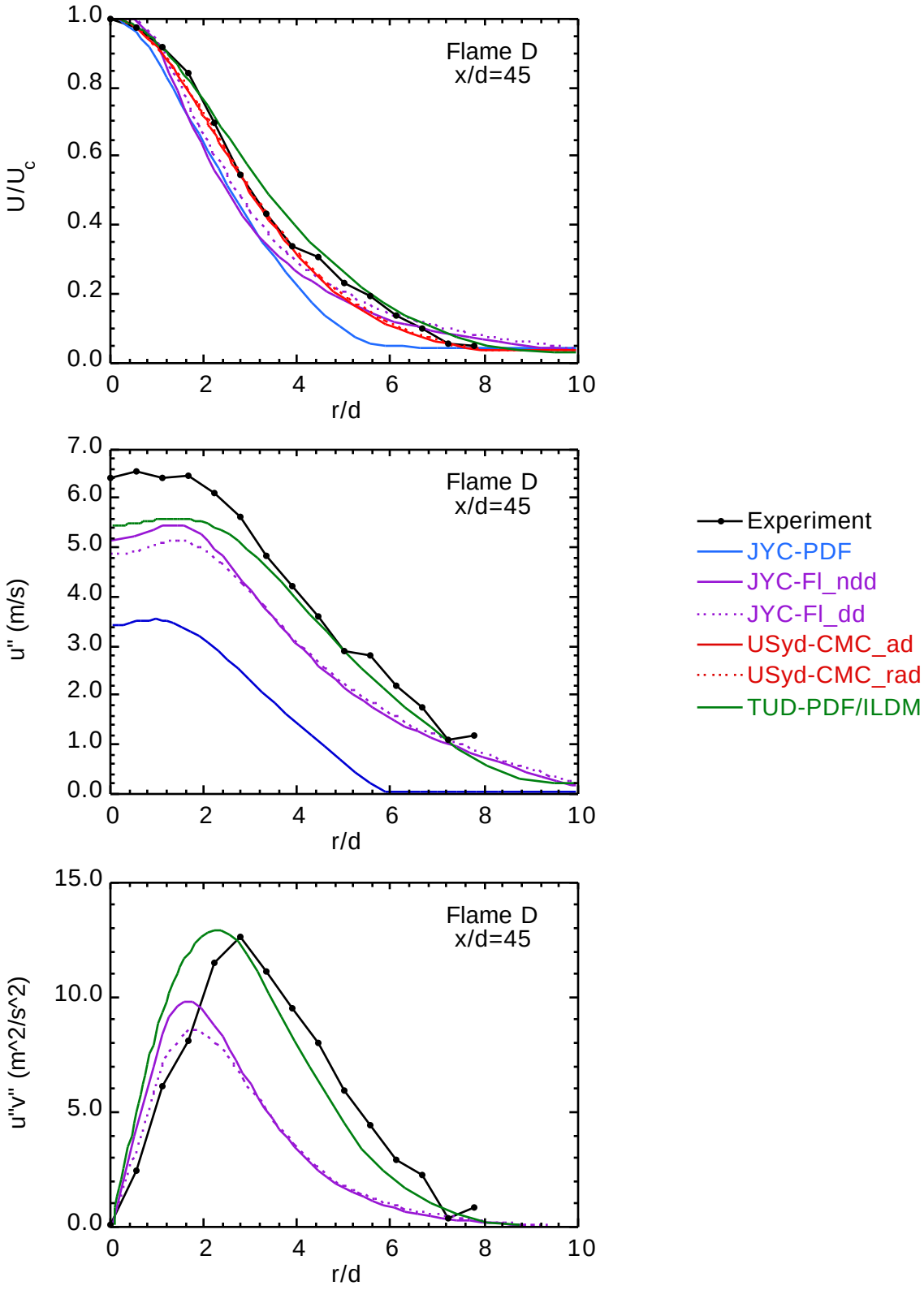

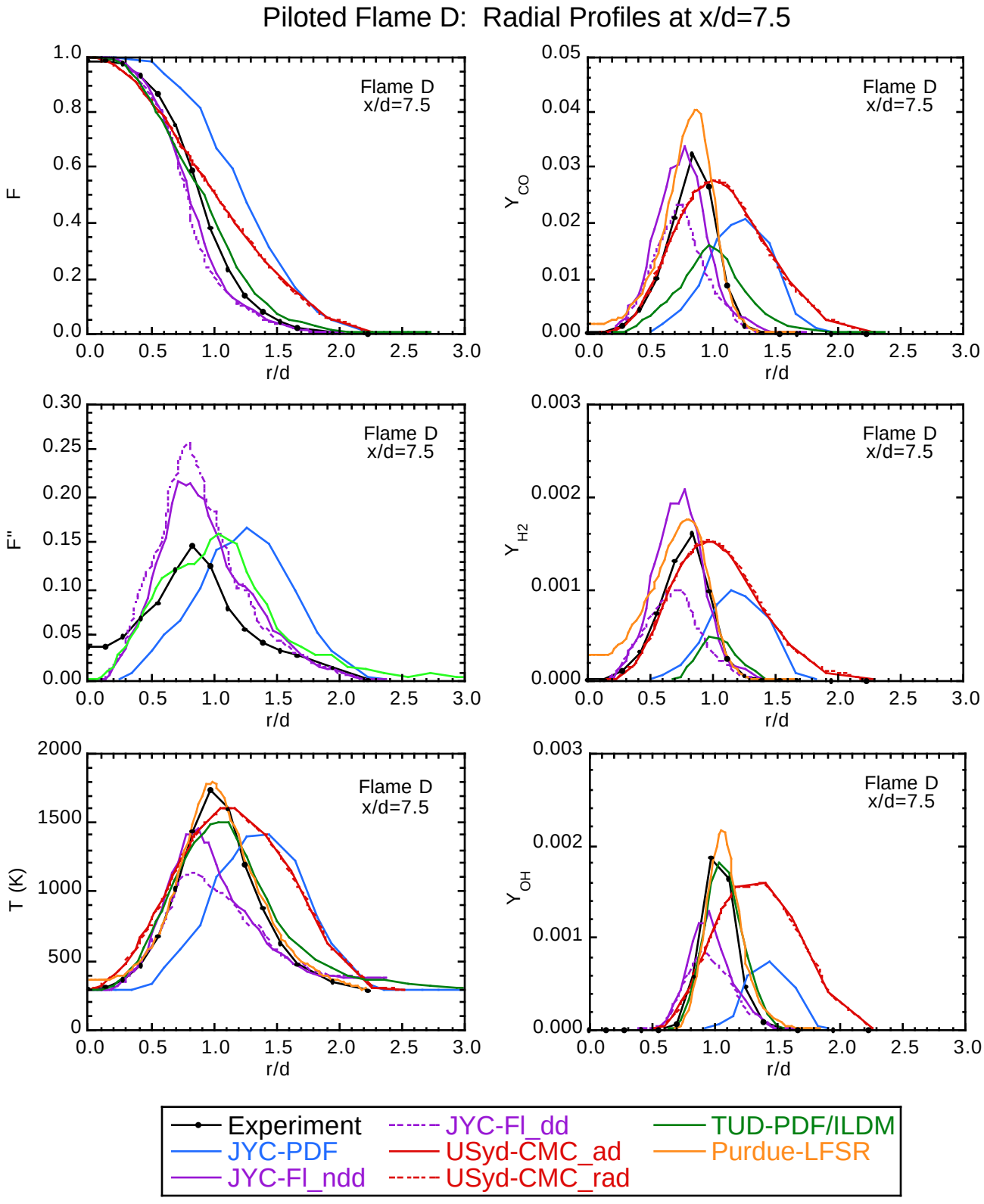
Piloted Flame D: Radial Profiles at x/d=7.5
Flame D
x/d=7.5
F
F''
T (K)
Y_{CO}
Y_{H2}
Y_{OH}
r/d
Experiment
JYC-PDF
JYC-Fl_ndd
JYC-Fl_dd
USyd-CMC_ad
USyd-CMC_rad
TUD-PDF/ILDM
Purdue-LFSR

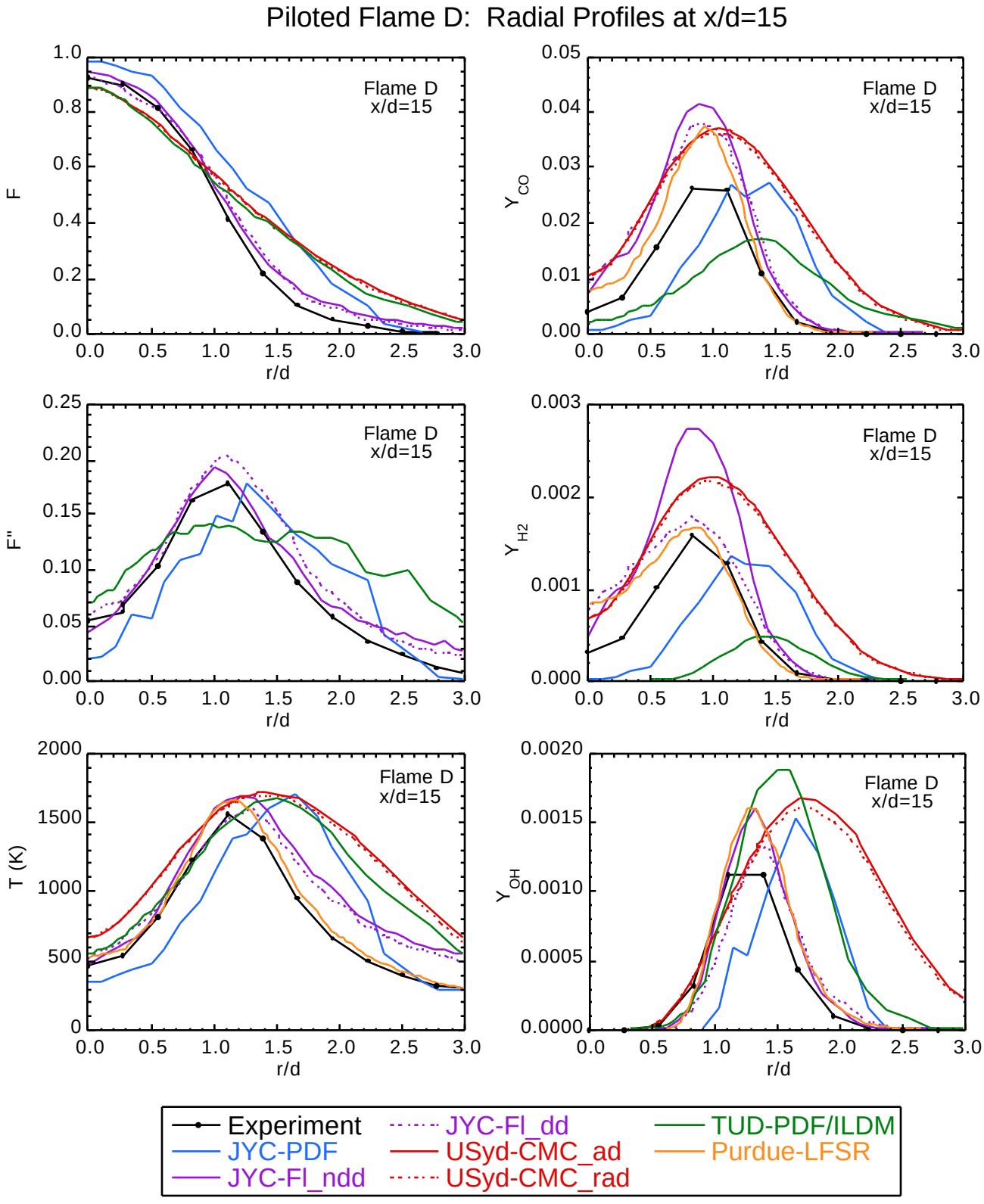
Piloted Flame D: Radial Profiles at x/d=15
Flame D
x/d=15
F
F"
T (K)
Y_{CO}
Y_{H2}
Y_{OH}
r/d
Experiment
JYC-PDF
JYC-Fl_ndd
JYC-Fl_dd
USyd-CMC_ad
USyd-CMC_rad
TUD-PDF/ILDM
Purdue-LFSR

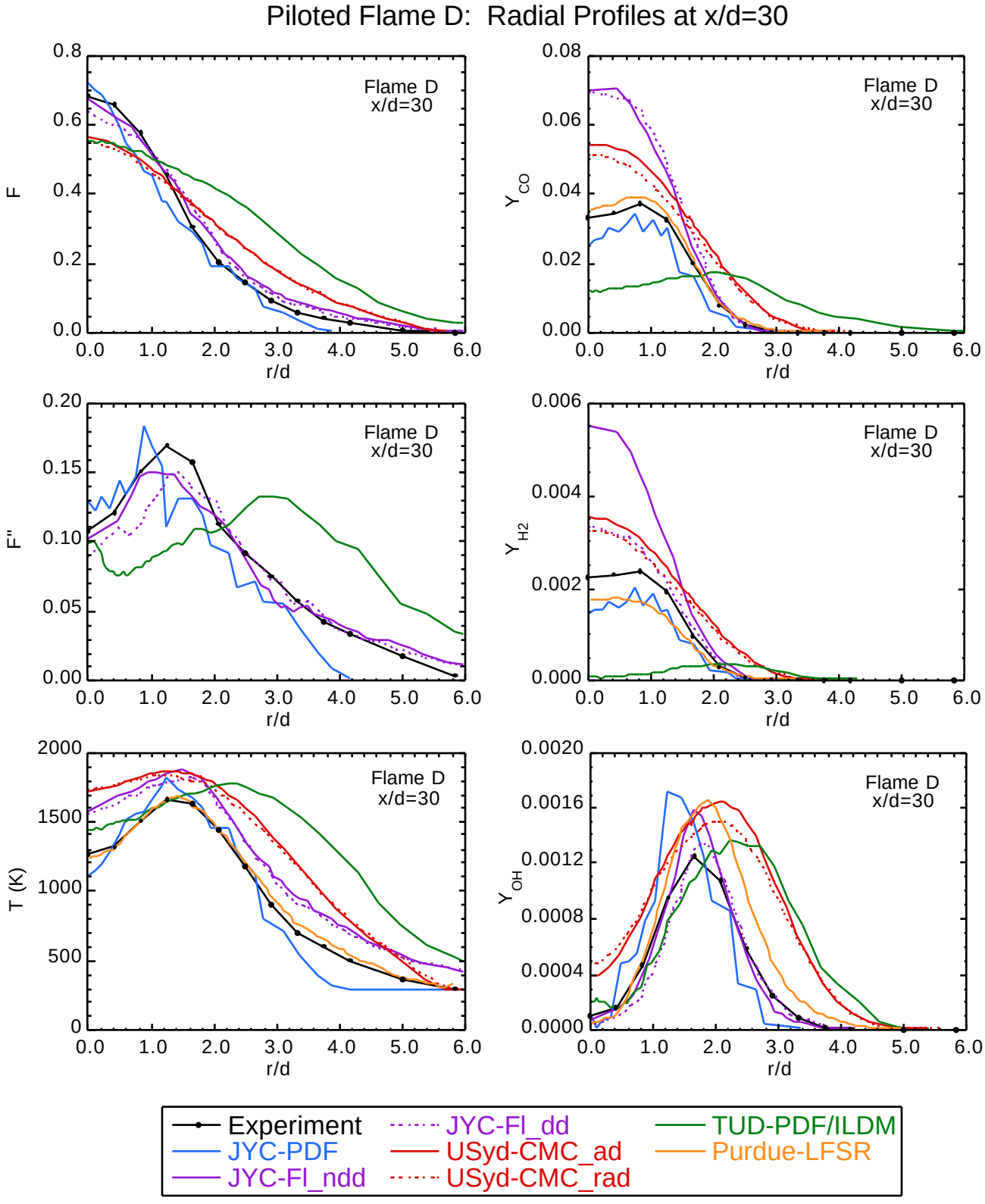
Piloted Flame D: Radial Profiles at x/d=30
Flame D
x/d=30
F
F''
T (K)
Y_{CO}
Y_{H2}
Y_{OH}
r/d
Experiment
JYC-PDF
JYC-Fl_ndd
JYC-Fl_dd
USyd-CMC_ad
USyd-CMC_rad
TUD-PDF/ILDM
Purdue-LFSR

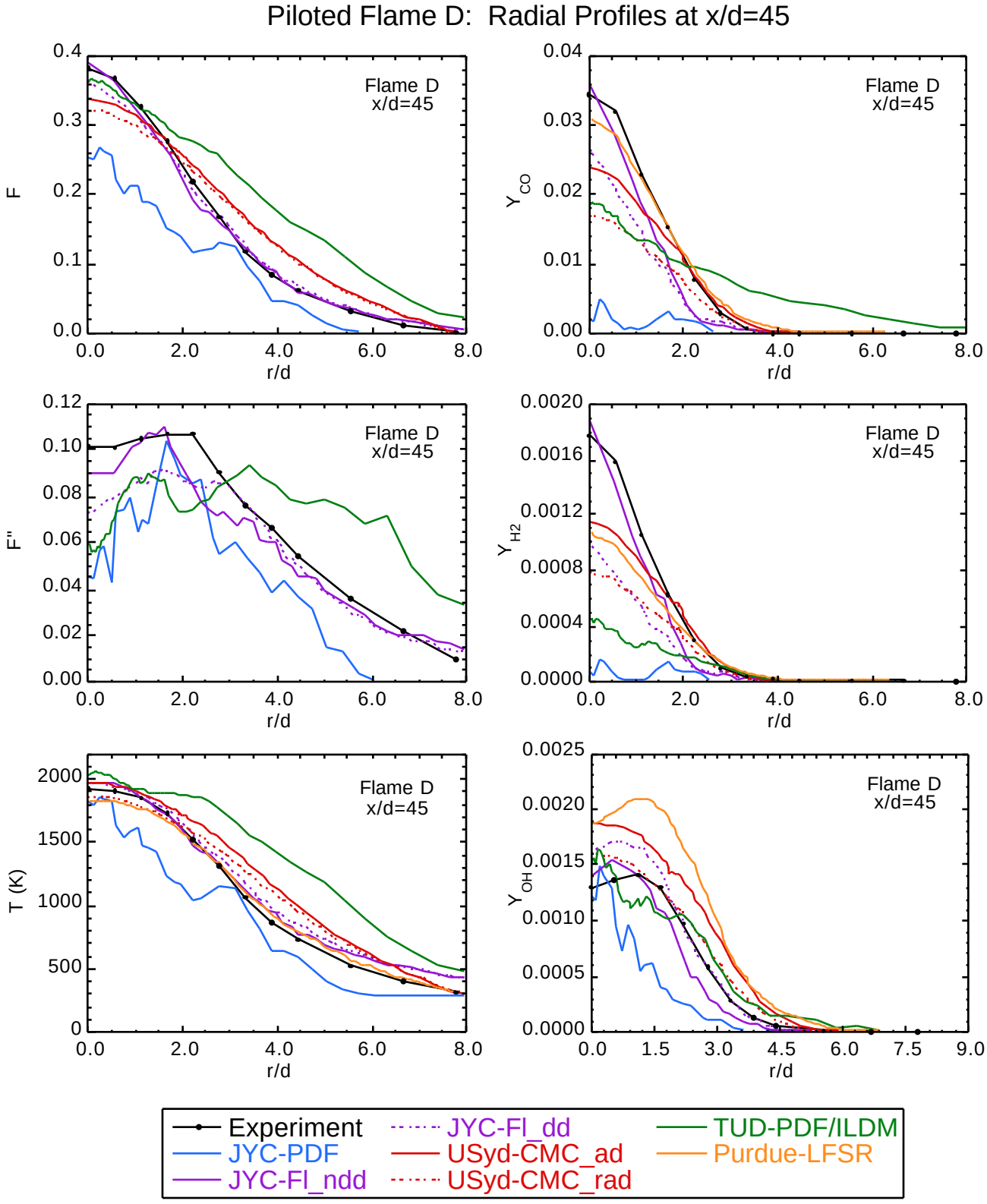
Piloted Flame D: Radial Profiles at x/d=45
Flame D
x/d=45
F
F''
T (K)
Y_{CO}
Y_{H2}
Y_{OH}
r/d
Experiment
JYC-PDF
JYC-Fl_ndd
JYC-Fl_dd
USyd-CMC_ad
USyd-CMC_rad
TUD-PDF/ILDM
Purdue-LFSR

Piloted Flame D: Radial Profiles at x/d=60

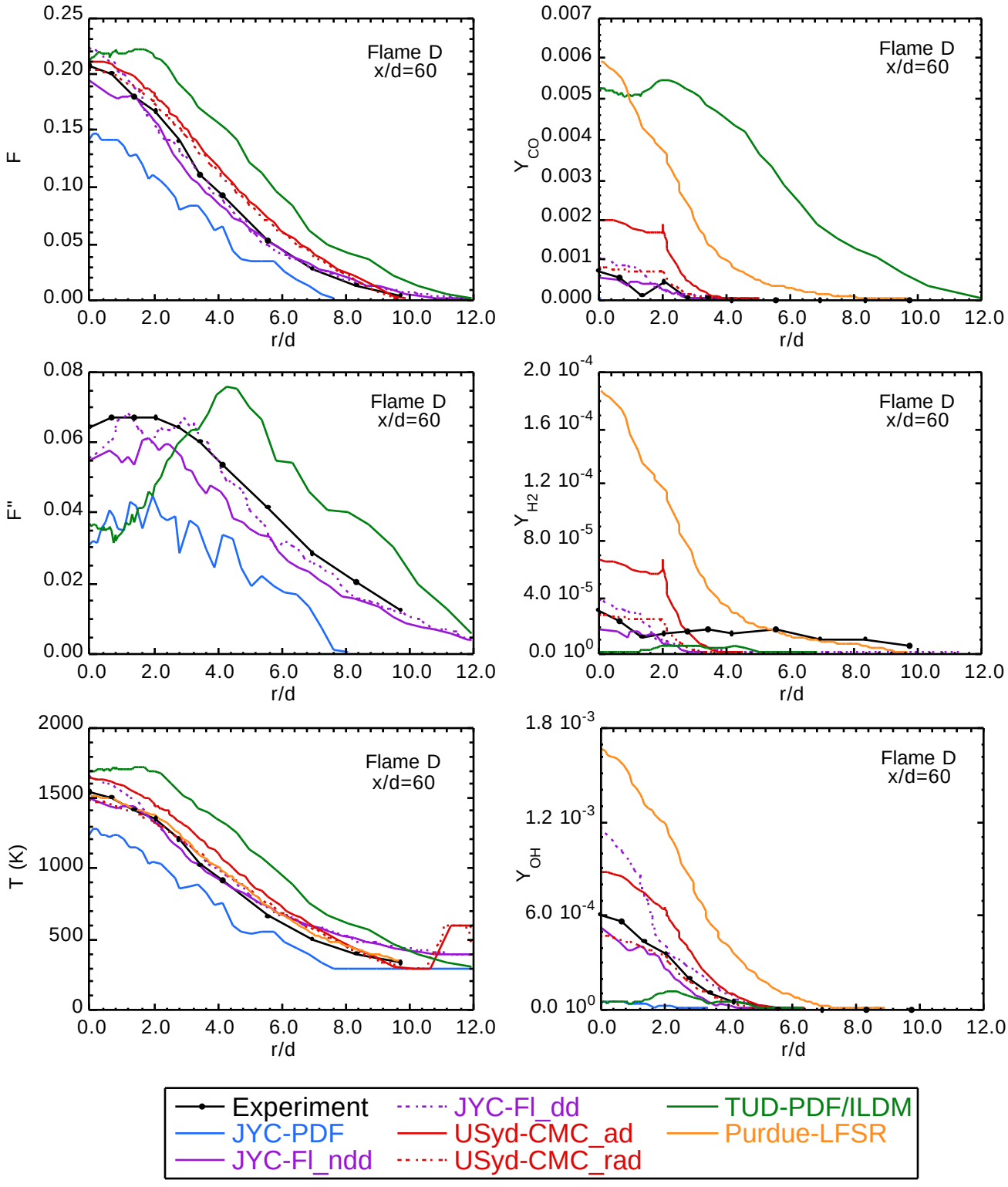

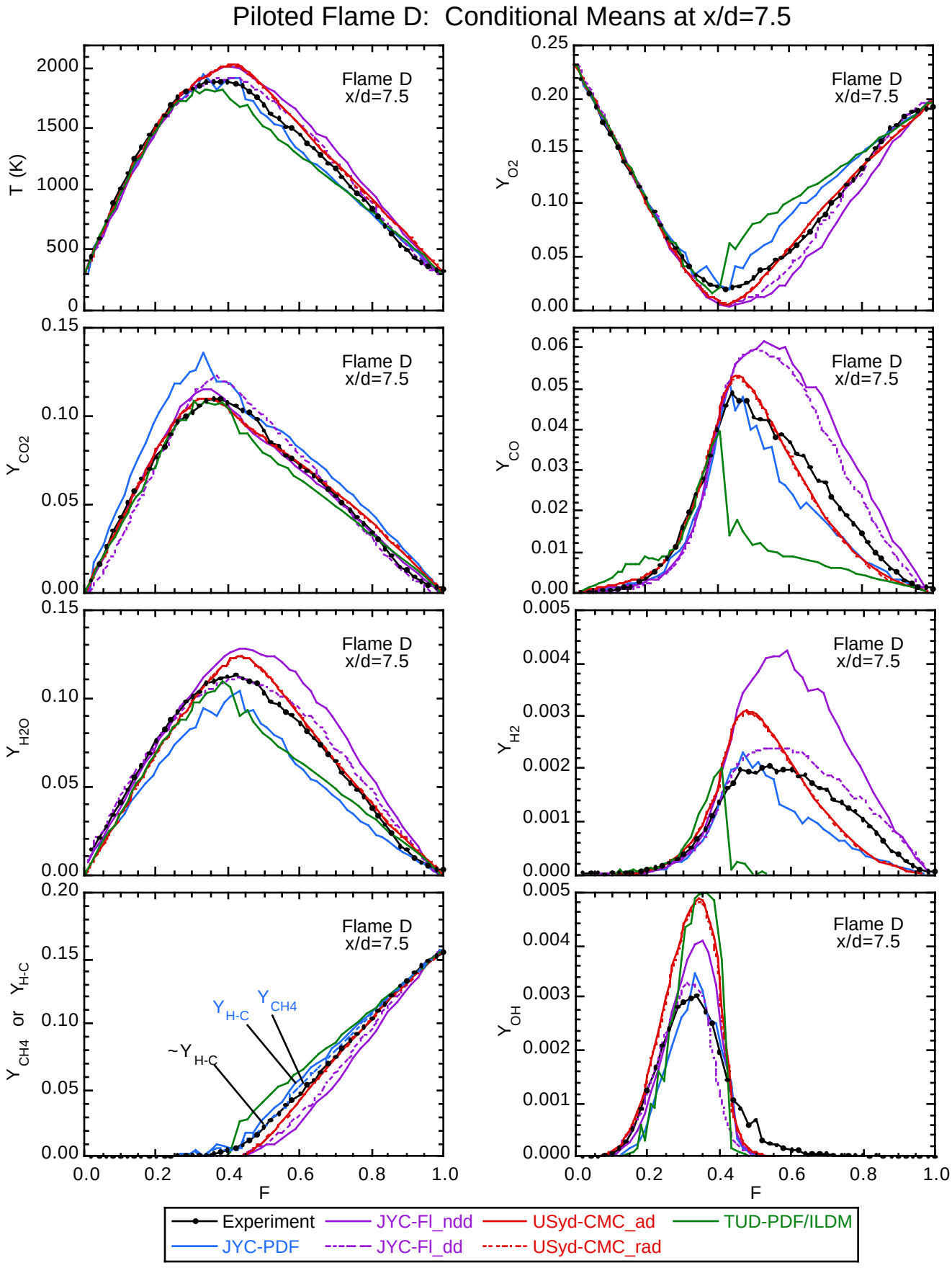
Piloted Flame D: Conditional Means at x/d=7.5
Flame D
x/d=7.5
T (K)
Y_{O2}
Y_{CO2}
Y_{CO}
Y_{H2O}
Y_{H2}
Y_{CH4} or Y_{H-C}
Y_{OH}
Y_{H-C}
Y_{CH4}
$\sim Y_{H-C}$
F
Experiment
JYC-PDF
JYC-Fl_ndd
JYC-Fl_dd
USyd-CMC_ad
USyd-CMC_rad
TUD-PDF/ILDM

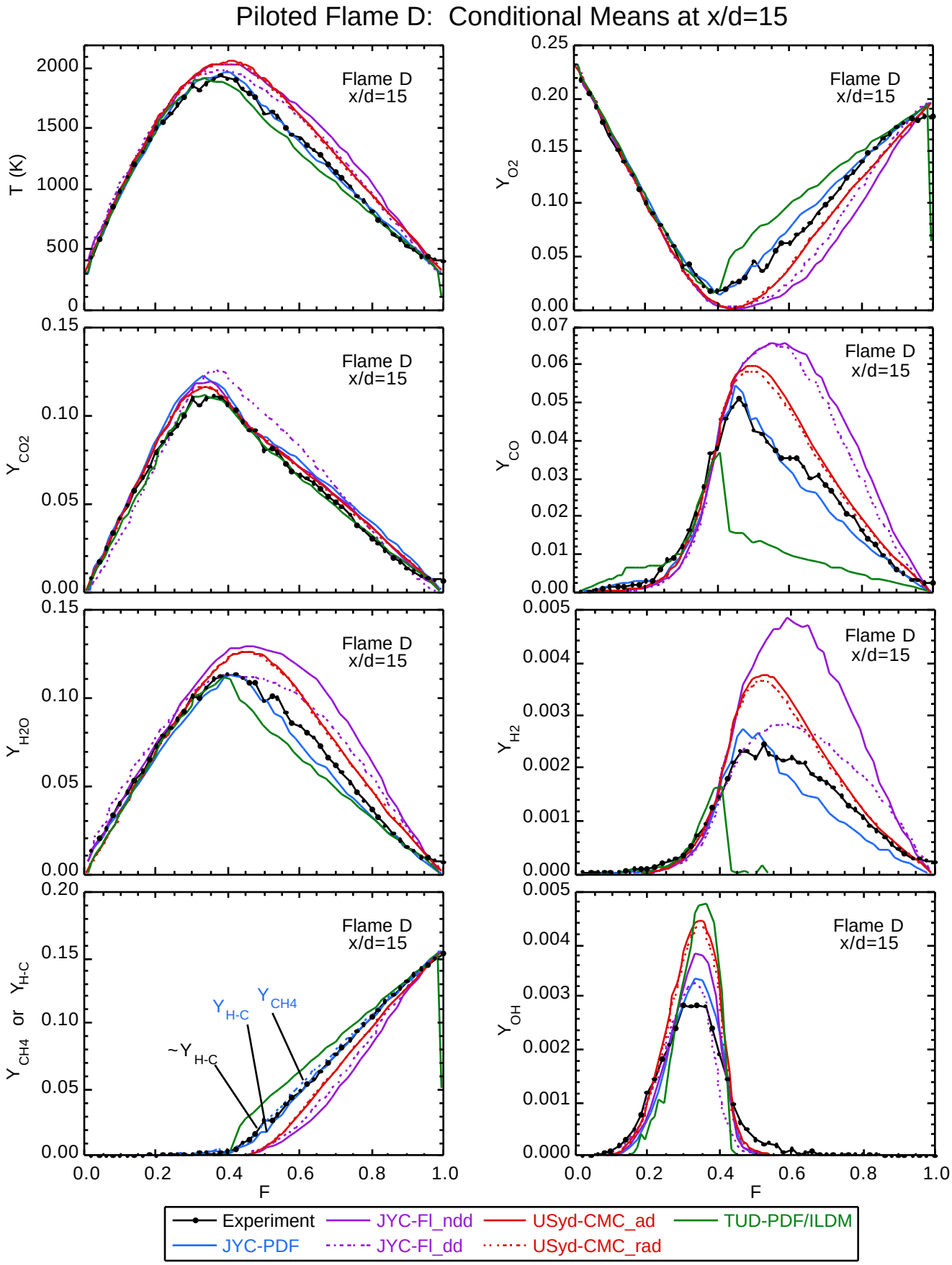
Piloted Flame D: Conditional Means at x/d=15
Flame D
x/d=15
T (K)
Y_{O2}
Y_{CO2}
Y_{CO}
Y_{H2O}
Y_{H2}
Y_{CH4} or Y_{H-C}
Y_{OH}
Y_{H-C}
Y_{CH4}
$\tilde{Y}_{H-C}$
F
Experiment
JYC-PDF
JYC-Fl_ndd
JYC-Fl_dd
USyd-CMC_ad
USyd-CMC_rad
TUD-PDF/ILDM

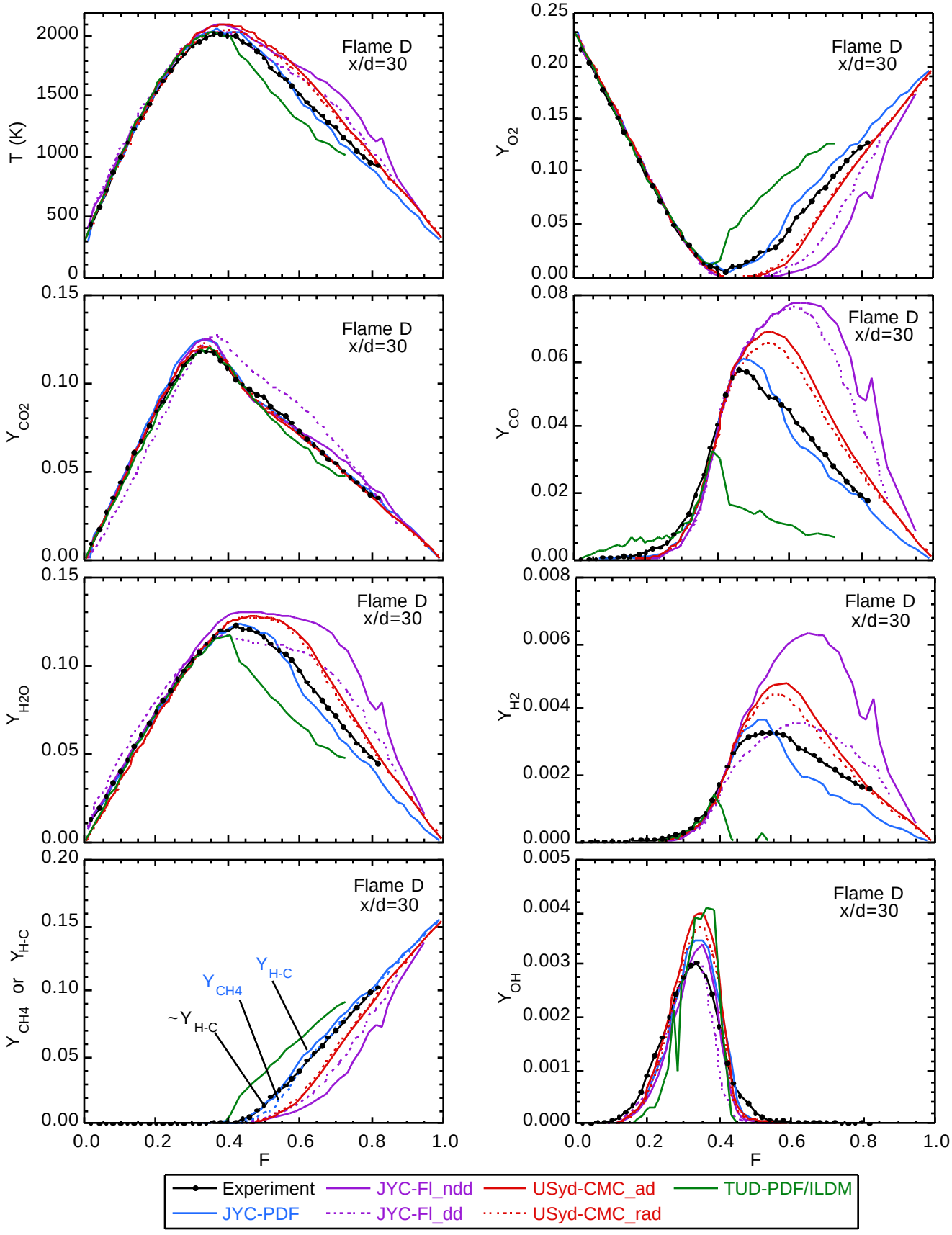
Piloted Flame D: Conditional Means at x/d=30
Flame D
x/d=30
T (K)
Y_{O2}
Y_{CO2}
Y_{CO}
Y_{H2O}
Y_{H2}
Y_{CH4} or Y_{H-C}
Y_{OH}
Y_{CH4}
Y_{H-C}
$\tilde{Y}_{H-C}$
F
Experiment
JYC-PDF
JYC-Fl_ndd
JYC-Fl_dd
USyd-CMC_ad
USyd-CMC_rad
TUD-PDF/ILDM

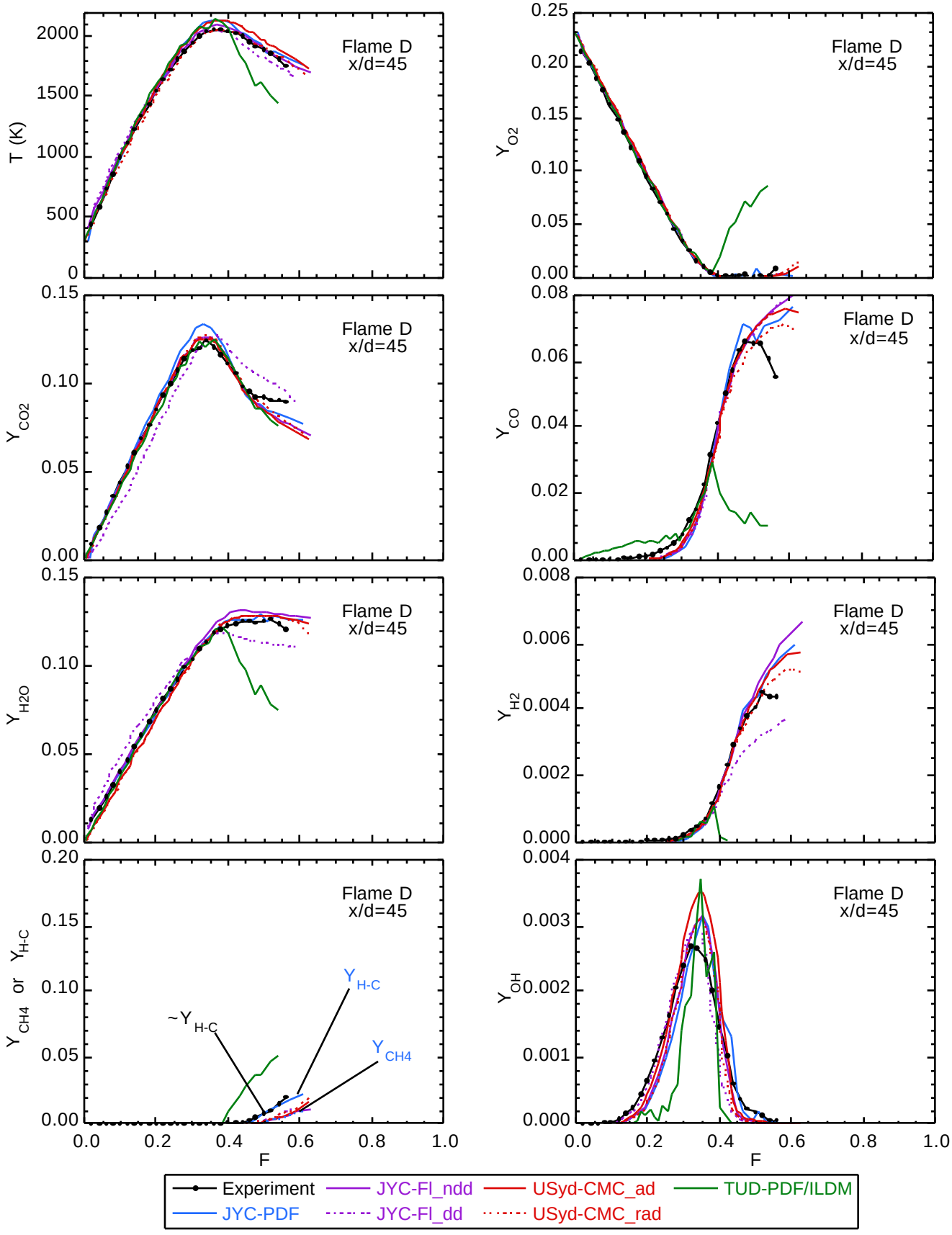
Piloted Flame D: Conditional Means at x/d=45
Flame D
x/d=45
T (K)
Y_{O2}
Y_{CO2}
Y_{CO}
Y_{H2O}
Y_{H2}
Y_{CH4} or Y_{H-C}
Y_{OH}
Y_{H-C}
$\sim Y_{H-C}$
Y_{CH4}
F
Experiment
JYC-PDF
JYC-Fl_ndd
JYC-Fl_dd
USyd-CMC_ad
USyd-CMC_rad
TUD-PDF/ILDM

Piloted Flame D: Conditional Means at x/d=60

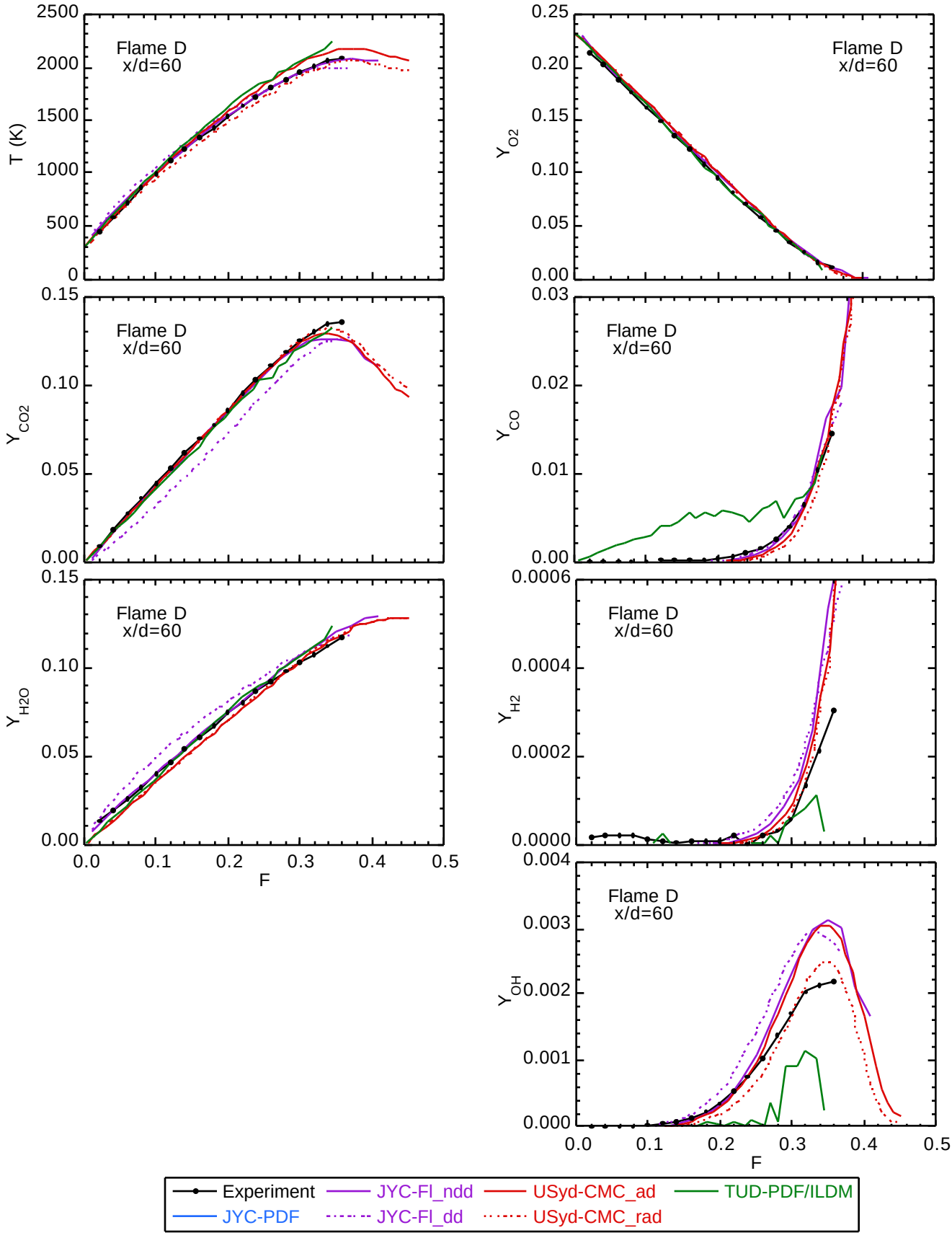

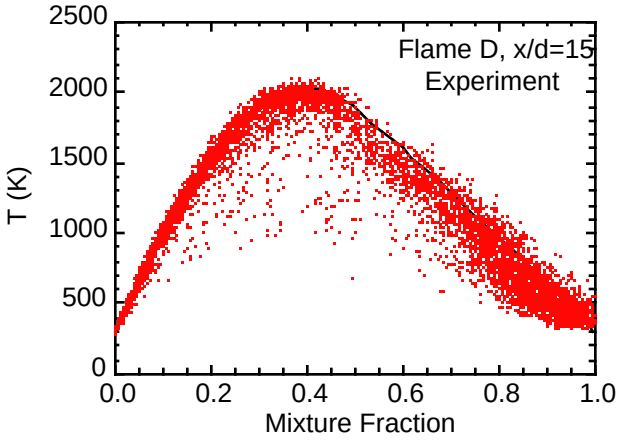
Flame D, x/d=15
Experiment
T (K)
Mixture Fraction
0
500
1000
1500
2000
2500
0.0
0.2
0.4
0.6
0.8
1.0

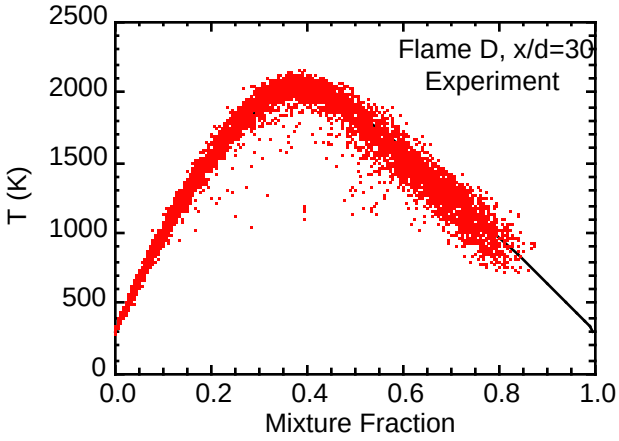
Flame D, x/d=30
Experiment
T (K)
Mixture Fraction
0
500
1000
1500
2000
2500
0.0
0.2
0.4
0.6
0.8
1.0

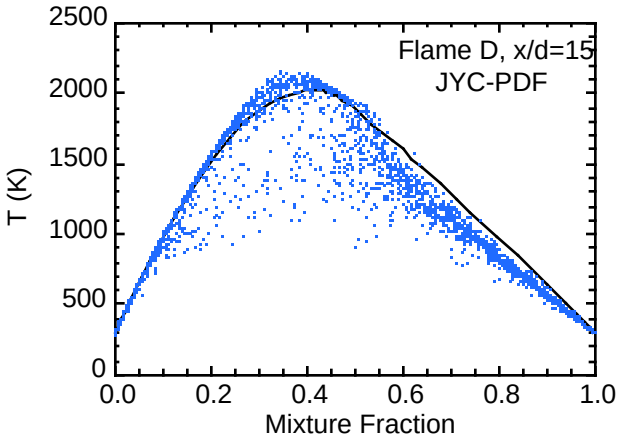
Flame D, x/d=15
JYC-PDF
T (K)
Mixture Fraction
0
500
1000
1500
2000
2500
0.0
0.2
0.4
0.6
0.8
1.0

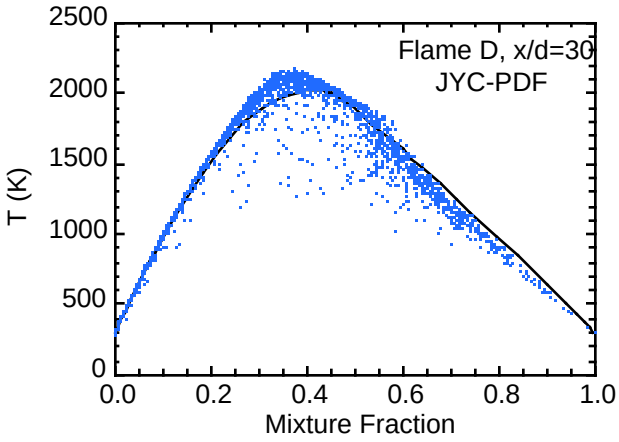
Flame D, x/d=30
JYC-PDF
T (K)
Mixture Fraction
0
500
1000
1500
2000
2500
0.0
0.2
0.4
0.6
0.8
1.0

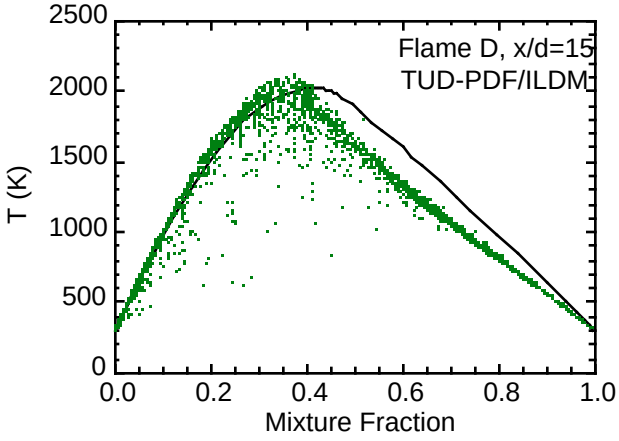
Flame D, x/d=15
TUD-PDF/ILDM
T (K)
Mixture Fraction
0
500
1000
1500
2000
2500
0.0
0.2
0.4
0.6
0.8
1.0

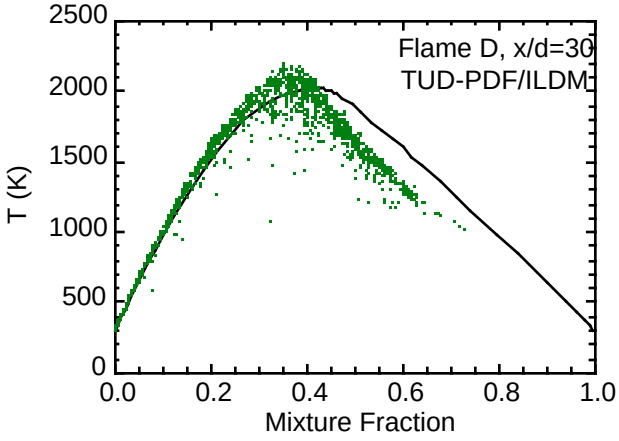
Flame D, x/d=30
TUD-PDF/ILDM
T (K)
Mixture Fraction
0
500
1000
1500
2000
2500
0.0
0.2
0.4
0.6
0.8
1.0

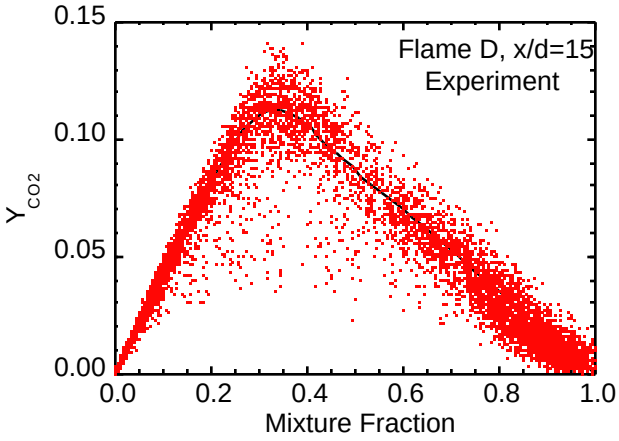
Flame D, x/d=15
Experiment
Y_{CO2}
Mixture Fraction
0.00
0.05
0.10
0.15
0.0
0.2
0.4
0.6
0.8
1.0

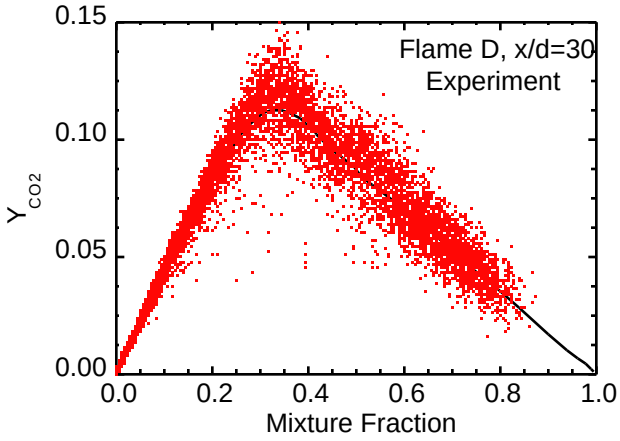
Flame D, x/d=30
Experiment
Y_{CO2}
Mixture Fraction
0.00
0.05
0.10
0.15
0.0
0.2
0.4
0.6
0.8
1.0

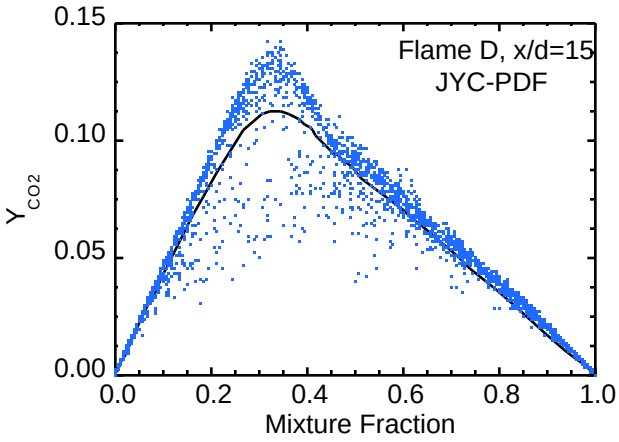
Flame D, x/d=15
JYC-PDF
Y_{CO2}
Mixture Fraction
0.00
0.05
0.10
0.15
0.0
0.2
0.4
0.6
0.8
1.0

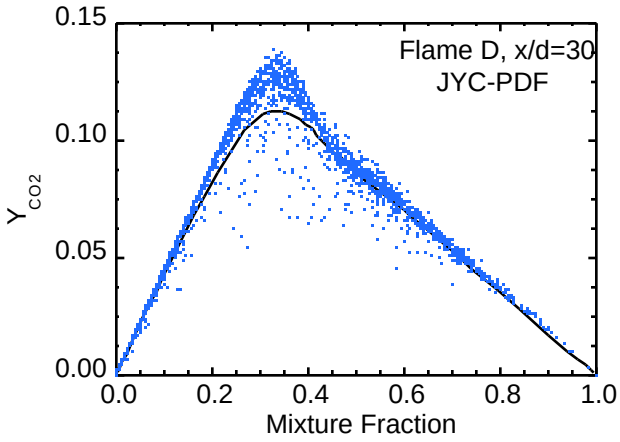
Flame D, x/d=30
JYC-PDF
Y_{CO2}
Mixture Fraction
0.00
0.05
0.10
0.15
0.0
0.2
0.4
0.6
0.8
1.0

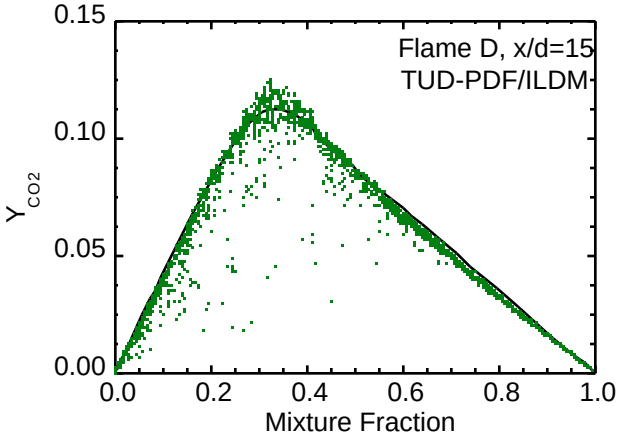
Flame D, x/d=15
TUD-PDF/ILDM
Y_{CO2}
Mixture Fraction
0.00
0.05
0.10
0.15
0.0
0.2
0.4
0.6
0.8
1.0

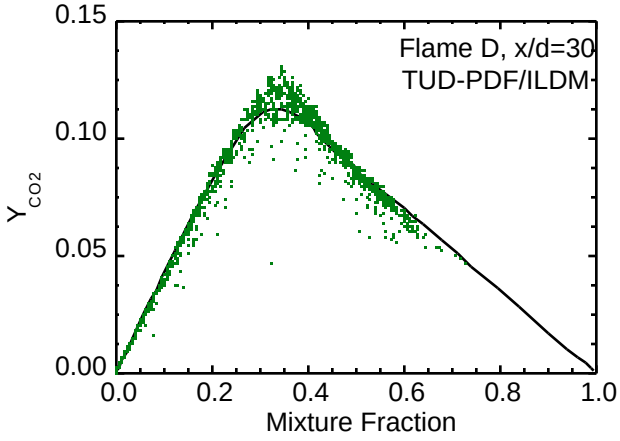
Flame D, x/d=30
TUD-PDF/ILDM
Y_{CO2}
Mixture Fraction
0.00
0.05
0.10
0.15
0.0
0.2
0.4
0.6
0.8
1.0

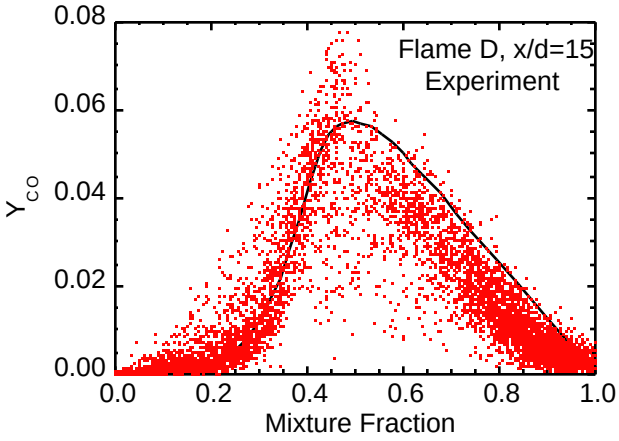
Flame D, x/d=15
Experiment
Y_{CO}
Mixture Fraction
0.00
0.02
0.04
0.06
0.08
0.0
0.2
0.4
0.6
0.8
1.0

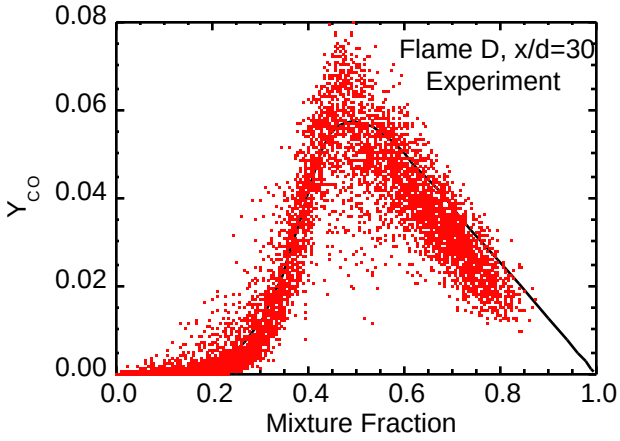
Flame D, x/d=30
Experiment
Y_{CO}
Mixture Fraction
0.00
0.02
0.04
0.06
0.08
0.0
0.2
0.4
0.6
0.8
1.0

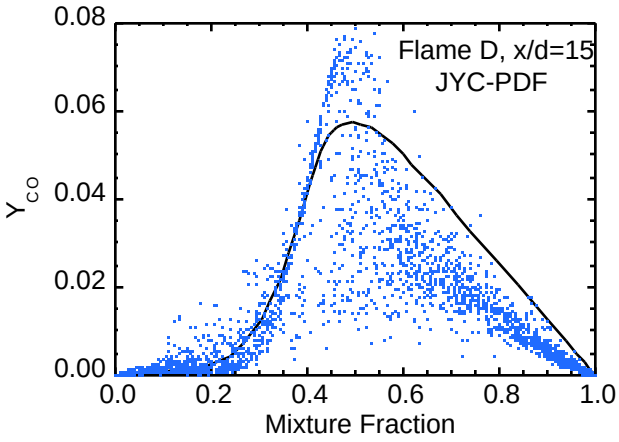
Flame D, x/d=15
JYC-PDF
Y_{CO}
Mixture Fraction
0.00
0.02
0.04
0.06
0.08
0.0
0.2
0.4
0.6
0.8
1.0

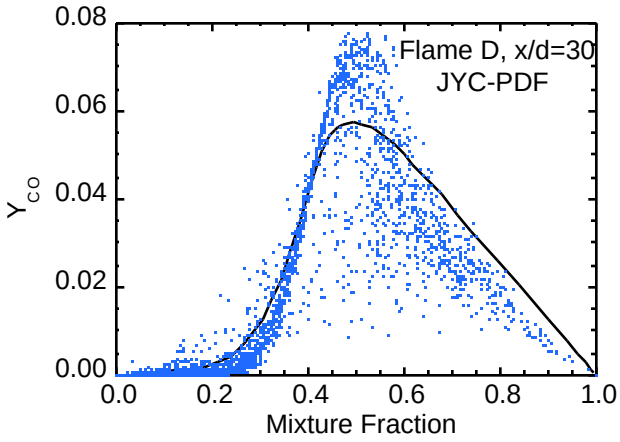
Flame D, x/d=30
JYC-PDF
Y_{CO}
Mixture Fraction
0.00
0.02
0.04
0.06
0.08
0.0
0.2
0.4
0.6
0.8
1.0

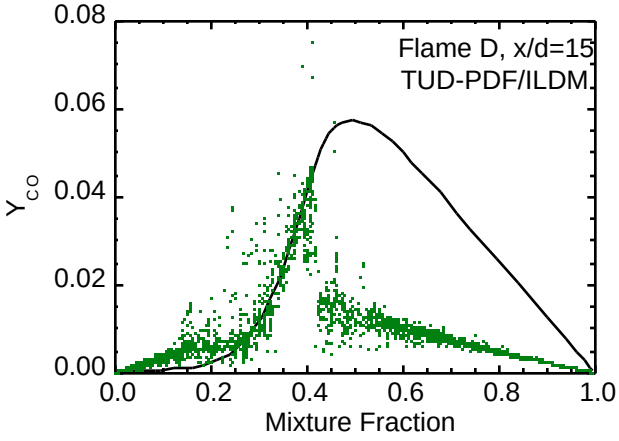
Flame D, x/d=15
TUD-PDF/ILDM
Y_{CO}
Mixture Fraction
0.00
0.02
0.04
0.06
0.08
0.0
0.2
0.4
0.6
0.8
1.0

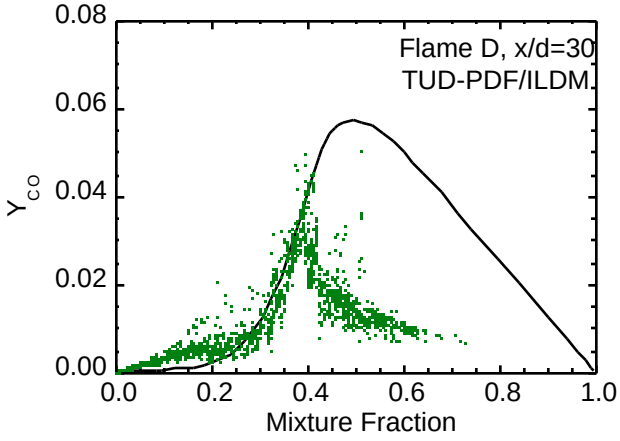
Flame D, x/d=30
TUD-PDF/ILDM
Y_{CO}
Mixture Fraction
0.00
0.02
0.04
0.06
0.08
0.0
0.2
0.4
0.6
0.8
1.0

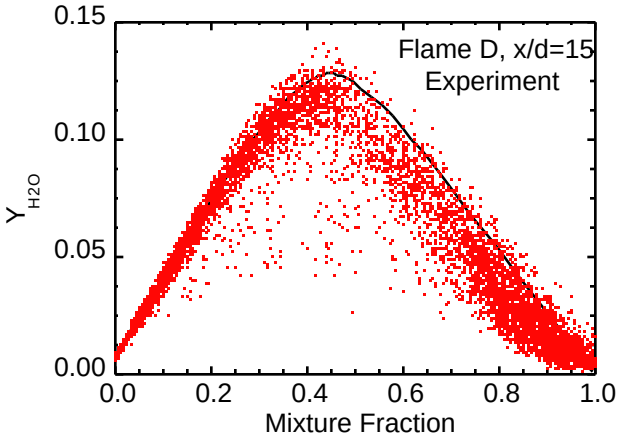
Flame D, x/d=15
Experiment
Y_{H2O}
Mixture Fraction
0.00
0.05
0.10
0.15
0.0
0.2
0.4
0.6
0.8
1.0

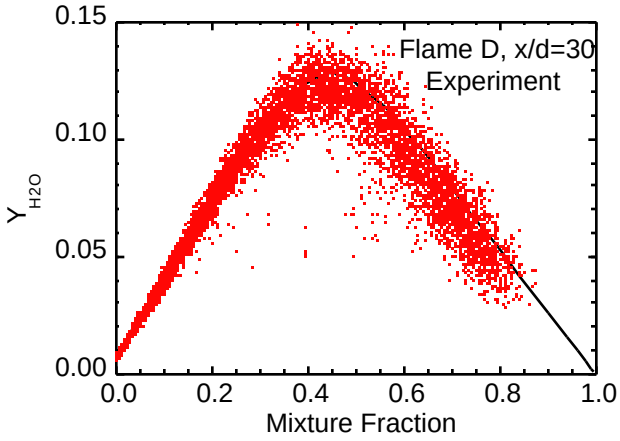
Flame D, x/d=30
Experiment
Y_{H2O}
Mixture Fraction
0.00
0.05
0.10
0.15
0.0
0.2
0.4
0.6
0.8
1.0

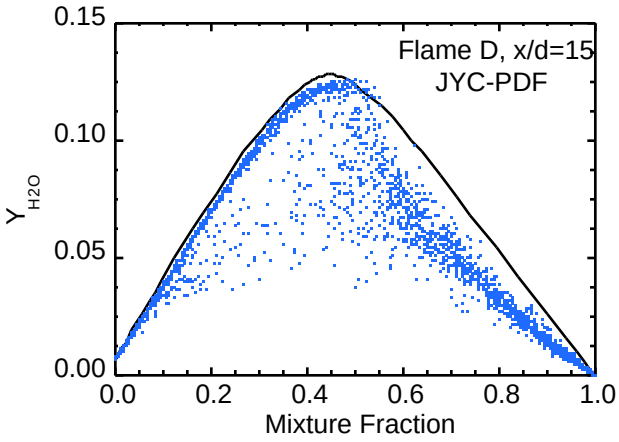
Flame D, x/d=15
JYC-PDF
Y_{H2O}
Mixture Fraction
0.00
0.05
0.10
0.15
0.0
0.2
0.4
0.6
0.8
1.0

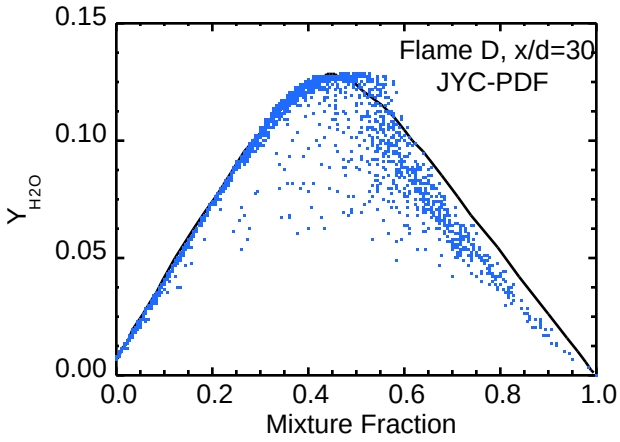
Flame D, x/d=30
JYC-PDF
Y_{H2O}
Mixture Fraction
0.00
0.05
0.10
0.15
0.0
0.2
0.4
0.6
0.8
1.0

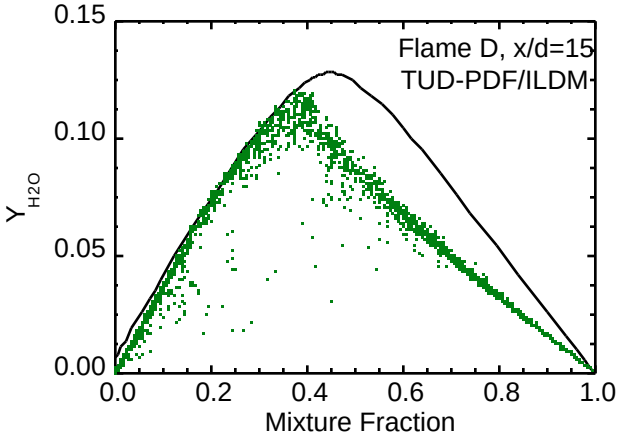
Flame D, x/d=15
TUD-PDF/ILDM
Y_{H2O}
Mixture Fraction
0.00
0.05
0.10
0.15
0.0
0.2
0.4
0.6
0.8
1.0

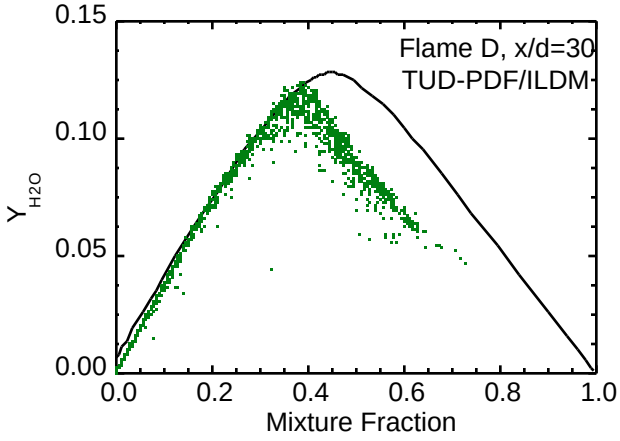
Flame D, x/d=30
TUD-PDF/ILDM
Y_{H2O}
Mixture Fraction
0.00
0.05
0.10
0.15
0.0
0.2
0.4
0.6
0.8
1.0

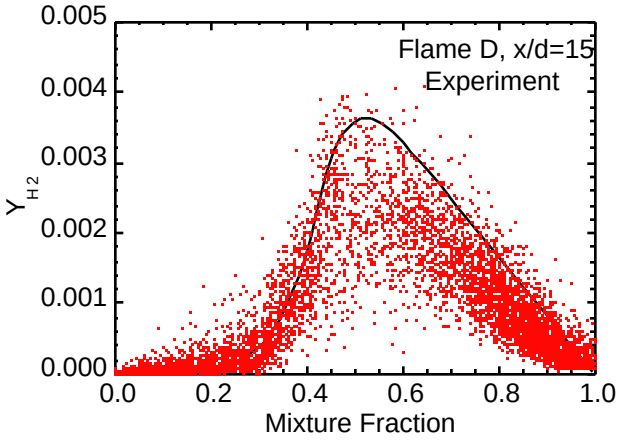
Flame D, x/d=15
Experiment
Y_{H2}
Mixture Fraction
0.000
0.001
0.002
0.003
0.004
0.005
0.0
0.2
0.4
0.6
0.8
1.0

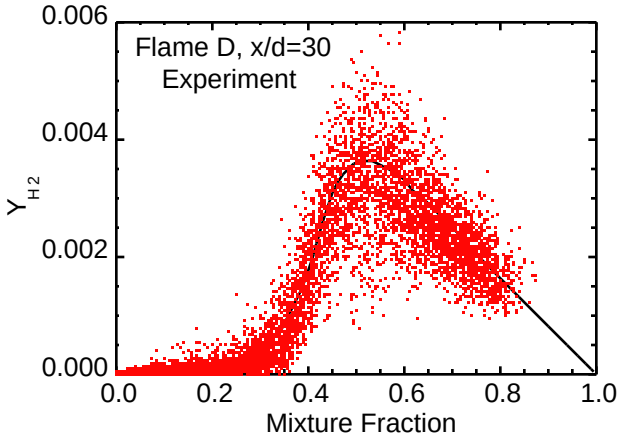
Flame D, x/d=30
Experiment
Y_{H2}
Mixture Fraction
0.000
0.002
0.004
0.006
0.0
0.2
0.4
0.6
0.8
1.0

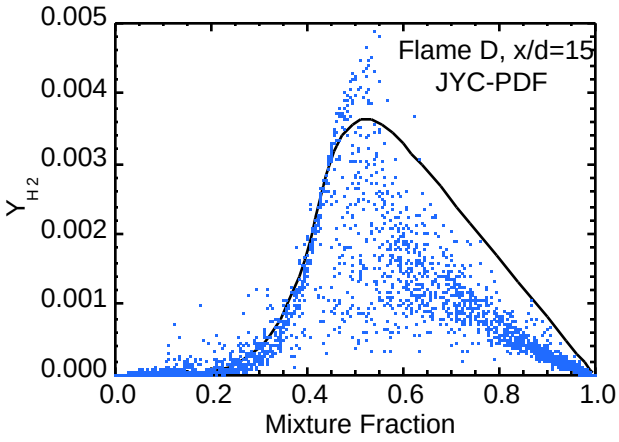
Flame D, x/d=15
JYC-PDF
Y_{H2}
Mixture Fraction
0.000
0.001
0.002
0.003
0.004
0.005
0.0
0.2
0.4
0.6
0.8
1.0

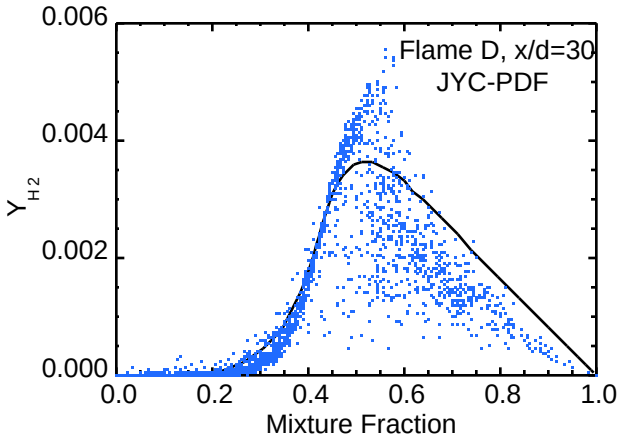
Flame D, x/d=30
JYC-PDF
Y_{H2}
Mixture Fraction
0.000
0.002
0.004
0.006
0.0
0.2
0.4
0.6
0.8
1.0

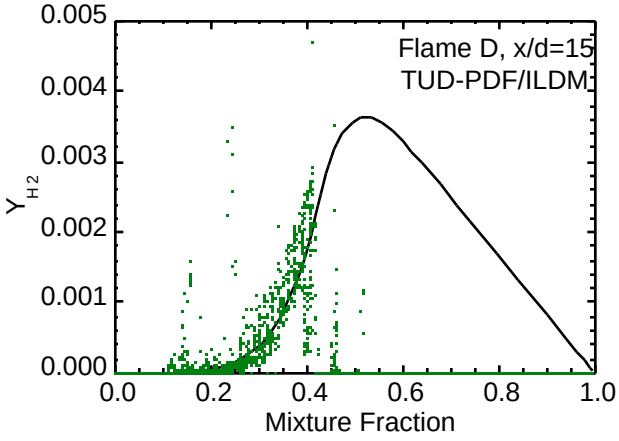
Flame D, x/d=15
TUD-PDF/ILDM
Y_{H2}
Mixture Fraction
0.000
0.001
0.002
0.003
0.004
0.005
0.0
0.2
0.4
0.6
0.8
1.0

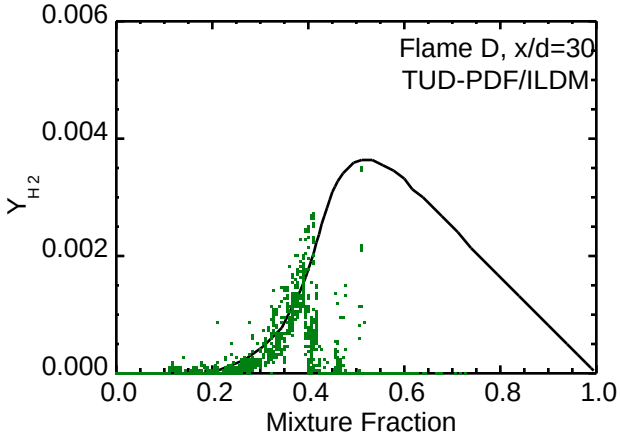
Flame D, x/d=30
TUD-PDF/ILDM
Y_{H2}
Mixture Fraction
0.000
0.002
0.004
0.006
0.0
0.2
0.4
0.6
0.8
1.0

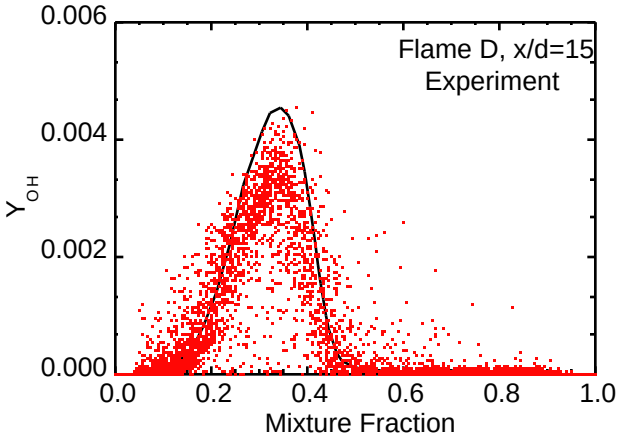
Flame D, x/d=15
Experiment
Y_{OH}
0.006
0.004
0.002
0.000
0.0
0.2
0.4
0.6
0.8
1.0
Mixture Fraction

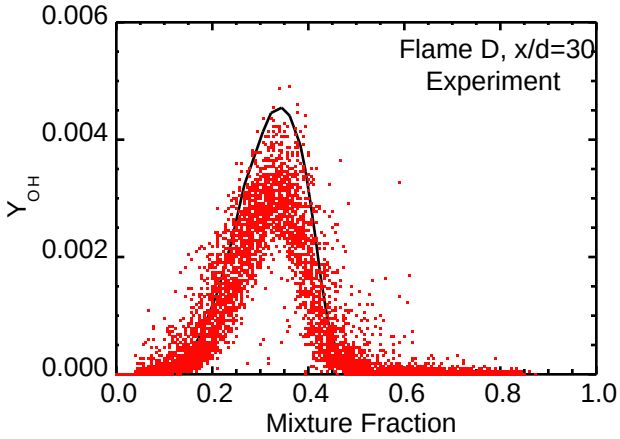
Flame D, x/d=30
Experiment
Y_{OH}
0.006
0.004
0.002
0.000
0.0
0.2
0.4
0.6
0.8
1.0
Mixture Fraction

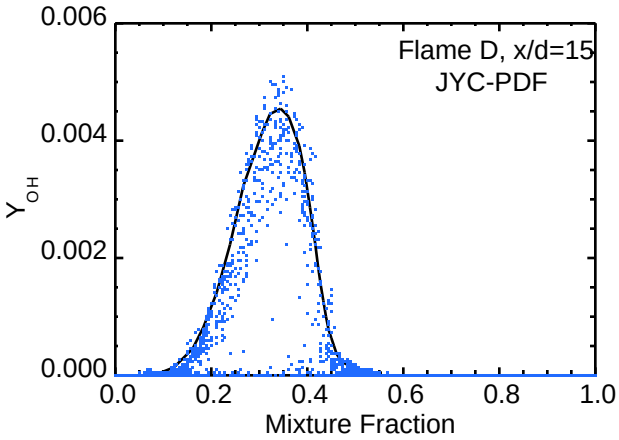
Flame D, x/d=15
JYC-PDF
Y_{OH}
0.006
0.004
0.002
0.000
0.0
0.2
0.4
0.6
0.8
1.0
Mixture Fraction

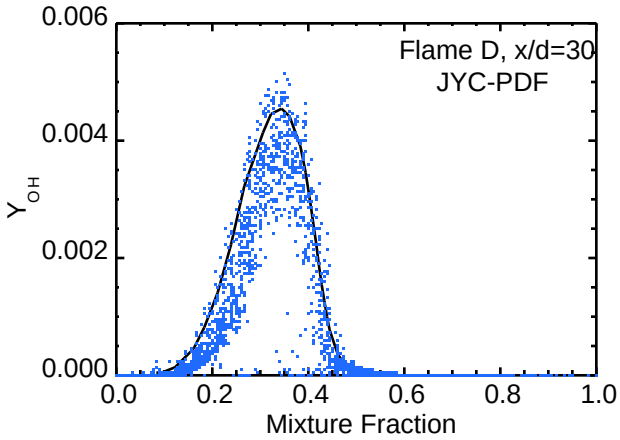
Flame D, x/d=30
JYC-PDF
Y_{OH}
0.006
0.004
0.002
0.000
0.0
0.2
0.4
0.6
0.8
1.0
Mixture Fraction

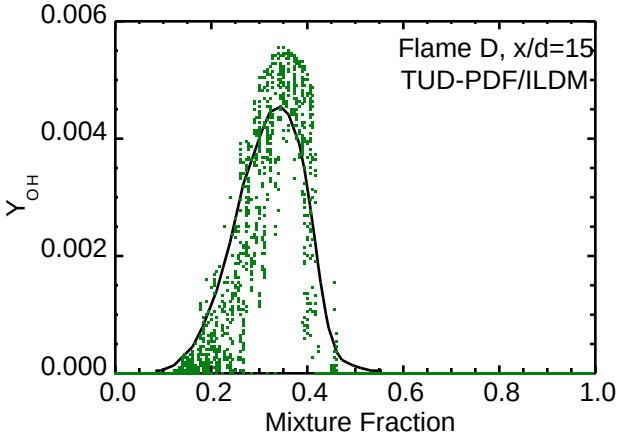
Flame D, x/d=15
TUD-PDF/ILDM
Y_{OH}
0.006
0.004
0.002
0.000
0.0
0.2
0.4
0.6
0.8
1.0
Mixture Fraction

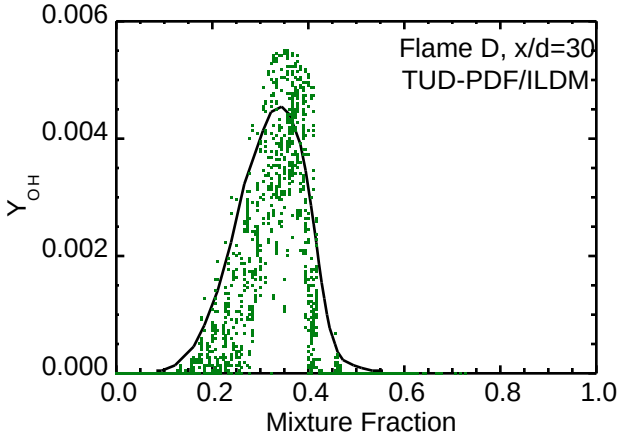
Flame D, x/d=30
TUD-PDF/ILDM
Y_{OH}
0.006
0.004
0.002
0.000
0.0
0.2
0.4
0.6
0.8
1.0
Mixture Fraction

Piloted Methane/Air Flame D - Preliminary Release

Updated 9-JAN-98

This information is under review by several participants in the TNF Workshop. There are likely to be some changes and additions to the velocity boundary conditions and the guidelines for model calculations. Check for updates. Comments are welcome.

UPDATE 4-NOV-97: Yno added to pilot flame boundary condition.
UPDATE 8-DEC-97: Typo in f-definition corrected, list of profiles expanded.
UPDATE 9-JAN-98: Addition of jet exit velocity profile and axial velocity profile from LDV measurements by the group at TU Darmstadt.

Robert Barlow and Jonathan Frank*
Mail Stop 9051
Sandia National Laboratories
Livermore, CA 94551-0969
barlow@ca.sandia.gov
http://www.ca.sandia.gov/tdf/Lab.html
http://www.ca.sandia.gov/tdf/Workshop.html

*(now at PSI in Andover, Massachusetts)

ABSTRACT

This file provides preliminary documentation for the 1997 Sandia data set of multiscalar measurements in piloted methane jet flames. Measured scalars include temperature, mixture fraction, N_2, O_2, H_2O, H_2, CH_4, CO, CO_2, OH, and NO. CO is measured by Raman scattering and by LIF. The complete data set includes results for several flames over a range of Reynolds number and includes axial and radial profiles of Reynolds- and Favre-average mass fractions, conditional statistics, pdfs, and complete scatter data for all measured scalars.

This preliminary information is being made available as part of the International Workshop on Measurement and Computation of Turbulent Nonpremixed Flames to allow modellers to set up calculations of a flame that has been selected as one of the targets for the 1998 Workshop in Boulder. The data included here are limited to boundary conditions, an axial profile, and four radial profiles for Flame D, which has a jet Reynolds number of Re=22400.

Additional information on the experimental methods and results will be made available on the web page for the Turbulent Diffusion Flame (TDF) Laboratory at the Sandia Combustion Research Facility (www.ca.sandia.gov/tdf/Lab.html). The complete data set will be put on the web at a later date.

Velocity measurements in these flames are in progress at the Technical University of Darmstadt but are not yet available. The initial velocity profiles included here are based on information from similar flames studied at Sydney University.

USE OF THE DATA

Please contact the authors at the above address if you use these data or if additional information is needed to initiate calculations. This will ensure that you will be on the mailing list for updates regarding these and other relevant data. Please also report any problems with this preliminary release.

These scalar data were obtained by R. Barlow and J. Frank during January 1997 and are not yet published. The data are being made available with the understanding they will not be included in published work unless i) permission is obtained from the above authors, or ii) the above authors publish the data in the open literature, or iii) the above authors lift this restriction in a subsequent electronic release of the data.

Similarly, permission should be obtained from Egon Hassel (hassel@hrz1.hrz.tu-darmstadt.de) before inclusion of the velocity data from TU Darmstadt in any published work.

NOTICE

GENERAL DESCRIPTION OF THE FLAME

The burner geometry is the same as used in numerous previous investigations of piloted flames at Sydney University and Sandia. The jet fluid is a mixture of three parts air and one part CH_4. This mixture significantly reduces the problem of fluorescence interference from soot precursors, allowing improved accuracy in the scalar measurements. Partial premixing with air also reduces the flame length and produces a more robust flame than pure CH_4 or nitrogen-diluted CH_4. Consequently, the flames may be operated at reasonably high Reynolds number with little or no local extinction, even with a modest pilot. The mixing rates are high enough that these flames burn as diffusion flames, with a single reaction zone near the stoichiometric mixture fraction and no evidence of premixed reaction in the fuel-rich CH_4/air mixtures. Flame D has a small degree of local extinction which is not expected to complicate comparisons with models. The pilot is a lean (phi=0.77) premixture of C_2H_2, H_2, air, CO_2, and N_2 with the same nominal enthalpy and equilibrium composition as methane/air at this equivalence ratio. The energy release of the pilot is approximately 6% of the main jet. The burner exit is approximately 15 cm above the exit of the vertical wind tunnel in the TDF lab. The flame is unconfined.

BURNER DIMENSIONS

```
Main jet inner diameter, d   = 7.2 mm
Pilot annulus inner diameter = 7.7 mm  (wall thickness = 0.25 mm)
Pilot annulus outer diameter = 18.2 mm
Burner outer wall diameter   = 18.9 mm (wall thickness = 0.35 mm)
Wind tunnel exit             = 30 cm by 30 cm
```

BULK FLOW CONDITIONS

```
Coflow velocity  (Ucfl)      = 0.9 m/s (+/- 0.05 m/s) @ 291 K, 0.993 atm
Main jet composition         = 25% CH4, 75% dry air by volume
Main jet velocity, Ubulk     = 49.6 m/s (+/- 2 m/s) @ 294K, 0.993 atm
Main jet kinematic viscosity = 1.58e-05 m^2/s (from chemkin)
```

Elemental mass fractions in the jet and coflow that are used in calculating the mixture fraction are given below, under the definition of mixture fraction.

The flame stabilizer in the pilot is recessed below the burner exit, such that burnt gas is at the exit plane. (A photo of the pilot may be viewed on the TDF Lab web page.) The boundary condition for the pilot is determined by matching the measurements at x/d=1 with calculations (by J-Y Chen) of laminar unstrained premixed CH_4/air flames and then extrapolating to the conditions at burner exit plane, based on the estimated convective time up to x/d=1. The pilot burnt gas velocity is determined from the cold mass flow rate and the density at the estimated exit condition. The resulting pilot flame boundary conditions are tabulated below. Separate calculations were performed to demonstrate that there are negligible differences in burnt gas composition for the pilot mixture vs. CH4/air at the same total enthalpy and equivalence ratio.

The pilot composition measured in the (nearly) flat portion of the radial profile at x/d=1 is:

```
phi       = 0.77
Fch       = 0.27
T         = 1908 K (+/- 50 K)
Yn2       = 0.734
Yo2       = 0.056
Yh2o      = 0.092
Yco2      = 0.110
Yoh       = 0.0022
```

The pilot composition at the burner exit is taken as that of an unstrained CH_4/air premixed phi=0.77 flame at the point in the flame profile where T=1880 K, following the process outlined above.

```
phi       = 0.77
Fch       = 0.27
T         = 1880 K
rho       = 0.180 kg/m^3
Yn2       = 0.7342
Yo2       = 0.0540
Yo        = 7.47e-4
Yh2       = 1.29e-4
Yh        = 2.48e-5
Yh2o      = 0.0942
Yco       = 4.07e-3
Yco2      = 0.1098
Yoh       = 0.0028
Yno       = 4.8e-06
```

The pilot velocity corresponding to this composition and the measured mass flow rate is:

```
Uplt = 11.4 m/s (+/- 0.5 m/s)
```

We note that a similar composition (within experimental uncertainty) is obtained from a laminar diffusion flame calculation with the present fuel-air boundary conditions, equal species diffusivities, and a relatively low strain rate (a ~ 20/s) at 0.27 mixture fraction. The sensitivity of model predictions to uncertainty the pilot boundary conditions may be an important consideration, especially with regard to flame stability and local extinction.

VELOCITY BOUNDARY CONDITIONS (Updated 9-JAN-98)

Two component velocity measurements are in progress at the Technical University of Darmstadt. Complete results are not yet available. However, a jet exit profile (at 1 mm from the nozzle) and an axial velocity profile have been made available by Chris Schneider (cschneid@hrz2.hrz.tu-darmstadt.de), Stefan Geiss, and Egon Hassel.

Calculations of this burner have typically used the 1/7th power law to estimate the mean velocity profile. Relative to the jet centerline, this gives:

```
U/Umax = (1 - r/R)^(1/n),    n=7,
```

and

```
U/Ubulk = (1 - r/R)^(1/n) * [(n+1)(2n+1)/2n^2],
```

where U is velocity, r is radius, and R=3.6 mm. This gives a ratio of centerline velocity to bulk velocity of 1.22 and a centerline velocity of 60.5 m/s.

The 1/7th power law is a high Reynolds number fit and does not provide a very good fit to the measured mean velocity profile for the Reynolds number of Flame D. (The power law profile is too flat.) The stability of piloted flames can be quite sensitive to velocity boundary conditions. Therfore, we recommend that modelers use the measured velocity profile. Figure 1 shows a plot of the measured mean velocity and turbulence profiles. Jet exit profiles of U/Uc,o and u'/Uc,o are tabulated below, with Uc,o=63.1 m/s being the measured centerline velocity in the exit profile. For convenience we have averaged the symmetric measurements for positive and negative coordinates, and we have set values to zero at r=R.

r/R	U/Uc,o	u'/Uc,o
0.000	1.000	0.0309
0.065	0.999	0.0307
0.130	0.995	0.0327
0.194	0.988	0.0366
0.259	0.978	0.0409
0.324	0.967	0.0450
0.389	0.951	0.0504
0.453	0.933	0.0550
0.518	0.912	0.0604
0.583	0.887	0.0648
0.648	0.858	0.0693
0.712	0.824	0.0726
0.777	0.785	0.0773
0.842	0.732	0.0863
0.907	0.613	0.1230

```
0.972   0.291   0.0991
1.000   0.000   0.0000
```

The pilot velocity profile is assumed to be flat, except for thin boundary layers. Here we have specified a piecewise-linear profile that takes the half velocity points to be mid-way across the burner walls, such that the thickness of the inner and outer walls is neglected.

```
r/R     U/Uplt  u'/Uplt
1.00    0.00    0.00
1.07    0.50    0.01
1.13    0.99    0.01
1.14    1.00    0.01
2.51    1.00    0.01
2.52    0.99    0.01
2.57    0.50    0.01
2.62    0.00    0.00
```

The boundary layer in the coflow is taken to have the same shape as specified by Sydney University, except that we have shifted the profile to correspond to the measured 18.9-mm outer dimension of the burner. Also, a free stream turbulence intensity of 1% is assumed.

```
r/R     U/Ucfl  u'/Ucfl
2.62    0.000   0.000
2.74    0.219   0.100
2.88    0.340   0.124
2.90    0.370   0.130
3.12    0.495   0.128
3.62    0.660   0.101
4.12    0.780   0.073
4.62    0.850   0.053
5.12    0.900   0.035
5.62    0.940   0.021
6.12    0.970   0.010
6.62    0.990   0.010
7.12    1.000   0.010
40.0    1.000   0.010
```

AXIAL VELOCITY PROFILE

The axial profile for Flame D (measured by the group at TU Darmstadt) is listed below as Uc/Uc,o and u'/Uc vs. x/d, where Uc is the mean centerline velocity, Uc,o is the centerline velocity at the jet exit, and u' is the rms fluctuation of axial velocity. Figure 2 shows a plot of the axial profiles of mean velocity and turbulence.

```
x/d     Uc/Uc,o u'/Uc
0.130   1.000   0.0307
0.518   1.000   0.0309
1.04    0.998   0.0317
1.55    0.999   0.0326
2.07    1.000   0.0359
2.59    0.994   0.0361
3.89    0.984   0.0385
5.18    0.974   0.0452
6.48    0.962   0.0494
7.77    0.946   0.0554
9.07    0.929   0.0625
10.4    0.909   0.0694
11.7    0.888   0.0789
13.0    0.866   0.0878
```

14.2	0.841	0.101
15.5	0.817	0.113
16.8	0.790	0.126
18.1	0.758	0.161
19.4	0.723	0.166
20.7	0.695	0.172
22.0	0.670	0.179
23.3	0.646	0.186
24.6	0.623	0.193
25.9	0.601	0.198
28.5	0.558	0.207
31.1	0.508	0.232
33.7	0.465	0.247
36.3	0.426	0.262
38.9	0.378	0.279
41.5	0.347	0.289
44.0	0.322	0.296
46.6	0.296	0.296
49.2	0.273	0.301
51.8	0.248	0.309
54.4	0.227	0.317
57.0	0.209	0.316
59.6	0.193	0.314
62.2	0.179	0.321
64.8	0.171	0.303
67.4	0.163	0.287
69.9	0.149	0.317
72.5	0.146	0.307
75.1	0.135	0.298
77.7	0.133	0.288
80.3	0.120	0.313
82.9	0.120	0.291
85.5	0.116	0.283

MIXTURE FRACTION DEFINITION

Mixture fraction is defined following Bilger, except that only H and C are included. This is because the jet- and coflow boundary conditions for the elemental oxygen mass fraction are relatively close, and shot noise in the measurements of elemental oxygen mass fraction causes excessive noise in the mixture fraction as normally defined. The mixture fraction based on C and H is tabulated in the data files. Calculations can use the normal definition of the Bilger mixture fraction, since the two will be identical unless the calculation includes differential diffusion.

$$F = \frac{0.5(YH-Y2H)/WTH + 2(YC-Y2C)/WTC}{0.5(Y1H-Y2H)/WTH + 2(Y1C-Y2C)/WTC}$$

where

YH = H element mass fraction in the measured sample
YC = C element mass fraction in the measured sample

Y1H = H element mass fraction in main jet stream
Y1C = C element mass fraction in main jet stream

Y2H = H element mass fraction in coflow stream
Y2C = C element mass fraction in coflow stream

and WTH = 1.008, WTC = 12.011

The elemental mass fractions used in the data reduction process are listed below. Here the ambient humidity in the coflow air is included, and the composition of dry air is taken to be 21% O_2 and 79% N_2 (Ar and CO_2 content are neglected).

```
Jet:     Y1H=0.0393, Y1C=0.1170, Y1O=0.1965, Y1N=0.6472

Coflow:  Y2H=0.0007, Y2C=0.0000, Y2O=0.2413, Y2N=0.7580
```

The stoichiometric value of the mixture fraction is Fstoic=0.351

MEASUREMENT LOCATIONS and GLOBAL PARAMETERS

The axial profile includes locations x/d = 5, 10, 15,...,80
The radial profiles are at x/d = 1, 2, 3, 7.5, 15, 30, 45, 60, and 75.

The visible flame length is approximately:

```
Lvis ~ 67d (48 cm)
```

The stoichiometric flame length based upon interpolation of the axial profile of Favre average mixture fraction is:

```
Lstoic = 47d (33.8 cm)
```

The total flame radiation was measured by J. Frank, using a calibrated wide-angle, heat flux radiometer (Medtherm) with a ZnSe window. The total radiative flux was 0.887 kW, or ~5.1% of the ~17.3 kW power of the flame plus pilot.

```
Frad = 0.051
```

AVAILABLE DATA and FILE DESCRIPTIONS

This preliminary release for Flame D includes the axial profile and radial profiles at x/d=1, x/d=2, x/d=15, and x/d=45. Files include Favre averaged scalars (mean and rms), with species listed as mass fractions.

Temperatures are from Rayleigh scattering measurements, except in the radial profile at x/d=1, where scattering from the burner causes the Rayleigh temperatures to be less reliable. Temperatures listed for x/d=1 are determined from Raman/LIF total number densities and the perfect gas law.

CO mass fractions from Raman and LIF are included. Differences are relatively small and will be documented at a later date. The CO-LIF measurements should be used for comparisons with model predictions.

Experimental uncertainties will be documented at a later date. Generally, the accuracies are comparable to or better than for recently published measurements from the TDF lab. The CO measurements, in particular, are improved relative to previous measurements in hydrocarbon flames. The probe volume is roughly 0.75 mm in diameter and length. Consequently, there is significant spatial averaging in regions of steep gradients near the nozzle, and data should be interpreted with caution.

Files include column labels. The column labels and the data are separated by 1 or more spaces.

```
File name       Description

DCL.Yfav        Flame D, axial (centerline) profile, Favre average mass fractions

D01.Yfav        Flame D, radial profile at x/d=1,   Favre mass fractions
D02.Yfav        Flame D, radial profile at x/d=2,   Favre mass fractions
D03.Yfav        Flame D, radial profile at x/d=3,   Favre mass fractions
D075.Yfav       Flame D, radial profile at x/d=7.5, Favre mass fractions
D15.Yfav        Flame D, radial profile at x/d=15,  Favre mass fractions
D30.Yfav        Flame D, radial profile at x/d=30,  Favre mass fractions
D45.Yfav        Flame D, radial profile at x/d=45,  Favre mass fractions
D60.Yfav        Flame D, radial profile at x/d=60,  Favre mass fractions
D75.Yfav        Flame D, radial profile at x/d=75,  Favre mass fractions
```

Some representative plots of conditional means and scatter data are available on the TNF Workshop web page (www.ca.sandia.gov/tdf/Workshop.html) under the descriptions of target flames for the 3rd TNF Workshop.

PRELIMINARY GUIDELINES FOR MODEL CALCULATIONS

To allow useful comparisons of the details of scalar results from various calculations in the context of the TNF Workshop, we recommend the following. We encourage discussion on these modeling guidelines and on the list of results to be compared. Please address comments to R. Barlow.

1) Adjust the turbulence/mixing code to match the measured axial velocity profile and the stoichiometric flame length (Favre average), and report adjustments. Agreement within +/- 5% (if practical) on the stoichiometric flame length will ensure that no two predictions will differ by more than 10% in flame length. For some modeling approaches it may be necessary to adjust separate parameters to match both the velocity and mixture fraction profiles. Comparisons of detailed scalar results will be ambiguous, at best, if the overall flow and mixing fields are not in reasonable agreement.

2) If NO is calculated, it would be useful to have both adiabatic and radiative calculations. Radiative calculations should use the approach documented on the Workshop Web page (www.ca.sandia.gov/tdf/Workshop.html). If only one calculation is done, it should be the adiabatic calculation.

3) If possible, use methane chemistry based on some derivative of the Warnatz mechanism that was discussed at the Heppenheim Workshop. This mechanism is available on the web. Modellers interested in ILDM tables or reduced mechanisms should contact U. Maas or J-Y Chen, respectively.

4) Please plan to provide results in a format similar to the experimental data. (Mass fractions, Favre mean and rms, Axial and radial profiles, Conditional mean and rms, File headers with identifying information and column labels, Columns separated by spaces or tabs.)

SECTION 3

Delft Piloted Natural Gas Flame III

Coordinated by Tim Peeters

Current Status of the Delft Piloted Jet Diffusion Flames

T.W.J. Peeters
Delft University of Technology, Dept. of Applied Physics, ThermoFluids Section, The Netherlands
E-mail: T.Peeters@tn.tudelft.nl

1 Introduction

The Delft III flame was selected as one of the target flames for the Third TNF Workshop. In this report, an update of the current status of the experimental data and the numerical simulations is presented.

In 1996, the Delft III flame was the topic of a European Workshop on simulation and validation of turbulent combustion models. At that time, the experimental data were incomplete. Turbulent velocity data, CARS temperature data, and OH LIF data were available, but there were still uncertainties with respect to the usefulness of these data. In 1997, Pieter Nooren of TU Delft went to Sandia, and conducted a series of Raman/Rayleigh/LIF experiments together with Rob Barlow and his coworkers. As a result, there now is a complete experimental dataset for the 'Delft' flame for two different Reynolds numbers, comprising all major species, temperature, NO, and OH.

In parallel to these new experimental data, the Delft group has improved their own CARS temperature measurement and post-processing technique. The latest results, obtained in July 1998, show that within experimental error, the latest CARS data and the Sandia Raman/Rayleigh temperature data agree with each other. This is considered as very encouraging and will be explained in more detail at the Workshop itself, since the new CARS data are very fresh.

So far, the data are limited to two cases: the Delft III flame, considered the near-equilibrium base case with only a small amount of local extinction and the Delft IV flame, with higher annular air velocity, and exhibiting stronger local extinction. Currently, the improved CARS technique is now applied to the Delft IV flame in order to compare with the Sandia measurements.

At the Second TNF Workshop held in Heppenheim, Germany, none of the participating simulation groups showed any particular interest in attempting to perform model calculations on the Delft flame. By June 1998, only one person (Dr. M. Nutini, Pirelli Company, Milano, Italy) submitted results, additional to the detailed calculations performed by the Delft group (Pieter Nooren, Tim Peeters, Dirk Roekaerts). Nutini used an eddy-break-up model with a one-step global reaction (Magnussen's model) in Fluent 5.0. Because of the major differences in modeling approach between Nutini's and Nooren's data, especially with respect to chemistry modeling and turbulence-chemistry interaction modeling, it is not considered worthwhile at this stage to show detailed comparisons between calculations and experiments. It is evident that before definitive conclusions can be drawn, one requires more groups to participate in the simulation of the Delft flame (at the next Workshop?).

In the next chapters, the data of Pieter Nooren's Thesis will be briefly discussed. The aim is to provide information important for future modelers of the Delft flames. The details of the experimental and numerical models will not be given; they can be found elsewhere, particularly in Pieter Nooren's Thesis and earlier Theses produced by the Delft group. The comparison of Nooren's calculations with the experimental data will be summarized in the conclusions.

2 Raman-Rayleigh-LIF measurements

The Raman-Rayleigh-LIF measurements performed in 1997 at Sandia National Laboratories on the Delft burner provide time- and space-resolved data on temperature and the concentrations of CO_2, O_2, CO, N_2, CH_4, H_2O, H_2, OH and NO. As all these quantities are measured simultaneously, information on the joint statistics of important thermochemical scalars is obtained, that can be directly compared to model predictions.

The Raman-Rayleigh-LIF measurements complement the existing experimental data for the Delft piloted diffusion flame burner collected earlier in the Heat Transfer Section of the Applied Physics Department, Delft University of Technology, The Netherlands. This database includes

- Laser Doppler Anemometry (LDA) measurements of the flow field (Stroomer, 1995)
- Laser-Induced Fluorescence (LIF) data on the OH radical concentration (De Vries, 1994)
- Coherent Anti-Stokes Raman Spectroscopy (CARS) measurements of mean temperature and temperature statistics (Mantzaras and Van der Meer, 1997) and improved measurements by Versluis and Zong (1998).

- Infrared emission/absorption tomography data on temperature and the volume fractions of H_2O, C_2H_2 and soot (Van den Bercken, 1998).

The Raman-Rayleigh-LIF measurements were performed in the Turbulent Diffusion Flame Laboratory of the Combustion Research Facility, Sandia National Laboratories[1], Livermore, USA, in a collaboration with R.S. Barlow and J.H. Frank.

2.1 Delft piloted diffusion flame burner

The Delft piloted diffusion flame burner, designed in the Heat Transfer Section, is used to produce a number of well-defined, laboratory-scale axisymmetric turbulent diffusion flames. The burner is described in detail by De Vries (1994) and Stroomer (1995).

2.1.1 Burner geometry

The burner consists of a central fuel jet, surrounded by two concentric coflows of air. Figure 1 shows the burner head. The fuel jet nozzle is 6 mm in diameter. It is separated from the primary air stream by a rim of outer diameter 15 mm. Pilot flames, necessary for the stabilization of the flame on the burner, are issued from holes located on this rim. The outer diameter of the primary air annulus is 45 mm.

[1]The Sandia contributions were supported by the United States Department of Energy, Office of Basic Energy Sciences, Division of Chemical Sciences.

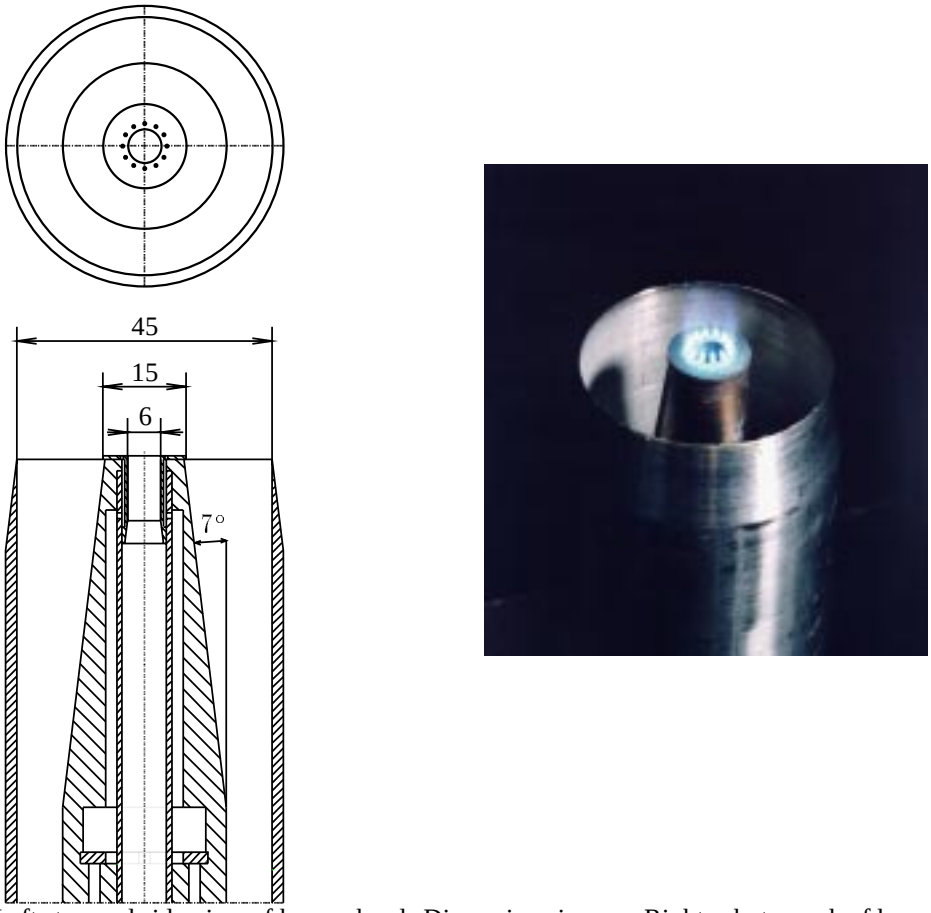

Figure 1: Left: top and side view of burner head. Dimensions in mm. Right: photograph of burner head with pilot flames. (Photograph courtesy of R.S. Barlow, Sandia National Laboratories.)

Table 1: Inlet conditions for two different flames. U is the mean exit velocity, T the temperature and Re the Reynolds number. The subscripts fuel and ann refer to the fuel and primary air stream, respectively. L_f is the visible flame length from De Vries (1994).

flame	Fuel jet			Primary air flow			L_f
	U_{fuel} (m/s)	T_{fuel} (K)	$\mathrm{Re}_{\mathrm{fuel}}$	U_{ann} (m/s)	T_{ann} (K)	$\mathrm{Re}_{\mathrm{ann}}$	(m)
III	21.9	295	9700	4.4	295	8800	0.85
IV	21.9	295	9700	8.0	295	16000	0.70

The length of the burner is 100 cm. In the first 94 cm, the inner diameter of the primary air annulus is 30 mm, decreasing to 15 mm in the final 6 cm. This gives rise to a small negative radial velocity component of the primary air in the exit plane of the nozzle. The initial diameter of the central fuel pipe is 8 mm. A pilot flame insert placed in the exit of the fuel pipe causes a decrease in diameter to 6 mm starting at a position 16 mm upstream of the nozzle exit. Although the decrease in diameter is gradual, with an 8° angle, the flow leaving the fuel pipe cannot be considered to be fully developed pipe flow.

In the experiments performed in the Heat Transfer Section the burner is placed in an octagonal chamber (figure 2), dimension 57 cm from side to side. A low-velocity secondary air stream provided through the throat prevents a large-scale recirculation in the burner chamber.

2.1.2 Boundary conditions

In the Heat Transfer Section, experiments are performed for six different sets of inlet boundary conditions. Here, we focus on two cases only, denoted as case IIIand IV. The flow rates of the fuel and air streams are varied to study the effect of different turbulent mixing rates. In addition, the fuel and air streams can be preheated in the LIF and CARS experiments. Table 1 gives an overview of the inlet boundary conditions of the two flames.

For both flames, the secondary air stream is kept at room temperature, approximately 295 K, with a velocity of

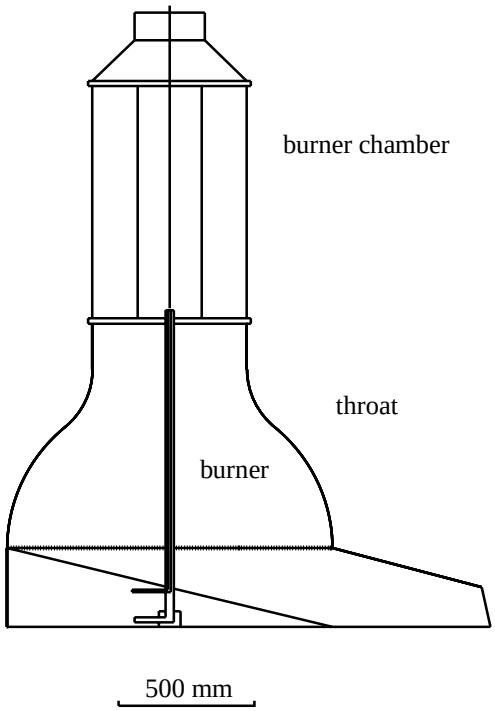

Figure 2: Burner placed in burner chamber.

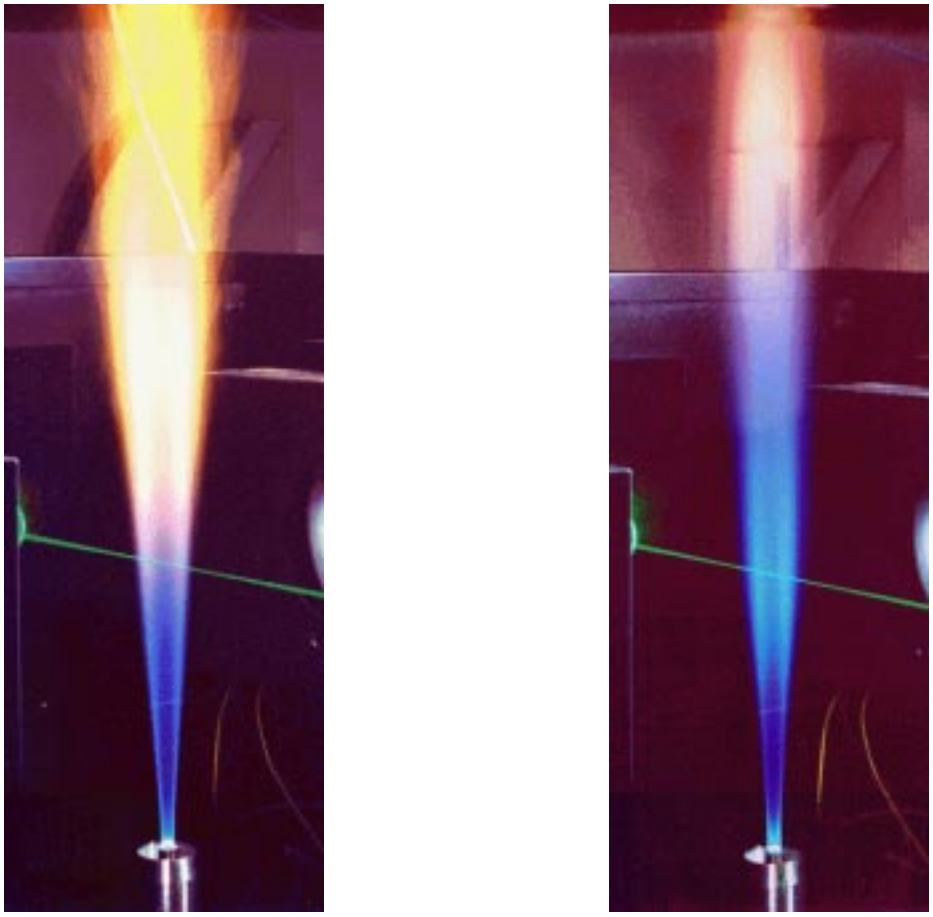

Figure 3: Photographs of flame III (left) and flame IV (right). The area covered is approximately 72 (height) $\times$ 25 (width) cm. (Courtesy of R.S. Barlow, Sandia National Laboratories.)

0.3 m/s. The fuel used in the experiments is Dutch natural gas, consisting mainly of methane and nitrogen. The detailed composition is given in Nooren's thesis.

The present Raman-Rayleigh-LIF measurements are performed for flames III and IV. Figure 3 shows photographs of these flames, taken in the Turbulent Diffusion Flame Laboratory. Flame III is considered as a reference flame or 'base case'. For this flame, LDA measurements of the equivalent non-reacting flow, with the natural gas in the fuel stream replaced by air, are available. This allows for a test of the turbulence model in a situation analogous to the reacting flow, without the added complication of chemical reaction.

2.1.3 Pilot flames

Pilot flames are necessary to stabilize the turbulent diffusion flame on the burner rim. The pilot flames are issued from twelve 0.5 mm diameter holes, situated on a 7 mm diameter ring on the rim separating the fuel and primary air streams, see figure 1. The pilot flames are fed with an acetylene/hydrogen/air premixture, equivalence ratio $\Phi = 1.4$. The C/H ratio is the same as that of the natural gas. The cold, unburnt velocity of the pilot flames is 12 m/s, the burnt velocity is estimated at 100 m/s. The heat release in the pilot flames is about 1% of the total thermal power of flame III.

A small recirculation zone, located directly above the 4.5 mm wide rim separating the fuel and primary air streams, provides a second possible mechanism for flame stabilization.

2.2 Experimental set-up for Raman-Rayleigh-LIF diagnostics

The Raman-Rayleigh-LIF set-up in the Turbulent Diffusion Flame Laboratory is extensively described elsewhere (Nguyen *et al.*, 1996; Barlow and Carter, 1994; Carter and Barlow, 1994; Dally *et al.*, 1996; Barlow *et al.*, 1990), except for the two-photon LIF (TPLIF) system for CO, which is a recent addition to the set-up. The description presented here follows the article by Nguyen *et al.* The spectroscopic principles on which the Raman, Rayleigh and LIF techniques are based can be found in Herzberg (1989). The application of these techniques to combustion diagnostics is described in numerous texts, *e.g.* Eckbreth (1996) and the references therein.

An overview of the Raman-Rayleigh-LIF set-up is shown in figure 4. Detailed schematics of the Raman-Rayleigh and LIF systems are presented in Nooren (1998).

The Raman-Rayleigh system is used to measure temperature and the concentrations of CO_2, O_2, N_2, CH_4, H_2O and H_2. Three separate LIF systems are used for the probing of OH, NO and CO. As the aim is to collect data on the time-resolved joint statistics of temperature and the major and minor species, the Raman-Rayleigh and LIF laser systems are fired almost simultaneously, with timing delays of typically 100 ns. This also allows for a quantitative correction for collisional quenching of the LIF signals. The timing delays are used to avoid interferences between the different systems. The delays are small compared to the chemistry and turbulence time scales in the flames studied here, so that the measurements can indeed be considered simultaneous. The set-up operates at 10 Hz.

The burner is positioned in an unconfined, 0.3 m/s air flow, produced by a wind tunnel with an exit cross-section of 254 $\times$ 254 mm. The fuel is California natural gas (composition approximately 94.7 mol% CH_4, 3.5 mol% C_2H_6, 0.1 mol% C_3H_8 and higher hydrocarbons, 1.0 mol% N_2 and 0.7 mol% CO_2) diluted with nitrogen. By adding 0.160 mole of N_2 to every mole of California natural gas, a fuel mixture with 81.7 mol% CH_4, 3.0 mol% C_2H_6, 0.1 mol% C_3H_8 and higher hydrocarbons, 14.6 mol% N_2 and 0.6 mol% CO_2 is obtained, which is very close to the composition of Dutch natural gas. The stoichiometric mixture fraction and adiabatic flame temperature of the nitrogen-diluted mixture are within 0.0005 and 1 K of the values for Dutch natural gas, respectively.

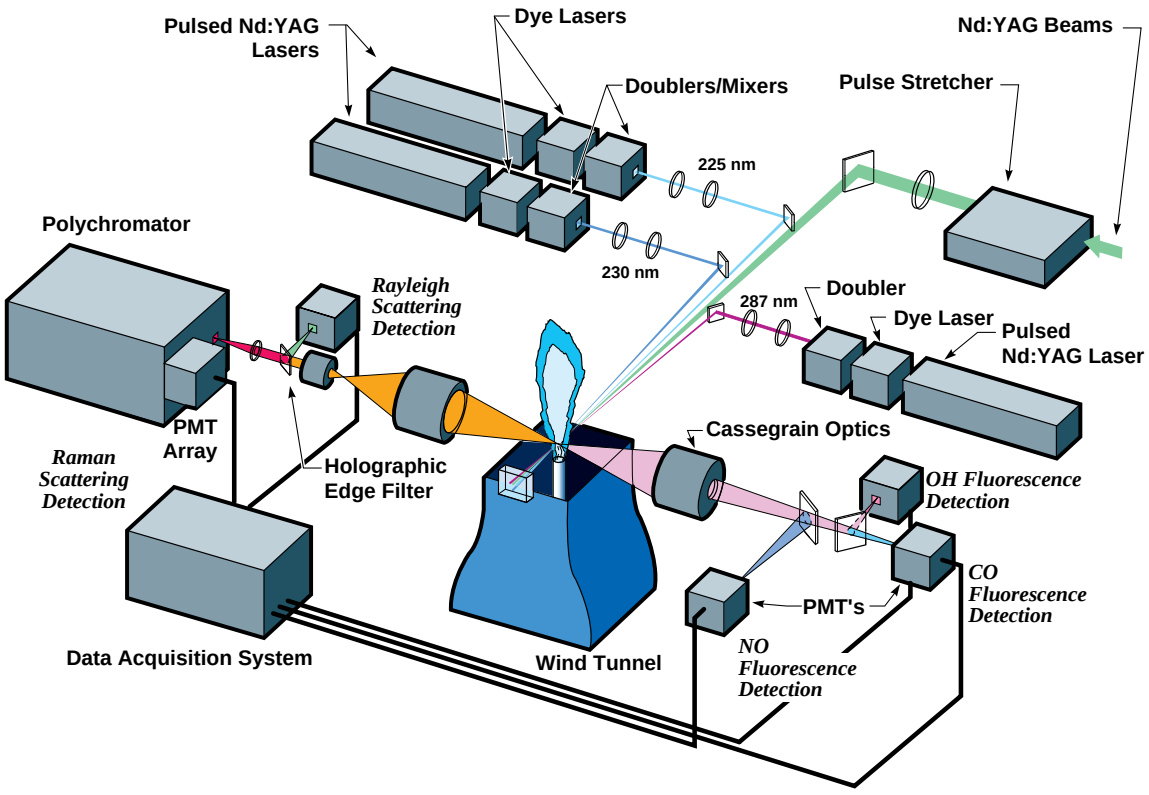

Figure 4: Overview of the Raman-Rayleigh-LIF set-up. (Courtesy of R.S. Barlow, Sandia National Laboratories.)

2.3 Treatment of interferences

2.3.1 Raman system

The interference contributions to the measured Raman signals originate from two main sources (Masri *et al.*, 1996). The first type of interference is caused by Raman scattering from other species. The second source of interferences is the non-resonant fluorescence from heavy hydrocarbons such as polycyclic aromatic hydrocarbons (PAHs) and other soot precursors (Masri *et al.*, 1987; Eckbreth, 1996). The spectrum of the fluorescence interferences in hydrocarbon flames depends on, among other things, the laser wavelength, the fuel composition and dilution level, the instantaneous mixture fraction, the turbulent mixing rate and the residence time of soot precursors in the flame. Especially in undiluted hydrocarbon flames, fluorescence interferences can be important. Other sources of interference are due to chemiluminescence and the resonant excitation of minor species like C_2. Although the spectral structure of this last type of interference exhibits distinct peaks, the overall character of the fluorescence interferences in CH_4 flames is found to be broadband.

In the Raman data reduction procedure, this broadband behaviour is exploited to identify the interference contributions to the Raman signals. The interferences are monitored by PMTs positioned at spectral locations in between the Raman channels. Because of the broadband character of the interferences, linear correlations exist between the signals from the fluorescence monitors and each of the Raman signals. These correlations are used to correct the Raman signals for the N_2 species for the interferences.

The fluorescence interferences are associated primarily with the presence of heavy hydrocarbon species, which occur in rich mixtures only. It is seen that the interference levels recorded in the two flames III and IV differ significantly. As shown later, the temperatures in the bottom of flame IV are substantially lower than those found in flame III. Combined with the smaller mean residence time of the fluid particles, caused by the larger annular air velocity, this is expected to give lower concentrations of heavy hydrocarbons. At x = 150 mm, the interference levels in flame III are about five times higher than those in flame IV.

Analysis of the data taken in flame III shows that in this flame, the interference on the CO_2 Raman channel cannot be corrected for using the same procedure as for N_2. In the processing of the data collected in flame III, it is therefore preferred not to use the CO_2 Raman signals from points with instantaneous signals on the 615 nm fluorescence monitor channel above a certain threshold. *For these points, the CO_2 concentration is obtained from an indirect procedure using the measured Rayleigh temperature and data from a laminar flamelet calculation instead.* In this procedure, it is assumed that the thermochemical composition in the flame is close to that in a laminar flamelet with strain rate a = 100 s^{-1}. A progress variable based on the Rayleigh temperature, introduced below, is used to describe small deviations from this composition. Simulations show that flame III exhibits a wide range of strain rates. However, realistic CO_2 concentrations can be obtained with a procedure based on a single representative strain rate.

The same procedure is used to obtain the O_2 concentration in flame III. It is found that in flame III, the fluorescence interference on the O_2 Raman channel cannot be adequately corrected for using a linear correlation with the 615 nm interference signal. The O_2 levels obtained in this way are unrealistically high, suggesting a large degree of local extinction. It is therefore preferred to obtain the O_2 from the progress variable/laminar flamelet (PVLF) procedure as well. The calculations of the CO_2 and O_2 concentrations are integrated in one procedure and performed simultaneously.

It is emphasized that the CO_2 and O_2 concentrations obtained from the PVLF procedure should not be used for a direct comparison to other experimental data or model predictions. Obviously, the resulting CO_2 and O_2 concentrations are strongly correlated with temperature. As such, they provide no independent information on the interaction between the turbulent flow field and the chemistry. The main purpose of the procedure is to obtain CO_2 and O_2 concentrations that are adequate for the evaluation of the mixture fraction and the effective Rayleigh cross-section.

2.3.2 LIF systems

Compared to the Raman signals, the recorded LIF signals are stronger and therefore generally less affected by fluorescence interferences from heavy hydrocarbons. However, the widths of the spectral intervals from which the LIF signals are collected are considerable. As a result, some interference contributions will still be present in the LIF signals recorded in the natural-gas flames.

It is seen that for $r < 5$ mm, where $\widetilde{\xi} > 0.4$, nearly all of the recorded LIF signal originates from interferences. At the positions where the maximal resonant OH signals are measured, the non-resonant contribution is only about

2%. The other graph shows the distribution in mixture fraction space of the OH concentration calculated from the uncorrected resonant signal. Clearly, the non-zero OH concentrations for $\xi > 0.40$ stem from interferences: the OH is expected to be confined to a narrow zone located around stoichiometric mixture fraction.

The flamelets in the laminar flamelet library for natural gas do not show significant levels of OH for $\xi > 0.10$. The non-resonant contributions to the measured OH concentrations can therefore be removed by setting the OH concentrations to zero for mixture fraction values above a certain threshold. The threshold value employed in this work is 0.20. This value is not critical: threshold values of 0.10 and 0.30 give nearly identical results for the mean OH concentration. The effect of the correction is shown in figure 5. Unphysical non-zero OH levels found near the centerline position in the uncorrected profile are eliminated. In the zones with high OH concentrations around r = 14 mm, the non-resonant contributions are negligible and the corrected and uncorrected profiles coincide.

A different approach is employed to suppress the non-resonant contributions to the NO signal. Scatterplots show that the structure of the NO off-resonance signal in mixture fraction space does not allow for a correction analogous to that used for OH. However, the non-resonant signal exhibits a distinct correlation with the 615 nm interference channel. This correlation is used to subtract the interference contributions from the resonant signal before the NO concentration is calculated.

The CO non-resonant signal is found to exhibit a correlation with the 615 nm interference channel, although it is not as distinct as in the case of NO. This correlation is incorporated in the response matrix $\underline{\underline{C}}$ used in the inverse Raman signal problem. Using this approach, the non-resonant contributions are reduced to about 5%.

In flame IV, the absolute non-resonant OH signals at x = 150 mm are found to be typically four times smaller than those in flame III. The absolute OH concentrations are somewhat smaller as well. The non-resonant contribution near the centerline is about 50%. The non-resonant NO and CO signals at x = 150 mm in flame IV are typically six and three times smaller than those at the same position in flame III, respectively.

2.4 Accuracy

For a useful comparison of the measurements to numerical predictions or other experiments, it is essential to have an adequate estimate of the overall accuracy of the data. Random and systematic uncertainties can be introduced in laser-diagnostic combustion measurements by a number of error sources (*e.g.* Eckbreth, 1996; Masri *et al.*, 1996).

Barlow *et al.* (1996) give estimates of random and systematic errors for a number of scalars measured in a turbulent H_2/N_2–air diffusion flame. These measurements were collected in the same set-up used in this study. However, in the case of the natural-gas flames additional uncertainties are introduced by fluorescence interferences not found in

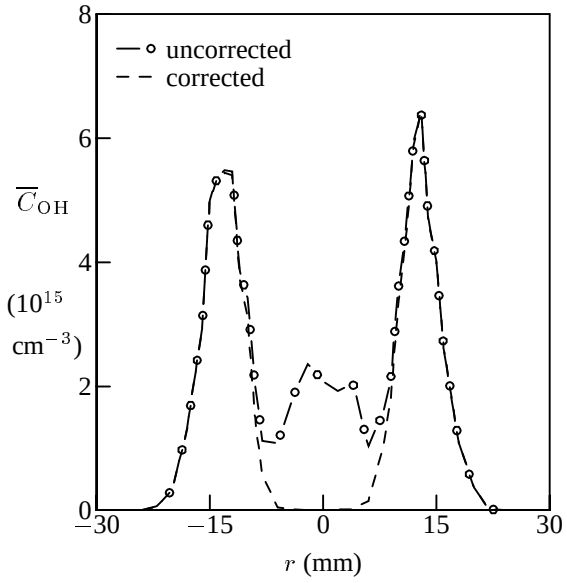

Figure 5: Effect of interference correction on mean OH concentration at x = 150 mm in flame III.

Table 2: Estimated relative random errors and potential systematic uncertainties in the Raman-Rayleigh-LIF measurements. The systematic uncertainties are given separately for lean/stoichiometric mixtures and for rich mixtures in flames III and IV. The species entries are for concentrations (moles dm^{-3}). The superscript IV denotes estimates valid in flame IV only, t and m refer to typical and maximum values, respectively.

quantity	random error (%)	potential systematic uncertainty (%)			
		lean/ stoich.	rich		main source(s)
			flame III	flame IV	
CO_2	8^{IV}	4	—	10	interferences
O_2	6^{IV}	3–12	—	3–12	calibration: 3% at 1300 K, 12% at 2000 K
N_2	3	2	5	5	interferences
CH_4	2	2–10	2–10	2–10	calibration: 6% at 1500 K, 10% at 2100 K
H_2O	7	4	11	8	interferences
H_2	17	5	20	15	calibration, interferences
OH	8	10	10	10	calibration
NO	12	10	20	15	calibration, non-resonant signal
CO	7	13	18	18	calibration, non-resonant signal
ξ	4	2	5^t, 20^m	2^t, 5^m	CH_4 calibration, PVLF correction flame III
T	1	2	2^t, 8^m	1^t, 3^m	CH_4 calibration, PVLF correction flame III, excluding spatial averaging

hydrogen flames. These interferences give rise to larger potential systematic errors.

The estimated random and systematic errors for the quantities obtained from the Raman-Rayleigh-LIF measurements are presented in table 2. No estimates are given for the inaccuracies of CO_2 and O_2 in flame III, as these concentrations are obtained from the PVLF procedure. Details can be found in Nooren (1998).

2.5 Results of NO measurements

The Raman-Rayleigh-LIF data for NO have so far not been used for the assessment of model predictions performed so far in Delft. From the experiments, the amount of NO in the bottom part of flame IV is significantly lower than that at the same position in flame III. This is attributed to the more frequent occurrence of local extinction and corresponding lower temperatures in flame IV. Calculations are required to confirm this.

3 Conclusions and future prospects

The Delft piloted diffusion flame burner burner has been designed to produce a number of well-defined turbulent natural-gas jet diffusion flames. The differences between the two flames described here, flames III and IV, originate from their different primary air flow rates. In flame IV, the primary air flow rate is nearly twice as large as in flame III.

3.1 Raman-Rayleigh-LIF measurements

The Raman-Rayleigh-LIF measurements provide simultaneous point data on temperature and the concentrations of CO_2, O_2, CO, N_2, CH_4, H_2O, H_2, OH and NO. The application of the Raman technique in the undiluted natural-gas flames considered here proves to be very challenging because of the high fluorescence interference levels. The interference contributions to the recorded Raman signals are identified and subtracted using empirical correlations between the Raman signals and the signals on the interference monitor channels. This procedure proves to be adequate for most species. However, it is found that the empirical approach cannot be used to remove the interference contributions to

the CO Raman signal. This also holds for the CO_2 and O_2 signals in flame III, the flame with the highest interference levels. The concentrations of these species are determined using alternative approaches. Because of the fluorescence interferences, the acquired Raman-Rayleigh-LIF dataset has certain limitations, the most important of which is the absence of independent CO_2 and O_2 measurements in flame III. The Raman-Rayleigh-LIF experiments nonetheless provide nearly all of the desired simultaneous measurements of temperature and major species concentrations. The Raman-Rayleigh-LIF data therefore form a valuable and useful extension of the existing database for the Delft piloted diffusion flame burner. So far, the improved CARS technique is consistent with the Raman-Rayleigh-LIF temperature data. The 'old' OH LIF data obtained at Delft also compare well with the Raman-Rayleigh-LIF data.

3.2 Turbulence models

It has been shown by Peeters and Nooren that a k-ϵ model with modifications for round-jet mixing already do a good job in predicting the mean flow field of the Delft flames. In order to predict the turbulence anisotropy, a basic Reynolds stress closure is recommended, but in general this does not bring about major changes in the mean flow field or the thermochemistry. The only difficulty lies in the fact that RSM requires more model constants to be selected, and so far no detailed investigations have been undertaken to assess the optimal RSM set of constants.

3.3 Micro-mixing models

The performance of the IEM, C/D and mapping closure micro-mixing models has been investigated using the experimental data on flame III. In the simulations, the thermochemistry in the flame is described by the single-scalar constrained-equilibrium chemistry model. The three micro-mixing models give very similar results for the mean mixture fraction and temperature fields. Marked differences are found between the higher moments of the temperature distribution obtained with the IEM model on one side and those from the C/D and mapping closure models on the other side. The measured temperature standard deviations and PDF shapes are generally reproduced well by the C/D and mapping closure models. The IEM model, in contrast, gives qualitatively incorrect predictions in parts of the domain. The inability of the IEM model to capture some of the essential properties of the fluctuating temperature is attributed to the small differences observed between the mixture fraction PDFs predicted by the IEM model on one side and those from the C/D and mapping closure models on the other side. Combined with the strongly non-linear dependency of temperature on mixture fraction around stoichiometry, these differences can have appreciable effects on the predicted temperature statistics. It is concluded that the choice of micro-mixing model can have a strong influence on the quality of the predictions. Based on the above analysis, the C/D and mapping closure models are preferred over the IEM model. It would be interesting to see these conclusions confirmed by calculations from other groups.

Unlike the C/D model, the mapping closure is local in composition space. It would therefore be very attractive to use the mapping closure in simulations employing multi-scalar chemistry. Unfortunately, the single-scalar mapping closure can only be generalized to multiple scalars under severe restrictions that preclude its use in combination with most multi-scalar chemistry models, including the ILDM reduced kinetics employed in other parts of this study. The ILDM simulations have therefore been performed with the C/D model.

3.4 Chemistry models

The performance of the constrained-equilibrium, laminar flamelet and ILDM models for non-premixed natural-gas combustion has been analyzed by Nooren using the experimental data on both flames III and IV. The eddy-break-up model of Nutini does not account for turbulent fluctuations of the thermochemical variables, and it gives rise to a fairly large overprediction of mean temperature if no 'dissociation correction' is included. It is hard to draw any further conclusions in this respect, because the whole approach of turbulence-chemistry interaction is fundamentally different between Monte Carlo methods and eddy-break-up models.

The comparison of predictions and measurements in flame III provides insight in the behaviour of the models in the near-equilibrium chemistry regime. The temperature and the CO_2 and H_2O mass fractions predicted by the three models are very similar. Comparison to the Raman-Rayleigh data suggests that the mean temperatures and peak mean H_2O mass fractions are somewhat overestimated. This can be caused by, among other things, a more frequent occurrence of local extinction in the Raman-Rayleigh experiments compared to the 'old' CARS experiments. New CARS measurements will have to be performed to confirm this.

It is concluded that the constrained-equilibrium, laminar flamelet and ILDM models are all successful at the prediction of the temperature and product mass fractions in this near-equilibrium flame. The correct prediction of the intermediates CO and H_2 proves to be more difficult. It is concluded that the constrained-equilibrium and laminar flamelet models cannot reproduce the measured CO and H_2 mass fractions over the entire mixture fraction range. The ILDM results for CO and H_2 are strongly affected by numerical problems in the construction of the low-dimensional manifold.

The predictions for OH clearly illustrate the different description of finite-rate kinetic effects in the laminar flamelet and ILDM models. Both models produce realistic super-equilibrium OH levels. However, a detailed analysis of the results shows that only the ILDM reduced kinetics correctly describe the relaxation of the super-equilibrium concentrations. It is concluded that the two reaction progress variables in the ILDM scheme are sufficient to account for the influence of the convective time scales on the slow processes governing the decay of the OH concentration towards equilibrium.

The Raman-Rayleigh measurements show that flame IV exhibits strong finite-rate kinetic effects. In the bottom part of this flame, the measured temperatures and H_2O mass fractions are substantially lower than in flame III. In the simulations, the turbulence time scales in the reaction zone in flame IV are approximately equal to those in flame III. It is therefore concluded that the more frequent occurrence of local extinction in flame IV is not caused by high turbulent mixing rates. Instead, the strong finite-rate kinetic effects are attributed to processes in the extreme upstream part of the flame. The higher primary air velocity reduces the residence time of (near-)stoichiometric mixtures in this region. The pilot-flame-induced stabilization process is therefore likely to be less effective than in flame III, leading to lower temperatures and product mass fractions.

The laminar flamelet model formulation used in this study cannot predict local extinction effects and has therefore not been applied in flame IV. Most laminar flamelet models described in literature can only predict finite-rate kinetic effects caused by high turbulent mixing rates. Furthermore, the use of laminar flamelet models for the prediction of local extinction in piloted flames is hampered by the difficulties encountered in the description of the flame stabilization mechanism. Based on these two observations, it is concluded that laminar flamelet models are not suitable for the prediction of the finite-rate kinetic effects in flame IV.

The ILDM scheme with its two reaction progress variables, on the other hand, provides an adequate description of the influence of the convective time scales on the chemistry in flame IV. The predicted conditional means of the temperature and product mass fractions are substantially lower than those in flame III. The fact that the overall reaction progress is still overpredicted can at least be partially attributed to the description of the pilot flames in the simulation. It is concluded that the ILDM reduced kinetics can, at least qualitatively, predict the stronger local extinction effects in flame IV.

Based on the performance of the chemistry models in flames III and IV, a number of recommendations can be formulated for their use in other turbulent flame calculations. The simple constrained-equilibrium model suffices for the prediction of the temperature and most major species concentrations in near-equilibrium flames. In situations where finite-rate kinetic effects are important, more advanced models have to be used.

In this context, it is useful to distinguish between two types or classes of finite-rate kinetic effects. The effects in the first class are caused by the coupling of the chemical kinetics with the convective time scales in the flow. The simulations and experimental data indicate that the super-equilibrium OH concentrations in flame III and the enhanced local extinction in flame IV both belong to this class. The laminar flamelet model cannot describe this type of flow field-chemistry interaction. The ILDM model, on the other hand, successfully predicts both phenomena and is therefore recommended for this class of finite-rate kinetic effects. The finite-rate kinetic effects in the second class result from the coupling of the chemical kinetics with high turbulent mixing rates. This type of flow field-chemistry interaction has not been encountered in this study. In principle, the ILDM and laminar flamelet models are both suitable for the prediction of this class of finite-rate kinetic effects. It is therefore left as a challenge to other groups to investigate the statement that local extinction phenomena in the Delft flames are attributed to convective effects rather than high turbulent mixing rates.

References

BARLOW, R.S. AND CARTER, C.D. (1994) Raman/Rayleigh/LIF measurements of nitric oxide formation in turbulent hydrogen jet flames. *Combustion and Flame*, **97**, pp. 261–280.

BARLOW, R.S., DIBBLE, R.W., CHEN, J.-Y. AND LUCHT, R.P. (1990) Effect of Damköhler number on superequilibrium OH concentration in turbulent nonpremixed jet flames. *Combustion and Flame*, **82**, pp. 235–251.

BARLOW, R.S., FIECHTNER, G.J. AND CHEN, J.-Y. (1996) Oxygen atom concentrations and NO production rates in a turbulent H_2/N_2 jet flame. In *Twenty-Sixth Symposium (International) on Combustion/The Combustion Institute*, pp. 2199–2205.

CARTER, C.D. AND BARLOW, R.S. (1994) Simultaneous measurements of NO, OH, and the major species in turbulent flames. *Optics letters*, **19**(4), pp. 299–301.

DALLY, B.B., MASRI, A.R., BARLOW, R.S., FIECHTNER, G.J. AND FLETCHER, D.F. (1996) Measurements of NO in turbulent non-premixed flames stabilized on a bluff body. In *Twenty-Sixth Symposium (International) on Combustion/The Combustion Institute*, pp. 2191–2197.

DE VRIES, J.E. (1994) *Study on turbulent fluctuations in diffusion flames using laser induced fluorescence*. PhD thesis, Delft University of Technology.

ECKBRETH, A.C. (1996) *Laser diagnostics for combustion temperature and species*. Combustion science and technology book series. Gordon and Breach Publishers, United Kingdom, Second edition.

HERZBERG, G. (1989) *Molecular spectra and molecular structure: I. Spectra of diatomic molecules.* Robert E. Krieger Publishing Company, Malabar, Florida, Second edition.

MANTZARAS, J. AND VAN DER MEER, TH.H. (1997) Coherent Anti-Stokes Raman Spectroscopy measurements of temperature fluctuations in turbulent natural gas-fueled piloted jet diffusion flames. *Combustion and Flame*, **110**, pp. 39–53.

MASRI, A.R., BILGER, R.W. AND DIBBLE, R.W. (1987) "Fluorescence" interference with Raman measurements in nonpremixed flames of methane. *Combustion and Flame*, **68**, pp. 109–119.

MASRI, A.R., DIBBLE, R.W. AND BARLOW, R.S. (1996) The structure of turbulent nonpremixed flames revealed by Raman-Rayleigh-LIF measurements. *Prog. Energy Combust. Sci.*, **22**, pp. 307–362.

NGUYEN, Q.V., DIBBLE, R.W., CARTER, C.D., FIECHTNER, G.J. AND BARLOW, R.S. (1996) Raman-LIF measurements of temperature, major species, OH, and NO in a methane-air Bunsen flame. *Combustion and Flame*, **105**, pp. 499–510.

NOOREN, P.A. (1998) *Stochastic modeling of turbulent natural-gas flames.* PhD thesis, Delft University of Technology.

STROOMER, P.P.J. (1995) *Turbulence and OH structures in flames.* PhD thesis, Delft University of Technology.

VAN DEN BERCKEN, R.E.J. (1998) *IR emission/absorption tomography in flames.* PhD thesis, Delft University of Technology.

SECTION 4

Sydney Bluff-Body Flow and CH_4/H_2 Flame

Coordinated by Assaad Masri

Third International Workshop on Measurement and Computation of Turbulent Nonpremixed Flames

Boulder, Colorado

July 30 - August 1, 1998

Computation of Bluff-Body Stabilised Jets and Flames

Coordinator

A.R. Masri

Department of Mechanical and Mechatronic Engineering

The University of Sydney

NSW, 2006, Australia

Burner Geometry

The bluff-body stabilised burner is located in a coflowing stream of air. The flame is not enclosed. The face of the burner is made of ceramic. A layout of a typical bluff-body stabilised flame and a sketch of the bluff-body burner are shown in Figures 1 and 2 respectively.

Wind tunnel at exit plane:	305×305mm
Diameter of bluff-body:	50.8mm
Diameter of central fuel jet	3.6mm

Computed Cases

Non-Reacting (NR)

- Fuel: C_2H_4
- Coflow air velocity = 20 m/s
- Bulk jet velocity = 62 m/s

Reacting (RX)

- Flame HM1
- Fuel Mixture: CH_4/H_2 = 1/1 (by volume)
- Bulk jet velocity = 118 m/s
- Coflow air velocity = 40 m/s

Submissions

Computations were received from the four research groups listed here. All flowfield calculations were based on either k-ϵ or Reynolds stress (RS) models of turbulence. The constants used by each group are listed in this report. A modification to one of the standard constants was adopted by few some groups. The following terminology is used here:

RS-S	Standard Reynolds Stress Model with $c_{epsilon1} = 1.44$
RS-M	Modified Reynolds Stress Model with $c_{epsilon1} = 1.60$
k-ϵ-S	Standard k-ϵ model with $c_{epsilon1} = 1.44$
k-ϵ-M	Modified k-ϵ model with $c_{epsilon1} = 1.60$

Contributing groups:

- Department of Fuel and Energy
  Leeds University, UK
  Contact person: **Dr Graham Spence**
- Department of Mechanical Engineering
  The University of Sydney
  Contact person: **Dr Bassam Dally**
- Department of Mechanical Engineering
  Pohang University of Science and Technology
  Pohang, Korea
  Contact person: **Prof. Kang, Y. Huh**
- Technische Universiteit Delft
  Department of Applied Physics
  Delft, The Netherlands
  Contact person: **Dr Tim Peeters**

Table 1: Summary of computations

	Summary of computations										
Group	Case	Turb.	PDF	Grid	Start	Xmax	Ymax	Conv.	Init.	Chem.	
		Model		size	x=	(mm)	(mm)	crit.	Con.	model	
Delft	RX	k-ϵ-M	beta	120x120	-100	200	100	1e-7	bulk	Full-Eq	
	RX	k-ϵ-M	beta	120x120	-100	200	100	1e-7	bulk	Part-EQ	
	RX	RS-M	beta	120x120	-100	200	100	1e-7	bulk	Full-EQ	
	RX	RS-M	beta	120x120	-100	200	100	1e-7	bulk	Part-EQ	
	RX	RS-M	beta	120x120	-100	200	100	1e-7	bulk	FLT 100	
	RX	RS-JM	beta	120x120	-100	200	100	1e-7	bulk	Full-EQ	
Korea	NR	k-ϵ-S	-	52x43	0	100	50	1e-10	web	-	CMC
	RX	k-ϵ-S	beta	52x43	0	100	50	1e-10	web	Warnatz	CMC
Leeds	NR	RS-S	-	58x144	-100	2000	152	1e-6	bulk	-	
	RX	RS-S	beta	58x144	-100	2000	152	1e-6	bulk	FLT 10	
	RX	RS-S	beta	58x144	-100	2000	152	1e-6	bulk	FLT 100	
	RX	RS-S	beta	58x144	-100	2000	152	1e-6	bulk	FLT1000	
Sydney	NR	k-ϵ-M	beta	60x100	-100	300	70	1e-7	bulk	-	
	NR	RS-M	beta	60x100	-100	300	70	1e-7	bulk	-	
	RX	k-ϵ-M	beta	60x160	-100	700	70	1e-7	bulk	M-I-B	
	RX	RS-M	beta	60x160	-100	700	70	1e-7	bulk	M-I-B	

Legend

NR	Non-Reacting
RX	Reacting
RS-JM	Reynolds Stress Model, Jones-Musonge
web	Initial conditions as specified on the web
bulk	Initial conditions based on bulk velocities
Full-Eq	Full equilibrium, fast chemistry assumption
Part-Eq	Partial, constrained equilibrium assumption
FLT 10	Flamelet model with a stretch rate of a=10/s
FLT 100	Flamelet model with a stretch rate of a=100/s
FLT 100	Flamelet model with a stretch rate of a=100/s
M-I-B	Mixed-Is-Burned (fast Chemistry assumption)

Model Constants

Sydney	k-ϵ-M	c_ν=0.09	$c_{\epsilon 1}$=1.6	$c_{\epsilon 2}$=1.92	
		σ_k=1.0	σ_ϵ=1.3	σ_ϕ=0.7	
		$c\xi(v1)$=2.8	$c\xi(v2)$=2.0		
Sydney	RS-M	c_ν=0.09	$c_{\epsilon 1}$=1.6	$c_{\epsilon 2}$=1.92	
		σ_k=1.0	σ_ϵ=1.3	σ_ϕ=0.7	
		c_{p1}=1.8	c_{p2}=0.6	c_{p3}=0.5	
		c_S=0.22			
Delft	k-ϵ-M	c_ν=0.09	$c_{\epsilon 1}$=1.6	$c_{\epsilon 2}$=1.92	
		σ_k=1.0	σ_ϵ=1.3	σ_ϕ=0.7	
		$c\xi(v1)$=2.8	$c\xi(v2)$=2.0		
Delft	RS-M	c_ν=0.09	$c_{\epsilon 1}$=1.6	$c_{\epsilon 2}$=1.92	
		σ_k=1.0	σ_ϵ=1.3	σ_ϕ=0.7	
		c_{p1}=1.8	c_{p2}=0.6	c_{p3}=0.55	
		$c_{1\phi}$=3.0	$c_{2\phi}$=0.5	$c_{3\phi}$=0.5	
		c_S=0.22	c_{SE}=0.18	c_{SF}=0.22	c_{SV}=0.22
Delft	RS-JM	c_ν=0.09	$c_{\epsilon 1}$=1.4	$c_{\epsilon 2}$=1.90	
		Other constants specified elsewhere			
Korea	k-ϵ-S	c_ν=0.09	$c_{\epsilon 1}$=1.44	$c_{\epsilon 2}$=1.92	
Leeds	RS-S	c_ν=0.09	$c_{\epsilon 1}$=1.44	$c_{\epsilon 2}$=1.92	
		σ_k=1.0	σ_ϵ=1.3	σ_ϕ=0.7	
		c_{p1}=1.8	c_{p2}=0.6	$c_{\epsilon 3}$=0.2	
		c_S=0.22			

The various computations performed by Leeds and the Delft groups were plotted separately. Each set of runs was compared with experimental data. The most appropriate cases were selected for further comparisons. For the Delft runs it was that the RS-JM calculations are way off. The RS-M calculations with flamelet chemistry (a=100/s) was found to be the most relevant. For the Leeds computations, the flamelet with an intermediate stretch rate (a=100/s) was chosen. The following cases were selected for further comparisons:

Non-Reacting

Group	Reference	Line format
Korea, NR, k-ϵ-S	K-NKES	blue-dashed
Sydney, NR, k-ϵ-M	S-NKEM	red-dashed
Leeds, NR, RS-S	L-NRSS	black-solid
Sydney, NR, RS-M	S-NRSM	purple-solid

Reacting

Group	Reference	Line format
Korea, RX, k-ϵ-S, CMC	K-RKES	blue-dashed
Sydney, RX, k-ϵ-M, M-I-B	S-RKEM	red-dashed
Delft, RX, RS-M, FLT 100	D-RRSM	green-solid
Leeds, RX, RS-S, FLT 100	L-RRSS	black-solid
Sydney, RX, RS-M, M-I-B	S-RRSM	purple-solid

Discussion

Non-Reacting Case

Flowfield
Figures 3 and 4
All cases perform rather well in the upstream regions at x=10 and 20mm. Differences start to appear toward the end of the recirculation zone at x=40 where the modified models become superior. The standard models, both k-ϵ and RS overpredict the jet decay rate. The standard k-ϵ model overpredicts the spreading rate of the jet. The turbulence field predictions are adequate although the scatter in the turbulence data appears to be significant.
Note:
The modified RS model predicts a stronger recirculation at x=10 and 20mm. The reasons for this need to be investigated. Both standard and modified RS models fail to predict the correct turbulence levels in the jet, however, the turbulence data may not be reliable in certain regions of this flow.

Mixing field
Figure 5
The standard k-ϵ model overpredicts the spreading rate which is captured very well by the modification. The standard RS model gives the best predictions for the mean mixture fraction. The modified k-ϵ model gives the closest predictions for the rms fluctuations of mixture fraction except at x=65mm where the centreline values are higher than the computed ones.

Reacting Case

Flowfield
Figures 6, 7, 8 and 9
As in the non-reacting case, all models perform well at x=10 and 20mm. Differences start to appear at x=30mm where the standard models give faster decay rates. The Modified RS models give superior predictions of the decay and spreading rates both in the recirculation zone and further downstream at x=90mm. The turbulence field is adequately predicted by the modified RS model except at x=45 and 90mm where all models fail. The scatter in the turbulence data is significant and this may be a cause of uncertainty.

Mixing field
Figures 10 and 11

Unlike in the non-reacting case, both standard k-ϵ and RS models overpredict the decay rate of the jet. The modified k-ϵ and RS models yield much better predictions down to x=120mm which is way downstream of the recirculation zone. The modified RS model also gives superior predictions for the rms fluctuations of mixture fraction.

Note: Flame HM1, which is chosen here for comparison with predictions, is at 50% off the blow off limit. Single-point data collected near the burner's exit plane show that this flame experiences slight liftoff which leads to an intermittent behaviour in the reactive scalar data collected close to the burner. This leads to artificially lower averages of temperature and reactive species mass fractions. Flame HM2 (178m/s) which is at 75% off blow off does not show this intermittent behaviour at the nozzle exit plane. Measured averages of mixture fraction, temperature and mass fractions of OH for flame HM2 are, therefore, also shown for locations close to the burner's exit plane at x=10 and 20mm. This is justified since it has been shown in Dally's PhD thesis that, within the recirculation zone, the fast chemistry assumption may be made regardless of the jet velocity (as long as the flame is burning in a stable mode)

Reactive scalar field
Figures 12 and 13

Radial profiles of mean temperature indicate that within the recirculation zone (profiles at x=13, 30 and 45), the modified turbulence model (k-ϵ-M and RS-M) along with the fast chemistry assumption yield the best results. Using flamelet modeling is not necessary is this region of the flow and the fast chemistry assumption is adequate.

Further downstream, at x=90 and 120mm, the fast chemistry assumption fails, as expected and for this particular flame the flamelet model along with the modified RS model is more appropriate. It should be noted here that, at higher jet velocities, the flame will approach extinction and this flamelet formulation will no longer be adequate unless scalar dissipation rate effects and transient effects are accounted for.

None of the approaches used here produces adequate computations for the hydroxyl radical, OH. The flamelet model calculations give broader profiles of OH with peak values that are generally higher than the measured ones. The CMC approach with detailed chemistry gives profiles of OH that are too narrow with higher peak values as well.

Conclusions

The following conclusions may be drawn:

- The modified k-ϵ or RS models should be used for computing bluff-body stabilised jets and flames (Constant $c_{\epsilon 1}$ should be changed from 1.44 to 1.6).
- Convergence for RS models is hard to achieve. The modified k-ϵ model should therefore be used whenever possible.
- In the non-reacting jet (NR), the modified RS model gives stronger flow reversals in the recirculation zone. The reasons for this need to be investigated.
- More flowfield data are needed for reacting and non-reacting bluff-body stabilised flows.

- The fast chemistry assumption is quite adequate in the recirculation zone of bluff-body stabilised flames. However, this will give good predictions for the mean temperature field and possibly those of stable species only. Reactive scalars such as hydroxyl radicals require more complex chemistry models.
- Flamelet models based on a single variable formulation do not have any particular advantage in the recirculations zone.

Ackowledgement
Thanks to all the groups who have contributed their computations for the comparisons presented here. Special thanks to Dr Bassam Dally for plotting the results.

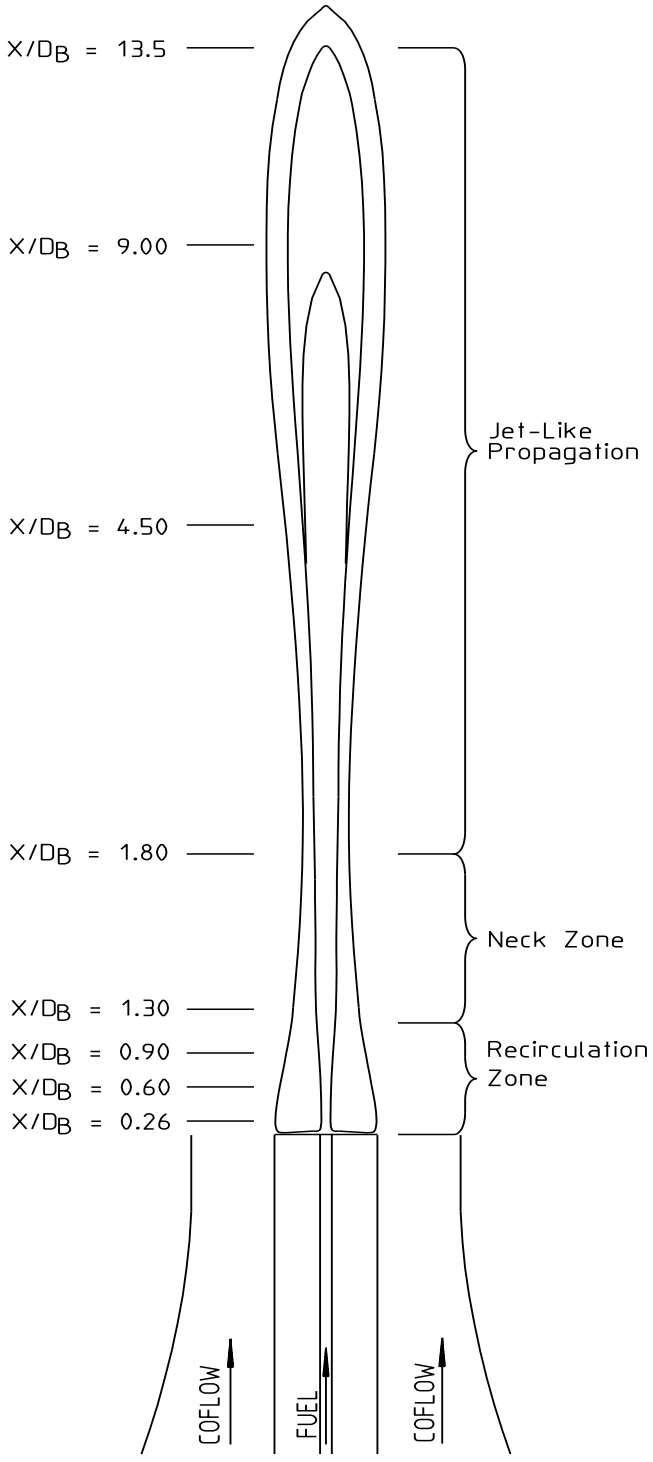

Figure 1: Sketch of a typical bluff-body stabilised flame and the measurement locations.

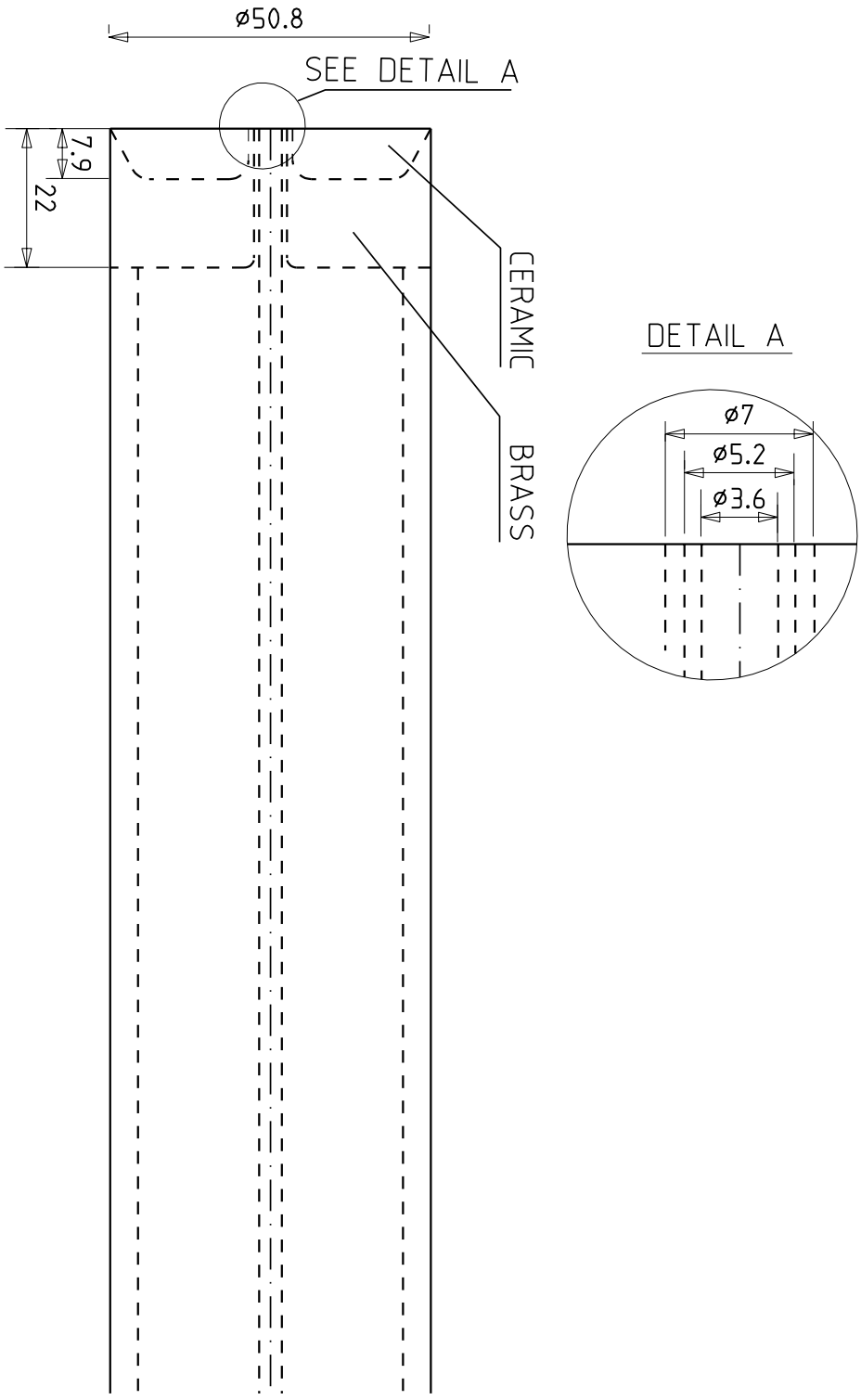

Figure 2: Detailed engineering drawing of the top section of the bluff-body burner.

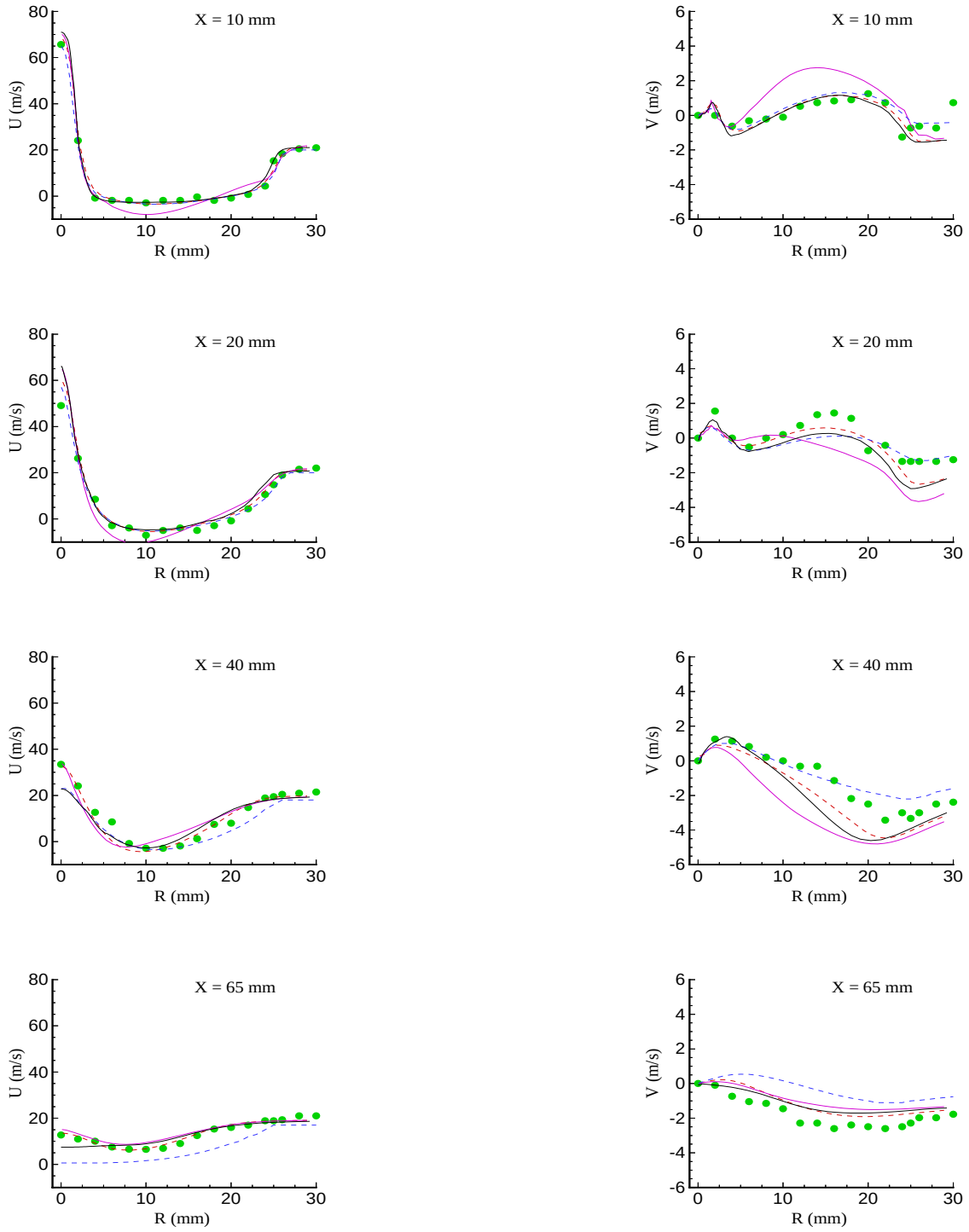

Figure 3: Radial profiles of mean axial (U) and radial (V) velocity in the non-reacting C_2H_4 jet (bulk jet velocity = 62m/s, coflow air velocity =20m/s). Green solid dots: Experimental data; red-dashed line : Sydney, k-ϵ-M (S-NKEM); blue-dashed line: Korea, k-ϵ-S (K-NKES); black-solid line: Leeds, RS-S (L-NRSS).

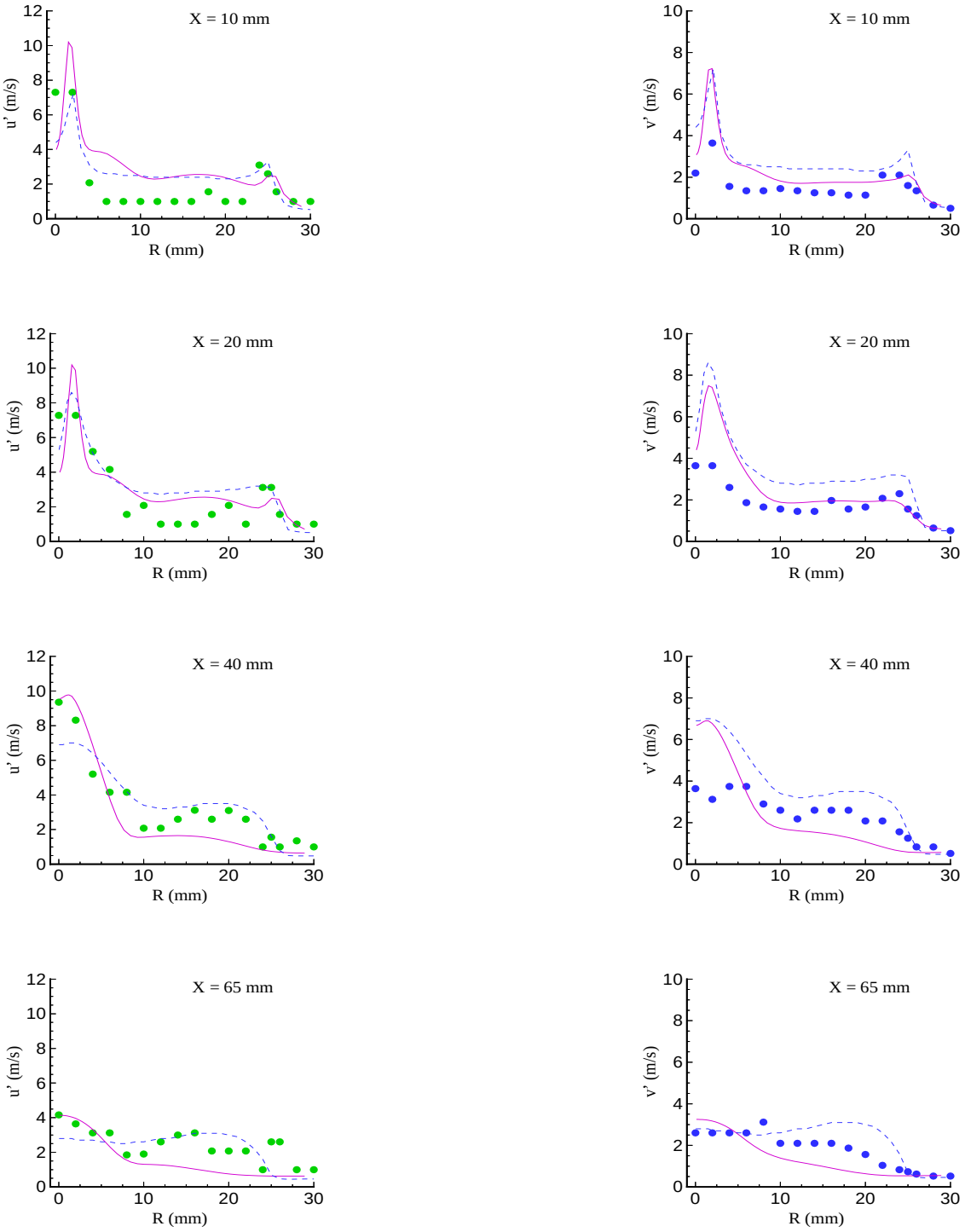

Figure 4: Radial profiles of rms fluctuations of axial (u') and radial (v') velocity in the non-reacting C_2H_4 jet (bulk jet velocity = 62m/s, coflow air velocity =20m/s). Legend as in Fig. 1.

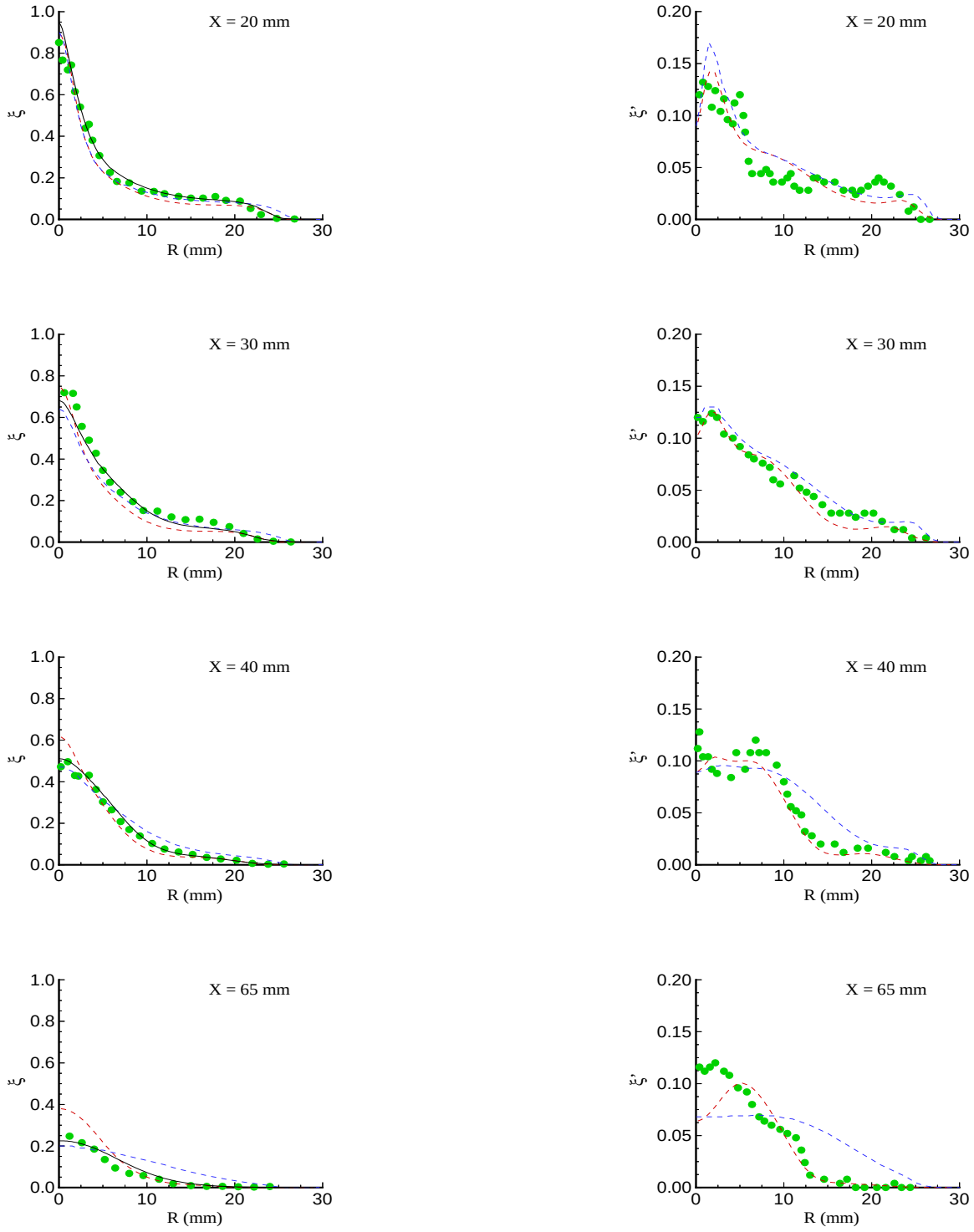

Figure 5: Radial profiles of mean mixture fraction (ξ) and its rms fluctuations (ξ') for the non-reacting C_2H_4 jet (bulk jet velocity = 62m/s, coflow air velocity =20m/s). Legend as in Fig. 1.

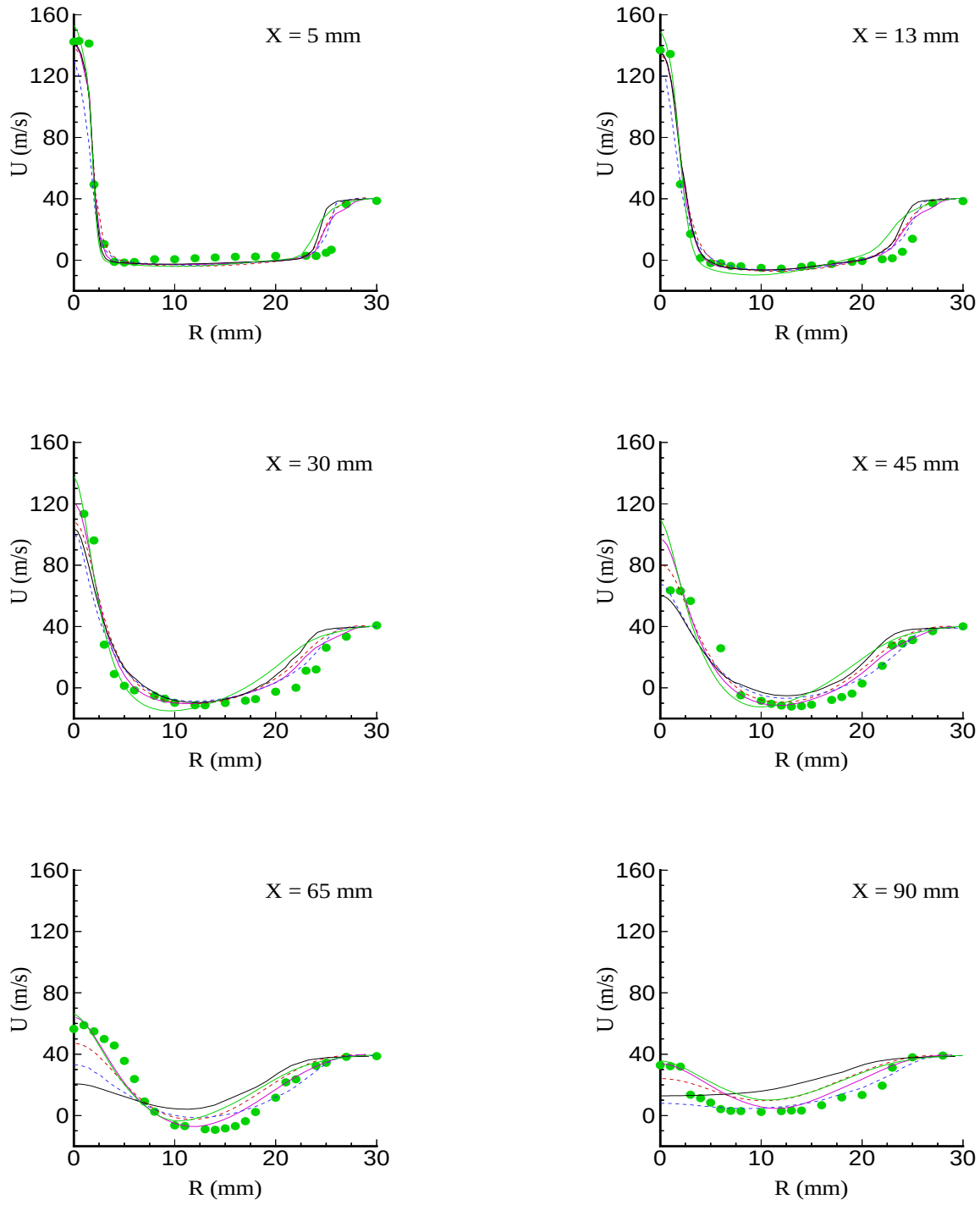

Figure 6: Radial profiles of mean axial (U) velocity in the reacting jet (case HM1) (CH_4/H_2 fuel, bulk jet velocity = 118m/s, coflow air velocity =40m/s). Green solid dots: Experimental data; blue-dashed line: Korea, k-ϵ-S (K-NKES); red-dashed line : Sydney, k-ϵ-M (S-NKEM); green-solid line: Delft, RS-M (D-RRSM); black-solid line: Leeds, RS-S (L-NRSS); purple-solid line: Sydney, RS-M (S-RRSM).

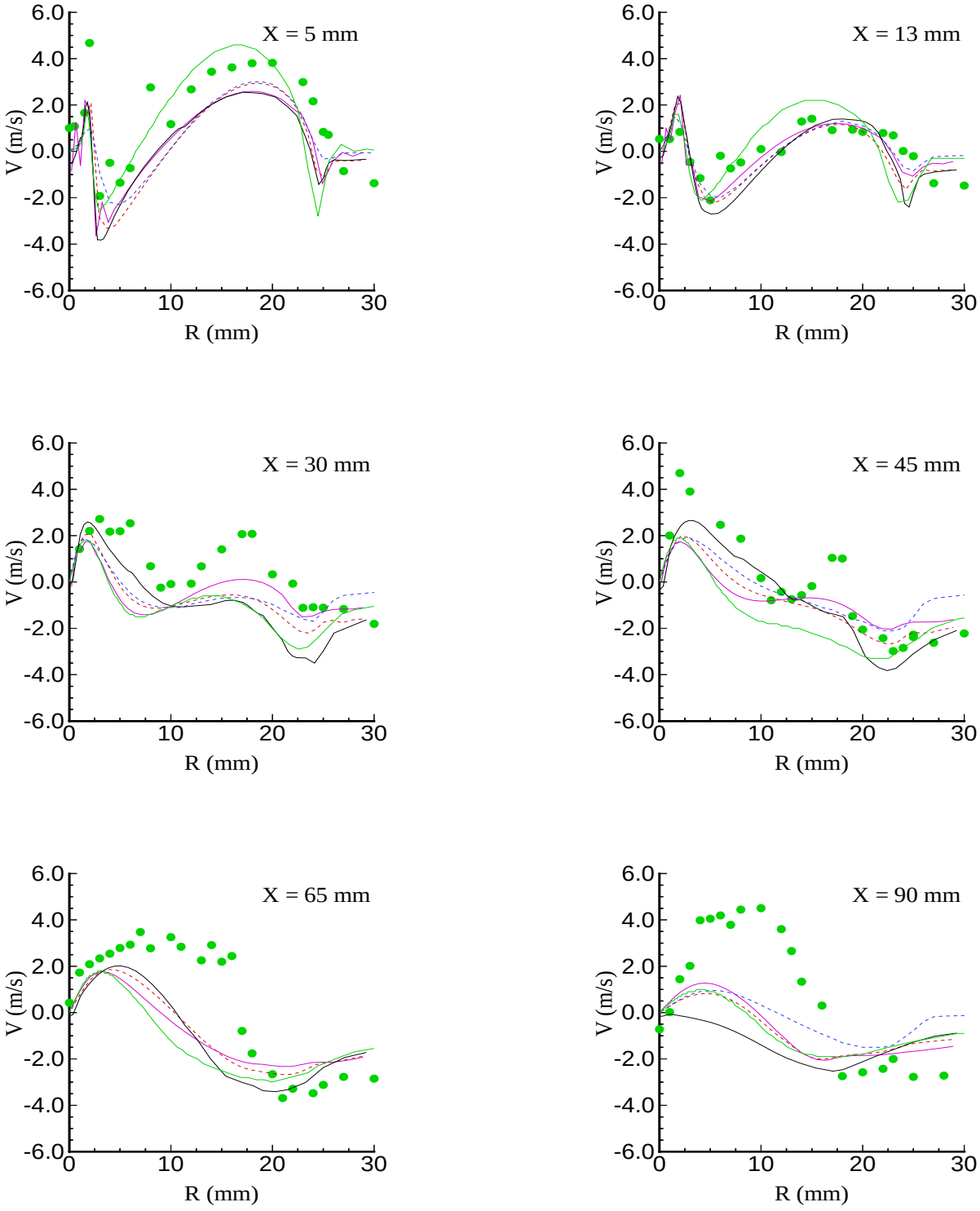

Figure 7: Radial profiles of mean radial (V) velocity in the reacting jet (case HM1) (CH_4/H_2 fuel, bulk jet velocity = 118m/s, coflow air velocity =40m/s). Legend as in Fig. 4.

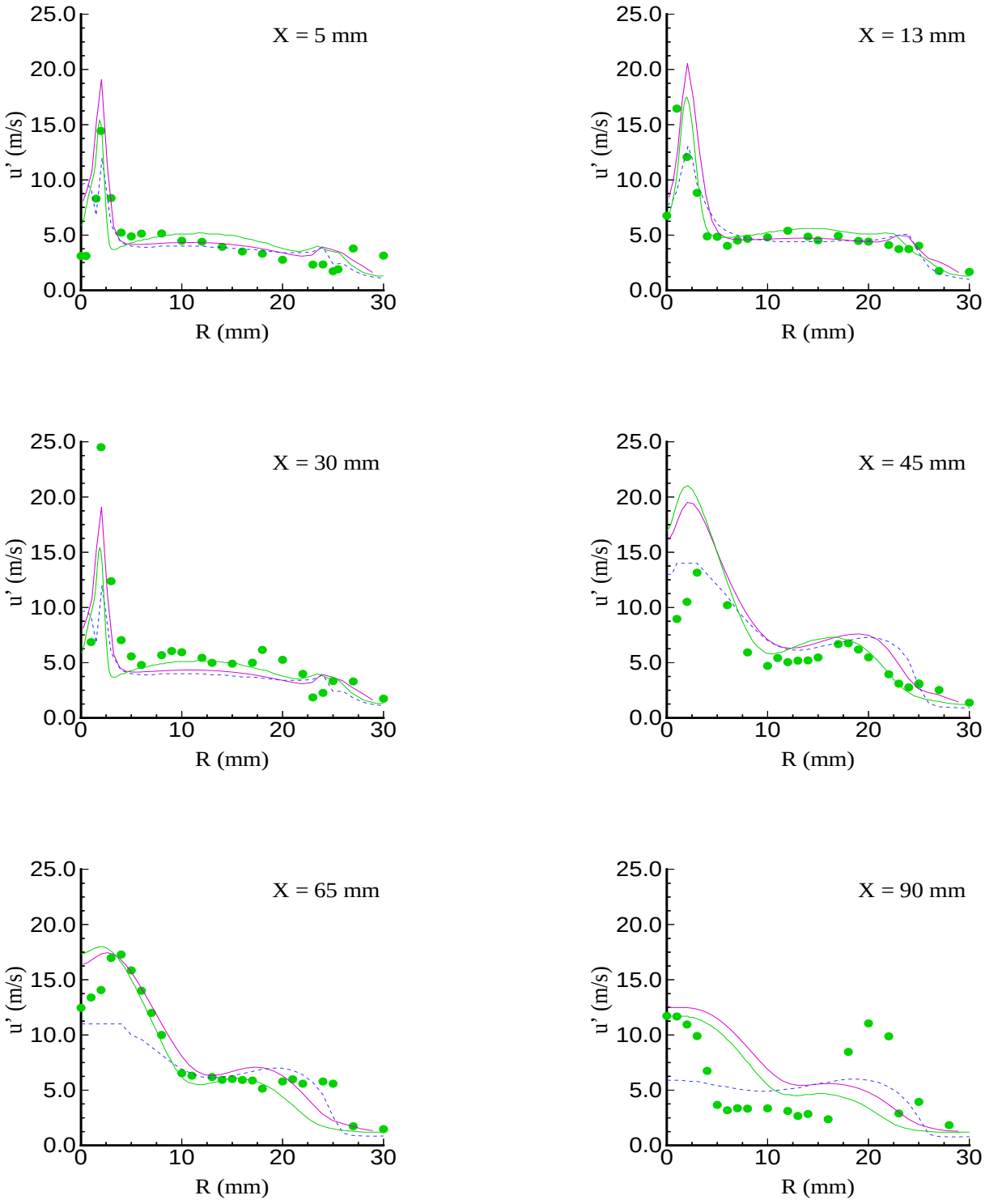

Figure 8: Radial profiles of rms fluctuations of the axial velocity (u') in the reacting jet (case HM1) (CH_4/H_2 fuel, bulk jet velocity = 118m/s, coflow air velocity =40m/s). Legend as in Fig. 4.

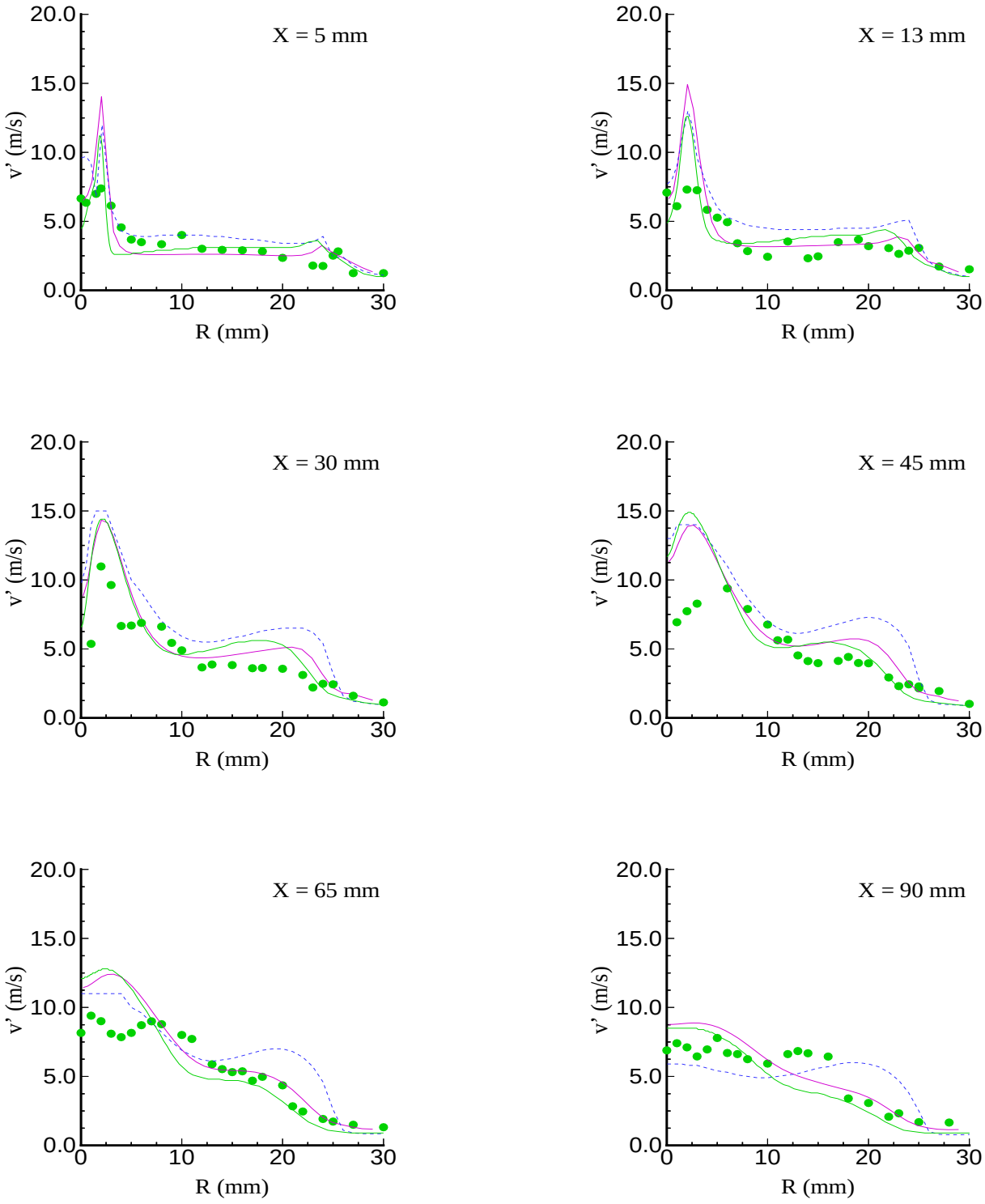

Figure 9: Radial profiles of rms fluctuations of the radial velocity (v') in the reacting jet (case HM1) (CH_4/H_2 fuel, bulk jet velocity = 118m/s, coflow air velocity =40m/s). Legend as in Fig. 4.

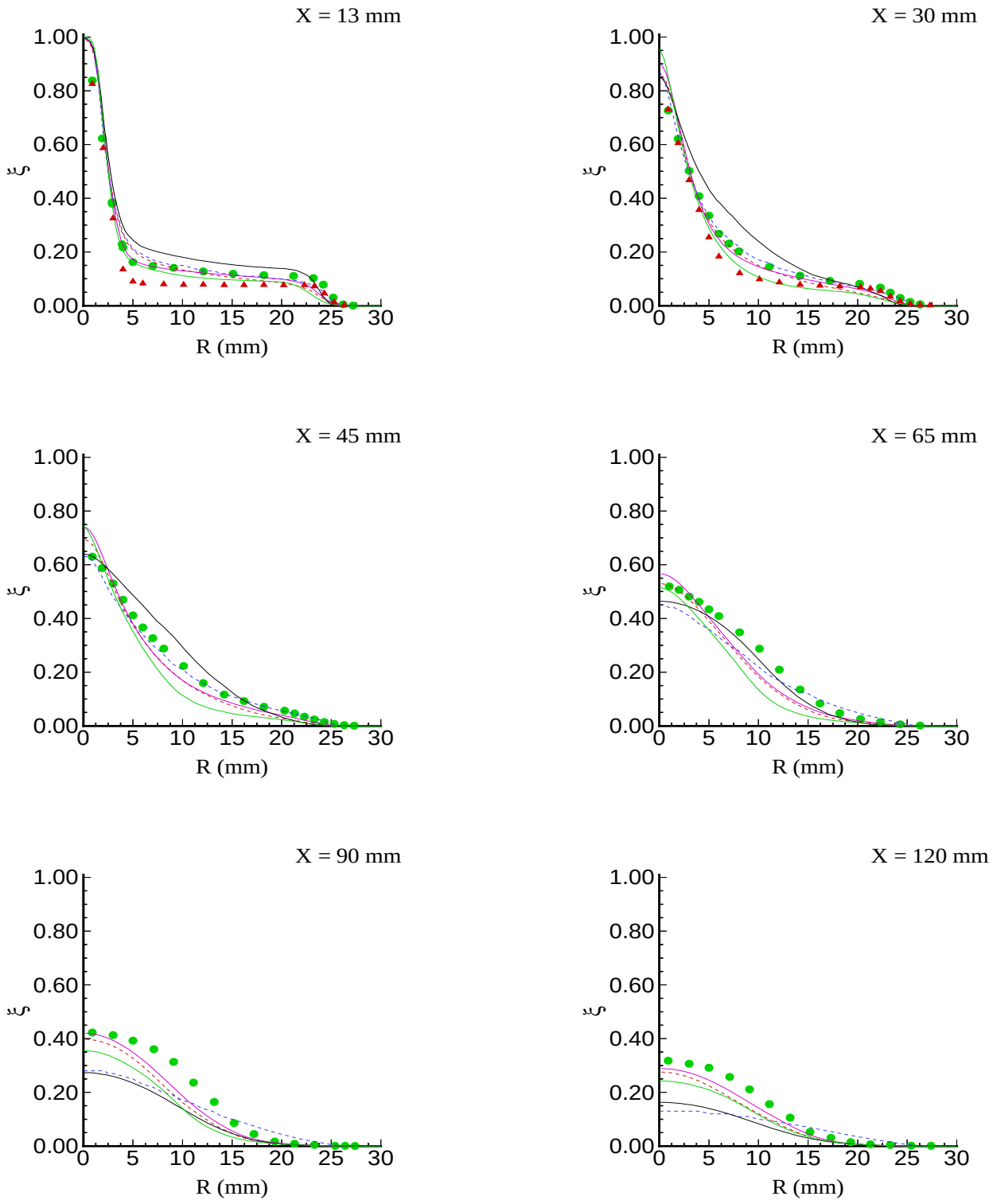

Figure 10: Radial profiles of mean mixture fraction (ξ) in the reacting jet (case HM1) (CH_4/H_2 fuel, bulk jet velocity = 118m/s, coflow air velocity =40m/s). Legend as in Fig. 4. Note: Red solid triangles shown for x=13 and 30mm are for flame HM2 which has a bulk jet velocity of 178m/s)

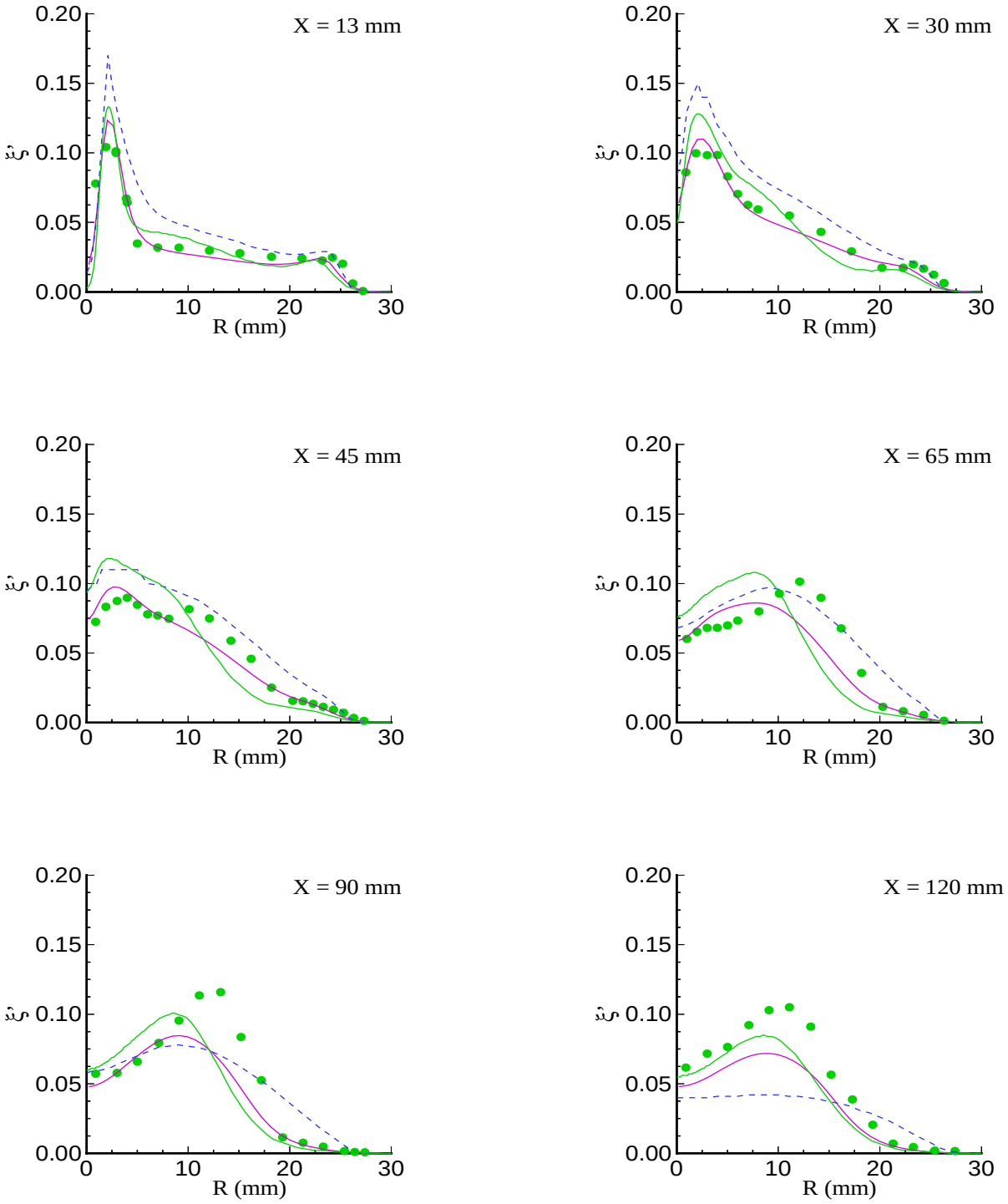

Figure 11: Radial profiles of the rms fluctuations of mixture fraction (ξ') in the reacting jet (case HM1) (CH_4/H_2 fuel, bulk jet velocity = 118m/s, coflow air velocity =40m/s). Legend as in Fig. 4.

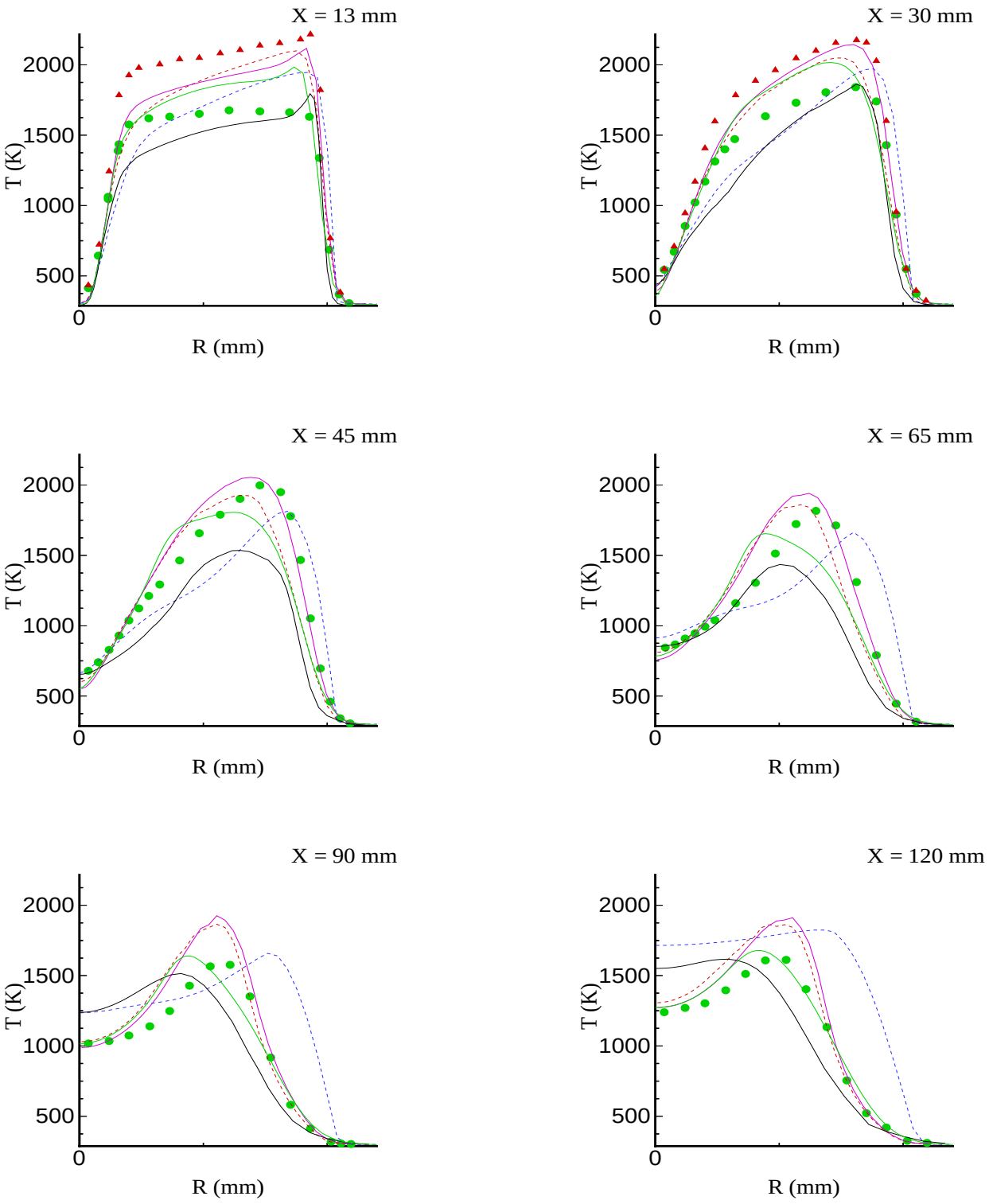

Figure 12: Radial profiles of mean temperature in the reacting jet (case HM1) (CH_4/H_2 fuel, bulk jet velocity = 118m/s, coflow air velocity =40m/s). Legend as in Fig. 4. Note: Red solid triangles shown for x=13 and 30mm are for flame HM2 which has a bulk jet velocity of 178m/s)

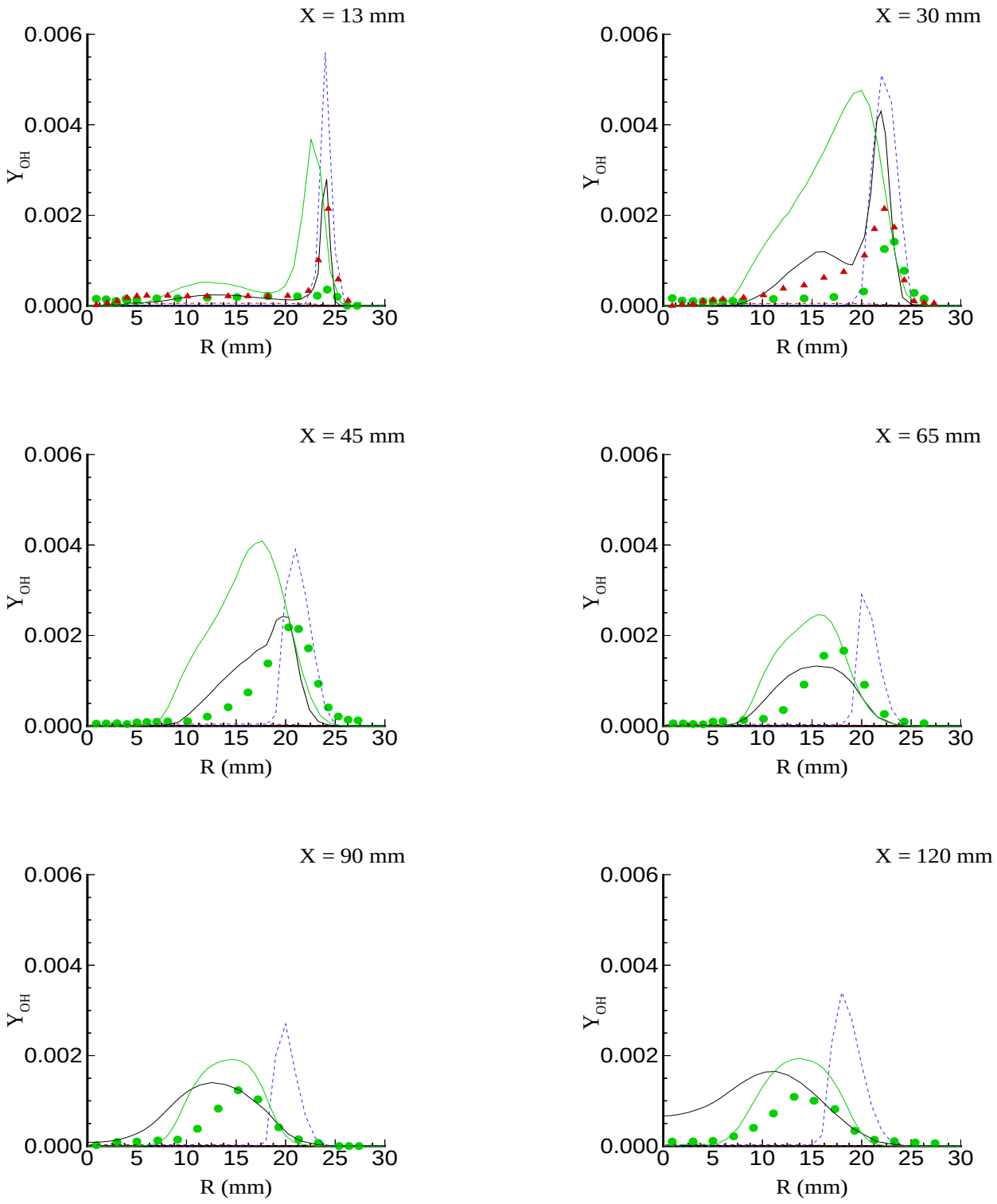

Figure 13: Radial profiles of mean mass fraction of OH in the reacting jet (case HM1) (CH_4/H_2 fuel, bulk jet velocity = 118m/s, coflow air velocity =40m/s). Legend as in Fig. 4. Note: Red solid triangles shown for x=13 and 30mm are for flame HM2 which has a bulk jet velocity of 178m/s)

SECTION 5

Poster Abstracts

ABSTRACTS

R.S. Barlow and J.H. Frank
"Experimental Results on Differential Molecular Diffusion in Piloted Methane-Air Jet Flames"

B. Bédat, F.N. Egolfopoulos and T. Poinsot
"Direct Numerical Simulation of NO_x Formation in Turbulent Non-Premixed Flames"

E.S. Bish
"An Evaluation of Practical Numerical Approaches for Modeling the Near Field Dynamics in a Step Swirl Combustor"

E.A. Brizuela and V. Echaniz
"Limits to the Scalar PDE's When Using a 4-Step Reaction Scheme"

S. Caillat, M.S. Cabot and G. Cabot
"Measurements and Modeling of NO_x Emission in CH_4/Wet Air Swirl Diffusion Flame"

C. M. Cha, G. Kosály and J.C. Kramlich
"Comment on the Quasi-Steady Modeling of a Hydrogen/Air Jet Flame"

B. B. Dally and A.R. Masri
"Evaluation of Differential Diffusion in Turbulent Nonpremixed Flames"

T. Echekki, A.R. Kerstein and J.-Y. Chen
"Modeling of Turbulent Nonpremixed Flames Using One-Dimensional Turbulence"

J. Fielding, A.M. Schaffer and M.B. Long
"Three-Scalar Measurements for Mixture Fraction Determination in Nonpremixed Methane Flames"

J.H. Frank and R.S. Barlow
"Mixture Fraction Measurements with Two Scalars in Turbulent Nonpremixed Methane Air-Flames"

G. Grünefeld, H. Finke, A. Gräber, A. Diekmann, S. Krüger and J. Bartelheimer
"Species, Temperature, and Velocity Measurements in a Turbulent Jet Flame and a Laminar Unsteady Flame"

A. Hinz, E.P. Hassel and J. Janicka
"Numerical Simulation of a Turbulent Piloted Methane/Air Jet Flame (Flame D) Using a Finite-Volume-Monte-Carlo-PDF Code"

T. Landenfeld, A. Kremer, E.P. Hassel and J. Janicka
"SMC Modeling of Strongly Swirling Natural Gas Flames"

R. P. Lindstedt, J.P.H. Sanders and E.M. Váos
"Joint Scalar PDF Monte Carlo Simulations of a H_2/CO_2 Turbulent Jet Diffusion Flame with Comprehensive Chemistry"

W. Malalasekera, J.C. Jones and M. Hossain
"Modeling of Turbulence-Radiation Interactions in Combustion Systems"

W. Meier, O. Keck, D. Wolff, V. Bergmann, V. Jörres and W. Stricker
"Investigation of a Turbulent CH_4/H_2N_2 Jet Diffusion Flame: Survey of Experimental and Theoretical Results"

S. Menon
"Parallel Large-Eddy Simulations of Reacting Single- and Two-Phase Flows using a Subgrid Combustion Model"

J.H. Miller
"Stretching Exercises: Flickering Flames as a Test of Our Understanding of Chemistry-Turbulence Interaction"

V. Nilsen and G. Kosály
"Differential Diffusion in Turbulent Reacting Flows"

P. A. Nooren, H.A. Wouters, T.W.J. Peeters and D. Roekaerts
"Monte Carlo PDF Calculations of the Delft III Flame"

P. A. Nooren, R.S. Barlow and J.H. Frank
"Rayleigh-Raman-LIF Measurements in the Delft III and IV Flames"

R.N. Paul, Y.R. Sivathanu and J.P. Gore
"Computation of Sandia Piloted CH_4/Air Jet Flames using Laminar Flamelet State Relationships"

T.W.J. Peeters, H.A. Wouters, and D. Roekaerts
"Second Moment Closure and PDF Calculations of a Bluff-Body Stabilized CH_4/H_2 Flame"

H. Pitsch, M. Chen and N. Peters
"Unsteady Flamelet Modeling of a Turbulent CH_4/H_2N_2 Diffusion Flame"

W. M. Pitts
"Resolution Requirements for Scalar Dissipation Measurements in Turbulent Jets and Flames"

M. Pourkashanian, G. Spence and A. Williams
"Assessment of Strained-Flamelet Prediction of a CH_4/H_2 Turbulent Non-Premixed Flame"

M.W. Renfro, S.D. Pack, A. Lakshmanarao, G.B. King and N.M. Laurendeau
"Quantitative Hydroxyl and Temperature Time-Series Measurements in Turbulent Nonpremixed Flames"

M.R. Roomina and R.W. Bilger
"Conditional Moment Closure (CMC) Predictions in Methane-Air Piloted Jet Flames"

T. Settersten, C. Fisher, N. Middleton and M. Linne
"Mode-Locked, Picosecond Laser-Based Diagnostics and Novel Sensors for Turbulence Measurement"

F. Takahashi, M.D. Vangsness, M.D. Durbin and W.J. Schmool
"Turbulence Structure of Swirling Hydrogen Jet Diffusion Flames"

M. Versluis, P. Nooren, R. Knikker, M.-C. Zong and T. van der Meer
"CARS Temperature Measurements in the Delft Jet Diffusion Flame: Flame III"

K. Xiao, D. Schmidt and U. Maas
"PDF Simulation of a Recirculating Stabilized Turbulent Nonpremixed Flame"

J. Xu and S.B. Pope
"PDF Modeling of Turbulent Non-Premixed Methane Flame: Numerical Aspects"

B. Zamuner, and F. Dupoirieux
"Numerical Simulation of a Swirl-Stabilized Turbulent Diffusion Flame with a Presumed Probability Density Function (PDF) Model"

EXPERIMENTAL RESULTS ON DIFFERENTIAL MOLECULAR DIFFUSION IN PILOTED METHANE-AIR JET FLAMES

R. S. Barlow and J. H. Frank
Sandia National Laboratories
Livermore, California
USA

The relative importance of differential molecular diffusion and turbulent transport is investigated in a series of methane-air jet flames by analyzing multiscalar point measurements. A piloted burner developed by Sydney University is operated with the composition of the main jet being 25% CH_4 and 75% by volume. Temperature and the mass fractions of N_2, O_2, CH_4, CO_2, H_2O, CO, H_2, and OH are measured using simultaneous Rayleigh scattering, Raman scattering, and laser-induced fluorescence. Six flames, having Reynolds numbers ranging from 1,100 (laminar) to 44,800 (turbulent with significant localized extinction), are considered. These flames are also described in a 27th Combustion Symposium paper [1], which reports conditional probability density functions of species mass fractions. This poster presents results on the differential diffusion parameter, *z*, which indicate that turbulent transport becomes dominant over molecular diffusion in determining major species mass fractions within the range of flow conditions and measurement locations considered in these experiments.

Elemental mixture fractions of hydrogen and carbon are calculated from the measured mass fractions. The degree of differential diffusion is then quantified as the difference between these elemental mixture fractions, $z=F_H-F_C$. The conditional mean and rms fluctuation of *z* are compared in the series of flames, with the conditioning variable being the mixture fraction defined as:

$$F_{HC} = \frac{(Y_H - Y_{H,2})/2w_H + 2(Y_C - Y_{C,2})/w_C}{(Y_{H,1} - Y_{H,2})/2w_H + 2(Y_{C,1} - Y_{C,2})/w_C}$$

where *Y*'s are elemental mass fractions, *w*'s are atomic weights, and subscripts 1 and 2 refer to the main jet and coflowing air stream, respectively. Partial premixing with air causes boundary conditions for the elemental mass fraction of oxygen to be relatively close, and this leads to excessive noise in the mixture fraction if oxygen is included in the calculation. The stoichiometric value of the mixture fraction is F_{HC}=0.351 in these flames.

Figure 1 shows that results from the laminar jet flame (Re=1,100) are in good agreement with results from steady, opposed-flow calculations using the Sandia Tsuji-flame code and the Chemkin transport package. Both show hydrogen deficits for mixture fractions in the approximate interval $0.25<F_{HC}<0.80$, with *z* dipping to about -0.1 near F_{HC}=0.45, and both show excess hydrogen outside this interval. As Reynolds number is increased through transitional and turbulent flames, as shown in Fig. 2, the magnitude of the conditional mean of *z* decreases. At the measurement location 15 nozzle diameters from the jet exit in the highest Reynolds number flames (Re=33,600 and 44,800) the conditional mean of *z* is comparable to that measured in the products above a premixed CH_4-air, where the small non-zero result is due to 1-2% systematic error in the calibrations (Fig. 3). The rms fluctuations of *z* in the highest Re flames are comparable to those measured in the steady premixed flat flames. These results show that differential diffusion effects in methane-air jet flames become too small to be measured with current diagnostic capabilities within the range of Reynolds numbers reported here. The implication is that turbulent transport becomes dominant over molecular diffusion within the ranges of flow conditions and streamwise location considered in this study.

1. Barlow, R. S. and Frank, J. H., "Effects of Turbulence on Species Mass Fractions in Methane/Air Jet Flames," *Twenty-Seventh Symposium (International) on Combustion*

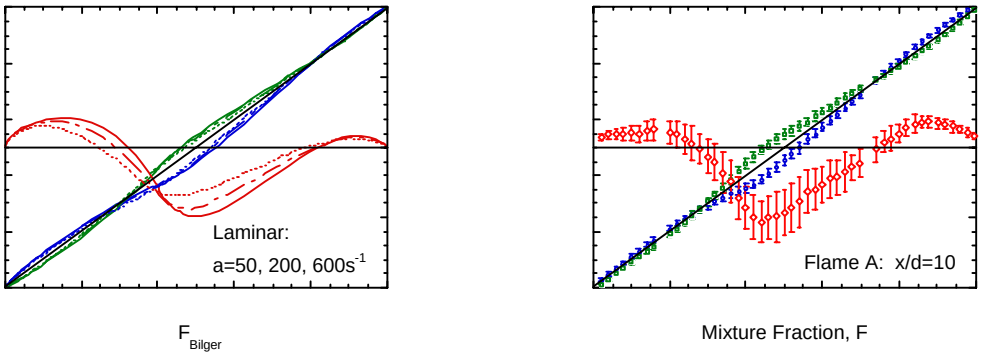

Fig. 1. Elemental mixture fractions, F_H and F_C, and the differential diffusion parameter, *z*, calculated for three steady, strained, opposed-flow laminar flames and measured in the laminar jet flame.

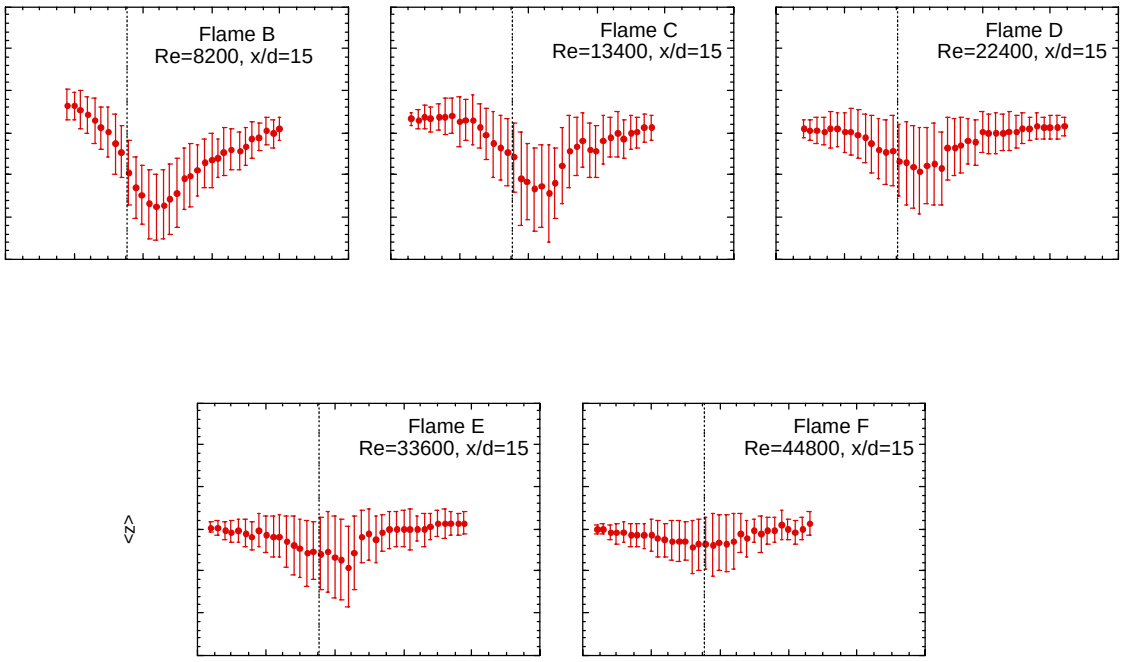

Fig. 2. Progression of the conditional mean and rms of *z* at x/d=15 in the turbulent flames.

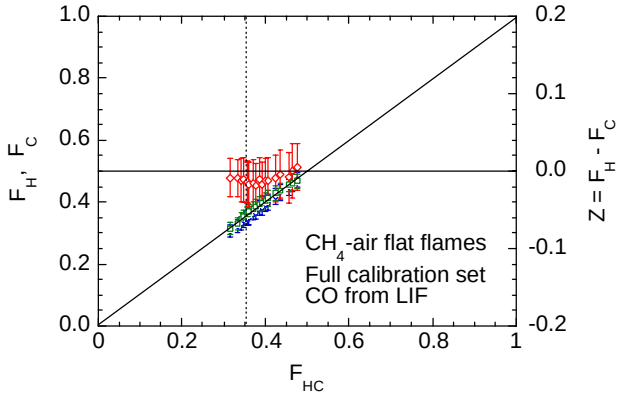

Fig. 3. Measured mean and rms of *z* in premixed laminar flat flames, where z=0 is expected.

Direct Numerical Simulation of NO_x formation in turbulent non premixed flames

Benoit Bédat[1], Fokion N. Egolfopoulos[2] and Thierry Poinsot[3]

(1)Centre de Recherche sur la Combustion Turbulente and Centre Européen de Recherche et de Formation Avancée en Calcul Scientifique, Toulouse, France
(2)Department of Mechanical Engineering, University of Southern California, Los Angeles, California, 90089-1453, USA
(3)CNRS, Institut de Mécanique des Fluides de Toulouse and Centre Européen de Recherche et de Formation Avancée en Calcul Scientifique, Toulouse, France

Direct Numerical Simulation (DNS) of turbulent reacting flows is a promising approach towards the understanding and modeling the physics of such flows. In the past, unreliable reduced chemical schemes have been incorporated in DNS and attempts to use complex chemistry and transport for kinetically simple systems, such as H_2/air and CH_4/air, resulted in excessive needs of memory and CPU time. Including a more realistic chemistry while keeping the need in computer resources low is the objective of this work. It presents a methodology (Integrated Combustion Chemistry (ICC)) capable of integrating complex chemistry effects. This methodology includes the use of a limited number of species and reactions with parameters which are derived to match a number of flame properties. It is illustrated through a four-step reaction mechanism appropriate for stoichiometric methane/air flame, and which compares favorably with predictions of the detailed GRI 2.1 mechanism. The proposed scheme includes one reaction for the methane oxidation, one for the thermal, one for the Fenimore and one for the non-premixed reburn chemical NO_x routes.

CH4+2O2	$\rightarrow$	CO2+2H2O	R1
N2 + O2	$\rightarrow$	2NO	R2
N2 + CH4 +02	$\rightarrow$	2NO + CH4	R3
2NO + CH4	$\rightarrow$	N2 + O2 +CH4	R4

The kinetic parameters for the hydrocarbon oxidation were determined by matching the GRI 2.1 predictions for laminar flame speed and adiabatic flame temperature, main reactants concentrations, and extinction strain rates for both premixed and non-premixed strained laminar flames (see schematic diagram, figure 1). Comparison between the GRI 2.1 and proposed reduced scheme is plotted on figure 2 and shows a good agreement. The kinetic parameters for the three steps corresponding to NO_x chemistry were determined through comparisons with the NO_x profiles obtained by using the GRI 2.1 scheme (see figure 3).

Finally, this four-step mechanism was used in two and three-dimensional turbulent non-premixed combustion DNS. It was found that the predominant formation mechanism is the Fenimore one and that the maximum of NO level is localized for rich mixture. A flamelet model has been derived from asymptotic theory with finite rate chemistry [1, 2, 3]. A shape relation between the scalar dissipation and the mixture fraction is introduced which takes into account non equilibrium effect on the chemistry.

$$\chi = \chi_f F_f(Z) \tag{1}$$

with

$$F_f(Z) = \left(\frac{\rho}{\rho_f}\right)^2 \left[\exp\left(erf^{-1}(1-2Z_f)^2 - erf^{-1}(1-2Z)^2\right)\right]^2 \tag{2}$$

where Z_f and ρ_f are the mixture and the density at the stochiometrix conditions. Compared to the shape function introduced by Peters [1], this formulation is valid for any Z_f. Three turbulent cases have been considered corresponding to three regimes; Steady laminar flamelet, Unsteady laminar flamelet with few quenching and Unsteady laminar flamelet with quenching [4].

Model (equations 1 and 2) is applied to turbulent conditions and shows its ability to predict the reaction rates. The precision is very good for Steady laminar flamelet case to good for Unsteady laminar flamelet with quenching case (see figure 4)

References

[1] N. Peters. *Combust. Sci. and Tech.*, 30:1–17, 1983.

[2] A. Linan. *Acta Astronautica*, 1:1007, 1974.

[3] B. Cuenot and T. Poinsot. *Comb. Flame*, 104(1/2):111–137, 1996.

[4] B. Cuenot and T. Poinsot. 25th Symp. (Int.) on Combustion, pages 1383–1390, Irvine, 1994. The Combustion Institute, Pittsburgh.

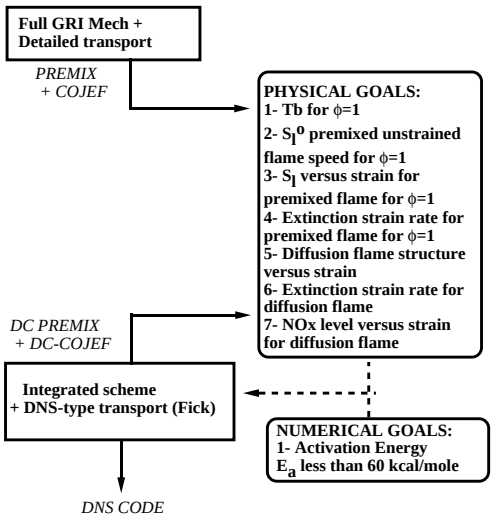

Figure 1: Schematic Diagram of ICC

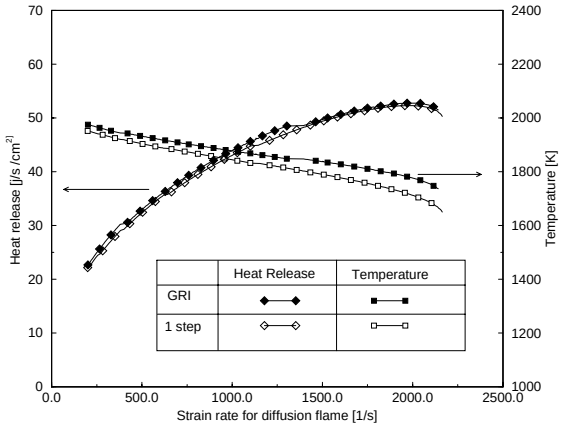

Figure 2: Response of the GRI 2.1 Mech and the hydrocarbon oxydation step in opposed jet flame configuration to a steady strain rate: integrated heat release across the flame and Maximum of temperature for non-premixed flame.

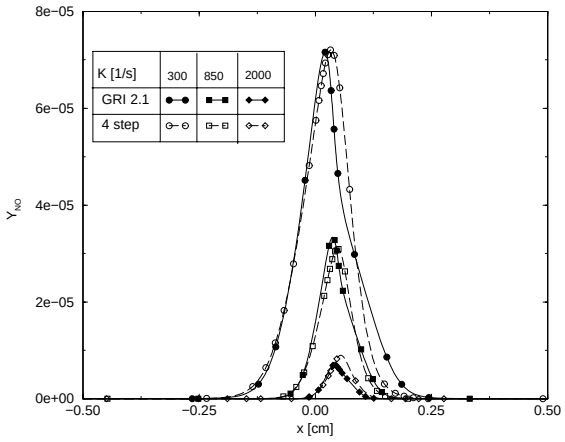

Figure 3: Comparison between the GRI 2.1 Mech with reduced NOx mechanism in non-premixed opposed jet flame configuration with a steady strain rate of 300, 850 and 2000 [1/s]

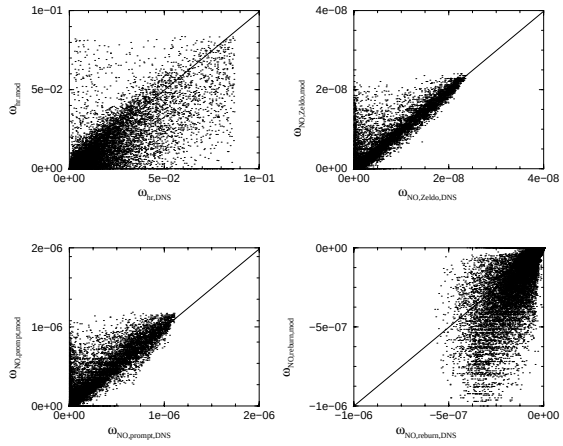

Figure 4: Point analysis for the three-dimensional turbulent case ($Re_t = u'L_t/\nu = 92$) corresponding to Unsteady laminar flamelet with quenching regime. Abscissa are DNS values and ordinate are model values. (a) heat release, (b) Zeldovitch reaction rate (R2), (c) Prompt reaction rate (R3) and (d) Reburn reaction rate (R4)

An Evaluation of Practical Numerical Approaches for Modeling the Near-field Dynamics in a Step Swirl Combustor

Eric S. Bish, Ph.D.
esb@fluent.com

Fluent Inc.
10 Cavendish Court
Lebanon, NH 03766-1442

The present study examines numerical simulations of a methane, step swirl combustor obtained using the CFD code FLUENT/UNS. These simulations follow the experimental investigation of Durbin *et al.*[1] The nonpremixed flame is stabilized by a swirl induced internal recirculation zone (IRZ) within the expanding near-burner region of the combustor. The major focus was to evaluate practical turbulence closure and turbulence-chemistry coupling models for flames of this type. The initial investigation involved simulations employing the Reynolds Stress Model (RSM) for turbulence closure and three different combustion chemistry models: the equilibrium chemistry PDF model[2] and an eddy break-up (EBU) model[3] using the originally derived rate constants and adjusted rate constants[4]. Consistent boundary conditions, fluid properties and discretization scheme were used for all cases to isolate the effects of closure models. Mean axial and swirl velocity and temperature profiles in the near-field region were compared with experimental measurements. These results show measurable differences in model predictions, with the simulation employing the EBU model with adjusted rate constants providing the most realistic flame shape and best predictions of swirl velocity. To examine the role of turbulence closure models, the same configuration was modeled using the EBU model with adjusted rate constants and replacing the RSM turbulence model with the two equation, standard k-ε and RNG k-ε models. Results show the inability of the standard k-ε model to capture the IRZ present within the combustor, leading to poor predictions of flame shape and velocity field. RNG k-ε results demonstrate strong agreement with experimental measurements, comparable to results obtained with the RMS model, despite the lack of accounting for nonisotropic turbulent shear stresses expected in the swirling flow. For confined, isothermal flows at comparable swirl numbers to the present study ($S \sim 0.4$), Durst & Wennerberg[5] suggest that the k-ε turbulence model can provide sufficiently good predictions of mean quantities, though the present results are more consistent with Favaloro *et al.*[6], who found the k-ε model inadequate. At higher swirl numbers, the RSM model has consistently demonstrated superiority over the standard k-ε turbulence model[7,8,9]. The strong agreement with experimental measurements demonstrated by the more economical RNG k-ε model is encouraging, but the applicability of the RNG k-ε model to swirl combustion applications is suspect at higher swirl numbers. Breussin *et al.*[10] obtained good agreement using the RSM model but poor results from both the k-ε and RNG k-ε models for a confined, reacting flow simulation with a swirl number of 1.0.

[1]Durbin, M.D., Vangsness, M.D., Ballal, D.R. & Katta, S.R. (1995) Study of flame stability in a step swirl combustor. ASME paper 95-GT-111, *Int'l Gas Turbine & Aeroengine Congress & Exp*., Houston, TX
[2]Bilger, R.W. *Prog. Energy Combust. Sci.* **16**, 109 (1976).
[3]Magnussen, B.F. & Hjertager, B.H. *16th Symposium (Int'l) on Combustion*. Combustion Institute, Pittsburgh, 1976, p 719.
[4]Visser, B.M., Smart, J.P., Van De Kamp, W.L. & Weber, R. *23rd Symposium (Int'l) on Combustion*. Combustion Institute, Pittsburgh, 1990, p 949.
[5]Durst, F. & Wennerberg, D. *Int. Jou. Num. Meth. Fl.*, **12**, 203 (1991).
[6]Favaloro, S. C., Nejad, A. S. & Ahmed, S. A. *J. Propulsion*, **7**, 348 (1989).
[7]Hogg, S. & Leschziner, M.A. *AIAA Jou.*, **27**, 57 (1989).
[8]Weber, R., Boysan, F., Swithenbank, J. & Roberts, P.A. *21st Symposium (Int'l) on Combustion*. Combustion Institute, Pittsburgh, 1986, p 1435.
[9]Weber, R., Visser, B. M. & Boysan, F. *Int. J. Heat Fluid Fl*, **11**, 225 (1990).
[10]Breussin, F., Pigari, F. & Weber, R. *26th Symposium (Int'l) on Combustion*. Combustion Institute, Pittsburgh, 1996, p 211.

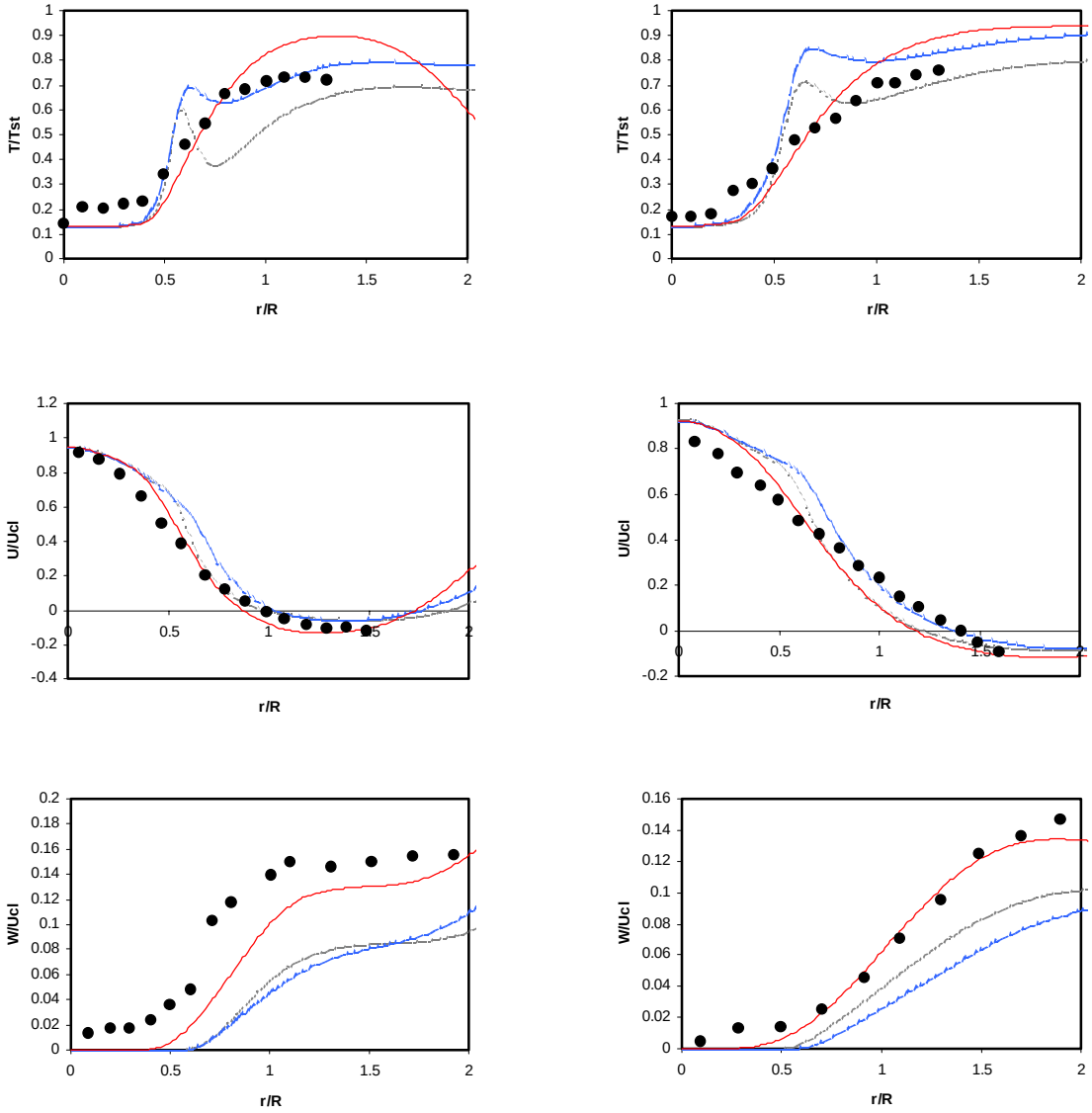

40 mm downstream

80 mm downstream

Radial profiles of mean temperature (top), axial velocity (middle) and swirl velocity (bottom) at locations 40 and 80 mm downstream of the burner exit. Measured data (circles) are compared with numerical simulations using the Reynolds stress turbulence closure model and three different combustion chemistry models: the equilibrium chemistry PDF model (gray dashed line) and an eddy break-up model using the originally derived rate constants (blue dot/dash line) and adjusted rate constants (red solid line). Only the simulation employing the EBU model with adjusted rate constants is seen to accurately predict the strength and location of recirculation zones established within the near field region of the combustor.

LIMITS TO THE SCALAR PDE´S WHEN USING A 4-STEP REACTION SCHEME

E. A. Brizuela* and V. Echaniz**

* Depto Mecanica y Naval, Fac. Ingenieria, Univ. de Buenos Aires, Paseo Colon 850, (1063) Capital, Argentina
E-mail: ebrizue@fi.uba.ar

** Depto Mecanica, Fac. Ingenieria, Univ. de Mar del Plata, J. B. Justo 4302, (7600) Mar del Plata, Argentina

INTRODUCTION

When using Reduced Reaction Schemes (RRS) to model tur-bulent diffusion flames, PDE´s are solved numerically for some of the scalars. It has been shown [1] that it is necessary to limit the ranges of the solutions to the PDE´s to avoid unphysical results, and accessible and allowable domains were defined. The accessible domain for the fuel mass fraction is obtained from the one-step reaction as [1][2] :

$$Y_{CH4,min} = f - \frac{1}{4}(1-f)Y_{O2,2} \quad (f \geq f_s),$$

and the allowable domain from the 4-step RRS as:

$$Y_{CH4,min} = f - (1-f)Y_{O2,2} \quad (f \geq 4f_S / (1-f_S)) \quad ,$$

whilst for both mechanisms $Y_{CH4,max} = f$.

For the oxidant, both mechanisms yield the limits

$$Y_{O2} \geq (1-f)Y_{O2,2} - 4f \qquad \text{(valid for } f \leq f_s)$$

$$Y_{O2} \leq (1-f)Y_{O2,2}$$

Figure 1 shows experimental data from [3] [2], plus allowable and accessible limits and an intermediate line:

$$Y_{CH4,min} = f - \frac{1}{2}(1-f)Y_{O2,2} \quad (f \geq f_S)$$

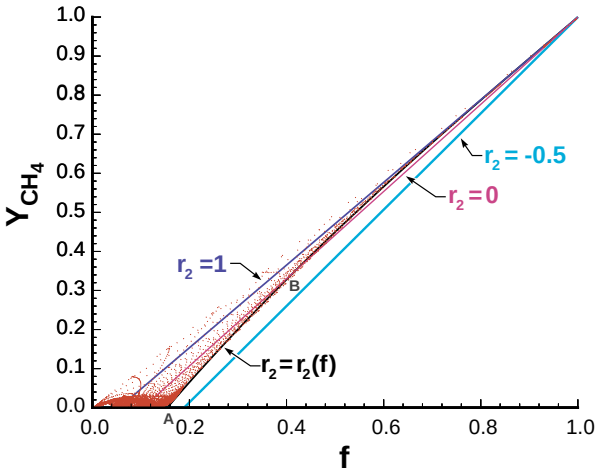

FIG 1: Mass fractions of fuel and limits

It is evidenced that the lower limit for fuel mass fraction lies between the allowable and accessible limits.

LIMITS FOR FUEL AND OXIDANT

To find a closer limit we consider the 4-step RRS:

$CH_4 + H_2O + 2H \rightarrow CO + 4H_2$	I
$CO + H_2O \leftrightarrow CO_2 + H_2$	II
$2H_2 + O_2 \rightarrow 2H_2O$	III
$3H_2 + O_2 \leftrightarrow 2H_2O + 2H$	IV

Neglecting convection and diffusion we may write $\Gamma_H = P_H - C_H \geq 0$, where Γ_H is the specific abundance of Hydrogen element, and P and C stand for production and consumption, respec-tively. By examination of the 4-step mechanism we may write:

$$C_{CH4} = P_{CO}$$
$$C_H = 2\,P_{CO}$$
$$P_H = 2\,C_{O2,IV}$$
$$C_{O2} = C_{O2,III} + C_{O2,IV} = C_{O2,IV}(1 + w_{III}/w_{IV}) = C_{O2,IV}(1 + r_2)$$

where we have defined the ratio of reaction rates $r_2 = w_{III} / w_{IV}$. To these we add the basic relations

$$C_{CH4} = f\,\Gamma_{CH4,1} - \Gamma_{CH4}$$
$$C_{O2} = (1-f)\,\Gamma_{O2,2} - \Gamma_{O2}$$

where 1 and 2 refer to the fuel and oxidant streams. From the above and for $f \geq 4\,f_s / (1-f_s)$:

$$Y_{CH4} \geq f - (1-f)Y_{O2,2} \Big/ 2(1 + r_2)$$

Note that for the one-step reaction ($r_2 = 1$) we recover the accessible limit, whilst for $r_2 = -0.5$ the allowable limit is obtained. It should also be noted that a value of $r_2 = -0.2$ was used in [2] as an acceptable average.

What is required is a model for $r_2 = r_2(f)$, stressing that the model is only required at the limit of maximum fuel con-sumption, not in the whole of the **f**-space.

Expressions for w_{III} and w_{IV} as functions of the reaction rates in the scheletal system are available [4]. However, the rate cons-tants available in the literature, particularly for the pyrolisis of CH_4, yield unsatisfactory results, in that w_{III} and w_{IV} are thence computed as sums of very small and similar numbers, and their ratio is unreliable.

A heuristic form may be substituted for r_2 , as follows: *at the mixture compositions found at the limit* we may assume that the reaction rates are only functions of temperature, of the form $w \propto \exp(-E / RT)$ and the maximum fuel consumption rate coincides with the maximum temperature at that composi-tion, which may be considered (again, at the limit) as a linear function of **f**. Also (see Figure 1), r_2 must be unity at f=1 and between 0 and -0.5 at the cutoff point. Hence, we posit the form

$$r_2 = 1 - \exp\left(\left(f - f_s\right) \Big/ \left((f-1) - f_s \Big/ \left(f_c\,(f-1)\right)\right)\right)$$

where f_c is the mixture fraction at which Y_{CH4}=0, which, from Figure 1, is taken as $f_c \approx 0.153$ (Point A).

This implies that $r_2 = 0$ at $f = f_s\,(1+1/f_c) \approx 0.42$. The $r_2 = 0$ line (shown in Figure 1) intersects the experimental results at $f \approx 0.43$ (Point B). Figure 1 shows that this is an acceptable model for the lower limit, between the 4-step and one-step limits.

It is remarked that the form presented for r_2 contains only one constant, which is supported by two items of experimental data: the cutoff mixture fraction and the mixture fraction at which $r_2 = 0$.

Limits for the oxidant may be found as follows: from the 4-step scheme we deduce

$$\Gamma_{H2} = P_{H2} - C_{H2} = C_{CH4}(4 + r_1) - 3C_{O2} \Big/ \frac{3 + 2\,r_1}{1 + r_1} \geq 0$$

which for the lean side (where $\Gamma_{CH4,min} = 0$, $r_2 = 1$) yields

$$Y_{O2} \geq (1-f)Y_{O2,2} - 4 / 5\; f\,(4 + r_1)$$

If $r_1 = 1$ we obtain the allowable (and accessible) limits.

Considering the experimental results shown in Figure 2, we choose an exponential form of a linear function of **f** and which yields $r_1 = 1$at f=0 and a value close to but below 1 at the cutoff point. Hence, we take

$$r_1 = \exp(-f / 2f_S)$$

It is noted that reaction II is reversible, whilst this form yields only positive values. However, the model chosen for r_1 is only valid at the limit of maximum consumption of oxidant, where it is never negative (Figure 2). Figure 2 shows the resulting lower limit for the oxidant, and the other limit lines.

LIMITS FOR OTHER SPECIES

The need for limits to the solutions of other species depends on the choice of which species are solved by PDE

and which are found by algebraic balances. For completeness we have derived limits for the remaining main species CO, H_2O, H, H_2 and CO_2 . For CO and H_2O we distinguish between regions separated by f_c :

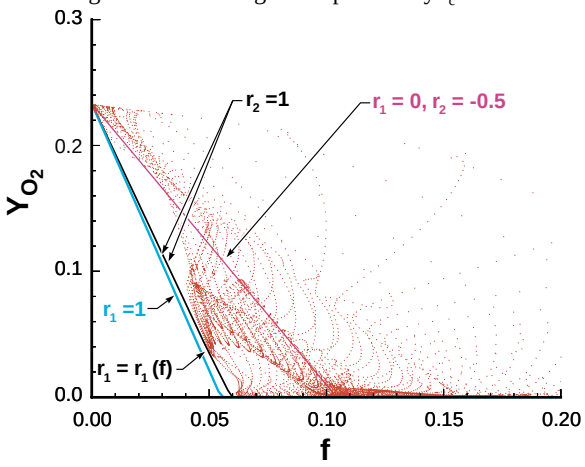

FIG 2: Mass fractions of oxidant and limits

$$Y_{CO} \le \frac{28}{32}\left[(1-f)Y_{O2,2} - Y_{O2,min}\right]\frac{2(1-r_1)}{(1+r_1)} \quad (f \le f_c)$$

$$Y_{CO} \le \frac{28}{16}(f - Y_{CH4,min})(1-r_1) \quad (f \ge f_c)$$

For H_2O, with $r_1 = 0$ to minimize consumption:

$$Y_{H2O} \le \frac{18}{16}\left[\left((1-f)Y_{O2,2} - Y_{O2,min}\right) - \left(f - Y_{CH4,min}\right)\right]$$

Figure 3 shows experimental results, the upper limit derived above, and the allowable and accessible limits. This new limit is considered particularly satisfactory.

An expression for Γ_{H2} was obtained above. In terms of mass fractions this is written:

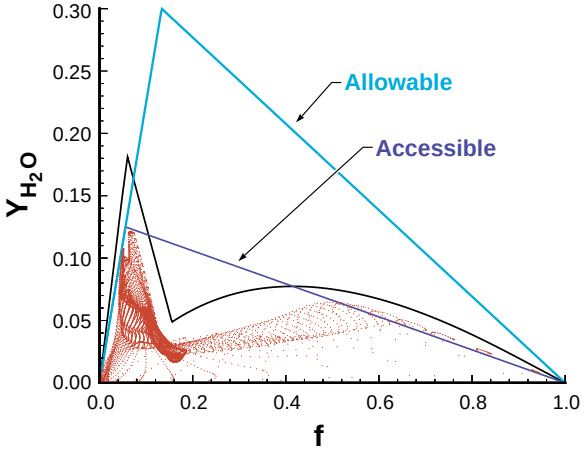

FIG 3: Mass fractions of H_2O and limits

$$Y_{H2,max} = \left(\frac{f - Y_{CH4,min}}{8}\right)(4+r_1) - \left(\frac{(1-f)Y_{O2,2} - Y_{O2,min}}{16}\right)\frac{3+2r_1}{1+r_1}$$

For H we obtain

$$Y_{H,max} = \left[\frac{(1-f)Y_{O2,2} - Y_{O2,min}}{16(1+r_2)}\right] - \left[\frac{f - Y_{CH4,min}}{8}\right]$$

For CO_2, it would seem obvious that $Y_{CO2,max}$ would correspond to nil CO, in which case

$$Y_{CO2,max} = \frac{44}{16}C_{CH4}$$

Figure 4 (curve **a**), shows this is not a satisfactory upper limit for carbon dioxide. A more satisfactory limit is found restricting r_1 to 2/3. In this case,

$$Y_{CO2} \le \frac{44}{32}\left(C_{O2}/(1+r_2) - 2\,r_1\,C_{CH4}\right)/2 \ .$$

This limit also is shown in Fig 4 (curve **b**).

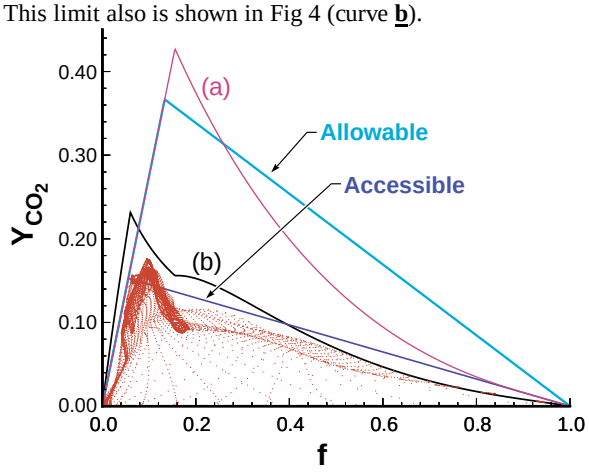

FIG 4: Mass fractions of CO_2 and limits

CONCLUSIONS:

Very simple heuristic models have been proposed for the ratios of reaction rates in the 4-step RRS. These models have the appropriate aymptotic behaviour and an adequate theoretical and experimental basis.

Limits to the main species PDE´s have been constructed with these models and basic concepts such as positiveness of species concentrations. These limits are much closer to experimental results than previously proposed allowable and accessible limits.

This is a report of work in progress, and certain points require further analysis, in particular the upper limit for the ratio r_1 re-quired to generate the limit for CO_2 . It is also necessary to test this work against more detailed and accurate experimental results.

REFERENCES

[1] CHEN, J.-Y, and DIBBLE, R. W.; "Application of reduced kinetic mechanisms for prediction of turbulent nonpremixed methane-air flames"; Chapter 9 of Lecture Notes in Physics 384, Springer-Verlag, Berlin.

[2] ECHANIZ, V.; LODI, S.; BRIZUELA, E. A., and BILGER, R. W.; "Numerical simulation of turbulent diffusion flame using a 4-step mechanism", *Proceedings*, ENCIT/LATCYM, Florianópolis, Nov. 1996.

[3] SPADACCINI, L. J. ; OWEN, F. K., and BOWMAN, C. T.; "Influence on aerodynamic phenomena of pollutant formation in combustion" ; Report No. EPA-600/2-76-247a, United Technology Research Centre, Connecticut, 1976.

[4] BILGER, R. W.; ESLER, M. B., and STARNER, S. H.; "On reduced mechanisms for methane-air combustion" ; Chapter 5 in [1].

MEASUREMENTS AND MODELLING OF NOx EMISSION IN CH_4 / WET AIR SWIRL DIFFUSION FLAME

S. CAILLAT, M. S. CABOT and G. CABOT
CORIA UMR CNRS 6614, Université de Rouen
76134 Mont Saint Aignan Cedex, France
Sebastien.Caillat@coria.fr, Gilles.Cabot@univ-rouen.fr

INTRODUCTION

Water injection is often used as a way to decrease NOx emission in industrial combustion devices like engines, gas turbines and, more recently, natural-gas boilers (Gaz de France [1]). This decrease is mainly due to the thermal effects of dilution leading to the reduction of flame temperatures. However, a few studies [2] have shown that added water vapor can participate in the reaction process.

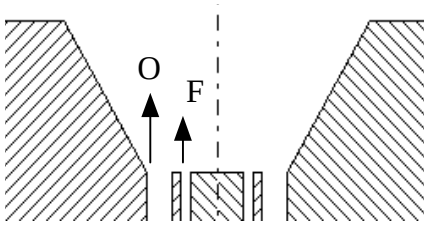

Fig. 1 : Nozzle description

In the present study, some measurements are first performed on industrial boilers using humid-air. The concentration of water vapor varies up to 150 g of water per kg of dry air (water/fuel ratio up to 3 kg/kg). From fig. 1 it is seen that the emission rate of NOx decreases essentially, but beyond a certain threshold a rate of CO production tends to increase.

In a second step, a laboratory CH_4/air diffusion flame is studied. A confined geometry is used in order to control the humidity of the combustion air and the air/fuel ratio. The flame is stabilized by a swirl. Measurements of chemical species concentrations and temperature are performed.

Experimental results are then compared with computations using Fluent numerical code [3]. A four-steps global mechanism [4] including CO, with simplified thermal NO production model is used for combustion.

LABORATORY BURNER

A laboratory burner based on the central annular fuel flow (∅int.: 8 mm, ∅ext.: 9 mm) is surrounded by a rotating air stream (∅int.: 10 mm, ∅ext.: 15.5 mm). The flame is stabilized inside a cone (30° angle, 16 mm high) then it develops in the combustion chamber (∅int.: 160 mm) at distance of about 100 mm. Four windows allowed optical and physical access for measurement instruments. Fuel injection velocity is 5 m/s. The airflow is set to maintain 3 Vol. $\%O_2$ in dry exhaust gases, which yields an air velocity around 14 m/s. Thin thermocouples (W-Re) are used for temperature profiles. Global values of species concentrations are measured at 850 mm from the nozzle. Inside the flame, local values are measured with an aspiration sonic probe. A non-dispersive infrared gas analyzer is used for CO, CO_2 and NOx, and a magnetic pressure type analyzer is used for O_2.

NUMERICAL SIMULATION

Two-dimensional axi-symmetric geometry for numerical simulation is represented with a 300 x 70 grid, on a height of 400 mm. Wall temperature is imposed equal to 200°C. Four-step global mechanism, including three intermediary species CH_2, H_2 and CO writes as [4]:

$$CH_4 \rightarrow CH_2 + H_2$$
$$CO + ½\ O_2 \rightarrow CO_2$$
$$CH_2 + ½\ O_2 \rightarrow CO + H_2$$
$$H_2 + ½\ O_2 \rightarrow H_2O$$

The classical k-ε turbulence model is used, and the reaction rate calculated by the Magnussen classical method [5]: min (W_{chem},W_{EBU}). A simplified Zeldovich thermal-NO mechanism [6] is implemented, based on the quasi-steady state assumption for nitrogen atoms: $dNO/dt = 2k_{O+N2\rightarrow NO+N}\ [N_2][O]$. Oxygen concentration is obtained from the partial equilibrium assumptions between O, H, OH, O_2, H_2 and H_2O:

$$[O] = (k_{H+O2}\ k_{OH+H2})/(k_{OH+O}\ k_{H+H2O})\ [O_2][H_2]/[H_2O].$$

RESULTS

The agreement between calculated and measured values of NO global exhaust emissions is rather satisfactory (see fig. 2). Still, predictions overestimate the water vapor addition effects on NOx reduction. Temperature profiles in the combustion zone at x=32 mm, r<20 mm are well predicted for any flow rate of water vapor (fig. 4). At x=32 mm, temperature is overestimated in the recirculation zone near the wall.

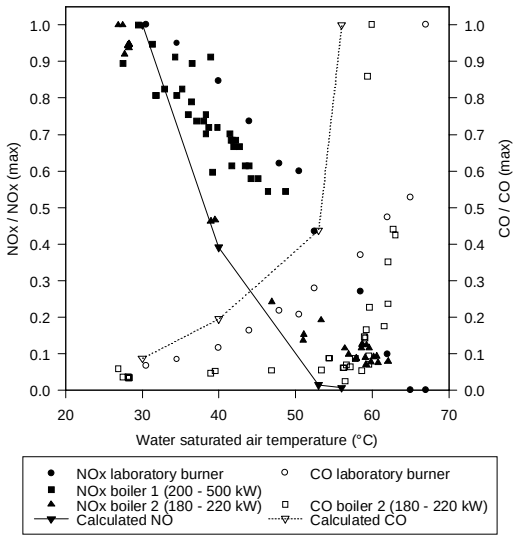

Fig. 2 : Experimental global CO and NO measurements

Downwards the combustion zone, at x=103 mm, gas temperature is also strongly overestimated on the axis. In the CO profiles (fig. 3) at x=22 mm, the computations gives nearly the same peaks positions and magnitudes as the measurements. However, the width and axis value of these peaks are underestimated by the calculation.

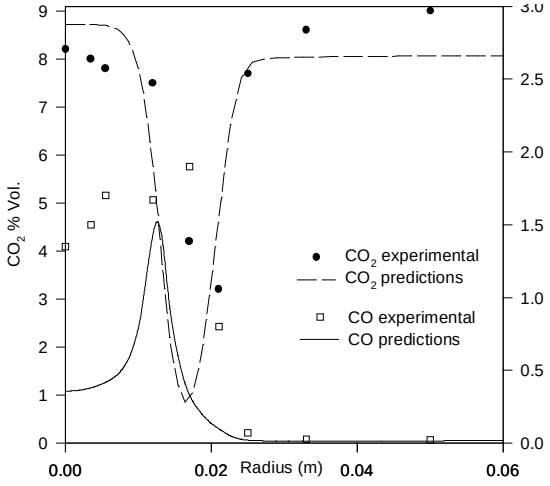

Fig. 3 :Calculated and measured CO and CO_2 profiles at x=32 mm

OUTLOOK

Wall treatement and turbulence modeling can easily be improved (rsm model for swirl). More complete kinetic schemes will be tested (5-steps [7,8] and 11-steps [9]) in order to understand the influence of H_2O chemistry on NOx formation.

REFERENCES

[1] Guillet R., Brunel G., Grehier A. Viltard J.C. (1995) "Porous Exchanger and Water Vapor Pump: the Altarex Boiler", International Gas Research Conference, pp. 663-72.

[2] Payne J. D., Seaba J. P. (1995) "Modeling the Effects of Water Vapor Addition on NO Chemistry in rich Methane - Air Flame", 15th Int. Col. on the Dynamics of Explosions and Reactives Systems, Comb. Sci. and Techn.

[3] Fluent 4.4 user's guide, 2ND edition, May 1997

[4] "Computation of Soot and NOx Emissions from Gas Turbine Combustors", NASA CR n° : 167930.

[5] J. Warnatz, U. Maas & R. W. Dibble (1996) "Combustion", Ed. Springer, ISBN 3-540-60730, pp. 219-222.

[6] Magnussen. B.F., Hjertager. B.H. (1976) ``On Mathematical Models of Turbulent Combustion with Special Emphasis on Soot Formation and Combustion", 16th Symp. (Int.) on Combustion, The Combustion Institute, pp. 15-20.

[7] D. G. Nicol et all. "Development of a 5 Step global Methane Oxidation – NO formation mechanism for lean premixed gas turbine combustion", to be presented at Int. Gas Turbine & Aeroengine Cong. Stockholm - June 2-5 1998.

[8] Miller J.A. & Bowman C.T. (1989) "Mechanism and Modeling of Nitrogen Chemistry in Combustion" Prog. Energy Combust. Sci. 15, pp 287-338.

[9] J.C Hewson, M. Bollig (1996) "Reduced Mechanisms for NOx Emissions from Hydrocarbon Diffusion Flames", 26th Symposium (Int.) on Combustion, The Combustion Institute, pp. 2171-2179.

Gaz de France is acknowledged for the financial support of the experimental part of this work.

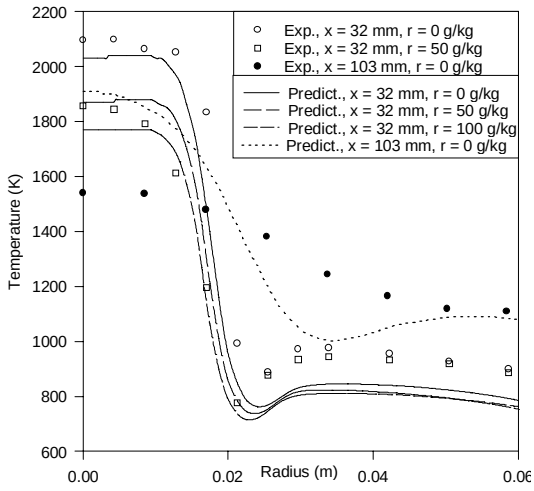

Fig. 4 : Calculated and measured temperature profiles at x=22 mm at x=32 and 103 mm

Comment on the Quasi-Steady Modeling of a Hydrogen/Air Jet Flame

Chong M. Cha† George Kosály John C. Kramlich
University of Washington, Department of Mechanical Engineering, Box 352600, Seattle, WA 98195

†Corresponding author: chongcha@u.washington.edu

In a recent paper, Barlow et al. [1] compared predictions obtained from the Conditional Moment Closure (CMC) method to data measured in hydrogen-air jet diffusion flames. The agreement between the data and the model predictions demonstrates the validity of the CMC approach. This poster investigates the possibility that the quasi-steady version of the CMC method (a lower-order approach) can provide nearly identical data comparisons as the full model. This possibility was briefly mentioned by Smith [2] in connection with a syngas flame. Buriko et al. [3] discuss a similar issue but looks at conditional averages only in an incompressible case. Note that the quasi-steady CMC model recovers the steady-flamelet approach [4] if the scalar dissipation and the mixture fraction are assumed to be independent and the influence of the fluctuations of the scalar dissipation rate is considered negligible.

With the presently available computer resources, the computation of a parabolic turbulent hydrogen-air jet is readily possible using the full CMC approach. The utilization of the quasi-steady version of the model can, however, be advantageous in three-dimensional problems and/or problems where large chemistry sets are required, *e.g.*, NO_x control via reburning. Large-eddy simulations (LES) require three-dimensional, time-dependent computations even for steady, axisymmetric problems, therefore, a quasi-steady approach is attractive in LES.

The fluid turbulence is modeled using a standard $k-\varepsilon-g$ model. In the description of the CMC approach, we follow [1]. The conditionally averaged mass fractions, Q_j with $j=1,\ldots,N$, the number of reacting species, along with the conditionally averaged standardized enthalpy, Q_h, are predicted by

$$\langle\rho u|\xi=\eta\rangle\frac{\partial Q_j}{\partial x}-\frac{1}{2}\langle\rho\chi|\xi=\eta\rangle\frac{\partial^2 Q_j}{\partial\eta^2} = \langle\dot{w}_j|\xi=\eta\rangle \quad (1)$$

$$\langle\rho u|\xi=\eta\rangle\frac{\partial Q_h}{\partial x}-\frac{1}{2}\langle\rho\chi|\xi=\eta\rangle\frac{\partial^2 Q_h}{\partial\eta^2} = \langle\dot{s}|\xi=\eta\rangle, \quad (2)$$

where $\dot{w}_j$ is the net chemical production term, $\dot{s}$ is the net radiative loss term, ρ is the density, u is the streamwise velocity, and χ is the dissipation rate of ξ, the conserved scalar.

Regarding the modeling of the conditionally averaged chemical production terms and the radiation sub-model we refer to [1]. The coefficients of the LHS of Eqs. (1)–(2) have been computed using two different models. In Model 1,

$$\widetilde{\xi}(x,y_{st})\equiv\xi_{st}: \quad \frac{\langle\rho u|\xi=\eta\rangle}{\langle\rho|\xi=\eta\rangle}=\widetilde{u}(x,y_{st}) \quad \text{and} \quad \frac{\langle\rho\chi|\xi=\eta\rangle}{\langle\rho|\xi=\eta\rangle}=\widetilde{\chi}(x,y_{st}) \quad (3)$$

below the stoichiometric flame-length, L_{st}, and are set identical to their centerline values above L_{st}. In Model 2,

$$\widetilde{\xi}(x,y_\eta)\equiv\eta: \quad \frac{\langle\rho u|\xi=\eta\rangle}{\langle\rho|\xi=\eta\rangle}=\widetilde{u}(x,y_\eta) \quad \text{and} \quad \frac{\langle\rho\chi|\xi=\eta\rangle}{\langle\rho|\xi=\eta\rangle}=\widetilde{\chi}(x,y_\eta) \quad (4)$$

for $0<\eta\leq\widetilde{\xi}(x,y=0)$. Above the centerline value $\langle\chi|\eta\rangle$ was linearly interpolated to zero at $\eta=1$, $\langle u|\eta\rangle$ was linearly interpolated to zero at unity, or was kept constant at its value at the centerline mixture fraction.

Fig. 1 shows the conditionally averaged mass fraction of OH in an undiluted hydrogen flame with radiation effects included. The data are from [1]; the computed curves use Models 1 and 2. For the major and radical species, the predictions do not appreciably change with either Model 1 or 2 (or cross-combinations of the models). Thermal NO is sensitive to all combinations of models for the coefficients. For the major and radical species, the insensitivity to the modeling of $\langle u|\eta\rangle$ is due to the secondary importance of the axial derivative term, the lack of sensitivity to the modeling of $\langle\chi|\eta\rangle$ is related to the large Damköhler values in this flame.

Next we investigate the ratio of the second term on the LHS of Eq. (1) to the reaction term. The quasi-steady approach is exact if this ratio is unity. Table 1 and 2 refer to $\eta=\xi_{st}$. Table 1 shows the adiabatic

results in the undiluted case. Table 2 refers to 40% dilution with He and accounts for radiation (L_{vs} = visual flame-length, $L_{st} \approx 0.75 L_{vs}$). Below the stoichiometric flame-length, the two terms balance quite closely indicating the approximate validity of the quasi-steady model (for the major and radical species). Presently, we are investigating the influence of the deviation from unity on the conditional averages of the species.

Acknowledgments

Partial support by GRI (Contract No. 5095–260–3504) and AFOSR (F49620–97–1–0092) is acknowledged.

References

[1] R. S. Barlow, N. S. A. Smith, J.-Y. Chen, and R. W. Bilger, submitted to Combustion and Flame (1998)

[2] N. S. A. Smith, PhD Dissertation, University of Sydney (1994)

[3] Y. Y. Buriko, V. R. Kuznetsov, D. V. Volkov, and S. A. Zaitsev, Combustion and Flame **96**: 104 (1994)

[4] N. Peters, Combustion Science and Technology **30**: 1 (1983)

TABLE 1: Adiabatic, 0% He dilution case: Ratio of the magnitudes of the diffusion term, $\frac{1}{2}\langle\rho|\eta\rangle\langle\chi|\eta\rangle\frac{\partial^2 Q_j}{\partial\eta^2}$, and the reaction term, $\langle\dot{w}_j|\eta\rangle$, for H_2O, OH, and NO. Magnitude ratios are at $\eta = \xi_{st} = 0.0283$.

x/L_{vs}	1/8	1/4	3/8	1/2	5/8	3/4	1
H_2O	1.00	0.99	0.99	0.99	0.97	0.96	0.95
OH	1.00	1.00	1.01	1.01	1.02	1.04	1.08
NO	0.95	0.93	0.90	0.89	0.81	0.69	0.52

TABLE 2: Radiative, 40% He dilution case: Ratio of the magnitudes of the diffusion term and reaction term at $\eta = \xi_{st} = 0.0634$.

x/L_{vs}	1/8	1/4	3/8	1/2	5/8	3/4	1
H_2O	1.00	0.99	0.98	0.97	0.94	0.90	0.88
OH	1.00	1.00	1.01	1.02	1.05	1.12	1.20
NO	1.02	0.89	0.86	0.82	0.74	0.67	0.62

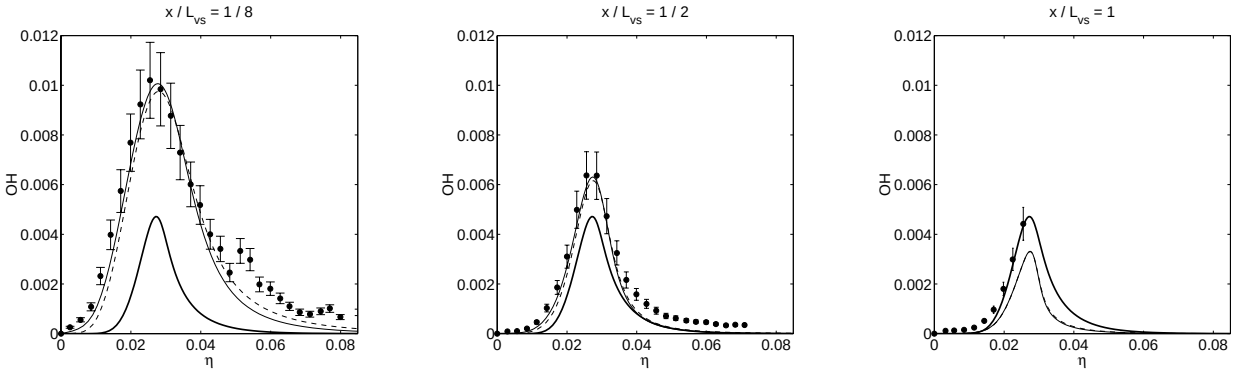

FIGURE 1: Radiative, 0% He dilution case: Comparisons of $\langle Y_{OH}|\xi = \eta\rangle$ predictions with experimental data of [1]. Bold solid = adiabatic equilibrium, solid line = Model 1, dash-dash = Model 2.

EVALUATION OF DIFFERENTIAL DIFFUSION IN TURBULENT NONPREMIXED FLAMES

B.B. DALLY[1] and A.R. MASRI

Department of Mechanical and Mechatronic Engineering
The University of Sydney, NSW, AUSTRALIA

Differential diffusion effects are usually assumed to be negligible in most conventional calculations of reacting and non-reacting turbulent flows. This, along with the unity Lewis number assumption, have been used conveniently by modelers, since they lead to a substantial simplification of the transport phenomena which is then represented by a single conserved scalar that is termed the mixture fraction. They also allow for the use of reduced chemistry to represent the reactive scalar field and substantially reduce the computational cost of turbulent reacting flows. Earlier investigations of differential diffusion in turbulent flames[1,2] have concluded that these effects decrease with Reynolds number, and hence their neglect in highly turbulent flow calculations, seemed justified. Recent advances in diagnostics and computational capabilities have rekindled interest in this issue. Experimental investigations such as those of Drake et al[2] and Smith et al[3] have confirmed earlier expectations that differential diffusion effects decrease and become negligible at sufficiently high Reynolds number flows.

Numerical efforts to model differential diffusion effects in reacting and non-reacting flows have recently been initiated[4,5,6] The scaling of the mean and the dominant variance of the differential diffusion variable, defined as $z = {}_A - {}_B$, where A and B are conserved scalars, with the Reynolds number has been proposed along with simplified models[5,6]. These scaling laws were suggested for isothermal flows and their applicability to reacting flows has been questioned[3]. Current understanding of differential diffusion remains very limited. Correlating it with the Reynolds number is empirical and does not account for the effects of chemical reaction and the nature of the parent fuel mixture. Advanced approaches to turbulent combustion modeling are in principle, capable of accounting for differential diffusion effects. This begs for reliable data for model validation.

In this poster, the differential diffusion parameters are evaluated from single-point data collected in turbulent nonpremixed flames of different fuel mixtures and for a wide range of Reynolds numbers. Flames stabilized on both piloted and bluff-body burners are presented. The effects of parent fuel mixture, chemical reaction, localized extinction and burner geometry on differential diffusion are investigated.

The differential diffusion variable is evaluated for flames of CH_3OH, H_2/CH_4 and H_2/CO fuel mixtures and over a range of jet Reynolds numbers. Table 1 shows the different flames studied and their parameters. These data are also accessible on the World Wide Web[7]. The effects observed in both bluff-body and pilot-stabilized flames are similar. Differential diffusion is generally found to decrease with increasing jet Reynolds number. The location of the reaction zone is found to be important in separating “hydrogen rich” regions on the lean side from “hydrogen deficient” on the rich side. This is true regardless of the parent fuel mixture. Profiles of mean z and its rms fluctuations are qualitatively similar in mixture fraction space, but in physical space, show a cross-stream dependence. These findings are useful for modeling differential diffusion effects in turbulent combustion.

[1] Author Current Address: Department of Chemical Engineering, The University of Sydney, bassam@chem.eng.usyd.edu.au

Fuel	Flame	U_J	$\mathbf{U_C}$	$\mathbf{Re_J}$	**%BO**	$_s$
CH_3OH	PML1	62	15	37080	47	0.135
	PML2	117		69430	88	
	PML3	127		74950	95	
	BML1	80	40	23700	55	
	BML2	121		35900	84	
	BML3	134		39700	93	
H_2/CO	BHC1	134		17500	18	
	BHC2	321		41990	43	
	BHC3	536		70120	74	
H_2/CH_4	BHM1	118		15800	50	0.05
	BHM2	178		23900	75	
	BHM3	214		28700	91	

Table 1: Summary of the flames studied. U_J is the jet velocity in m/s, U_C is the coflow air velocity in m/s, Re_J is the jet Reynolds number, %BO is the percent of blow off calculated as the ratio of the bulk jet velocity over the velocity at blow off and $_s$ is the stoichiometric mixture fraction. Flames with names that start with (P) are stabilized on a piloted burner while those names that start with (B) are stabilized on a bluff-body burner.

References

1. Bilger, R.W. and Dibble, R.W., "Differential Molecular Diffusion Effects in Turbulent Mixing", *Combus. Science and Tech.*, **28**:161--172, (1982)

2. Drake, M.C., Pitz, R.W. and Lapp, M., "Laser Measurements on Nonpremixed Hydrogen-Air Flames for Assessment of Turbulent Combustion Models", *AIAA 22nd Aerospace Sciences Meeting* January 9-12, 1984, Reno, Nevada.

3. Smith, L.L., Dibble, R.W., Talbot, L., Barlow, R.S. and Carter, C.D., *Combust. and Flame*, **100**:153-160 (1995)

4. Kerstein, ``Linear-eddy Modelling of Turbulent Transport. Part 3. Mixing and Differential Diffusion in Round Jets'', *J. Fluid Mech.*, **216**, pp. 411-420, (1990)

5. Kerstein, A.R., Cremer, M.A. and McMurtry, P.A., "Scaling Properties of Differential Molecular Diffusion Effects in Turbulence", Phys. Fluids, **7(8)**: 1999-2007, (1995)

6. Kronenburg, A. and Bilger, R.W., "Modelling of Differential Diffusion Effects in Nonpremixed Nonreacting Turbulent flow", *Phys. Fluids*, **9(5)**: 1435-1447, (1997)

7. Data-base available from Masri, A.R., Mechanical and Mechatronic Engineering, The University of Sydney, NSW, 2006, Australia. (http://www.mech.eng.usyd.edu.au/research/energy/energy.html)

Modeling of Turbulent Nonpremixed Flames using 'One-Dimensional Turbulence'

Tarek Echekki[1], Alan R. Kerstein[2]
Sandia National Laboratories
Livermore, CA 94551-0969
and Jyh-Yuan Chen[3]
Department of Mechanical Engineering, UC Berkeley
Berkeley, CA 94720-1740

A formulation of the novel one-dimensional turbulence (ODT) model [1], developed by Kerstein, is extended with the incorporation of variable-density, variable- property and finite rate kinetics within the framework of Chemkin [2]. The model is based on a mechanistic distinction between molecular processes (reaction and diffusion) and advective processes in a time-resolved simulation on a one-dimensional domain. Molecular processes, including diffusion and reaction, are computed deterministically by solving the unsteady reaction-diffusion equations. Advective processes are implemented stochastically using triple-mapping stirring events which emulate the compressive-strain and rotational folding effects of turbulent eddies. The formulation, then, allows for the accurate description of fine scale processes, including differential diffusion effects, and the detailed account of turbulence-chemistry interactions. The model has two constants of proportionality of order unity which relate the eddy characteristic time to the local eddy rate of shear and to the elapsed time for non-stationary flows.

Simulations of turbulent nonpremixed hydrogen-air and piloted methane-air flames were carried out using ODT. These simulations show that ODT reproduces some of the gross features of turbulent reacting jets at a relatively small cost of CPU time for individual realizations. Spatial intermittency of stirring events and cascading from larger to smaller eddies is demonstrated in the simulations. Eddy distributions as a function of height from burner show that that the range of scales is increased with downstream location.

Comparisons of ODT simulations using a five-step reduced mechanism for hydrogen-air [3] with experiments on turbulent jet hydrogen-air flames [4-6] show excellent agreements between axial profiles of mean and rms quantities of temperature, major species mass fractions

[1]Sandia National Laboratories, e-mail: techekk@ca.sandia.gov
[2]Sandia National Laboratories, e-mail: kerstein@ca.sandia.gov
[3]Univ. of California, Berkeley, e-mail: jychen@euler.berkeley.edu

and mixture fraction. The results also show that ODT is capable of reproducing differential diffusion effects. Some interesting chemistry and entrainment effects are also observed. Comparisons of ODT simulations using a twelve-step methane-air reduced mechanism [7] with Sandia experimental data on piloted methane-air jet diffusion flames [8-9] reproduce the ignition process of the reacting mixture by the pilot flame as well as the axial profiles of the major species and temperature. These agreements are obtained with the same set of parameters used in the hydrogen-air flame simulations.

1. Kerstein, A.R., One-Dimensional Turbulence. Part 1: Homogenous Turbulence and Shear Flows, in press *J. Fluid Mech.* (1997).

2. Kee, R.J., Miller, J.A. and Jefferson, T.H., CHEMKIN: A General Purpose Problem-Independent, Transportable, Fortran, Chemical Kinetic Program Package, Sandia National Laboratories Report SAND83–8003 (1983).

3. Chen, J.-Y., Chang, W.-C., and Koszykowski, M., Numerical Simulation and Scaling of NOx Emissions from Turbulent Hydrogen Jet Flames with Various Amounts of Helium Dilution, *Combust. Sci. Tech.* 110-111: 505-529 (1995).

4. Meier, W., Vyrodov, A.O., Bergmann, jV. and Stricker, W., Simultaneous Raman/LIF Measurements of Major Species and NO in Turbulent H_2/air Diffusion Flames, *Appl. Phys. B* 63: 79–90 (1996).

5. Meier, W., Prucker, S., Cao, M.-H., and Stricker, W., Characteristization of Turbulent H_2/N_2/Air Jet Diffusion Flames by Single-Pulse Spontaneous Raman Scattering, *Combust. Sci. Tech.* 118: 293–312 (1996).

6. DLR hydrogen-air diffusion flame data: www.st.dlr.de/EN-CV/flamedat/intro.htm#refer

7. Chen, J.Y., private communications (1998).

8. Barlow, R.S. and Frank, J.H., Effects of Turbulence on Species Mass Fractions in Methane/Air Flames, accepted for publication at the Proceedings of the Twenty-Seventh International Symposium on Combustion, Boulder, Co, 1998.

9. Sandia piloted methane-air flame data: www.sandia.gov/tdf/Workshop.html

Three-Scalar Measurements for Mixture Fraction Determination in Nonpremixed Methane Flames

Joseph Fielding, Andrew M. Schaffer, and Marshall B. Long†
Yale University
Department of Mechanical Engineering and Center for Laser Diagnostics
New Haven, Connecticut 06520-8284, USA

† Corresponding Author: Professor Marshall B. Long
email: mblong@cld3.eng.yale.edu

Abstract

Two simultaneous methods of imaging mixture fraction have been investigated using planar Rayleigh, fuel Raman, and nitrogen Raman scattering in nonpremixed flames of argon/oxygen diluted methane. One method for constructing a conserved scalar used in this work is through the simultaneous measurement of temperature (T) and fuel concentration [1]. The conserved scalar β, is defined based on fuel mass fraction (Y_F) and enthalpy and takes the form:

$$\beta = Y_F + c_p \mathrm{T}/Q \qquad (1)$$

where Q is the lower heat of combustion and c_p is the specific heat at constant pressure. This two-scalar formulation, which assumes unity Lewis number and idealized one-step reaction between fuel and oxidizer, relates mixture fraction to the measured signals through the expression:

$$\xi^{FT} = \frac{\mathrm{C}_1 \sigma}{W\,Ra} Rm + \frac{\mathrm{C}_2}{Q}\left(c_p \frac{\sigma}{Ra} - c_{p,air}\,\mathrm{T}_{air}\right) \qquad (2)$$

where Rm is the measured fuel Raman scattering and Ra is the Rayleigh scattering. The parameter σ, which is proportional to the Rayleigh cross section, the mixture molecular weight W, and the specific heat c_p, are dependent on the mixture fraction. Strained counterflow flame calculations provide appropriate functional forms for these parameters which are incorporated into an iterative scheme for determining ξ. The remaining constants C_1 and C_2 must be determined from calibration experiments.

This approach has been applied successfully [2,3], however there is a need to improve the certainty in the mixture fraction calculation around the stoichiometric contour. At this location, the fuel concentration approaches zero and the Rayleigh signal remains nearly constant.

The second method for determining mixture fraction is through the use of the N_2 Raman channel as an independent passive conserved scalar. To provide sufficient signal variation between regions of pure air and pure fuel, experiments were performed in which the fuel stream contained no nitrogen. Under these conditions, the conserved scalar can be written in terms of nitrogen mass fraction:

$$\beta^{N_2} \equiv Y_{N_2} \qquad (3)$$

with the mixture fraction:

$$\xi^{N_2} = 1 - \frac{Y_{N_2}}{Y_{N_2,\mathrm{air}}} = 1 - \frac{\mathrm{C}_3 \sigma}{W\,Ra} Rm_{N_2} \qquad (4)$$

where Rm_{N_2} is the nitrogen Raman signal, and C_3 is an additional calibration constant. This formulation requires measurement of the temperature and nitrogen concentration, and thus, represents an additional two-scalar approach. Both techniques were applied in laminar and turbulent flames of methane diluted with argon and oxygen (3/1 diluent/fuel by volume). The stochiometric mixture fraction for this fuel is 0.41 which puts the reaction zone well inside the shear layer.

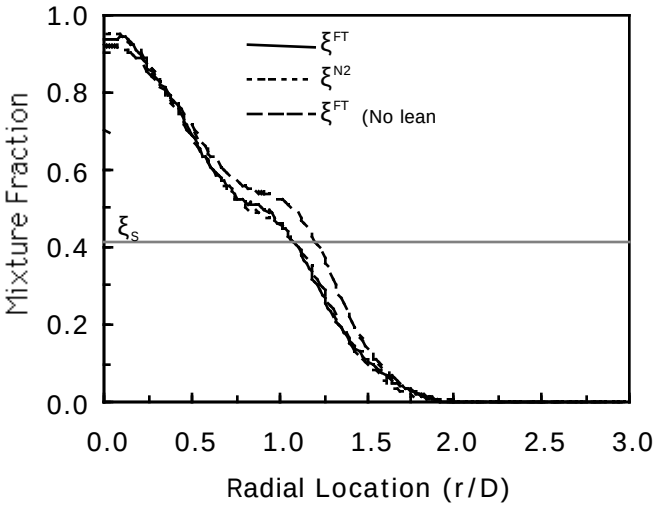

Figure 1. Radial variation of mixture fraction calculated from fuel-temperature (solid line) and nitrogen-temperature (short dashes) two-scalar approaches 15*D* downstream in the laminar flame. ξ^{FT} overpredict the fuel-temperature mixture fraction in regions around and lean of stoichiometric (long dashes).

Figure 1 shows line plots of mixture fraction from a laminar flame (Re=1600) at a location 15 nozzle diameters downstream (*D*=6.1 mm). Two curves are shown for ξ^{FT}, which differ in the parameterization of the

mixture fraction dependent terms appearing in Eqn. 2 (i.e. σ, W, c_p). The curve marked "No lean correction" uses flame calculation terms parameterized by "actual" mixture fraction determined from the Bilger formula [4]. Figure 2 shows that this approach incorporates a departure of ξ^{FT} from the more rigorous formulation, as indicated by laminar flame calculations (100 s^{-1}). Deviation from one-step chemistry (i.e. loss of parent fuel to intermediate species) is compensated in the curve marked ξ_{cor} by using a weighting term [5]. The curve for ξ^{N_2} exhibits liitle deviation from the actual mixture fraction. By assigning functional dependences based on the predicted ξ^{FT} from flame calculations, the ξ^{FT} curve shown in Fig. 1 is obtained showing improved agreement with ξ^{N_2}.

Applying this technique to single-pulse imaging in turbulent nonpremixed flames provides similar results, although the N_2 Raman signal is increasingly affected by noise, especially in regions of high mixture fraction. Figure 3 shows images taken 25*D* downstream from a *Re*=15,000 turbulent flame; the Raman images have been contour smoothed [6]. Qualitatively, the scalar dissipation fields, χ (defined as $\chi \equiv 2D \quad \xi \quad \xi$, where *D* is the diffusivity), appear similar, revealing the same main structural features, with peak scalar dissipation apparent along the edge of the main jet. The position of the stoichiometric mixture fraction contour is highlighted (black lines) in these images. Experiments are presently underway to provide complementary velocity data for this and other flames examined as part of this study.

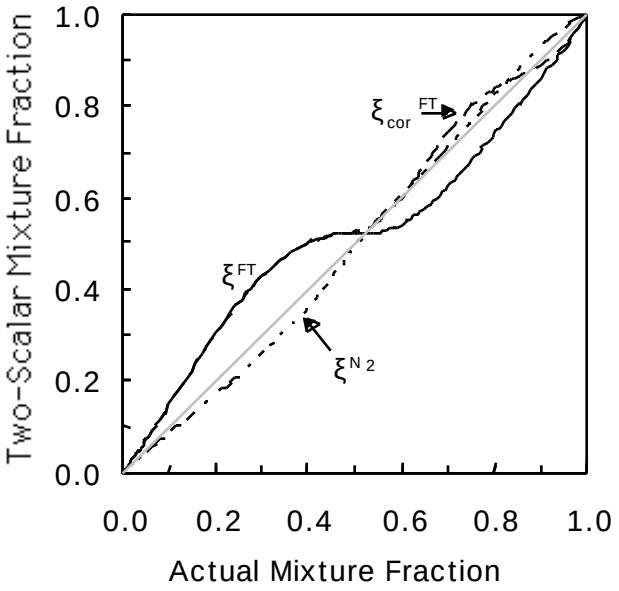

Figure 2. Mixture fraction calculated from strained laminar flame calculations (100 s^{-1}) using the fuel-temperature (solid line) and nitrogen-temperature (short dashes) two-scalar approaches plotted against mixture fraction calculated using the formula proposed by Bilger [1]. The effect of fuel correction on ξ^{FT} is shown (long dashes).

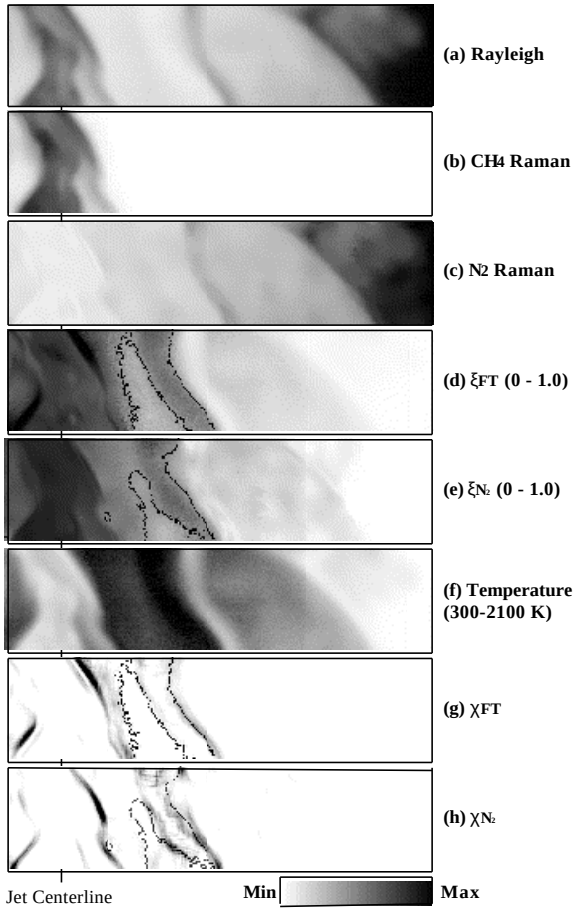

Figure 3. Instantaneous (a) Rayleigh, (b) CH_4 Raman, (c) N_2 Raman images of the turbulent flame. Also shown are the computed mixture fraction images (d) ξ^{FT}, (e) ξ^{N_2}, (f) temperature, and scalar dissipation images (g) χ^{FT}, and (h) χ^{N_2}. Each image size is 4.3*D* × 1*D*.

References

1. Stårner, S.H., Bilger, R.W., Dibble, R.W., and Barlow, R.S., *Combust. Sci. and Tech.* 86:223-236 (1992).
2. Stårner, S.H., Bilger, R.W., Lyons, K.M., Frank, J.H., and Long, M.B., *Combust. Flame.* 99:347-354 (1994).
3. Kelman, J.B., and Masri, A.R., *Combust. Sci. and Tech.* 122:1-32 (1997).
4. Bilger, R.W., Stårner, S.H., and Kee, R.J., *Comb. and Flame*, 80:135-149 (1990).
5. Stårner, S.H., Bilger, R.W., Long, M.B., Frank, J.H., and Marran, D.F., *Combust. Sci. Tech.* 129:141-163 (1997).
6. Stårner, S.H., Bilger, R.W., and Long, M.B., *Combust. Sci. and Tech.* 107:195-203 (1995).

Mixture Fraction Measurements with Two Scalars In Turbulent Nonpremixed Methane-Air Flames

JONATHAN H. FRANK
Physical Sciences Inc.
20 New England Business Center
Andover, MA 01810, USA
E-mail: frank@psicorp.com

ROBERT S. BARLOW
Combustion Research Facility
Sandia National Laboratories
Livermore, CA 94551, USA

Abstract

Techniques for multi-dimensional mixture fraction measurements are essential for determining gradients and scalar dissipation rates, which are commonly used in modeling turbulent nonpremixed flames. Previous studies have demonstrated the potential for instantaneous two-dimensional measurements of mixture fraction using simultaneous Rayleigh and fuel Raman scattering [1-8]. In the present work, a detailed evaluation of this technique is performed using multi-scalar point measurements in turbulent nonpremixed methane-air flames. Simultaneous measurements of temperature and species (CH_4, O_2, N_2, H_2O, CO_2, H_2, CO, NO, OH) are obtained using a combination of Rayleigh scattering, Raman scattering, and laser-induced fluorescence. An accurate measure of the instantaneous mixture fraction (f) is obtained using the following equation:

$$f = \frac{\left(Z_H - Z_{H,Ox}\right)/2W_H + 2\left(Z_C - Z_{C,Ox}\right)/W_C - \left(Z_O - Z_{O,Ox}\right)/W_O}{\left(Z_{H,Fu} - Z_{H,Ox}\right)/2W_H + 2\left(Z_{C,Fu} - Z_{C,Ox}\right)/W_C - \left(Z_{O,Fu} - Z_{O,Ox}\right)/W_O} \tag{1}$$

where Z_i is the mass fraction of element i, W_i is the atomic weight of element i, and the subscripts Ox and Fu indicate the oxidizer and fuel streams, respectively. The less accurate two-scalar method of determining mixture fraction can then be compared with values of f on a shot-to-shot basis.

The two-scalar technique of determining mixture fraction uses simultaneous Rayleigh and Raman scattering to obtain temperature (T) and fuel-concentration measurements. The mixture fraction is calculated using a formulation based on the fuel mass fraction (Y_F) and the enthalpy ($H = c_p T/Q$) with assumptions of unity Lewis number and a one-step reaction between fuel and oxidizer. The resulting expression for mixture fraction is as follows:

$$f^{FT} = \frac{Y_F + \left(c_p T - c_{p,Ox} T_{Ox}\right)/Q}{Y_{F,Fu} + \left(c_{p,Fu} T_{Fu} - c_{p,Ox} T_{Ox}\right)/Q} \tag{2}$$

where Q is the lower heat of combustion, and c_p is the specific heat at constant pressure. A more detailed derivation of Eq. (2) is presented elsewhere [1,2]. The instantaneous methane mass fraction, temperature, and specific heat are determined from the multi-scalar measurements.

We consider four partially premixed methane-air flames (3/1 Air/CH_4 by volume) with different Reynolds numbers. These flames correspond to Flames A, B, D, and F from Barlow and Frank [9] with Reynolds numbers of 1100, 8200, 22400, 44800, respectively. The flame is stabilized on an axisymmetric piloted burner with a nozzle diameter of 7.2 mm, and the burner is surrounded by filtered co-flowing air. The stoichiometric mixture fraction in

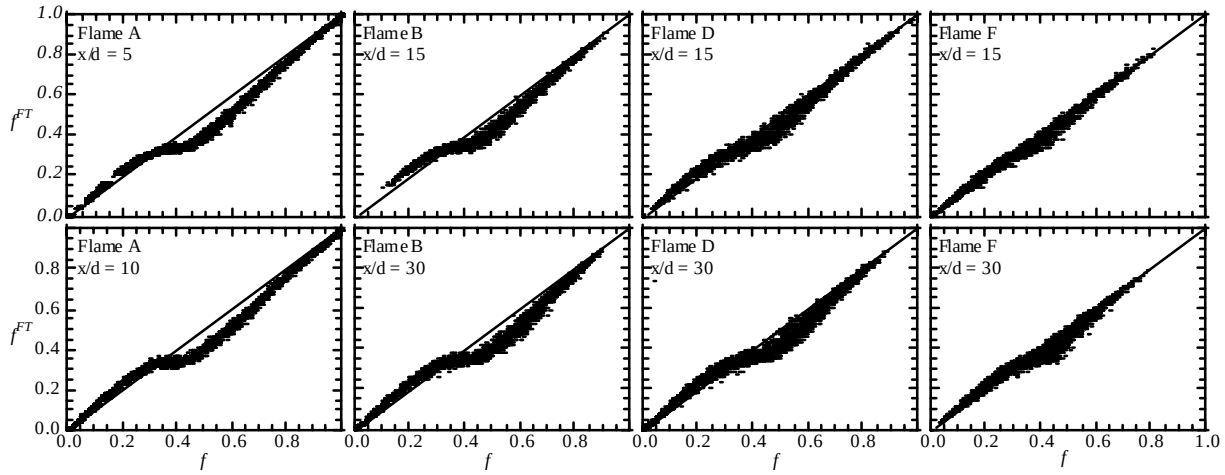

Fig. 1 Scatter plots of f^{FT} vs. f for methane-air flames with four different Reynolds numbers.

these flames is 0.351, and the mean visible flame length is approximately 67 nozzle diameters. Figure 1 shows scatter plots of f^{FT} vs. f for two different axial locations in each of the four different flames. Each point is obtained from an instantaneous measurement. The solid line in each plot represents the ideal case in which $f^{FT} = f$. The agreement between f^{FT} and f is quite good in the fuel lean region ($f < 0.351$). On the fuel rich side ($f > 0.351$), the values of f^{FT} fall well below the actual mixture fraction because of the loss of parent fuel to intermediate species. This discrepancy is a result of the one-step chemistry assumption used in the f^{FT} formulation. Although attempts can be made to compensate for this effect, considerable care must be used because these corrections directly effect the evaluation of mixture fraction gradients. As the Reynolds number increases, the scatter in the plots increases, and the overall distribution of points moves closer to the $f^{FT} = f$ line. Flame F shows the best agreement between f^{FT} and f. This is primarily the result of considerable local extinction in Flame F. In extinguished regions of the flame, fuel and oxidizer mix without any loss of parent fuel. Extinction is more probable at x/d=15 than at x/d=30, and accordingly the agreement of f^{FT} and f is better at x/d=15.

The accuracy of this two-scalar technique for determining mixture fraction varies with Reynolds number and location in the flame. Improvements to the technique may be possible by adding a third scalar measurement.

Acknowledgments: This research was conducted at Sandia National Laboratories and was supported by U. S. Department of Energy, Office of Basic Energy Sciences.

References

1. Stårner, S. H., Bilger, R. W., Dibble, R. W., and Barlow, R. S., *Combust. Sci. and Tech.* 86:223-236 (1992).
2. Frank, J. H., Lyons, K. M., Marran, D. F., Long, M. B., S. H. Stårner, and R. W. Bilger, *Proceedings of the Twenty-Fifth Symposium (International) on Combustion*, The Combustion Institute, Pittsburgh, 1994, p.1159-1166.
3. Stårner, S. H., Bilger, R. W., Lyons, K. M., Frank, J. H., and Long, M. B., *Combust. Flame* 99:347-354 (1994).
4. Marran, D. F., Frank, J. H., Long, M. B., S. H. Stårner, and R. W. Bilger, *Opt. Lett.* 20:791-793 (1995).
5. Stårner, S. H., Bilger, R. W., Frank, J. H., Marran, D. F., Long, M. B., *Combust. Flame* 107:307-313 (1996).
6. Stårner, S. H., Bilger, R. W., Long, M. B., Frank, J. H., Marran, D. F., *Combust. Sci. Technol.* 129:141-163 (1997).
7. Kelman, J. B., Masri, A. R., Stårner, S. H., Bilger, R. W., *Proceedings of the Twenty-Fifth Symposium (International) on Combustion*, The Combustion Institute, Pittsburgh, 1994, p.1141-1147.
8. Kelman, J. B., and Masri, A. R., *Combust. Sci. and Tech.* 129:17-55 (1997).
9. Barlow, R. S. and Frank, J. H., to appear in the *Twenty-Seventh Symposium (International) on Combustion.*

SPECIES, TEMPERATURE, AND VELOCITY MEASUREMENTS IN A TURBULENT JET FLAME AND A LAMINAR UNSTEADY FLAME

GERD GRÜNEFELD, HANSJÖRG FINKE, ASTRID GRÄBER, ANDRE DIEKMANN, SASCHA KRÜGER, JÖRN BARTELHEIMER

University of Bielefeld, Faculty of Physics,
Postf. 100131, 33501 Bielefeld
Germany

E-mail address of the corresponding author: gruenefe@physik.uni-bielefeld.de

The feasibility of simultaneous multi-species, temperature and velocity field measurements is demonstrated in nonpremixed flames. Multi-species and temperature measurements are done along a line (7mm length) using 1-D Raman and Rayleigh scattering, which is excited simultaneously by a strong ultraviolet laser [1]. Single-shot measurements can be done in this way.
In addition a new technique called Gaseous Imaging Velocimetry (GIV) for velocity field measurements in flames is employed. This technique is capable of providing quantitative velocity field information in a plane around the 1-D multi-species and temperature measurements. The GIV technique is based on two consecutive laser pulses similar to Particle Imaging Velocimetry (PIV). Thus instantaneous velocity fields can be measured using GIV. In contrast to PIV no particles are needed for seeding the flowfield. Instead gaseous tracers like NO, which can be detected efficiently by planar laser-induced fluorescence (LIF), are used. Thus the velocity field can be measured simultaneously with the temperature by Rayleigh scattering, because the Rayleigh scattering is not obscured by Mie scattering from particles. This offers the possibility of measuring instantanous correlations of densities and velocities in turbulent flames. This was done only a few times before using point-wise techniques [2].
In addition instantaneous gradients of majority species densities and velocities can be measured by the combined Raman/Rayleigh/GIV technique. LIF from OH can be excited at the same time using the focused laser beam of the Raman/Rayleigh measurements [1]. Thus relative OH densities can also be provided by the combined Raman/Rayleigh/LIF/GIV technique.
It is also demonstrated that double-pulse Raman/Rayleigh/GIV measurements can be done in turbulent diffusion flames, so that the temporal evolution of the chemical composition, temperature and flow field can be studied using two consecutive laser pulses with an arbitrary delay [3]. In this way the instantaneous 1-D chemistry - 2-D flow field interaction can be investigated.
The GIV technique is applied to a turbulent hydrogen/air diffusion flame (Re=13900) by seeding NO as a tracer gas into the flame and the ambient air. It turned out that the flame is not considerably altered, with regard to the majority species concentrations and temperatures, by this procedure using very low NO concentrations (sub-percent). Thus the data that is obtained by this technique can be combined to previously measured data of such flames [4].

Two tunable KrF excimer lasers are used for Raman/Rayleigh/LIF and velocity measurements. Raman and Rayleigh scattering are excited by the focused 248 nm beams. After passing the probe volume the 248 nm beams are converted to 226 nm beams by stimulated Raman scattering. The 226 nm beams are formed to sheets and used for GIV after passing a delay line. Only two laser sources are used in this way to perform the combined Raman/Rayleigh/LIF/GIV measurements.
The recently developed GIV method is also applied to a laminar unsteady hydrogen/air diffusion flame. This flame is pulsed using a speaker that modulates the hydrogen fuel flow similar to a set-up described previously [5]. The radial flow field in this flame is essentially two-dimensional in a center plane. Thus less problems with velocity components perpendicular to the measured velocity field occur. The capability of the GIV technique to measure instantenous velocity fields in such unsteady flames is verified. The flame is also characterized by OH imaging using LIF so that the flame front is visualized. The interaction of the flow field and the flame front are studied.
It is also demonstrated that GIV, which is a two-dimensional imaging technique at the present state, can also be applied to three-dimensional flowfields in turbulent multi-phase flows and flames. For this purpose certain strategies to identify velocity components perpendicular to the imaging plane are presented.

References

[1] W. Reckers, L. Hüwel, G. Grünefeld, P. Andresen: "Spatially resolved multispecies and temperature analysis in hydrogen flames", Appl. Opt. 32 (6), S. 907-918, 1993.
[2] S.C. Johnston, R.W. Dibble, R.W. Schefer, W.T. Ashurst, W. Kollman: "Laser measurements and stochastic simulations of turbulent reacting flows“ AIAA Journal 24 (6), S. 918-93, 1984.
[3] G. Grünefeld, A. Gräber, A. Diekmann, S. Krüger, P. Andresen: "Measurement System for Simultaneous Species Densities, Temperature and Velocity Double-Pulse Measurements in Turbulent Hydrogen Flames“, accepted for Combust. Sci. and Tech. (Special Issue), 1998.
[4] Brockhinke, A., Andresen, P., Kohse-Höinghaus, K., "Quantitative one-dimensional single-pulse multi-species concentration and temperature measurement in the lift-off region of a turbulent H_2/air diffusion flame", Appl., Phys. B 61 (6), S. 533-545, 1995.
[5] G.S. Lewis, B.J. Cantwell, U.Vandsburger, C.T. Bowman, „An investigation of the structure of a laminar non-premixed flame in an unsteady vortical flow“, 22nd Symp. (Int.) on Comb. S. 515-522, 1988.

Numerical Simulation of a Turbulent Piloted Methane / Air Jet Flame (Flame D) using a Finite-Volume - Monte-Carlo-PDF Code

Alexander Hinz, Egon P. Hassel, Johannes Janicka

FG Energie– u. Kraftwerkstechnik, Technische Universität Darmstadt,
Petersenstr. 30, 64287 Darmstadt, Germany
phone: +49-6151/16 2502, fax: +49-6151/16 6555, e-mail: ekt@hrzpub.tu-darmstadt.de

This work presents numerical simulation results of the piloted methane/air flame, known as *Flame D* [Barlow98]. The code used solves for the Eulerian-composition PDF in coupling with a finite-volume simulation of the velocity field.
The following overview summarizes the sub-models applied in the simulation:

Turbulence model	$k-\varepsilon$-model with modified constants C_2, C_μ [Launder72]
Chemistry model	ILDM method with two reaction progress variables [Maas92]
Mixing model	Modified Curl model [Janicka79]
Coupling model	Eulerian composition PDF [Pope81, Chen96]

The plots of the results contain axial profiles of the mean axial velocity, turbulent kinetic energy, mixture fraction, temperature and mass fraction of CO_2 and CO. Radial profiles are shown for mixture fraction and mass fraction of CO_2. In addition to that conditional means of CO_2 and CO are plotted.

The axial mean velocity and the turbulent kinetic energy are in good agreement with experimental data (Fig. 1a). The major species distributions are in reasonable agreement with the experiments (Fig. 1b, d, e, g). According to that, the flame length matches the peak values of temperature (Fig. 1c). Problems arise with the prediction of CO. This becomes appearant from the mean mass fraction along the axis and also for the conditional mean at $x/d = 15$ (Fig. 1d, h). Two reaction progress variables in the ILDM method seem to be insufficient to predict CO accurately in the rich flame zone. In addition to that, similar problems emerge for the H_2 concentration (not shown here). According to the radial profiles (Fig. 1e, g), the spreading of the jet is too large, probably due to mispredictions of the turbulence model. But the conditional mean plots of major species (e.g. Fig. 1f) show that the results are consistent with regard to the chemistry model.

References:

Barlow, R., Frank, J.H. (1998), 27^{th} *Symp (Int.) Comb.*, accepted
Chen, J.-Y., Chang, W.-C. (1996), 26^{th} *Symp (Int.) Comb.*, pp. 2207-2214
Janicka, J., Kolbe, W., Kollmann, W. (1979), *J. Non-Equil. Thermodyn.*, 4, pp. 2292-2307
Launder, B.E., Morse, A., Rodi, W., Spalding, D.B. (1992), *Tech. Report, NASA SP-311*
Maas, U., Pope, S.B. (1992), *Comb. Flame*,88 (3), pp. 239-264
Pope, S.B. (1981), *Combust. Sci. Technol.*, 25, pp. 159-174

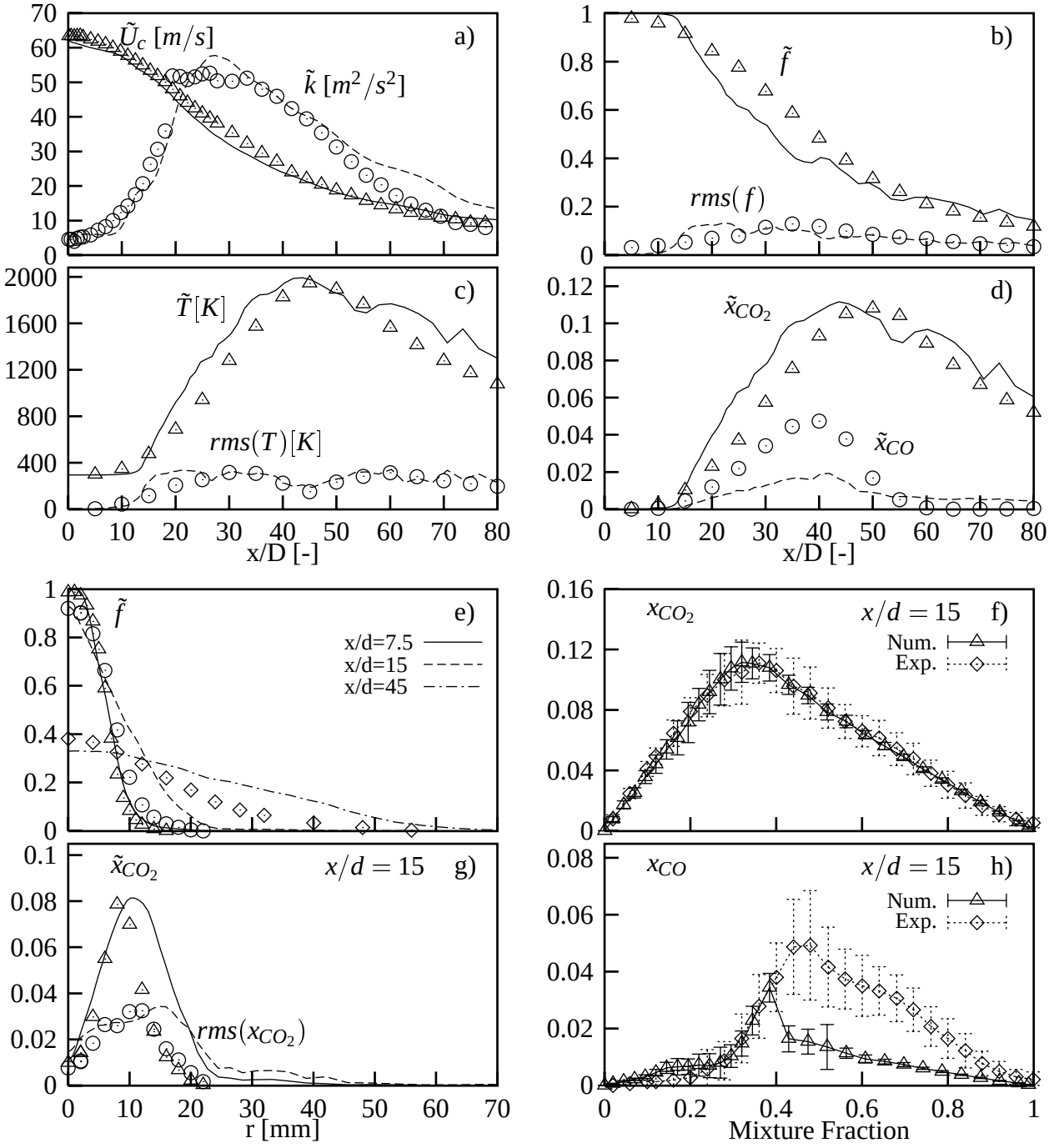

Fig.1: a) – d): Axial profiles; e), g): Radial profiles; f), h): Conditional distributions. In plots a) – e), and g), lines show numerical results, symbols represent the respective experimental data.
a) Mean axial velocity, turbulent kinetic energy; b) Mixture fraction: mean and rms; c) Temperature: mean and rms; d) Mass fraction CO_2 and CO: mean; e) Mixture fraction: mean; f) Mass fraction CO_2: conditional mean; g) Mass fraction CO_2 , mean and rms; h) Mass fraction CO, conditional mean

SMC Modeling of Strongly Swirling Natural Gas Flames

T. Landenfeld, A. Kremer, E. P. Hassel, J. Janicka

Fachgebiet Energie– und Kraftwerkstechnik, TU Darmstadt
Petersenstr. 30, 64287 Darmstadt
E-Mail: ekt@hrzpub.tu-darmstadt.de Internet: http://www.tu-darmstadt.de/fb/mb/ekt

Modern and elaborated techniques of turbulence and combustion modeling are essential to describe the turbulent reactive flow in technical combustion systems with high accuracy. Statistical turbulence models and especially the second order moment closures (SMC) are up to now the only feasible approach to model reactive flows with high anisotropies of turbulence and strong streamline curvature. Combustion models beyond the assumption of infinitely fast chemistry have become available on different levels of complexity.

The focus of this work is directed towards the simulation of complex flames. Linear vs. non-linear SMC calculations are evaluated in coupling with the well known flamelet approach. In an outlook simulations with the ILDM model are presented. A standard way of implementation are presumed probability density functions (pdf).

Attention in this study is drawn to a strongly swirling natural gas flame from the TECFLAM project for which valuable modeling experience has been gathered over the last two years, e.g [6, 7, 3]. The swirl and Reynolds numbers and thermal power are $S = 0.62$, $Re = 42000$ and $P = 150$ kW, respectively, thus representing an object close to engineering applications. The swirl is generated by a movable-block as described in the listed references. The turbulent flow field has been extensively measured with the LDV technique by [4, 5]. Temperature measurements with Rayleigh scattering and LIF investigations of the OH radical are described in [7].

The performance of Reynolds stress models in flames has already been object of intensive investigations (see e.g. [2, 6]), where relatively simple chemistry models, i.e. flamelet model with low strain rate, have been applied. In this study a step further is taken and more sophisticated chemical submodels are incorporated. Since methane flames do not satisfy the infinitely fast chemistry assumption, nonequilibrium effects need to be accounted for. The flamelet model capturing all the necessary strain rates in the flow field including the blowoff limit is one valid approach. Alternatively, the ILDM model, developed by [8], provides a description of the chemical reactions which locally considers the slowest chemical time scales. In this study, two progress variables together with the mixture fraction, are used to represent the current state in reaction space. A threedimensional pdf is defined via triple presumed betafunctions, after appropriate scaling of the progress variables in order to achieve statistical independence. The pdf is a function of the means of the mixture fraction and the two progress variables and also of their variances. Using a six dimensional lookup table, the source terms of the progress variables and other relevant thermochemical properties are evaluated efficiently in a preprocessing step.

Fig. 1 shows the radial distributions of mean velocity. In Fig. 2 calculated temperature contour-plots are to be seen. Both plots prove the method to work correctly. Issues of optimization regarding the size and shape of the look-up table are still under progress.

References

[1] J.Y. Chen and W.C. Chang. In TwentySixth Symposium (International) on Combustion, pp. 2207-2214, 1996.

[2] M. Fairweather, W.P. Jones, H.S. Ledin, and P. Lindstedt. In TwentyFourth Symposium (International) on Combustion, pp. 1067-1074, 1992.

[3] P. Habisreuther, P. Schmittel, P. Idda, H. Eickhoff, and B. Lenze. In VDI Berichte 1313, pp. 127-132, 1997.

[4] A. Kremer, E. P. Hassel, and J. Janicka. VDI Engineering Research, 8, 1997.

[5] A. Kremer, T. Landenfeld, E. P. Hassel, and J. Janicka. In VDI Berichte 1313, pp. 139-144, 199.

[6] T. Landenfeld, A. Kremer, E. P. Hassel, and J. Janicka. In Eleventh Symposium on Turbulent Shear Flows, pp. 18-1–18-6, 1997.

[7] T. Landenfeld, A. Kremer, E.P. Hassel, T. Janicka, Schäfer, J. Kazenwadel, C. Schulz, and Wolfrum J. To be presented at Twenty-Seventh Symposium (International) on Combustion, 1998.

[8] U. Maas and S.B. Pope. Combustion and Flame, 88, pp.239-264, 1992.

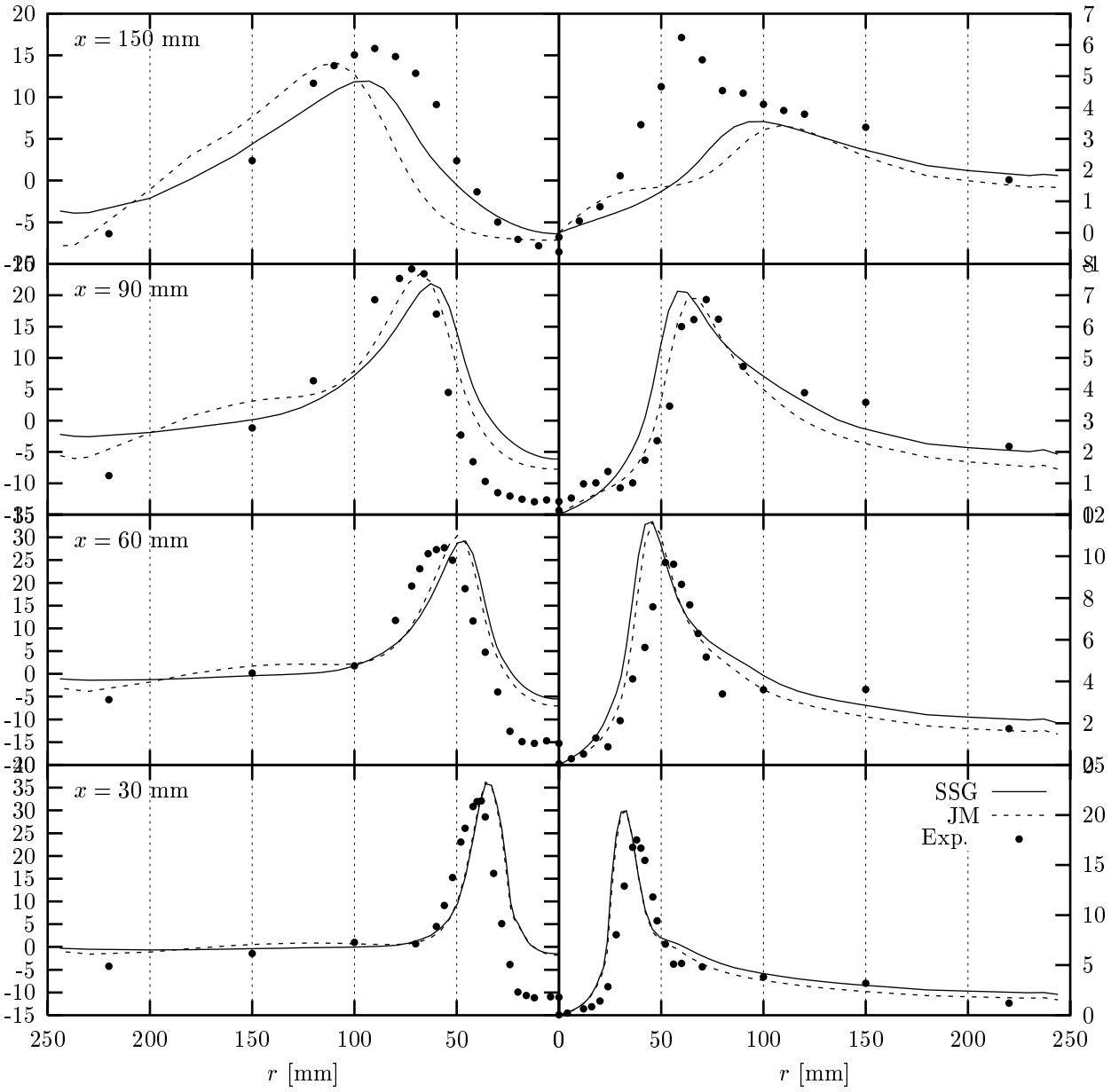

Figure 1: Radial distribution of axial mean velocity $\tilde{u}$, shear stress $\widetilde{u''v''}$ (left) and tangential velocity $\tilde{w}$, shear stress $\widetilde{u''w''}$ (right)., symbols: $\odot$ Exp. — SSG, − − − JM

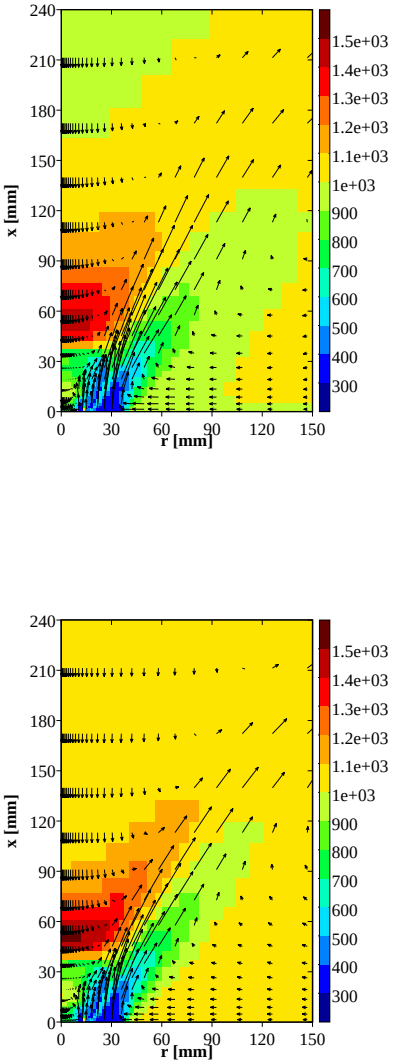

Figure 2: Mean Temperature distribution of SMC simulation, non-linear SMC model (top), linear SMC model (bottom)

Joint scalar PDF Monte Carlo simulations of a H_2/CO_2 turbulent jet diffusion flame with comprehensive chemistry

R.P. Lindstedt, J.P.H. Sanders and E.M. Váos

e-mail: p.lindstedt@ic.ac.uk

Imperial College of Science, Technology and Medicine
Mechanical Engineering Department
London SW7 2BX, U.K.

The $H_2 : CO_2$ (5:95) piloted turbulent ($Re = 15000$) diffusion flame of Masri et al. [1] has been modelled using the transported scalar Probability Density Function (PDF) approach. The flame consists of an axi-symmetric fuel jet with a mean velocity of 130 m/s and an ambient air co-flow of 15 m/s. The flame is stabilised by a rich ($\phi = 1.39$) premixed pilot flame of 10 m/s.

The flow field is modelled using the SSG (Speziale, Sarkar and Gatski [2]) second moment closure. The $C_{\varepsilon 2}$ constant in the dissipation rate equation is adjusted from 1.92 to 1.8 in order to improve the predicted spreading rate. Molecular mixing is modelled via the modified Curl's model [3]. The equations are solved using a Monte Carlo approach featuring moving particles in a Lagrangian frame of reference [4]. The flame is computed using a parabolic formulation with 50 cross stream nodes each containing on average 400 particles. About 4500 axial steps are used to cover 100 jet diameters. The chemistry is based on the reduced mechanism of Lindstedt and Selim [5] and features 14 solved (H_2, O_2, H_2O,H, O, OH, HO_2, CO, CO_2, CHO, CH_2O, NO, N_2O and N_2) and 8 steady state (H_2O_2, HNO, NNH, N_2H_2, N, NH_2, NH and NH_3) species.

The overall agreement with experimental data is good, as shown in Figs. 1-3, where conditional averages of experimental and computational data (50 bins) are presented. Fig. 1 shows that the predictions at $x/D = 6$ are closer to equilibrium than the experimental data. Fig. 2 and Fig. 3 imply that the rate of spread is reasonably well predicted as the computational and experimental results are truncated at the same point in mixture fraction space.

The influence of the composition of the pilot flame is found to be negligible at the first downstream measurement location of $x/D = 6$. Similarly, the effect of including CHO and CH_2O chemistry is found to be modest. The largest difference $\sim 10\%$ is found in the CO level at $x/D = 39$. The implication is that the flame can be computed with reasonable accuracy using only CO and CO_2 as carbon containing species.

The predicted CO level at $x/D = 6$ is higher than the experimental value, while the OH level shows good agreement with measurements. Further downstream ($x/D = 39$), the CO level remains overpredicted ($\sim 10\%$), while the OH levels are $\sim 66\%$ of the experimental peak value. The fact that CO and OH predictions are on different sides of the experimental data may indicate a problem with the experimental accuracy.

The rate for the $CO + OH \overset{\rightarrow}{\leftarrow} CO_2 + H$ reaction was further investigated through the use of the rate of Warnatz [6] (c.f. Lindstedt and Skevis [7]) and the CEC recommendation by Baulch et al. [8] (c.f. Leung and Lindstedt [9]). As anticipated by the study of laminar premixed flames by Lindstedt and Skevis [7], the slower Warnatz rate rate decreases the CO level by $\sim 15\%$ and generally improves agreement.

References

[1] Masri, A.R., Dibble, R.W. and Barlow, R.S., *Comb. Flame* 91:285-309 (1992).

[2] Speziale, C.G., Sarkar, S. and Gatski, T.B., *J. Fluid Mech.* 227:245-272 (1991).

[3] Janicka, J. and Kollmann, W., *J. Non-equilib. Thermodyn.* 4:47 (1978).

[4] Hulek, T. and Lindstedt, R.P., *Combust. Sci. Tech.* to appear, 1998.

[5] Lindstedt, R.P. and Selim, M.A., *Combust. Sci. Tech.* 99:277-298 (1994).

[6] Warnatz, J., Rate coefficients in the C/H/O system. In *Combustion Chemistry* (W.C. Gardiner Jr., Ed.), p. 197, Springer-Verlag, New York, 1984.

[7] Lindstedt, R.P. and Skevis, G., *Combust. Sci. Tech.* 125:73-137 (1997).

[8] Baulch, D.L., Cobos, C.J., Cox, R.A., Esser, C., Frank, P., Just, Th., Kerr, J.A., Pilling, M.J., Troe, J., Walker, R.W. and Warnatz, J., *J. Phys. Chem. Ref. Data* 21:411 (1992).

[9] Leung, K.M. and Lindstedt, R.P., *Combust. Flame* 102:129-160 (1995).

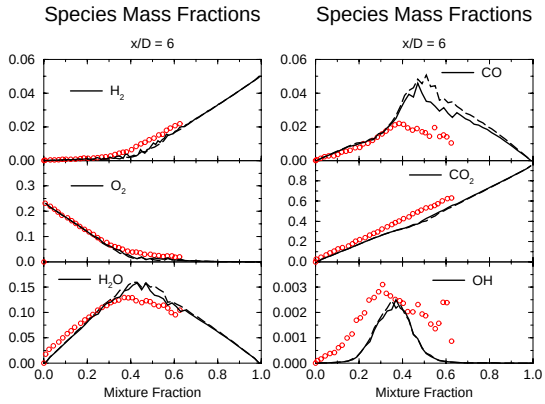

Figure 1: *Radial species profiles in mixture fraction space at $x/D = 6$. The circles and lines are conditional averages of experimental [1] and computed data. The solid and long-dashed lines represent calculations with the rates of Warnatz [6] and Baulch et al. [8] for the $CO + OH$ reaction respectively.*

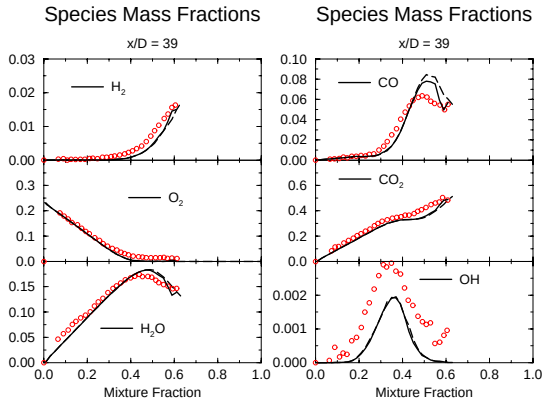

Figure 2: *Radial species profiles in mixture fraction space at $x/D = 39$. The circles and lines are conditional averages of experimental [1] and computed data. The solid and long-dashed lines represent calculations with the rates of Warnatz [6] and Baulch et al. [8] for the $CO + OH$ reaction respectively.*

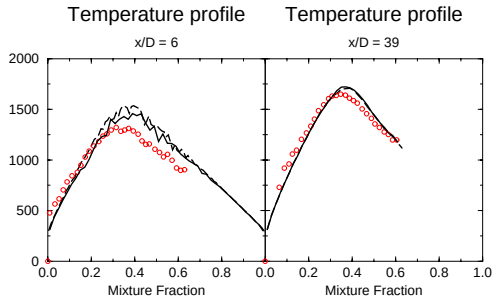

Figure 3: *Radial temperature profiles in mixture fraction space at $x/D = 6$ and 39. The circles and lines are conditional averages of experimental [1] and computed data. The solid and long-dashed lines represent calculations with the rates of Warnatz [6] and Baulch et al. [8] for the $CO + OH$ reaction respectively.*

MODELLING OF TURBULENCE-RADIATION INTERACTION IN COMBUSTION SYSTEMS

W. Malalasekera, J. C. Jones and M. Hossain
Department of Mechanical Engineering
Loughborough University
Loughborough, Leics. LE11 3TU, United Kingdom

ABSTRACT

In high intensity combustion systems, temperature and radiation fluctuations can be significant and the modelling of such systems requires the inclusion of temperature and absorption coefficient fluctuations in radiation calculations. There are a number of studies, both experimental and theoretical, which have attempted to investigate the effects of turbulence/radiation interactions in combustion. The experimental and modelling work of Kounalakis et al. [1] on non-premixed hydrogen/air flames observed measured intensity fluctuations of 20 - 110 % in their flames, providing direct evidence of the importance of turbulence/radiation interactions. Koch et al. [2] have reported spectral and time resolved radiation measurements in a model gas turbine combustor where the time resolved spectral intensity fluctuations have shown to be more than 30 % of the average value. Song and Viskanta [3] used concentration correlation functions to calculate the intensity fluctuations in a two dimensional axisymmetric geometry and showed that the intensity level, scale of turbulence and system dimensions affect the radiance. In a coupled simulation with combustion they showed that the calculated flux distributions can be significantly different when radiation fluctuations are included. The present study attempts to quantify the effects of temperature and absorption coefficient fluctuations on radiative heat transfer. A series of one-dimensional case studies have been considered to illustrate individual effects on radiation heat flux and the study also attempts to identify fluctuation effects on source terms which are used to couple radiation calculations to CFD combustion modelling procedures. The one-dimensional case studies show that temperature fluctuations cause significantly larger fluctuations in fluxes than those due to absorption coefficient fluctuations, due to the non-linear nature of temperature coupling. An increase in temperature from its mean value causes a considerably large percentage increase of flux from its mean. Temperature fluctuations also cause considerable source term fluctuations and, depending on local conditions, source term fluctuations can be out of phase causing large temperature gradients within the field. Based on one-dimensional observations a time-averaged method based on the discrete transfer technique is proposed in this study. It is demonstrated that the proposed time-average method is capable of reproducing the exact results obtained using the quasi-transient approach, Fig. 1. The time-averaged method is further used to demonstrate its applicability in modelling radiation fluctuations in a practical furnace system, as shown in figure 2. The study shows that in the case where temperature fluctuations are 10% of the mean values, the error occurring from the non inclusion of these fluctuations is approximately 2.5% and for a situation where temperatures fluctuate up to 25%, the error increases to 13%.

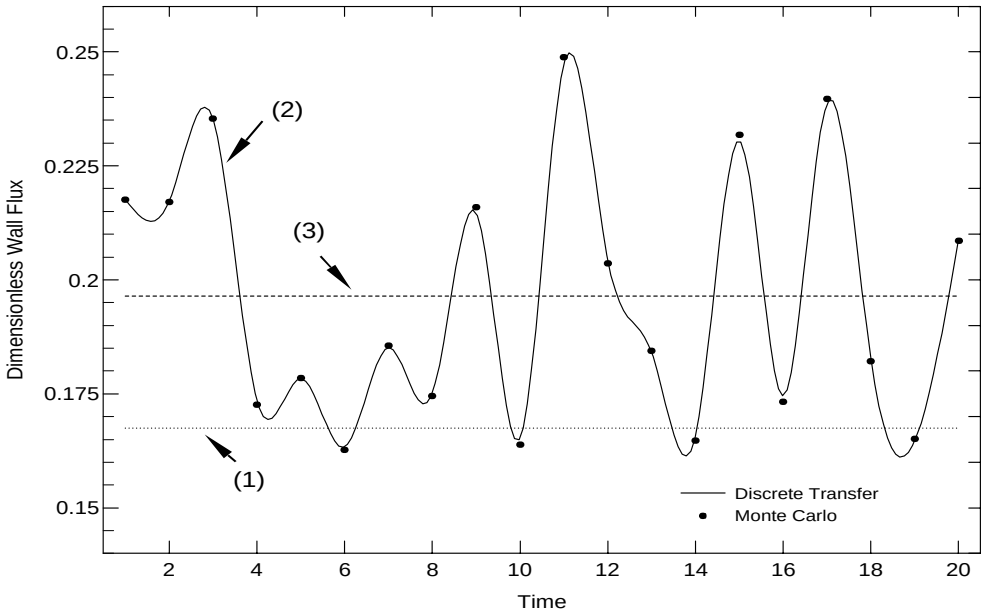

Figure 1. 1D case. Resulting wall flux from random temperature fluctuations. (1) Uniform medium, (2) Instantaneous wall flux, (3) Mean of instantaneous flux equal to the time-averaged result.

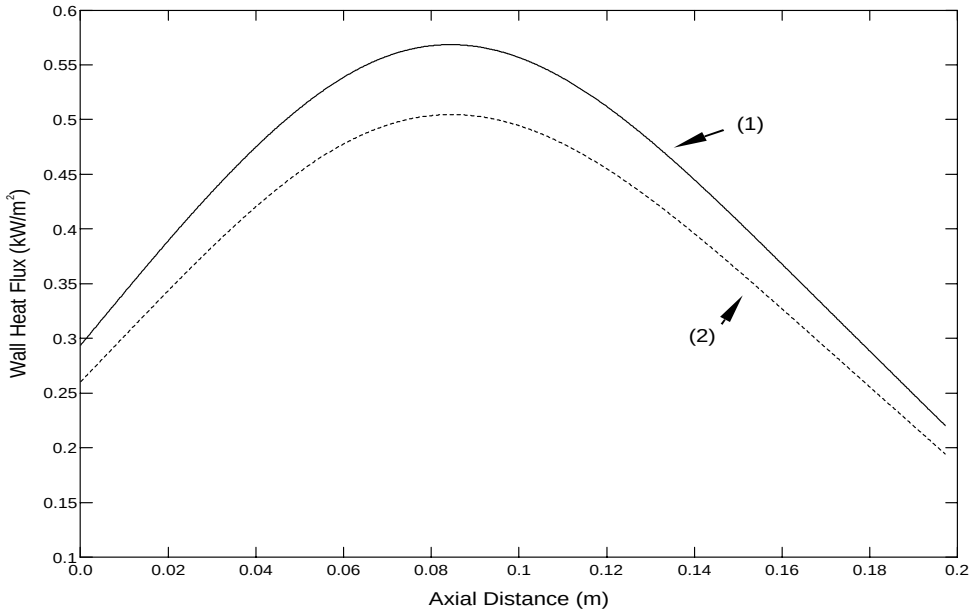

Figure 2. 2D case. Incident flux on axial wall of furnace. Showing the results from the time-average approach (1), and from using the mean temperatures (2).

REFERENCES

[1] Kounalakis, M. E., Gore, J. P. and Faeth, G. M., *Twenty-Second Symposium (International) on Combustion*, The Combustion Institute, Pittsburgh, 1981, pp. 1281-1290.

[2] Koch, R., Krebs, W., Jeckel, R., Ganz, B. and Wittig, S., ASME. 94-GT-403, 1994.

[3] Song, T. H. and Viskanta, R., *J. Thermophysics* 1: 56-62 (1986)

Investigations of a Turbulent $CH_4/H_2/N_2$ Jet Diffusion Flame: Survey of Experimental and Theoretical Results

W. Meier, O. Keck, D. Wolff, V. Bergmann, V. Jörres, W. Stricker

Institut für Physikalische Chemie der Verbrennung
DLR Stuttgart, Pfaffenwaldring 38, D-70569 Stuttgart
wolfgang.meier@dlr.de

An unconfined jet diffusion flame (Re=15200) fueled by a mixture of CH_4, H_2, and N_2 has been investigated experimentally by spontaneous Raman/Rayleigh scattering, two-dimensional laser-induced fluorescence, and laser Doppler velocimetry. The main goal of this work was a detailed characterization of the flame in order to establish a data base which can be used for the validation of mathematical flame models. A comparison between the experimental and theoretical results from PDF calculations is given.

The burner for the unconfined jet diffusion flame consisted of a straight tube (i.d. 8 mm) with a thinned rim at the exit and a coflow-nozzle (i.d. 140 mm) supplying the flame with dry air [1,2]. The fuel composition of 22.1% CH_4, 33.2% H_2, and 44.7% N_2 was chosen for the following reasons: (1) to study the chemistry of carbon containing species in turbulent jet flames; (2) to stabilize the flame by H_2 without changing the simple flow field of a straight tube; (3) dilution by N_2 to reduce signal background from laser-induced fluorescence of PAHs and C_2 radicals; (4) to get a nearly constant Rayleigh scattering cross section throughout the flame in order to apply 2D Rayleigh thermometry. From the Raman signals, excited by a flashlamp pumped dye laser, the PDFs of the major species concentrations (CH_4, H_2, O_2, N_2, H_2O, CO_2, CO) have been determined in quantitative pointwise measurements with a spatial resolution of 0.6 mm. The temperature was deduced from the total number density and, in addition, from the Rayleigh scattering signals using the actual Rayleigh cross section determined from the Raman data [3]. The radial profiles of the mean values and rms fluctuations which have been derived from the PDFs yield a general characterization of the flame and the correlations between various quantities give an insight into processes like differential diffusion and flame stretch. In addition to the point measurements, two-dimensional distributions of OH, CH, NO, and temperature have been measured in order to visualize the structures within the flame and to determine temperature gradients [2]. The flowfield was characterized by LDA measurements performed in J. Janicka's group at the TU Darmstadt. Radial profiles of the mean axial velocity U and radial velocity V, as well as the Reynolds-stress tensor components u'u' and u'v' have been determined at 7 downstream locations. An axial profile of U and u'u' has also been measured.

This flame and some experimental results from it have been presented at the second TNF Workshop in Heppenheim in 1997. Meanwhile, the data set has been completed by the LDA measurements and results from model calculations are also available. J.-Y. Chen from UCB has performed calculations with a parabolic code using Reynolds stress with joint scalar PDF approach, a 10-step reduced chemistry, and a modified Curl's mixing model. The comparison between the experimental and calculated results reveals a good agreement for the mixing and

velocity fields, but deviations for the temperature and some species mole fractions are clearly seen in the start region of the jet.

We expect further theoretical results from other modellers by the time of the workshop so that we can discuss the merits and shortcomings of various mathematical flame models. In the poster we will give an overview of the activities concerning this flame and summarize the results.

[1] F. Lipp, J. Hartick, E.P. Hassel, J. Janicka: In 24th Symp. (Int'l) on Combustion (The Combustion Institute, Pittsburgh, PA 1992), pp. 287

[2] V. Bergmann, W. Meier, D. Wolff, W. Stricker: Appl. Phys. B 66, 489 (1998)

[3] http://www.st.dlr.de/EN-CV/

Parallel Large-Eddy Simulations of Reacting Single and Two-Phase Flows using a Subgrid Combustion Model

Suresh Menon
School of Aerospace Engineering
Georgia Institute of Technology

Most practical combustion systems as in gas turbine engines, internal combustion engines, liquid-fueled rockets, etc., employ liquid fuel and gaseous oxidizer for the combustion process. As a result, many physically important processes (e.g., atomization, droplet vaporization, and fuel-air mixing) occur prior to the actual combustion process. The heat released during combustion in turn will modify the turbulence in the flow resulting in a fully coupled evolution of the fluid flow and chemical processes. All these processes are highly unsteady and in most real systems, occur in a highly turbulent environment. Current understanding of this type of flow field is severely limited and comes primarily from experiments carried out using simplified test configurations. Future advancement in engine design and increase in efficiency (i.e., reduced fuel consumption and pollutant emission) will require a more in-depth understanding of the combustion processes. However, experimental studies of real combustors are difficult primarily because of the difficulty in accessing the reaction zone with non-intrusive instruments. Furthermore, diagnostic tools currently available can only provide information on only a few species and in most cases, can provide only limited information on the dynamics of the processes. In addition, parametric experiments on complex real engines can easily become prohibitively expensive.

An alternate method would be to employ numerical methods since they are more cost effective. However, at present there are no modeling tools available to address this type of unsteady flow primarily due to (a) the lack of physically accurate models and (b) the lack of adequate computing resources. With the availability of massively parallel systems and the recent development of a physically accurate simulation model (discussed in this paper), these limitations can be relaxed to some extent so that it becomes feasible to address simulation of high Reynolds number reacting, turbulent, single- and two-phase flows. However, it is worth noting here that in spite of the recent development of parallel systems with terraflop capability, simulations of such flows in practical systems are still considered impossible since both the memory and processing speed requirements are far beyond the current capability. However, the development and validation of a physically accurate method of simulation using current facilities will go a long way towards establishing a viable tool for simulating such complex flows in the future when petaflop machines become available. Here, we report on the development of such a simulation tool. It is also shown here that this development requires the availability of parallel processing systems both due to the nature of the model and due to the processing power needed to evaluate the model's performance.

The present study employs the technique of large-eddy simulations (LES). In LES, the scales larger than the grid are computed using a time- and space-accurate scheme, while the unresolved smaller scales are modeled. The Navier-Stokes equations that govern the conservation of mass, momentum and energy in a fluid are filtered to obtain the LES equations. The filtering operation results in terms in these equations that must be modeled. Closure of momentum and energy transport equations can be achieved using a subgrid eddy viscosity model since the small scales primarily provide a dissipative mechanism for the energy transferred from the large scales. A local dynamic model for the subgrid turbulent kinetic energy has been developed for the closure of the subgrid terms in the momentum and energy equations. Application of this subgrid model in turbulent flows shows that this model is capable of accurately representing the effect of unresolved terms even when relatively coarse grids are employed. The details of the LES equations and the subgrid closure employed have been reported in the cited papers and therefore, are avoided here for brevity.

Subgrid closure of this manner (i.e., based on an eddy viscosity model) cannot be used for modeling the scalar transport since for combustion to occur, the species must first mix at the molecular level. The small scales of motion control this stage of mixing, which are typically unresolved in LES. Thus, ad hoc models for the subgrid (unresolved) scales cannot be used.

To address these issues, recently a subgrid combustion model was developed and implemented within the LES formulation. This model separately and simultaneously treats the physical processes of molecular diffusion and small scale turbulent convective stirring. This is in contrast to probability density function closure which phenomenologically treats these two processes by a single model, thereby removing experimentally observed Schmidt number variation of the flow. In the present approach, the resolved scale momentum transport is simulated on a conventional grid using a conventional LES method. However, no scalar transport is simulated on the LES grid. Rather, within each LES cell, a subgrid one-dimensional (1D) domain is defined and within this 1D domain, turbulent small-scale mixing, molecular transport and chemical kinetics are explicitly modeled. The local 1D domain can be visualized as a stochastic instantaneous slice of the local 3D flame brush and the resolution in this domain is chosen to resolve all relevant length scales. As a result, the chemical reaction-diffusion equations can be solved without any assumptions (i.e., as a direct simulation).

The gas-phase methodology has been extended to two-phase flows to capture accurately the process of phase change and turbulent mixing. The method has also been further refined and used to study vaporization and the subsequent chemical reactions. Both infinite and finite-rate kinetics have been investigated. The two-phase simulation model is part of a suite of simulation codes developed at the Computational Combustion Laboratory in Georgia Tech. These codes (of increasing complexity and applicability) have been used to methodically develop the new subgrid combustion simulation approach. The goal of these studies is to develop and validate a scheme that can be used to investigate and design the next generation gas turbine engines. The present methodology is computationally much more expensive when compared to codes currently being employed. However, the potential increase in accuracy and the projected ability of the new approach to capture complex phenomena and radical kinetics justifies the added expense. Furthermore, with the increase in computational power, such intensive calculations may become acceptable in the future especially when even more massively parallel systems (i.e., with processors > 1000 CPU's) become available.

The present approach combines features of both Eulerian-Eulerian (gas-liquid) and Eulerian-Lagrangian (gas-liquid) modeling approaches. In this approach, gas phase calculations are carried out using an Eulerian LES method while the liquid droplets are tracked within the Eulerian gas phase using a Lagrangian particle tracking method. The droplets are integrated in time in each of the gas phase LES cells and are transported across the Eulerian domain. In this process, the droplets exchange mass, momentum and energy with the local gas phase. In conventional two-phase modeling, all droplets smaller than a pre-specified cut-off size are assumed to instantaneously vaporize and mix. However, results have confirmed that this assumption is highly erroneous unless the cutoff size is very small. Increasing the cutoff size without sacrificing accuracy is of great interest since this would reduce the computational time significantly. This issue has been addressed here such that the droplets below the cut-off are carried into the subgrid using a void fraction Eulerian formulation to simulate the effect of droplets all the way till the liquid phase completely vaporizes and mixes at the smallest scales.

We will report on LES results obtained for various problems of current interest: scalar mixing/combustion in turbulent shear layers, opposed jet diffusion flame, stagnation point flames, highly swirling premixed flames in real combustor and two-phase vaporizing flows in mixing layers.

Stretching Exercises: Flickering Flames as a Test of Our Understanding of Chemistry-Turbulence Interaction

J. Houston Miller
Department of Chemistry
The George Washington University
Washington, DC 20052
(202) 994-7474
houston@gwu.edu

The interactions between chemistry and turbulence are critically important in the production of pollutants and in determining flame stability. For example, two of the mechanisms for the production of NO in flames involve radical species, CH and O atoms, whose concentrations depend upon the local strain rate. A second example is the formation of soot particles and the emission of smoke from flames. The chemistry that leads to particle inception is relatively slow and would also be expected to depend on not only radical species concentrations, but also on the particle residence time in flame regions conducive to this growth chemistry.

Over the past several years numerous research groups have initiated studies of either flames that are naturally flickering or have either or both of the air and fuel flow rates acoustically-coupled. For example, an experimental facility to study time-varying, hydrocarbon diffusion flames using optical imaging techniques has been developed at the National Institute of Standards and Technology (NIST). Axisymmetric flames have been acoustically locked to a pulsed dye laser system at 10 Hz, allowing interrogation of the flame dynamics as a function of height, phase angle, and forcing amplitude. These flames exhibit reproducible structure and a much range of local strain and scalar dissipation rates than those found in steady, co-flowing laminar flames. Experimental imaging results have been obtained on OH , polycyclic aromatic hydrocarbons, and soot particles in these time-varying flames. One of the most striking results is the observation that soot production in these flames is significantly enhanced (by more than a factor of 4-5) compared to steady laminar flames. In our laboratory, we have reproduced the NIST experiment and have used Tunable Diode Laser Absorption Spectroscopy to map carbon monoxide, carbon dioxide, and methane. The mass fraction of these three species may be used to estimate mixture fraction both spatially and temporally.

Although an effort is underway at GWU to model this flame, the purpose of this poster is to propose this, or similar flames , as a target of opportunity for the turbulence modeling community.

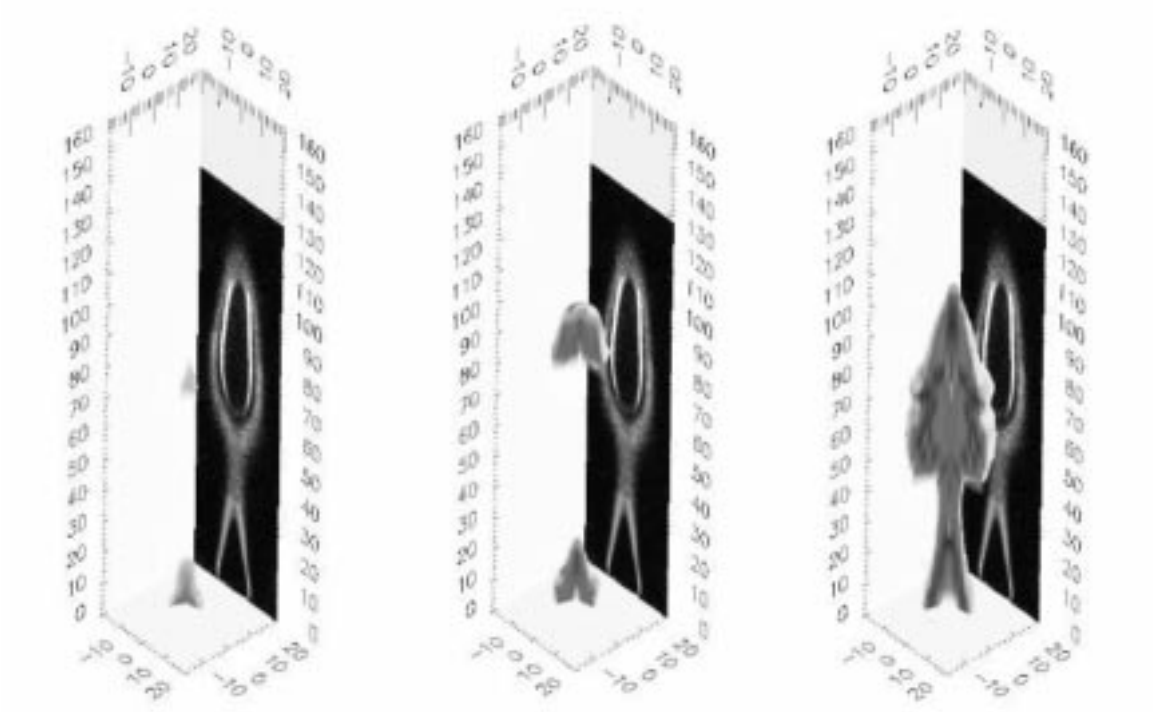

Figure 1: *Foreground*: profiles of methane, carbon monoxide, and carbon dioxide in time varying, methane/air, non-premixed flame (time = 70 ms relative to node in sinusoidal excitation of fuel flow rate). *Background:* hydroxyl radical laser-induced fluorescence and soot particle scattering data courtesy of Kermit Smyth (NIST).

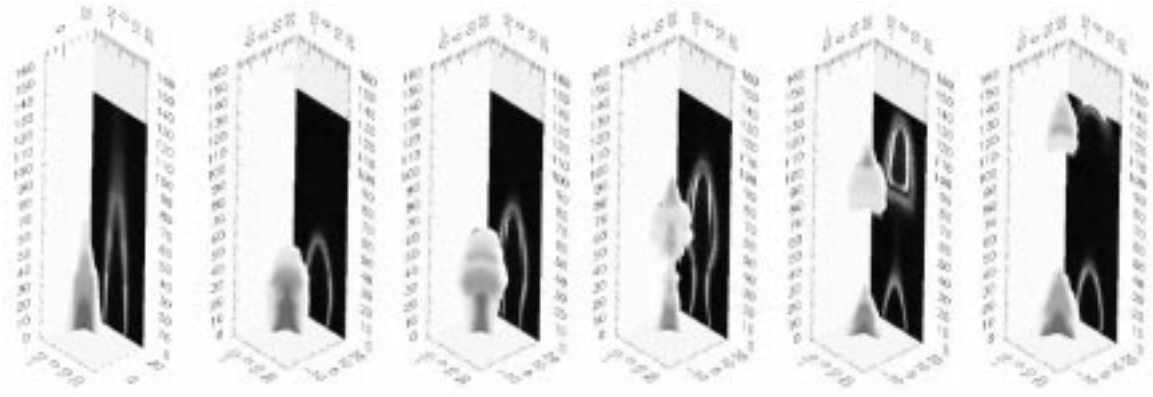

Figure 2: Contours of mixture fraction in steady flame (left panel) and in time-varying flame (images separated by 20 ms). Color versions of these and other time-varying flame media can be found at http://www.gwu.edu/~gwchem/jhm_images.

Differential Diffusion in Turbulent Reacting Flows

Vebjørn Nilsen: Combustion Research Facility, Sandia National Laboratories, Livermore, CA 94551-0969 and George Kosály: Department of Mechanical Engineering, University of Washington, Seattle, WA 98195

Corresponding author: Vebjørn Nilsen, e-mail: vebjorn@thor.ran.sandia.gov

Abstract

Data obtained from direct numerical simulations are presented to examine effects due to differential diffusion on reacting scalars in isotropic, decaying turbulence. In the simulations fuel and oxidant react via a one-step, isothermal reaction.

The data demonstrated that the influence of differential diffusion on ensemble averages of the mass fractions and the reaction rates diminishes with increasing Reynolds numbers (Re). With increasing Damköhler numbers, however, differential diffusion effects became more pronounced.

The equations satisfied by the average fuel and oxidant mass fractions conditioned on values of a unity Schmidt number conserved scalar, Z, are attractive starting points of modeling efforts. The conditionally averaged mass fractions are denoted as $\widetilde{Q}_i(\eta,t) \equiv \langle \widetilde{Y}_i | Z=\eta \rangle_t$; i = F, O. If the conditional fluctuation terms are neglected the Conditional Moment Closure (CMC) [1] model equations are ($Sc_F < 1, Sc_O = 1$):

$$\frac{\partial \widetilde{Q}_F}{\partial t} - \frac{1}{2Sc_F}\langle \chi|\eta\rangle_t \frac{\partial^2 \widetilde{Q}_F}{\partial \eta^2} - \frac{(1-Sc_F)}{Sc_F}\langle \Theta|\eta\rangle_t \frac{\partial \widetilde{Q}_F}{\partial \eta} = -A\widetilde{Q}_F\widetilde{Q}_O, \tag{1a}$$

$$\frac{\partial \widetilde{Q}_O}{\partial t} - \frac{1}{2}\langle \chi|\eta\rangle_t \frac{\partial^2 \widetilde{Q}_O}{\partial \eta^2} = -rA\widetilde{Q}_F\widetilde{Q}_O \tag{1b}$$

where $\langle \chi|\eta\rangle_t \equiv 2\nu\langle \nabla Z\cdot\nabla Z|Z=\eta\rangle_t$ and $\langle \Theta|\eta\rangle_t \equiv \nu\langle \nabla^2 Z|Z=\eta\rangle_t$. The conditional averages of the mass fractions are assumed to satisfy the usual initial and boundary conditions:

$$\widetilde{Q}_F(\eta,t=0)=\eta, \quad \widetilde{Q}_O(\eta,t=0)=1-\eta, \tag{2a}$$

$$\widetilde{Q}_F(\eta,t) = \begin{cases} 1, & \text{when} \quad \eta\to 1 \\ 0, & \text{when} \quad \eta\to 0 \end{cases} \quad \text{and} \quad \widetilde{Q}_O(\eta,t) = \begin{cases} 0, & \text{when} \quad \eta\to 1 \\ 1, & \text{when} \quad \eta\to 0. \end{cases} \tag{2b}$$

Model equations similar to Eqs. (1a,b) have been proposed recently by Pitsch and Peters [2] who used flamelet arguments in the development. Equations (1a-2b) will therefore be referred to as the Conditional Moment Closure - Flamelet (CMC-FL) model equations of differential diffusion.

In the absence of differential diffusion the terms associated with the conditional fluctuations can be neglected [1]. The conditional fluctuations, however, play an important role in the modeling of differential diffusion. The neglection of the conditional fluctuations leads to an overestimation of the influence of differential diffusion and results in erroneous Re dependence of the average mass fractions and reaction rates. Indeed, as Fig. 1 illustrates, CMC-FL predicts that the influence of differential diffusion on the average fuel reaction rate increases with increasing Re which contradicts the true behavior. Note that $\langle w_F \rangle$ refers to

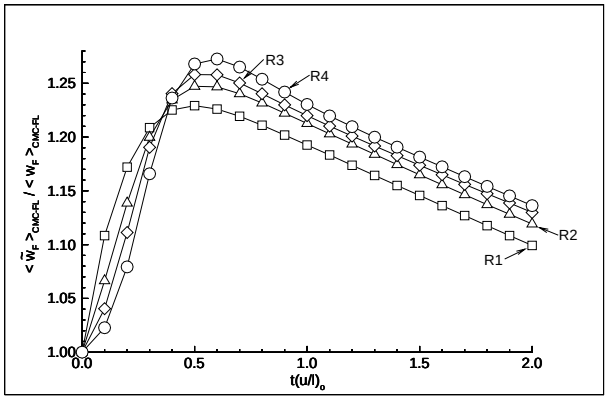

Figure 1: $\langle \widetilde{w}_F \rangle / \langle w_F \rangle$ versus $t(u'/\ell)_o$ as computed from CMC-FL for the R1 ($-\Box-$), R2 ($-\triangle-$), R3 ($-\diamond-$) and R4 ($-\bigcirc-$) velocity fields ($A = 8$, $Sc_F = 0.5$).

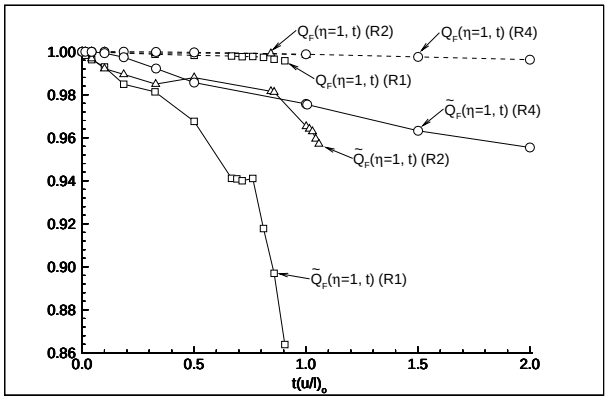

Figure 2: The average fuel mass fraction conditioned on $Z = 1$ versus $t(u'/\ell)_o$ for the R1 ($-\Box-$), R2 ($-\triangle-$) and R4 ($-\bigcirc-$) velocity fields. The solid and dashed curves refer to the $\mathcal{D}_F = 4\nu$ and $\mathcal{D}_F = \nu$ case, respectively ($A = 8$)

the average reaction rate in the absence of differential diffusion and that the velocity fields R1-R4 are in order of increasing Reynolds numbers.

The boundary condition $\widetilde{Q}_F(1,t) = 1$ cannot be established mathematically when there is differential diffusion. Figure 2 shows that there is a substantial violation of this boundary condition, especially at low Re values. However, the use of the erroneous boundary condition did not lead to significant error in the predicted average mass fraction and reaction rates provided the conditional fluctuation terms are accounted for.

Acknowledgements

Partial support by NSF (CTS-9415280) and AFOSR (F49620-97-1-0092) is acknowledged.

References

[1 R. W. Bilger, "Conditional moment closure for turbulent reacting flow," *Phys. Fluids A*, **5**, 436 (1993)

[2 H. Pitsch and N. Peters, "A Consistent Flamelet Formulation for Non-Premixed Combustion Considering Differential Diffusion Effects ," (*Accepted for publication by Combust. Flame, 1997*)

Monte Carlo PDF calculations of the Delft III flame

P.A. Nooren[*] , H.A. Wouters[**] , T.W.J. Peeters and D. Roekaerts

J.M. Burgers Centre, Department of Applied Physics, Thermal and Fluid Sciences,
Delft University of Technology, P.O. Box 5046, 2600 GA Delft, The Netherlands
E-mail: roekaerts@tn.tudelft.nl

Model predictions of the "Delft III flame", the piloted turbulent natural gas diffusion flame selected for this workshop, are obtained with a Monte Carlo Probability Density Function (PDF) model and are compared to experimental data reported in Refs. [1-3] (LDA, OH-LIF, CARS) and [5] (Raman-Rayleigh-LIF). The main objective was to investigate the performance of different micro-mixing models and simplified descriptions of the combustion chemistry needed in the PDF approach. Details of the investigation reported here can be found in Refs. [4,5]. The fact that the RR-LIF measurements of [5] show lower temperatures than the CARS results of [3] complicates the model validation. This issue is also addressed in other contributions to this workshop [6, 7].

First, the numerical accuracy obtained with the computational grids and the number of Monte Carlo particles typically used in the calculations is investigated. It is shown that the accuracy achieved in the simulations is sufficient for an adequate evaluation of the submodels. Next, the predictions for the velocity field are discussed. In general, the k-ε model with round jet correction can correctly describe the mean axial velocity and turbulent kinetic energy in the upstream part of the flame. At the highest axial position considered, x = 250 mm, the width of the jet is somewhat under predicted. Constrained equilibrium calculations are performed using three different models for scalar micro-mixing: the Interaction by Exchange with the Mean (IEM), Coalescence-Dispersion (C/D) and mapping closure models. The different descriptions of micro-mixing yield very similar results for the mean mixture fraction field and give good agreement with the CARS data of Ref. [3] for the mean temperature. Temperature standard deviation and PDF shapes are generally predicted well by the C/D and mapping closure models. The IEM model, in contrast, produces qualitatively incorrect results in parts of the domain. The inability of the IEM model to capture some of the essential properties of the fluctuating temperature is attributed to the small differences observed between the mixture fraction PDF predicted by the IEM model on one side and those from the C/D and mapping closure models on the other side. Combined with the strongly non-linear dependency of temperature on mixture fraction around stoichiometry, these differences can have appreciable effects on the predicted temperature statistics. It is concluded that the choice of micro-mixing model can have a strong influence on the quality of the predictions.

The other two chemistry models that are studied are the laminar flamelet model and the ILDM reduced chemical kinetics. In both approaches, the description of the flame stabilisation process induced by the pilot flames plays a crucial role. Unfortunately, some of the characteristics of the pilot flames, such as their three-dimensional geometry and exact thermochemical composition, cannot be represented in the simulations. In the laminar flamelet description used here, lift-off of the turbulent flame is prevented by excluding extinguished flamelets from the laminar flamelet library. Local extinction effects can therefore not be predicted in the laminar flamelet computation. In the ILDM simulations, flame stabilisation is achieved by enhancing scalar micro-mixing by a factor of two compared to the standard value used in the constrained equilibrium calculations.

* Present address: KPN Research, Leidschendam, The Netherlands
** Present address: Corporate Research Lab., Hoogovens BV, IJmuiden, The Netherlands

The temperature fields from the laminar flamelet model and ILDM simulations are in good agreement with the data presented in Ref. [3] and the constrained equilibrium results. The ILDM reduced kinetics were found to predict only a small amount of local extinction. The CO_2 and H_2 O mass fractions, which can, just as temperature, be considered as global reaction progress variables, agree well with the constrained equilibrium data. The measured peak mean H_2 O mass fractions are smaller than the predicted values.

In the Raman-Rayleigh-LIF measurements, CO and H_2 mass fractions significantly above steady laminar flamelet values were observed. Scatter plots show that the laminar flamelet model predicts the CO mass fraction well in rich mixtures. The radial profiles of the mean CO mass fraction are reproduced well in the laminar flamelet model simulation. However, it is concluded that the constrained equilibrium and laminar flamelet model descriptions cannot successfully predict the CO levels over the entire mixture fraction range. The same holds for H_2. By construction, the ILDM scheme employed here [4] gives zero CO and H_2 for compositions outside the domain where solutions for the low-dimensional manifold are available. This leads to a strong underestimation of the CO and H_2 levels.

Comparison of the measured OH concentrations to the constrained equilibrium values showed that, as expected, OH is in super-equilibrium in the upstream part of the flame. Although the laminar flamelet model and ILDM descriptions both produce realistic super-equilibrium OH levels, it is concluded that only the ILDM reduced kinetics correctly describe the decay of the OH concentrations towards equilibrium. The good performance of the ILDM kinetics was attributed to the two reaction progress variables in the scheme. The progress variables can successfully describe the slow chemical processes governing the relaxation of the super-equilibrium OH concentration.

From the observation that the turbulent mixing frequency is rather insensitive to primary air flow rate, with frequency of local extinction being sensitive, it is concluded that the finite-rate kinetic effects in the Delft flames III and IVare not caused by a high mixing rate but can be attributed to processes in the extreme upstream part of the flame which can be expected to be very sensitive to the inlet boundary conditions.

Acknowledgements

The ILDM table was constructed by U. Maas and D. Schmidt (University Stuttgart). The work of P.A. Nooren was carried out in the program of the Foundation for Fundamental Research on Matter (FOM), The Netherlands.

References

[1] P.P.J. Stroomer, *Turbulence and OH structures in flames*, PhD thesis. TU Delft, 1995
[2] J.E. de Vries, *Study on turbulent fluctuations in diffusion flames using laser induced fluorescence*, PhD thesis, TU Delft, 1994
[3] J. Mantzaras and Th.H. van der Meer, Coherent Anti-Stokes Raman Spectroscopy measurements of temperature fluctuations in turbulent natural gas-fueled piloted jet diffusion flames, *Combustion and Flame*, **110**, 39-53, 1997
[4] Nooren, P.A., Wouters, H.A., Peeters, T.W.J., Roekaerts, D., Maas, U. and Schmidt, D., Monte Carlo PDF modeling of a turbulent natural-gas diffusion flame, *Combust. Theory Modeling*, **1**, 79-96, 1997
[5] P.A. Nooren, *Stochastic modeling of turbulent natural-gas flames*, PhD thesis, TU Delft, 1998
[6] P.A. Nooren, R.S. Barlow and J.H. Frank, *Rayleigh-Raman-LIF measurements in the Delft III and IV flames*, this workshop
[7] Michel Versluis, Pieter Nooren, Ronnie Knikker, Ming-Cheng Zong and Theo van der Meer, *CARS temperature measurements in the Delft III flame*, this workshop

Rayleigh-Raman-LIF measurements in the Delft III and IV flames

P.A. Nooren *
J.M. Burgers Centre, Dept. of Applied Physics, Thermal and Fluid Sciences,
Delft University of Technology, P.O. Box 5046, 2600 GA Delft, The Netherlands
*New address: KPN Research, Leidschendam, The Netherlands
E-mail: P.A. Nooren@research.kpn.com

R.S. Barlow and J.H. Frank
Diagnostics and Reacting Flow Department, MS 9051 Sandia National Laboratories,
Livermore, CA 94551-099, USA
E-mail: barlow@ca.sandia.gov

Simultaneous point measurements of species concentrations and temperature in the "Delft III flame", the piloted turbulent natural gas diffusion flame selected for this workshop, were obtained at the turbulent diffusion flame laboratory at Sandia National Laboratories, using Rayleigh-Raman-LIF (RR-LIF)[1]). These measurements complement the existing experimental data for the this flame collected earlier at Delft University of Technology: LDA measurements of the flow field [2], LIF data on the OH radical concentration [3], Coherent Anti-Stokes Raman Spectroscopy (CARS) measurements of mean temperature and temperature statistics [4] and Infrared emission/absorption tomography data on temperature and the volume fractions of H_2O, C_2H_2 and soot [5]. The RR-LIF measurements provide simultaneous point data on temperature and the concentrations of CO_2 , O_2, CO, N_2, CH_4 , H_2O, H_2, OH and NO. In addition to measurements in flame III also measurements in flame IV, which differs from flame III only by an increase of the primary air flow rate with 42 %, were made. Details of the investigation reported here can be found in Ref. [1].

The application of the Raman technique in the undiluted natural-gas flames considered here proves to be very challenging because of the high fluorescence interference levels. The interference contributions to the recorded Raman signals are identified and subtracted using empirical correlations between the Raman signals and the signals on the interference monitor channels. This procedure proves to be adequate for most species. However, it is found that the empirical approach cannot be used to remove the interference contributions to the CO Raman signal. CO measurements are obtained using two-photon LIF. For certain mixture fractions conditions in flame III the interferences on the Raman signals for CO2 and O2 cannot be removed adequately. The concentrations of these species are determined using an alternative approach assuming that the thermochemical composition is close to that in a strained laminar flamelet (PVLF correction).

For comparison with model predictions and other measurements, it is important to consider the relative random errors and potential systematic uncertainties in the RR-LIF experiment. These data are summarised in Table 1.

The Raman-Rayleigh temperatures are generally lower than previous CARS measurements of [4]. Because of the systematic uncertainties, present in both Raman-Rayleigh and CARS data sets it is not possible to reach, on the basis of data presented in Refs. [1] and [4], a final conclusion as to whether the Raman-Rayleigh and CARS data sets are consistent. Part of the differences observed between the Raman-Rayleigh and CARS temperatures can be caused by small differences between the boundary conditions in the two experiments. Further analysis of the CARS measurement technique is presented by Versluis *et al.* in Ref. [6].

The RR-LIF measurements of the OH concentration compare well with the existing semi-quantitative one-dimensional LIF data [3]. For the assessment of model predictions of the OH concentrations RR-LIF data are preferred, as these provide truly quantitative concentrations.

Acknowledgement

The Sandia contributions to this project were supported by the United States Department of Energy, Office of Basic Energy Sciences, Division of Chemical Sciences. The work of P.A. Nooren was carried out in the program of the Foundation for Fundamental Research on Matter (FOM), The Netherlands.

Table 1: Estimated relative random errors and potential systematic uncertainties in the Raman-Rayleigh-LIF measurements. The systematic uncertainties are given separately for lean/stoichiometric mixtures and for rich mixtures in flames III and IV. The species entries are for concentrations (moles dm^{-3}). The superscript IV denotes estimates valid in flame IV only, t and m refer to typical and maximum values, respectively.

quantity	random error (%)	potential systematic uncertainty (%)			
		lean/ stoich.	rich		main source(s)
			flame III	flame IV	
CO_2	8^{IV}	4	—	10	interferences
O_2	6^{IV}	3–12	—	3–12	calibration: 3% at 1300 K, 12% at 2000 K
N_2	3	2	5	5	interferences
CH_4	2	2–10	2–10	2–10	calibration: 6% at 1500 K, 10% at 2100 K
H_2O	7	4	11	8	interferences
H_2	17	5	20	15	calibration, interferences
OH	8	10	10	10	calibration
NO	12	10	20	15	calibration, non-resonant signal
CO	7	13	18	18	calibration, non-resonant signal
ξ	4	2	5^t, 20^m	2^t, 5^m	CH_4 calibration, PVLF correction flame III
T	1	2	2^t, 8^m	1^t, 3^m	CH_4 calibration, PVLF correction flame III, excluding spatial averaging

References

[1] P.A. Nooren, *Stochastic modeling of turbulent natural-gas flames*, PhD Thesis, TU Delft, 1998, Promotors: D. Roekaerts and K. Hanjalić

[2] P.P.J. Stroomer, *Turbulence and OH structures in flames*, PhD Thesis, TU Delft, 1995

[3] J.E. de Vries, *Study on turbulent fluctuations in diffusion flames using laser induced fluorescence*, PhD Thesis, TU Delft, 1994

[4] J. Mantzaras and Th.H. van der Meer, Coherent Anti-Stokes Raman Spectroscopy measurements of temperature fluctuations in turbulent natural gas fueled piloted jet diffusion flames, *Combustion and Flame*, **110**, 39–53, 1997

[5] R.E.J. van den Bercken, *IR emission/absorption tomography in flames*, PhD Thesis, TU Delft, 1998

[6] Michel Versluis, Pieter Nooren, Ronnie Knikker, Ming-Cheng Zong and Theo van der Meer, *CARS temperature measurements in the Delft III flame*, this workshop

Computation of Sandia Piloted CH_4/Air Jet Flames using Laminar Flamelet State Relationships

R. N. Paul, Y.R. Sivathanu and J. P. Gore
gore@ecn.purdue.edu
Thermal Sciences & Propulsion Center
Purdue University, West Lafayette, IN 47907

Introduction

Sandia piloted partially premixed CH_4/Air turbulent jet flame, one of the target flames for the 3rd TNF Workshop, is considered using the laminar flamelet concept. Predictions of Favre averaged mean and RMS (root mean square) temperature, N_2, O_2, H_2O, H_2, CH_4, CO, CO_2, OH and NO are compared with the measurements. The main jet is a mixture of three parts air and one part CH_4 by volume yielding an equivalence ratio of 3.16. The laminar flamelet state relationships (LFSR) are generated using the OPPDIF code including the effects of radiation heat loss. Opposed flow partially premixed flames with velocities between 5 – 50 cm/s are computed to parametrically address the effects of stretch rate. A clipped Gaussian profile is assumed for the mixture fraction PDF. The parameters of the mixture fraction PDF are obtained from the Favre averaged mixture fraction and the mean square mixture fraction fluctuations. In the present calculations, these quantities are taken from the experimental data provided at the TNF Workshop web site. Favre averaged mean and RMS of all other scalars are computed. The predictions of mean and RMS temperature and major species concentrations are in good agreement with the data.

Results and Discussion

The Favre averaged mean and RMS of temperature, N_2, O_2, H_2O, H_2, CH_4, CO, CO_2, OH and NO are calculated using the LFSR and PDF approach. Results are then compared with the experimental data for all axial locations where data are available. Sample results with state relationships obtained from the 5 cm/s flames without the effects of radiation are plotted in Figures 1 and 2. The Favre averaged mean and RMS temperature profile are presented for axial locations x/d = 1, 7.5 and 30. At all locations the calculations show reasonable agreement with the experimental data. Calculations also capture the experimentally observed variations in T_{rms}, e.g., double peaks at x/d = 1.

The Favre averaged mean and RMS mass fractions for all major species are also compared with measurements and reasonable agreement is found. In Figures 3 and 4, the Favre averaged mean and RMS of mass fractions of CH_4, O_2, and CO_2 are compared with experimental data for x/d = 1, 7.5 and 30. The Favre averages for all of the major species shows good agreement with experimental data. The RMS values of these species also show reasonable agreement except at x/d =1, where calculated RMS for O_2 mass fraction is much larger than the data. The agreement for CO, H_2 and NO mole fractions is not good but improves when effects of stretch rate and radiation are considered. The above comparison between mean and RMS values of temperatures and major species concentrations shows that the laminar flamelet concept is applicable for the operating conditions of Sandia flame D.

The temperature and major species mole fraction predictions based on the state relationships involving an order of magnitude variation in stretch rates and radiation heat loss were also considered. These are in agreement with each other and with the results shown in Figs. 1-4 within the experimental uncertainty. For CO, H_2, and NO mole fractions, consideration of radiative heat loss improves the agreement between measurements and predictions significantly. However, for these species, the effects of higher stretch rates and those of radiative heat loss are qualitatively similar. Therefore, in spite of the encouraging agreement between measurements and predictions for major species concentrations, laminar flamelet state relationships with radiation heat loss and stretch-rate as parameters appear necessary, for minor species predictions.

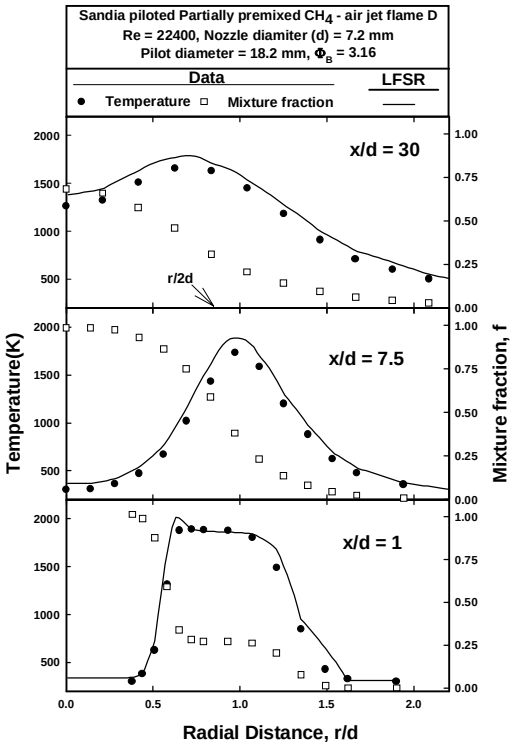

Fig. 1: Measurements and LFSR predictions of Favre averaged temperatures

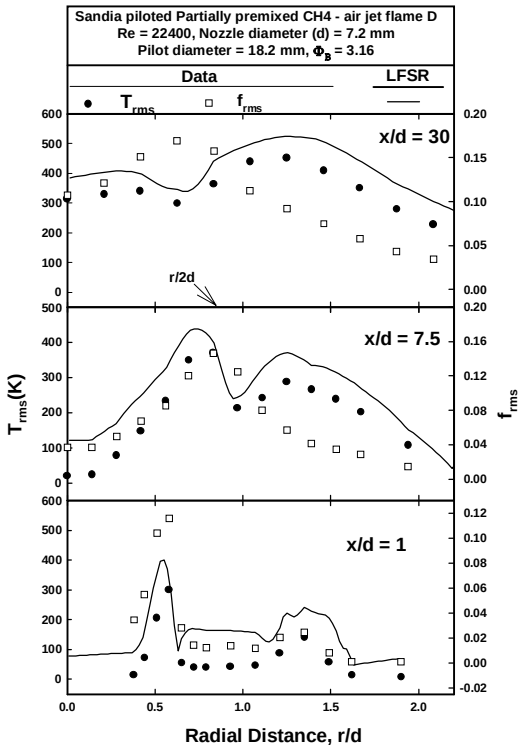

Fig. 2: Measurements and LFSR predictions of Favre averaged rms temperatures

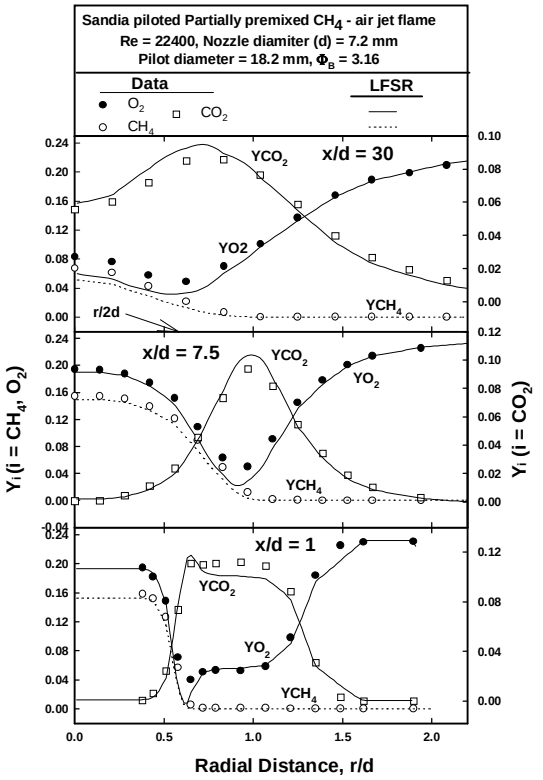

Fig. 3: Measurements and LFSR predictions of Favre averaged mass fractions

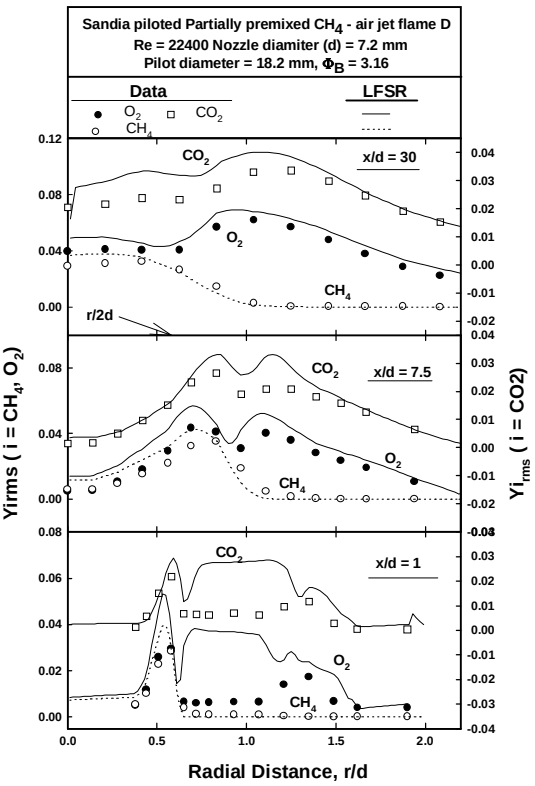

Fig. 4: Measurements and LFSR predictions of Favre averaged RMS species mass fractions

Second moment closure and PDF calculations of a bluff-body stabilized CH_4/H_2 flame

T.W.J. Peeters, H.A. Wouters*, D. Roekaerts**
Delft University of Technology, Dept. of Applied Physics, ThermoFluids Section, The Netherlands
E-mail: T.Peeters@tn.tudelft.nl
*New address: Corporate Research Lab., Hoogovens B.V., The Netherlands
**Also at: Shell Research and Technology Center, Amsterdam, The Netherlands

Introduction

One of the target flames of the Workshop is the bluff-body stabilized CH_4/H_2 flame, for which experimental data have been disclosed on the world-wide web by Masri [1]. Based on discussions in previous workshops, it was concluded that a careful and accurate numerical investigation is mandatory to establish an acceptable degree of consensus on appropriate models for chemistry, turbulence, and radiation. The poster will focus on the bluff-body stabilized flame, using accurate numerical methods, and different physical/chemical models to test their validity in this configuration:

- Standard eddy-viscosity modeling of the non-reacting and reacting test cases
- Full second-moment closure of the non-reacting and reacting test cases, using the so-called 'Basic Model' and the Jones and Musonge model (with terms and constants as disclosed by Janicka on his website [2]) Both the eddy-viscosity and second-moment closure models for the reacting test case employ a chemical equilibrium chemistry model, with an assumed-shape beta function for mixture fraction.
- Monte Carlo PDF simulations of the reacting test case, using a generalized Langevin model which is equivalent to the 'Basic Model' and the ISAT chemistry tabulation algorithm for detailed chemistry (involving 16 species in the C_1-mechanism).

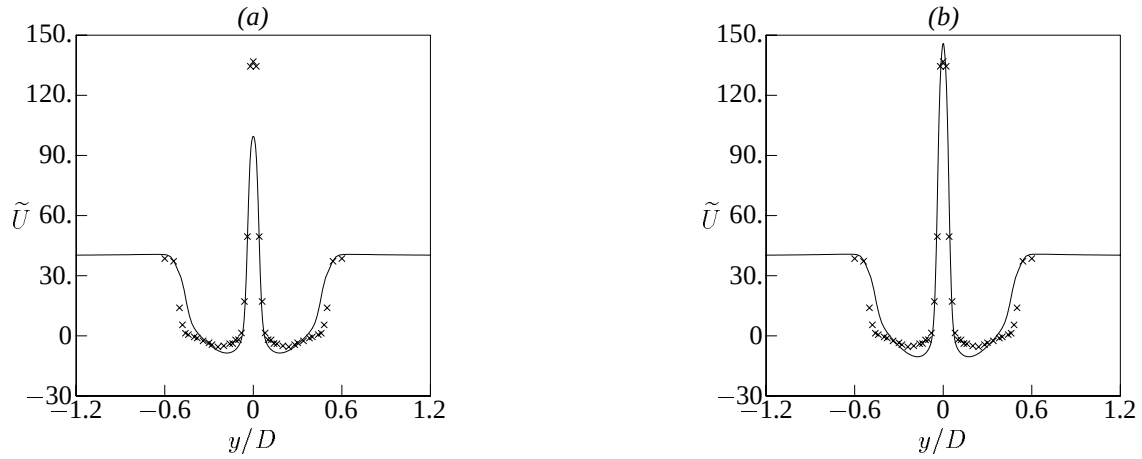

Figure 1: Comparison between eddy-viscosity model computations and experiments for the reacting case, with $U_{\rm jet} = 118$ m/s, at a height of $x/D = 0.26$ above the bluff body. *(a)* Experimental initial conditions, *(b)* Initial conditions based on bulk flow data.

Considerations on initial conditions

To compute the flow field around the bluff body, the following steps have been taken. At first the computational domain was selected to extend 0.2 m in axial direction and 0.1 m in radial direction. When applying the inlet boundary conditions recommended by Masri [3], the flow field could not be computed because of lack of convergence. It was then found to be important to move the inlet regions for fuel and air 0.1 m upstream, in order to relax the dependence on the experimental boundary conditions for velocity and turbulent quantities. This was achieved in our multi-block CFD code by using three separate domains for fuel stream, air stream, and region above the bluff body. Next, it turned out that the bulk mass flow rate and momentum flow rate of the fuel stream are seroiously underpredicted if the

experimental initial conditions of Masri are used (see Fig. 1). Since the inlet planes had been shifted upstream anyway, there was no numerical problem in applying the bulk flow data as initial conditions, rather than the experimental radial profiles. The fuel-stream flow field has sufficient time to form a developed pipe flow before exiting into the flow above the bluff body. This ensures better agreement with the experimental flow field data above the bluff body.

Numerical accuracy

The numerical method is based on the multi-block, non-orthogonal, colocated, finite volume discretization of Peric [4]. For the present test cases, however, the grid was chosen to be orthogonal. The computation of the flow field requires a sufficiently fine computational grid. The check grid independence, a coarse grid (1340 cells) was used as a starting point. In successive refinement steps, the number of grid cells was increased to 5360 and 21440 cells. The finest grid, however, still does not guarantee grid independent results. New calculations are under way to give results for the next grid refinement, in order to assess the numerical accuracy and grid independence. The first-order upwind scheme and several second-order schemes have been used for our finite-volume computations. For the Monte Carlo PDF calculations, the 21440-cell-grid with 50 to 100 particles per cell was used. Averaging over 500 time steps was used to obtain smooth profiles in the statistically stationary state.

Results and discussion

The influence of the different turbulence models is shown in Fig. 2a for the mean temperature predictions, using the equilibrium model for chemistry. It is clear that the use of the chemical equilibrium model gives too low temperatures in the fuel-rich zone of the flame, which is the region between the fuel jet and the temperature maximum.

We applied also a simplified flamelet model (using only one flamelet with strain rate 100 s^{-1}), but this gives nearly identical results for the major species and temperature. The fuel mixture used is relatively insensitive to moderate strain rates (< 300 s^{-1}). Monte Carlo PDF calculations with the ISAT method, based on a C_1-mechanism for methane combustion, produce much lower temperatures, as can be seen from the Fig. 2b, where we used the 'Basic' Reynolds-stress model for turbulence.

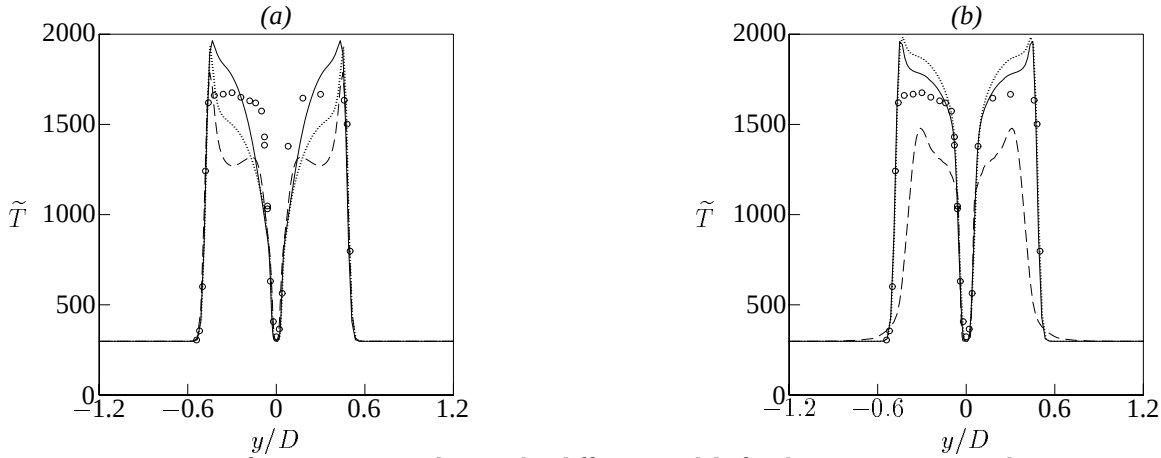

Figure 2: Comparison of temperature predictions by different models for the reacting case, with $U_{\rm jet} = 118$ m/s, at a height of $x/D = 0.26$ above the bluff body. *(a)* ∘ experiments, — eddy viscosity model, · · · Basic Reynolds-stress model, — — Jones Musonge model. *(b)* ∘ experiments, — constrained-equilibrium model, · · · single laminar flamelet $a = 100$ s^{-1}, — — ISAT.

References

[1] ftp://flame.mech.eng.usyd.edu.au/pub/Bluffb for B4F3 case.

[2] http://www.tu-darmstadt.de/fb/mb/ekt/flamebase/modeling/rsm

[3] ftp://flame.mech.eng.usyd.edu.au/pub/bvel/icbbody.dat

[4] J.H. Ferziger, and M. Perić *Computational Methods for Fluid Dynamics,* Springer-Verlag, 1996.

Unsteady Flamelet Modeling of a Turbulent $CH_4/H_2/N_2$ Diffusion Flame

H. Pitsch
Department of Applied Mechanics and Engineering Science
Center for Energy and Combustion Research
University of California San Diego
La Jolla, CA 92093-0411
e-mail: hpitsch@ames.ucsd.edu

M. Chen, N. Peters
Institut für Technische Mechanik
RWTH Aachen
Templergraben 64
52062 Aachen
e-mail: M.Chen@itm.rwth-aachen.de, N.Peters@itm.rwth-aachen.de

An unsteady flamelet model has been applied in a numerical simulation of a steady, turbulent $CH_4/H_2/N_2$ diffusion flame, which has been experimentally investigated by Bergmann et al. [1] and Hassel et al. [2].

In a recent study [3], transient effects in jet diffusion flames have been shown to be important if slow physical processes, such as radiation, or slow chemical processes, like the formation of NO_x, are considered. Moreover, unsteady effects have to be taken into account if the diffusion time scale is large compared to a typical time scale of the mean flow.

The unsteady flamelet model applied in the present study is described in detail in Ref. [3]. The flamelet equation for the temperature is of the kind

$$\rho\frac{\partial T}{\partial t} - \rho\frac{\chi}{2}\left(\frac{\partial^2 T}{\partial Z^2} + \frac{1}{c_p}\frac{\partial c_p}{\partial Z}\frac{\partial T}{\partial Z}\right) + \frac{1}{c_p}\left(\sum_{k=1}^{N} h_k \dot{m}_k + \dot{q}_R''' - \mathcal{H}\right) = 0\,, \tag{1}$$

where t denotes the time, Z the mixture fraction, T the temperature, χ the scalar dissipation rate, ρ the density, c_p the specific heat capacity at constant pressure, $\dot{q}_R'''$ the rate of radiative heat loss per unit volume. N is the number of chemical species, h_k the enthalpy, and $\dot{m}_k$ the chemical production rate per unit volume of species k. $\mathcal{H}$ accounts for the enthalpy flux by mass diffusion.The flow field has been calculated using the FLUENT code. To incorporate transient effects into the flamelet calculations, an unsteady flamelet has been solved interactively with the CFD solution. Since the boundary conditions of the flamelet, which are the temperatures and the composition of the fuel and the oxidizer stream, as well as the pressure, remain constant throughout the calculation, the only varying parameter influencing the flamelet solution is the scalar dissipation rate, describing the impact of the turbulent flow field on the diffusion flame structure. The unsteady flamelet has been calculated as a function of the flamelet time, which is related to the distance from the nozzle x as

$$t = \int_0^x \frac{1}{u(x')\Big|\left(\widetilde{Z} = Z_{\rm st}\right)}dx'\,, \tag{2}$$

where $\widetilde{Z}$ is the Favre average of the mixture fraction and $u(x)\Big|\left(\widetilde{Z} = Z_{\rm st}\right)$ is the axial velocity component at the radial position, where $\widetilde{Z} = Z_{\rm st}$, and the index st refers to stoichiometric conditions. Following Ref. [3] the development of the scalar dissipation rate as a function of the nozzle distance is obtained by determining its conditional mean value in each computational cell and spatially averaging for each radial cell layer. The solution for the turbulent diffusion flame is then obtained by recalculating the unsteady flamelet after a certain number of FLUENT iterations. Convergence is achieved if the change of the scalar dissipation rate used for the flamelet calculations is smaller than a prescribed tolerance. Typically, two flamelet calculations yield a satisfying accuracy.

Since Bergmann et al. [1] found differential diffusion effects only very close to the nozzle, where transient effects are unimportant because of the high scalar dissipation rates, the numerical simulations have been carried out with unity Lewis numbers for all chemical components.

The calculations have been performed with a reduced 14-step mechanism. Based on the skeletal mechanism given in Ref. [4] steady state assumptions have been introduced for some radicals, which are comsumed

by fast reactions. In the figures given below the results of the numerical simulation are compared with experimental data by Bergmann et al. [1] for turbulent mean values of mixture fraction, temperature, and species mass fractions and the variance of the mixture fraction. Moreover, turbulent mean values of the axial velocity are compared with experimental data by Hassel et al. [2]. The flow field data, represented by the axial velocity, the mean and the variance of the mixture fraction, and the mass fractions of the fuel components are predicted very accurately. The temperature is also well predicted in the rich part, but slightly underpredicted when the mixture fraction drops under its stoichiometric value. The mass fractions of O_2, CO, H_2O, and CO_2 are in reasonable agreement with the experimental data, although CO is overpredicted in the lean, CO_2 in the rich region of the flame. The comparison of radial profiles reveals similar accuracy and has been omitted for brevity.

To investigate the influence of the chemical reaction scheme, numerical simulations have also been performed using the chemical mechanism by Warnatz et al. [5] and the GRI-mechanism [6]. All three mechanisms lead to almost undistinguishable temperature developments. However, differences are obtained for the mass fractions of CO and CO_2, especially in the rich region. Both, Warnatz' mechanism and the GRI mechanism seem to perform better than the 14-step mechanism for CO_2. However, the CO mass fractions are overpredicted by these mechanisms.

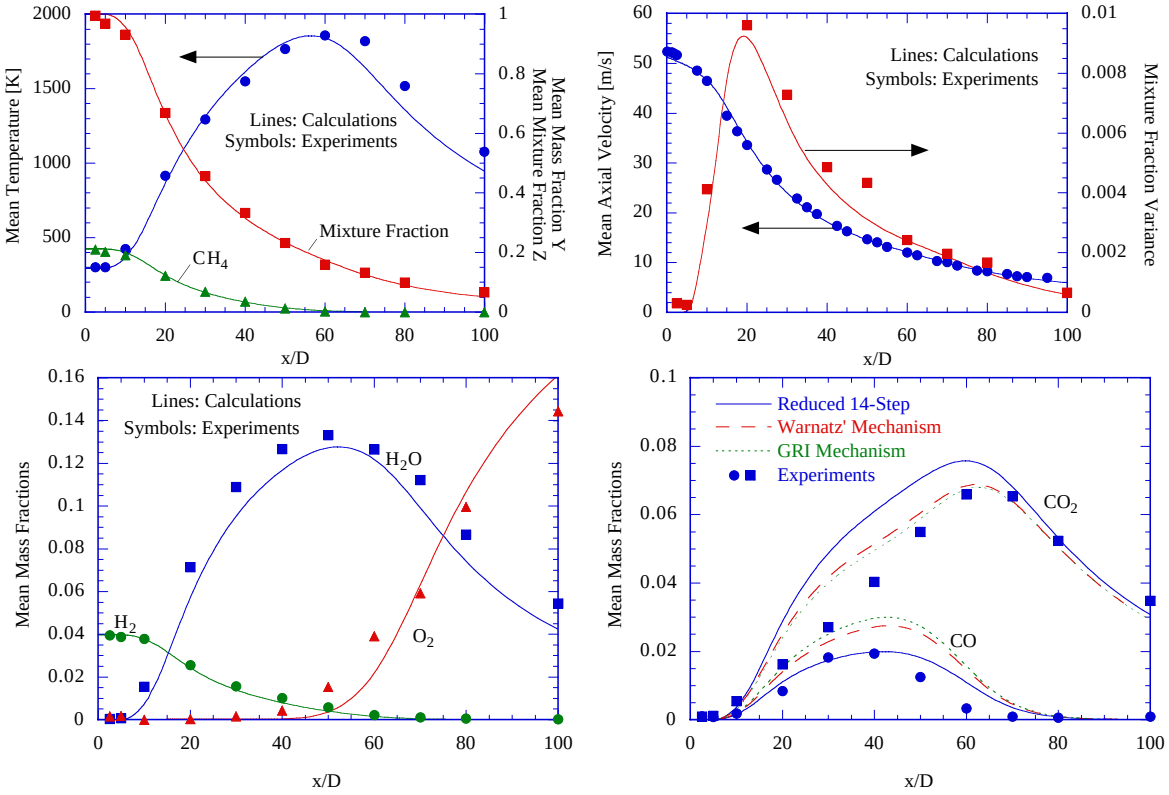

References

[1] Bergmann, V., Meier, W., Wolff, D., Stricker, W., Appl. Phys. B, accepted for publication, 1997.

[2] Hassel, E., private communication, 1998.

[3] Pitsch, H., Chen, M., Peters, N., Twenty-Seventh Symposium (International) on Combustion, accepted for presentation, 1998.

[4] Peters, N., in Reduced Kinetic Mechanisms for Applications in Combustion Systems (Peters and Rogg, Eds.), Springer, 1993.

[5] Warnatz, J., Maas, U., Dibble, R. W., in Combustion, Physical and Chemical Fundamentals, Modeling and Simulation, Experiments, Pollutant Formation, Springer Verlag, 1996.

[6] Bowman, C. T., Hanson, R. K., Davidson, D. F., Gardiner, Jr., W. C., Lissianski, V., Smith, G. P., Golden, D. M., Frenklach, M., Goldenberg, M., http://www.me.berkeley.edu/gri_mech/

RESOLUTION REQUIREMENTS FOR SCALAR DISSIPATION MEASUREMENTS IN TURBULENT JETS AND FLAMES

William M. Pitts
Building and Fire Research Laboratory
National Institute of Standards and Technology
Gaithersburg, MD 20899

Scalar dissipation, •, characterizes the rate of molecular mixing in a turbulent flow field. It is defined as

$$\chi = 2D\nabla\xi \cdot \nabla\xi, \tag{1}$$

where D is an appropriate molecular diffusion coefficient and ξ is a conserved scalar known as the mixture fraction. Scalar dissipation is related to the local rate of molecular mixing and is therefore of fundamental interest in turbulent mixing studies. This parameter also plays a central role in models of turbulent combustion[1,2] which require estimates for the mixture fraction and scalar dissipation.

Experimental estimates of scalar dissipation are typically obtained in one of two ways. In the first, values for the scalar are determined simultaneously at two or more appropriately spaced locations and the gradient is determined from the change of the values between the locations and knowledge of the separation distance(s) of the measurement points. Due to difficulties associated with recording scalar values in three dimensions, it is common that only one or two components of the scalar gradient are measured at a given time. It is necessary to invoke certain assumptions in order to estimate values of χ from these measurements (e.g., see Buch and Dahm[3]). In the second approach, real-time measurements of the scalar are made at a single point and Taylor's hypothesis is used to convert the temporal gradient to a spatial gradient by dividing by the time-averaged local flow velocity. Only a single component of χ is obtained, and the use of Taylor's hypothesis can introduce additional errors.[4,5]

In order to estimate values of χ as accurately as possible, it is necessary to have sufficient spatial and temporal resolution to ensure that the concentration gradient is effectively constant in space and time during the measurement. In other words, spatial fluctuations in the concentration gradient must occur on scales larger than the measurement volume and the product of the measurement time and local velocity. An important consideration is what spatial resolution is required. Traditionally, it was argued that the resolution had to be sufficient to resolve features on the same order of size as the Batchelor scale, η_B, which is given by[6]

$$\eta_B = \eta_K Sc^{-1/2} = \frac{\nu^3}{\varepsilon} Sc^{-1/2}, \tag{2}$$

where Sc is the Schmidt number equal to the ratio of the kinematic viscosity, ν, and D, η_K is the Kolmogorov scale, and ε is the average rate of turbulent energy dissipation. More recently, it has been suggested that the required spatial resolution may be roughly twelve times larger than η_B.[7,8] This latter relaxed estimate has been adopted for several recent studies, including one of the first direct measurements of χ for mixture fraction in a turbulent flame.[9,10,11]

Values of η_B are typically on the order of a few hundred μm for laboratory turbulent flows. Such lengths scales are close to the minimum resolvable with current optical and probe techniques. For this reason, a relaxation of the required resolution by a factor of 12 would result in more easily implemented experiments having significantly improved signal-to-noise ratios. Unfortunately, recent experiments have demonstrated that the larger estimate for the required spatial resolution is not valid. Lozano et al. used two-dimensional planar images of biacetyl fluorescence doped into an axisymmetric jet to show that the smallest scales for which scalar gradient variations were observed were comparable in size to η_B.[12] Antonia and Mi explicitly considered the effects of spatial separation of two probes used for gradient measurement and found that small corrections were still required for spatial

averaging when a probe separation corresponding to $2\eta_B$ was used.[13] Work by Anselmet et al.[14] and Tong and Warhaft[15] support this finding. Recent real-time measurements of scalar dissipation along a line in a propane axisymmetric jet have revealed significant temporal and spatial variations on scales close to the Batchelor scale.[16]

Taken together, these studies support earlier hypotheses that the spatial resolution required for scalar dissipation measurements should be very close to η_B (a value of $2\eta_B$ would seem to be a maximum) in order to fully spatially resolve scalar dissipation fluctuations for flows with $Sc \approx 1$. Interestingly, based on an extended analysis of the data presented by Dowling and Dimotakis, Dowling concluded that their original estimate for the multiplier to use with η_B should be reduced by a factor of 4 or 5. [17] It is important to recognize that the smaller estimated spatial resolution requirement is consistent with that required for analogous measurements of energy dissipation in air flows.[18,19,20] It seems reasonable that the smallest scales over which fluctuations of velocity and scalar occur would be on the same order of size since both are determined by molecular diffusion processes of roughly comparable magnitude.

Based on a review of previous investigations as well as the measurements at National Institute of Standards and Technology, it is concluded that the required spatial resolution for accurate measurements of χ is on the order of the Batchelor scale. Adoption of the proposed relaxed spatial resolution requirement will result in significant volume averaging.

References

1. N. Peters, *Twenty-First Symposium (International) on Combustion*, 1986, p. 1231.
2. R. W. Bilger, *Twenty-Second Symposium (International) on Combustion*, 1988, p. 475.
3. W. J. A. Dahm and K. A. Buch, *Phys. Fluids A* **1**, 1290 (1989).
4. J. Mi and R. A. Antonia, *Phys. Fluids* **6**, 1548 (1994).
5. W. J. A. Dahm and K. B. Southerland, *Phys. Fluids* **9**, 2101 (1997).
6. G. K. Batchelor, *J. Fluid Mech.* **5**, 113 (1959).
7. D. R. Dowling and P. E. Dimotakis, *J. Fluid Mech.* **218**, 109 (1990).
8. W. J. A. Dahm, K. B. Southerland, and K. A. Buch, *Phys. Fluids A* **3**, 1115 (1991).
9. L. L. Smith, R. W. Dibble, L. Talbot, R. S. Barlow, and C. D. Carter, *Phys. Fluids* **7**, 1455 (1995).
10. L. Su and N. T. Clemens, "Measurements of the Three-Dimensional Scalar Dissipation Rate Field in Gas-Phase Planar Turbulent Jets," *AIAA 97-0074*, Thirty-Fifth Aerospace Sciences Meeting, Reno, NV, Jan. 6-10, 1997.
11. A. Brockhinke, P. Andresen, and K. Kohse-Höinghaus, *Twenty-Sixth Symposium (International) on Combustion*, 1996,, p. 153.
12. A. Lozano, I. Van Cruyningen, P. Danehy, and R. K. Hanson, "Planar Laser-Induced Fluorescence Measurements in a Turbulent Jet," in *Application of Laser Techniques to Fluid Mechanics* (Springer-Verlag, Berlin, 1991), pp. 19.
13. R. A. Antonia and J. Mi, *J. Fluid Mech.* **250**, 531 (1993).
14. F. Anselmet, H. Djeridi, and L. Fulachier, *J. Fluid Mech.* **280**, 173 (1994).
15. C. Tong and Z. Warhaft, *J. Fluid Mech.* **292**, 1 (1995).
16. W. M. Pitts, "Large- and Small-Scale Structures and Their Interactions in an Axisymmetric Turbulent Jet," to be submitted.
17. D. R. Dowling, *Phys. Fluids A* **3**, 2229 (1991).
18. A. A. Townsend, Proc. Royal Soc. (London) **208A**, 534 (1951).
19. J. C. Wyngaard, *J. Phys. E: Sci. Instrum.* **1**, 1105 (1968).
20. R. A. Antonia, B. R. Satyaprakash, and A. K. M. F. Hussain, *Phys. Fluids* **23**, 695 (1980).

Assessment of Strained-Flamelet Prediction of a CH_4/H_2 Turbulent Non-Premixed Flame

by

M. Pourkashanian, G. Spence* and A. Williams
Department of Fuel and Energy,
University of Leeds,
Leeds, LS2 9JT, UK.

ABSTRACT

The stretched laminar flamelet formalism provides an efficient mechanism for incorporating finite rate kinetics into computations of non-premixed flames. In the strained flamelet model two scalars, a mixture fraction ξ and scalar dissipation χ as a measure for flamelet stretch, determine unambiguously the local instantaneous thermo-chemical state in the turbulent flow. Using an existing validated mechanism[1], a flamelet library is constructed for CH_4/H_2 flames for stretch rates of 100/s, 200/s and 300/s. Computations with this flamelet library are benchmarked against a CH_4/H_2 non-premixed turbulent bluff body stabilised flame as investigated by Masri et al[2]. Fluctuations in mixture fraction ξ and scalar dissipation χ are accounted for using an assumed beta-function and delta-function shape at mean conditions, respectively. The calculations were performed with an elliptic flow solver to allow subsequent computations of more complex flows. Unstructured hanging node adaption techniques were employed to provide efficient localised gradient adaption. These techniques offer the advantage over structured CFD techniques by minimising the total number of cells required for adequate resolution of gradients encountered with complex flows. However, computational memory demands are increased. Fixed strained-flamelet calculations were compared with an equilibrium model. Calculations indicate that a characteristic constant strain rate calculation can be identified which is representative for similar flames. The success in predicting temperature depression, radical concentration and characteristics of a turbulent jet non-premixed flame was reviewed. The limitations of the modelling assumptions made and the advantages of the combustion models and solution methods are discussed.

Unlike turbulent non-premixed jet flames, turbulent non-premixed bluff body flames resemble practical engineering combustion problems due to the production of complex recirculation zones downstream of the bluff body. Computations were assessed against data obtained via simultaneous, space and time resolved, Raman-Rayleigh measurements of temperature, mass fractions of fuel, O_2, N_2, CO, CO_2, H_2, H_2O and OH[2]. Such data sets provide an essential tool for modellers in validating CFD codes and assessing the capabilities of different combustion models. Initial investigations were performed for a non-reacting flow with the fuel comprising of C_2H_4 and a co-flowing stream of air on the same burner geometry. Mixture fraction measurements for this particular flow were obtained using planar imaging of Rayleigh scattering. The purpose of such investigations was to assess the performance of the Computational Fluid Dynamics code at calculating the complex recirculating flow and mixing fields. Using the Reynolds Stress turbulence model, calculations were satisfactory and the length of the recirculation zone was predicted well, however the results show that even when chemistry isn't modelled the task of predicting the complex recirculating velocity profiles is formidable. For the reacting flow case, the bluff body stabilised flames fuel comprised of CH_4/H_2 on

an equal volumetric ratio, again the co-flow stream being air. The composition of the strained laminar flamelets was obtained via the code OPPDIF, developed at Sandia National Laboratories, and the GRI 2.11 mechanism for methane oxidation[1].

Figure 1(a-b) show the scatter plots of temperature and Y_{CO} verses mixture fraction (ξ) for the non-premixed bluff body stabilised CH_4/H_2 flame. The flamelet calculation is shown in the full curve. Flamelet calculations of a fixed strain rate yield satisfactory results, however measured peak levels of CO and CO_2 overshoot steady laminar flamelet calculations. These overshoots could be caused by fluorescence interference with the Raman signals. Furthermore, in the case of CO overshoots, unsteady effects may play a role as observed by Mauβ et al[3]. The results indicate that the agreement for temperature are qualitatively excellent and quantitatively good.

References

1. Bowman, C.T., Hanson, R.K., Davidson, D.F., Gardiner, Jr, W.C., Lissianski, V., Smith, P., Golden, D.M., Frenklach, M. and Goldenberg, M., http://www.me.berkeley.edu/gri_mech/
2. Combustion Database, The University of Sydney and The Combustion Research Facility, Sandia National Laboratories: http://www.mech.eng.usyd.edu.au/research/energy/#data
3. Mauβ, F., Keller, D. and Peters, N.: Twenty Third Symposium (International) on Combustion, p. 693, The Combustion Institute, 1990.

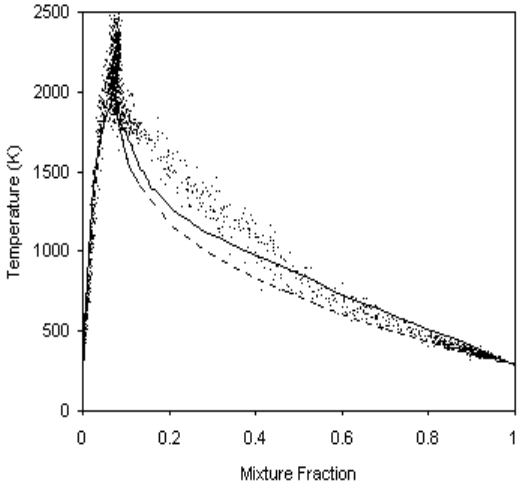

Figure 1a

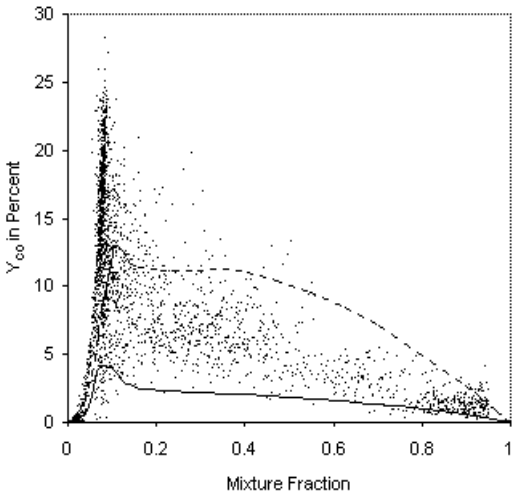

Figure 1b

Scatter plots of all data for temperature and Y_{CO} mass fraction in a bluff body burner turbulent non-premixed flame of CH_4/H_2 at x/D = 0.26. Full curves are for flamelet based CFD prediction with strain rate parameter a=100/s and dashed line are for equilibrium based calculation.

* Corresponding author e-mail: fuegts@sun.leeds.ac.uk

Quantitative Hydroxyl and Temperature Time-Series Measurements in Turbulent Nonpremixed Flames

M. W. Renfro[*]*, S. D. Pack, A. Lakshmanarao, G. B. King, and N. M. Laurendeau*
School of Mechanical Engineering
Purdue University
West Lafayette, Indiana 47907-1288

During the past several years, we have presented measurements of both CH- and OH-fluorescence time series via picosecond time-resolved laser-induced fluorescence (PITLIF) [1,2]. These measurements are unique since frequency statistics, such as the power spectral density (PSD), are not available for minor species by any other technique. However, the measurements so far have lacked corrections for variations in the quenching rate coefficient. The dependence on quenching is common to linear LIF measurements but can be avoided with high-powered lasers via laser-saturated fluorescence (LSF). Unfortunately, high-powered lasers do not have the necessary repetition rate for time-series measurements; thus, the quenching dependence must be accounted for by other methods. A rapid, gated photon-counting system, termed LIFTIME, has been built to allow on-the-fly quenching corrections to each point of a fluorescence time series. This photon-counting system divides the fluorescence decay into three equal temporal partitions and integrates the photon count within each of these areas. These three integrated counts are then used to compute the lifetime, the peak amplitude of the fluorescence decay, and the flame-emission background. The measured lifetime can then be used to correct the fluorescence time series point by point. Alternatively, the initial decay amplitude can be directly interpreted as concentration. Following this quenching correction, the time series are calibrated against well-characterized premixed flames. The result of the combination of PITLIF and LIFTIME is a system capable of quantitative time-series measurements of naturally-occurring minor-species concentrations in turbulent flames. These measurements will provide new spectral data for scalar fluctuations that can be used to develop or test combustion models. For example, the data can be used along with an assumed power spectral density and a laminar-flamelet analysis to investigate the interactions between turbulence and chemical reaction [3].

The photon-counting system design and results of lifetime and concentration measurements in a series of laminar flames have been presented recently [4,5]. These measurements were compared to both modeling and previous LSF measurements as verification of the system's capabilities. However, many of these measurements were obtained with reduced photon count rates so as to avoid pulse pileup in the system's discriminators. This approach is common to single photon counting (SPC) measurements. For application to time-series measurements in turbulent flames, the signal level must be increased above SPC guidelines such that the background in the computed PSD does not corrupt the desired information. A pulse pileup correction has been derived for correcting the measured data which utilizes a saturate-and-compare technique. This analysis is similar to convolute-and-compare techniques which are commonly used to account for instrumentation response in lifetime measurements. The corrected measurements are found to agree with the lower photon-rate measurements in our previous work. With this correction scheme, the system is capable of processing up to 40 million photoelectrons per second. This correction procedure will be presented in detail elsewhere.

[*] Corresponding author: renfro@ecn.purdue.edu

Here, measurements of OH concentration in a buoyant, flickering, laminar diffusion flame will be presented first, using the new system with pulse pile-up correction. This flame has a dominant 15-Hz frequency which is shown to appear in both the lifetime and concentration PSDs. However, the second-harmonic frequency is apparent only in the concentration PSD owing to the shapes of the lifetime and hydroxyl concentration radial profiles. This is compared to previous time-series measurements of OH fluorescence which were not corrected for quenching [2]. The computed PSDs are shown to differ with respect to this second harmonic, which underscores both the importance of on-the-fly quenching corrections and increased signal-to-noise ratio (decreased PSD background). Moreover, spatial variations in the quenching rate coefficient are shown to cause errors in the mean hydroxyl concentration if the correction is not applied to the measured data.

Measurements for turbulent nonpremixed flames will also be presented at a range of Reynolds numbers from 2800 to 19,000. These measurements represent the first known quantitative time series for OH concentration in a turbulent flame. The flames studied include a methane/air, a hydrogen/argon/air, and a hydrogen/methane/air diffusion flame. For the latter flame, the hydrogen/methane composition is chosen such that the scattering cross-sections are nearly constant across the flame front. Rayleigh scattering time-series measurements, using a cw-argon-ion laser, will be presented which can be directly interpreted as temperature in this special composition flame. Errors associated with variations in the cross-sections have been estimated at ±6% for the entire range of mixture fractions. In this way, temperature and hydroxyl concentration time series can be compared. In addition to the PSD, the probability density function (PDF) is computed for each of the reported time series. Although quantitative PDFs are available with low repetition rate lasers via LSF, LIFTIME offers the ability to determine the PDF in a much shorter period of time owing to the improved duty cycle of the laser. For example, a PDF computed from 2000 individual samples, which previously required ~3.5 minutes of data collection, can now be collected in ~0.2 seconds. Perhaps of more importance, the duty cycle of the PITLIF laser allows as many as 4000 photoelectrons to be collected during any 100-μs time period (approximately equal to the Kolmogorov time scale) without saturating the PMT owing to the relatively uniform temporal distribution of the photons. That is, the PMT can use the entire 100 μs for data collection, encompassing 8000 laser pulses. In contrast, single-shot, low repetition rate techniques require that all of the collected photons occur within a much shorter temporal window (often less than a few nanoseconds) since only one laser pulse occurs during the Kolmogorov time scale. Hence, in some cases, shot-noise can be reduced with the high-repetition rate laser.

1. Renfro, M. W., Klassen, M. S., King, G. B., and Laurendeau, N. M. (1997). *Opt. Let.* **22**, 175-177.
2. Renfro, M. W., Pack, S. D., King, G. B., and Laurendeau, N. M. (1998). *Combust. Flame*, **115**, 443-455.
3. Renfro, M. W., Sivathanu, Y. R., Gore, J. P, King, G. B., and Laurendeau, N. M. (1998), *Twenty-Seventh Symposium (International) on Combustion*, The Combustion Institute, Pittsburgh, PA, in press.
4. Pack, S. D., Renfro, M. W., King, G. B., and Laurendeau, N. M. (1998), *Opt. Let.* **23**, 1215-1217.
5. Pack, S. D., Renfro, M. W., King, G. B., and Laurendeau, N. M. (1998), Central States Section Meeting of The Combustion Institute, Lexington, KY.

Conditional Moment Closure (CMC) Predictions in Methane-Air Piloted Jet Flames

M. R. ROOMINA and R. W. BILGER

Department of Mechanical and Mechatronic Engineering
The University of Sydney, NSW 2006, AUSTRALIA
E-mail: roomina@mech.eng.usyd.edu.au; bilger@mech.eng.usyd.edu.au

INTRODUCTION

Reduction of pollutant emissions is important task of interest in combustion technology. The accurate prediction of pollutants of interest such as carbon monoxide, CO, nitric oxide, NO and soot requires employing complex chemical mechanisms and accounting for turbulence-chemistry interactions. Conditional Moment Closure (CMC) (Klimenko, 1990, Bilger, 1993) is a method for handling turbulence chemistry interactions which is capable of being used with large chemical mechanisms at modest computational cost. The basic idea of the method is that most of the fluctuation in temperature and composition can be associated with one variable and conditional averaging with respect to that variable allows closure of the conditional average chemical reaction rate terms. For the nonpremixed combustion systems considered here, the conditioning variable of choice is the mixture fraction. This is defined as the mass fraction of an inert tracer entering with the fuel, normalised to be unity in the unmixed fuel and zero in the unmixed oxidant.

Excellent results have been obtained for NO predictions in turbulent jet diffusion flames of hydrogen (Smith et al., 1992, 1995). Here we apply the method to predictions for a turbulent diffusion flame formed from a partially premixed jet of methane and air. The burner is an axisymmetric jet with a jet nozzle diameter of 7.2 mm and an outer annulus diameter of the pilot of 18.2 mm, centred in a stream of co-flowing air. The jet velocity is 49.6 m/s (±2 m/s) which has a jet Reynolds number of ~22400. The co-flow velocity is 0.9 m/s. The main fuel is a mixture of one part methane and three parts air by volume at temperature of 294 K. Results are compared with the laser measurements of Barlow and Frank (1997) and Schneider et al. (1998).

RESULTS AND DISCUSSION

The calculations are carried out down to x/D=100. The chemistry is represented by the GRI-Mech 2.11 mechanism. Radiative heat loss is modelled by RADCAL (Sivathanu and Gore, 1993) radiation sub-model. Adiabatic equilibrium compositions are employed for the reactive scalars down to five jet diameters, in order to assure the ignition of the flame in the near-field region due to high mixing rates.

The predicted mean mixture fraction on the centreline is in good agreement with the measurements of Barlow and Frank (1997). Fluctuations in mixture fraction, however, are somewhat over-predicted particularly for downstream. The stoichiometric flame length is predicted to be 44 jet diameters and the visible flame length is estimated from the predictions ~64 jet diameters. These are in very good agreement with the measured stoichiometric and visible flame lengths which are reported as 47 and 67 jet diameters, respectively. The total enthalpy lost to the surroundings in the computational domain is calculated by subtracting the radiative standardised enthalpy from the adiabatic standardised enthalpy and found to be 2.16 kW. This quantity when normalised by the total power of the flame (17.34 kW) represents the radiant fraction. The radiant fraction is predicted to be ~12%, which is 2.4 times greater than that measured (~5.1%) by radiometers by Barlow and Frank (1997). This is a large discrepancy and there should be a corresponding discrepancy in predicted and measured temperatures.

At x/D=30 predicted temperature levels are in very good agreement with measurements on the fuel-lean side. The predicted and measured peak conditional mean temperatures occur at η=0.38 with values of 2058K and 2022K respectively which shows very good agreement as well. On the fuel-rich side, however, the temperature levels tend to deviate from the measurements and higher levels of temperature (by 10%) are predicted. At x/D=60 the mixture is always fuel lean and the predictions for conditional averaged temperature are about 50K below the measurements. This is only about half of the discrepancy that can be inferred from the discrepancy in the radiation loss reported above. CMC predictions for reactive species are excellent on the fuel-lean side. Significant deviations from measurements are observed for CH_4, O_2, CO and H_2 on the fuel-rich side and these

are consistent with those found for temperature. Predicted CO levels on the fuel-lean side show fair agreement with measurement while the predicted peak carbon monoxide value shifts to the rich side of stoichiometric. Levels of H_2 are well predicted on the fuel-lean side but they are over-predicted on the fuel-rich side. The hydroxyl mass fractions are in reasonable agreement with measurements with the peak value, which occurs at stoichiometric, being over-predicted by 20%. It seems that the chemistry is poorly modelled on the fuel-rich side.

Predicted NO levels are in fair agreement with the measured levels. The predicted NO level peaks at stoichiometric as in the measurements. The predictions are high by ~50% on the fuel-lean side. Predictions show faster consumption of NO on the fuel-rich side and it is under-predicted there by ~20%. Smooke et al. (1996) investigate issues related to the computation and measurement of NO in laminar methane-air diffusion flames. They found that GRI-Mech produces excellent agreement for most of the features of the measured NO with the peak NO mole fractions underpredicted by less than 30% of the experimental value in the opposite direction to our finding. Their temperatures were quite a lot lower than in our flame. It is believed that the inadequacy of current chemical kinetics for reaction in nonpremixed flames could be a main cause for the discrepancies found. Other causes could be the need for a higher order closure for the conditional reaction rate (Kronenburg, et al., 1998) or numerical errors.

Favre averaged statistics are obtained by the weighting of the conditional mean statistics with the local pdf over the entire mixture fraction space. Therefore, the quality of predictions for Favre averaged statistics are affected by the quality of both the conditional mean statistics and the pdf of mixture fraction, and hence should not exceed the quality of the conditional averaged predictions. Radial profiles of Favre averaged quantities are in reasonable agreement, particularly at downstream locations. The agreement for temperature is very good and not significant lower than the measurements as the discrepancy in the radiation loss referred to above would imply. In the measurements there must be a small but significant radial variation of conditional average temperatures to account for the lack of discrepancy here that was apparent in the conditional values. The NO predictions are some 50% high.

CONCLUSION

The flow and mixing field results are in quite good quantitative agreement with the measurements. The k-ε-g turbulence model somewhat over-predicts the mixing rates near the nozzle and the predicted flame is slightly shorter than that reported in the experiment. Predicted temperature levels are in much better agreement with the measurements than would be expected from the discrepancy in the radiant loss. The radiation measurements need to be checked. Conversion of fuel to intermediates is over-predicted on the rich side of the flame. The NO predictions are high by ~50% on the fuel-lean side and this persists to the end of the flame. Predictions show faster consumption of NO on the fuel-rich side and it is under-predicted there by ~20%. It seems that the chemical mechanism used for methane oxidation is accurate on the fuel-lean side but is inadequate on the fuel-rich side. The NO part of the GRI mechanism gives over-predictions here, opposite to that found in laminar diffusion flames. It is possible that a higher order closure for the conditional reaction rate terms is needed.

ACKNOWLEDGMENT

This work is supported by the Australian Research Council.

REFERENCES

BARLOW, R.S. and FRANK, J., 1997, available from web site: http://www.ca.sandia.gov/tdf/workshop.html.
BILGER, R.W., *Phys. Fluids* A **5**(2):436-444, 1993.
GRI-Mech 2.11, available from Web site: http://www.me.berkeley.edu/gri_mech/.
KLIMENKO, A.Y., *Fluid Dynamics* **25**:327-334, 1990.
KLIMENKO, A.Y., *Phys. Fluids* **7** (2):446-448, 1995.
KRONENBURG, A., BILGER, R.W. and KENT J.H., *27th Symposium (International) on Combustion*, The Combustion Institute,1998 (to appear).
SCHNEIDER, C., GEISS, S. and HASSEL, E., 1998: http://www.ca.sandia.gov/tdf/workshop.html.
SIVATHANU, Y.R. and GORE, J.P., *Combustion and Flame*, **94**, 265-270, 1993.
SMITH, N.S.A., BILGER, R.W. and CHEN, J.Y., *24th Symposium (International) on Combustion*, The Combustion Institute, pp.263-269, 1992.
SMITH, N.S.A., BILGER, R.W., CARTER, C.D., BARLOW, R.S. and CHEN, J.Y., *Combustion Sci. and Tech.* **105**:357-375 (1995).
SMOOKE, M. D., ERN, A., TANOFF, M.A., VALDATI, B.A., MOHAMMED, R.K., MARRAN, D.F. and LONG, M.B. *26th Symposium (International) on Combustion*, The Combustion Institute, Pittsburgh, pp.2161-2170, 1996.

Mode-Locked, Picosecond Laser-Based Diagnostics and Novel Sensors for Turbulence Measurement

T. Settersten, C. Fisher, N. Middleton and M. Linne
Center for Combustion and Environmental Research
Colorado School of Mines, Golden, CO 80401
mlinne@mines.edu

J. Gord
Propulsion Directorate, Air Force Research Laboratory, Wright Patterson AFB, OH

G. Fiechtner
Innovative Scientific Solutions Inc., Dayton, OH

We are pursuing an unusual set of laser diagnostics using picosecond laser systems and new demodulation detectors. Our goal in this poster is to begin a series of discussions on how best to apply these diagnostics to turbulent flames. We will present a description of the diagnostic techniques currently under development, present some preliminary results and then discuss future applications.

In a review on turbulence, Pope[1] pointed out that composition fields contain length and time scales that are different than those of the velocity field. It is therefore necessary to make spatially and temporally resolved measurements of key species in turbulent flames. Pope adds that, "measurement of more detailed statistics are needed in order to discriminate between (various) models", and the development of models "will be greatly aided by … experimental techniques that are capable of resolving the fine scale composition fields". We began to work on high-speed measurement of concentration in 1993, our goal being to measure the kind of spectra described by review articles on turbulence.

In order to achieve these goals, we have focused on mode-locked, picosecond laser-based technology. We seek a method capable of: 1. Determination of absolute concentrations without calibrations or corrections, over a spatially resolved sample volume; 2. The observation of turbulence frequency spectra (up to 10 kHz) for species concentrations; and 3. Measurements at high pressure (representative of practical combustion systems). Our understanding of these techniques has been developing. In initial work, we showed that picosecond pump/probe is an absolute determination capable of acquiring fluctuation spectra[2,3].

Following those initial measurements, we have developed successively more sophisticated spectroscopic models for the interaction. In order to demonstrate conclusively that these diagnostics do what we claim, we have developed a quantum mechanically exact (for a two-level system) density matrix model for the pump/probe interaction. We find good agreement between this exact model and the more straightforward rate equation model used previously[2], when operating within the rate equation limit (agreement is within 7% and we know how to reduce that value). The density matrix results will be used to identify the regions in which the rate equation approach is appropriate, it will be used to evaluate the accuracy of the rate equations, and it will be compared with potassium measurements being performed over this summer.

We use potassium because we are performing detailed experimental validation of model results. Potassium has two strong ground state transitions in the fundamental tuning range of Ti:Sapphire. These lines are sufficiently spaced that a two-level interaction is appropriate. The dipole moment and broadening parameters for potassium are well known. We can therefore be certain that our model accurately describes the physical interaction.

The experiments employ a Spectra Physics regeneratively mode-locked Ti:Sapphire laser system . The beam diameter is approximately 100 μm at the sample volume. The laser is tuned to the $4^2S_{1/2}$-$4^2P_{1/2}$ transition of atomic potassium at 769.9 nm. Two sources of potassium will be used in experiments. A

low-pressure atomic vapor cell will be used initially to provide well-characterized number densities. This cell will have four windows arranged in a tee, so that we can perform spectrally resolved absorption measurements simultaneous with pump/probe determinations. This measurement will be made with narrow linewidth, tunable diode laser absorption spectroscopy, directed normal to the pump/probe beam. A Winefordner-style aspirating burner will also be used to seed potassium into an atmospheric methane/air flame. This device was used to simulate a combustion diagnostic more closely. Initial results will be presented in the poster.

Pump/probe is not a background-free technique, so it presents detection limit difficulties. We will discuss these difficulties in the context of flame species of interest (primarily CH and HCO). Estimated detection limits will be provided, together with a discussion on the feasibility of performing simultaneous background free measurements (e.g. pump/probe and DFWM).

In recent, related work, we have developed entirely new approaches to optical signal sensing and electrical signal processing. This effort has yielded a demodulating camera system capable of extracting weak, modulated images from a strong background[4]; and a single point sensor capable of improved signal-to-noise ratios (SNR) using signal processing concepts from entirely unrelated domains. The camera system has been completed during a collaborative interaction with Princeton Instruments, Inc. Our near-term goal in this work is to observe acetone in cold flow using pump/probe. This work will be performed at Wright Labs, in Dayton, OH. The camera will most likely be operated as a line sensor for the initial work, and a 50 kHz amplified Ti:sapphire system will be frequency doubled and used to perform pump/probe in the flow. This measurement will give a determination of scalar dissipation in real time. Initial results will be presented in the poster.

This camera system can also be used with an imaging spectrometer to obtain Raman spectra for major species concentrations, simultaneous with pump/probe measurements. This would make use of a Rubidium filter[5] in the collection optics, to block elastic scattering from the Ti:sapphire laser. A related topic is the use of a wavelength modulated diode laser with the rubidium filter to observe doppler profiles and hence acquire velocity without the use of a particle seed[6]. We will provide an explanation of these experiments as well, as an aid to discussion on future measurement possibilities.

This research has been supported by the National Science Foundation through grants CTS-9411391, CTS-9711889, and DGE-9554559, and by the US Air Force Wright Laboratories through grant number F33615-96-C-2632.

---

1. S. B. Pope, Twenty-Third Symposium (International) on Combustion/the Combustion Institute, Pittsburgh, PA , (1990).
2. G.J. Fiechtner and M.A. Linne, Combust. Sci. and Tech. **V100**:1-6, p. 11, (1994).
3. M.A. Linne and G.J. Fiechtner, Optics Letters, **19**, No. 9, (1994).
4. M. A. Linne, D. C. Morse, J. L. Skilowitz, G. J. Fiechtner, and J.R. Gord, Optics Letters, **20**, No. 23, 2414 - 2416, (1995).
5. P. Varghese, Phadke and M. Fink, AIAA 96-0176, (1996).
6. J. Mach and P. Varghese, AIAA 98-0510, (1998).

Poster Session at the Third International Workshop on Measurement and Computation of Turbulent Nonpremixed Flames
Boulder, Colorado, July 30-August 1, 1998

Turbulence Structure of Swirling Hydrogen Jet Diffusion Flames

Fumiaki Takahashi, Marlin D. Vangsness, Mark. D. Durbin, and W. John Schmoll
University of Dayton Research Institute, Dayton, Ohio, U. S. A.
E-mail: ftakahas@engr.udayton.edu

Turbulence and swirl play an essential role in enhancing fuel-air mixing, combustion intensity, and flame stabilization in practical combustion systems. Previous studies of turbulent jet diffusion flames focused mostly on nonswirling flames and rarely reported high-order moments, particularly triple correlations, of the probability-density functions (pdf) of velocity components. Furthermore, the velocity statistics are strongly influenced by the intermittent nature of near-field mixing of the fluids which originate from different flow channels and have different initial velocities. Hence, recent computational models; e.g., the joint velocity-scalar pdf method, are capable of calculating high-order moments for the fluids with different origins. Thus, demands for the detailed, conditionally sampled experimental data, particularly in swirling flows, have grown in recent years. The developing region of the jet flame is particularly important because various physical and chemical processes occur rapidly and affect the structure downstream.

This study provides the detailed velocity and temperature data in swirling and nonswirling turbulent hydrogen jet diffusion flames designed for model validation. The combustor (Fig. 1) consists of a central fuel tube (9.45-mm inner diameter, 0.2-mm lip thickness, 806-mm length) and a concentric annulus-air tube (26.92-mm inner diameter), centered in a vertical test section (150- × 150-mm square cross section with rounded corners, 486-mm length), through which external air is supplied. A helical vane swirler unit is placed in the annulus channel 96 mm upstream from the jet exit. The conditionally sampled, three-component laser-Doppler velocimetry measurements with a small probe volume were made to obtain the unbiased velocity data, including high-order cross-correlations. The coherent anti-Stokes Raman spectroscopy thermometry generated the temperature data without causing disturbances on the flame. Table 1 shows the experimental conditions, including the vane angle (θ) and the velocities of jet fluid (U_j), annulus air (U_a), and external air (U_e). The experimental data and a comparison with the computational results were reported in detail elsewhere [1, 2].

Increasing the jet velocity shifts the apparent turbulent flame zone inward (Fig. 2), makes the thermal layer thinner, and thus, strains the flame zone in the near field. On the other hand, swirl generally promotes turbulence and creates a positive radial velocity component even at the jet-exit plane (which, in turn, induces the radial velocity of the jet fluid), thereby shifting the flame zone outward and broadening the thermal layer. The outward flow deflection was not observed in nonreacting air jets studied previously. The peculiar result for the swirling flame is particularly important when applying the boundary conditions; the upstream boundary may need to be taken well below the jet exit outside the pressure field variation due to swirl if the jet-exit experimental results are not used as the boundary condition.

The distributions of second- and third-order velocity moments provide a physical insight into the generation and diffusion of turbulent kinetic energy (TKE). TKE is generated in the shear layer, where velocity gradient and Reynolds shear stress reach their peaks (Fig. 3). TKE diffuses inward and outward from the shear layer and then downstream in the outer region and upstream in the inner region (Fig. 4). Both skewnesses and kurtoses of velocity components in the near field were largely affected by the pipe-flow turbulence. The presence of swirl in the flame promoted early jet spread and turbulent stirring, thus accelerating the decay of the mean axial velocity and shifting the turbulence intensity peaks upstream. Bimodal temperature pdfs and, in turn, large rms values were observed on the air side of the flame zone.

Acknowledgments

This work was supported by the U. S. Air Force Research Laboratory, Propulsion Directorate, Propulsion Sciences and Advanced Concept Division, Wright-Patterson Air Force Base, Ohio, under Contract No. F33615-97-C-2719 (Technical Monitor: C. W. Frayne).

References

1. Takahashi, F., Vangsness, M. D., Durbin, M. D., and Schmoll, W. J., "Structure of Turbulent Hydrogen Jet Diffusion Flames With or Without Swirl," *Journal of Heat Transfer*, 877-884 (1996).
2. Anand, M. S., Takahashi, F., Vangsness, M. D., Durbin, M. D., and Schmoll, W. J., 1996, "An Experimental and Computational Study of Swirling Hydrogen Jet Diffusion Flames," *Journal of Engineering for Gas Turbines and Power* 119, 305-314 (1997).

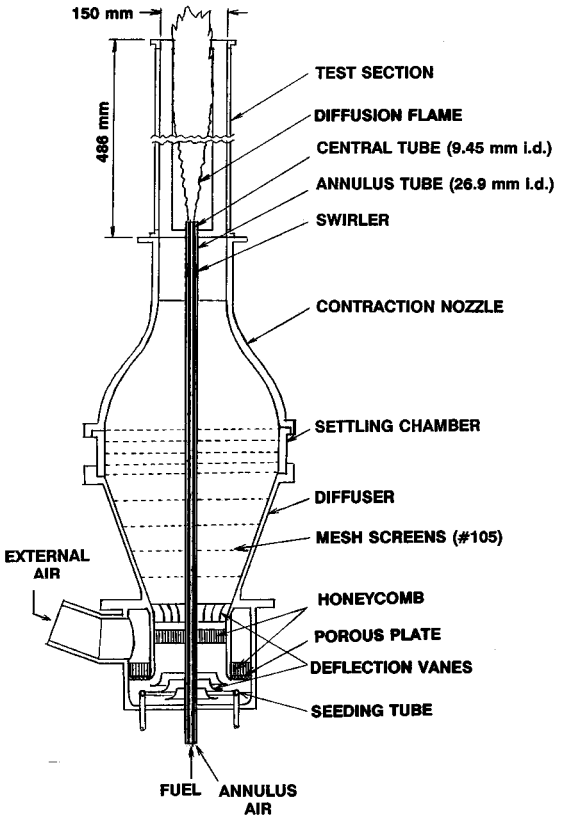

Fig. 1 Schematic of the combustor used.

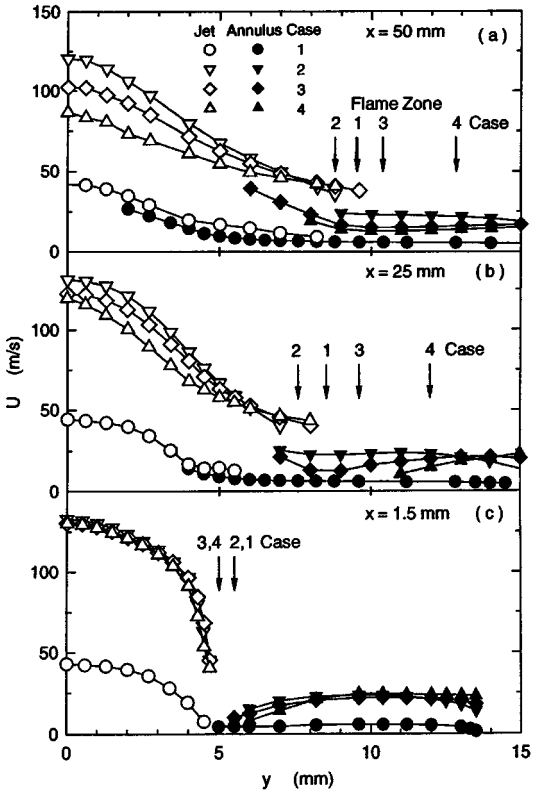

Fig. 2 Mean axial-velocity distribution across the hydrogen jet flame at three different heights.

Table 1. Experimental Conditions

Case No.	θ (°)	U_j (m/s)	U_a (m/s)	U_e (m/s)
1	0	25	4	1
2	0	100	20	4
3	30	100	20	4
4	45	100	20	4

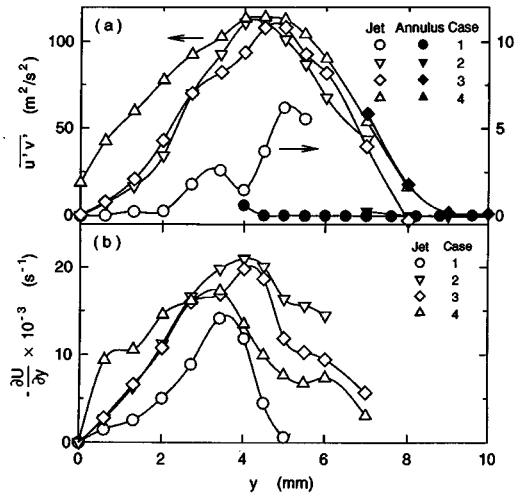

Fig. 3 (a) Reynolds shear stress and (b) axial-velocity gradient across the hydrogen jet flame at x = 25 mm.

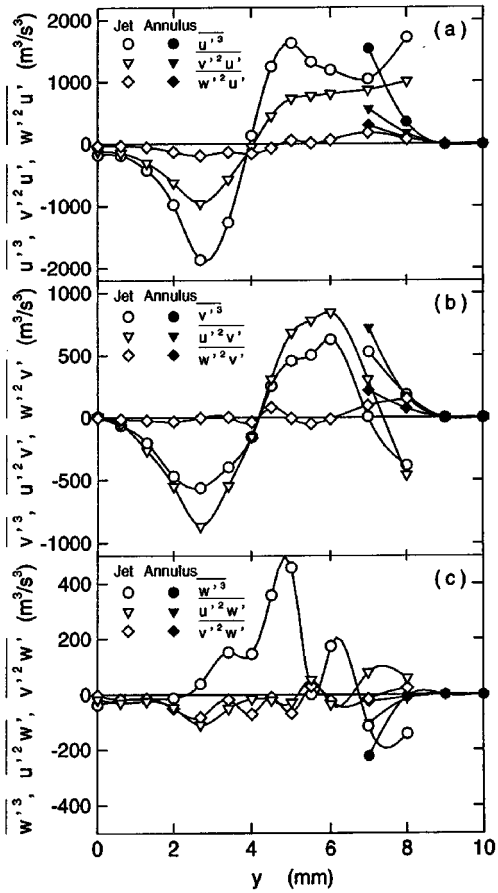

Fig. 4 Triple-correlation distribution across the hydrogen jet flame(Case 3) at x = 25 mm.

CARS temperature measurements in the Delft jet diffusion flame : Flame III

Michel Versluis, Pieter Nooren, Ronnie Knikker,
Ming-Cheng Zong and Theo van der Meer
Thermal and Fluid Sciences, Dept. of Applied Physics, Delft University of Technology
P.O. Box 5046, 2600 GA Delft, The Netherlands
E-mail: M.Versluis@tn.tudelft.nl

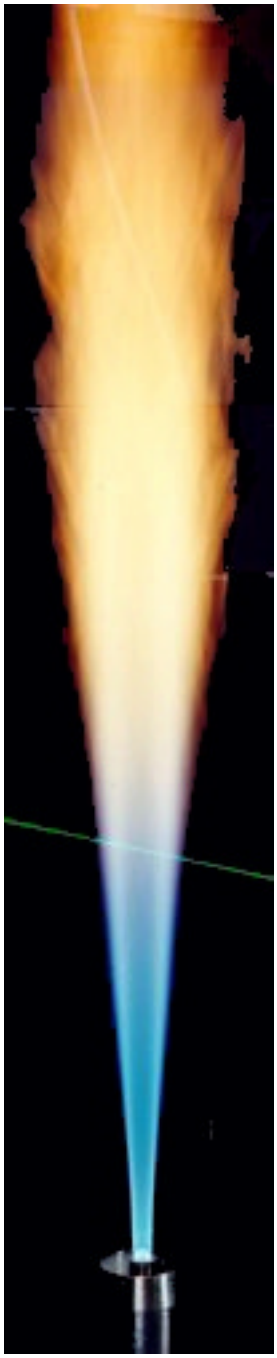

The Delft piloted diffusion flame burner is used to produce a number of well-defined laboratory scale axi-symmetric turbulent diffusion flames. The burner is described by Peeters et al.[1]. From the six different sets of inlet boundary conditions, Flame III is considered as a reference flame or 'base case'. For this flame an extensive set of experimental data is available, including laser-Doppler anemometry (LDA) of the flow field[1], 2D laser-induced fluorescence (LIF) data on the OH radical concentration[1] and coherent anti-Stokes Raman spectroscopy (CARS) measurements of the mean temperature and temperature statistics[2]. Recently, Raman-Rayleigh measurements of temperature and major species concentrations combined with LIF measurements of OH, NO and CO[3] complemented the experimental database for flame III. The experimental dataset has been used to validate various turbulence-chemistry interaction models[1,4]. The Delft Flame III is one of the three target flames selected at the 2nd TNF workshop in Heppenheim, Germany.

The recently acquired Raman-Rayleigh data complement the existing database for flame III by providing the major species concentrations. In addition, it also partially overlaps the database, since it provides the mean temperatures and temperature PDFs previously determined with CARS. This comparison of measurements obtained with different laser techniques is valuable from both experimental and modeling standpoints.

For the Raman-Rayleigh data both Reynolds-averaged and density-weighted (Favre-averaged) temperatures are available. From the comparison it followed that the CARS and Reynolds-averaged profiles are very similar. The comparison also revealed that the peak mean CARS temperatures from Mantzaras and van der Meer are about 150-250 K higher depending on the height in the flame. A comparison between these datasets is complicated by a number of systematic uncertainties, which will be addressed in this poster presentation. Part of the differences observed could be caused by small differences between the boundary conditions in the two experiments, which were performed in different laboratories. In addition, differences between the CARS and Raman-Rayleigh temperatures can be introduced by unequal biases due to spatial averaging effects.

The differences in the two experimental datasets lead us to collect new CARS data with an improved experimental setup and to reexamine our CARS fitting routines. The main systematic errors arise from the response characteristics of the IPDA detector, the long-term spectral shift of the dye laser, spatial averaging effects and the accuracy of the estimation of the experimental parameters in the CARS code fitting process. We have improved our CARS setup with the addition of a back-illuminated CCD camera. In the previous setup a 10:1 beam splitter setup was needed to overcome saturation problems due to the turbulent behavior of the flame. Now, with the very high dynamic range of the system the spectral resolution of the CARS spectra is significantly improved. In addition, the burner is now mounted on a traversing unit, thereby

eliminating alignment errors. Furthermore, the increased data acquisition speed will reduce errors related to the spectral shift of the broadband dye laser. We have also reexamined the CARS fitting routines. One of the complications in the fitting of CARS spectra of non-premixed flames is the large and unknown non-resonant susceptibility χ_{NR} in the fuel-rich parts of the flame. A two-parameter fit of the temperature and of the ratio of the probed species mole fraction to the average molecular background susceptibility is essential to avoid a substantial temperature overestimate. In the air-rich side of the flame a one-parameter fit of the temperature is sufficient. One of the difficulties is to determine where to switch from a one- to a two-parameter fit, since there is a diffuse transition region where both fuel-rich and air-rich pockets exist. We will describe ways to determine directly from the CARS spectrum if one or two parameters must be fitted. In addition, we have also investigated the possibility to perform a two-parameter fit at all positions in the flame (air-rich, fuel-rich and intermediate regions).

The figure below shows the mean temperature profile measured at x = 150 mm for the Raman-Rayleigh measurements together with the CARS data. For the Raman-Rayleigh data both the Reynolds-averaged and the Favre-averaged temperature is plotted. Favre averaging gives rise to lower mean temperatures. The CARS temperatures and the Reynolds-averaged temperatures show a very good agreement. The difference of 50 K that is observed in the center of the flame is well within the experimental uncertainties of both techniques. In addition the new CARS measurements shows an excellent agreement with the Reynolds-averaged Raman-Rayleigh measurements around the peak mean temperature.

References:

[1] T.W.J. PEETERS, P.P.J. STROOMER, J.E. DE VRIES, D.J.E.M. ROEKAERTS AND C.J. HOOGENDOORN. Comparative experimental and numerical investigation of a piloted turbulent natural-gas diffusion flame. *Twenty-Fifth Symposium (International) on Combustion*, pp. 1241-1248 (1994).

[2] J. MANTZARAS AND TH.H. VAN DER MEER. Coherent Anti-Stokes Raman Spectroscopy measurements of temperature fluctuations in turbulent natural-gas-fueled piloted jet diffusion flames. *Combustion and Flame* **110**, pp. 39-53 (1997).

[3] P.A. NOOREN, M. VERSLUIS, TH.H. VAN DER MEER, R.S. BARLOW AND J.H. FRANK. Raman-Rayleigh-LIF measurements of piloted turbulent natural-gas diffusion flames. *In preparation.*

[4] P.A. NOOREN, H.A. WOUTERS, T.W.J. PEETERS, D. ROEKAERTS, U. MAAS AND D. SCHMIDT. Monte Carlo PDF modeling of a turbulent natural-gas diffusion flame. *Combustion, Theory and Modeling* **1** pp. 79-96 (1997).

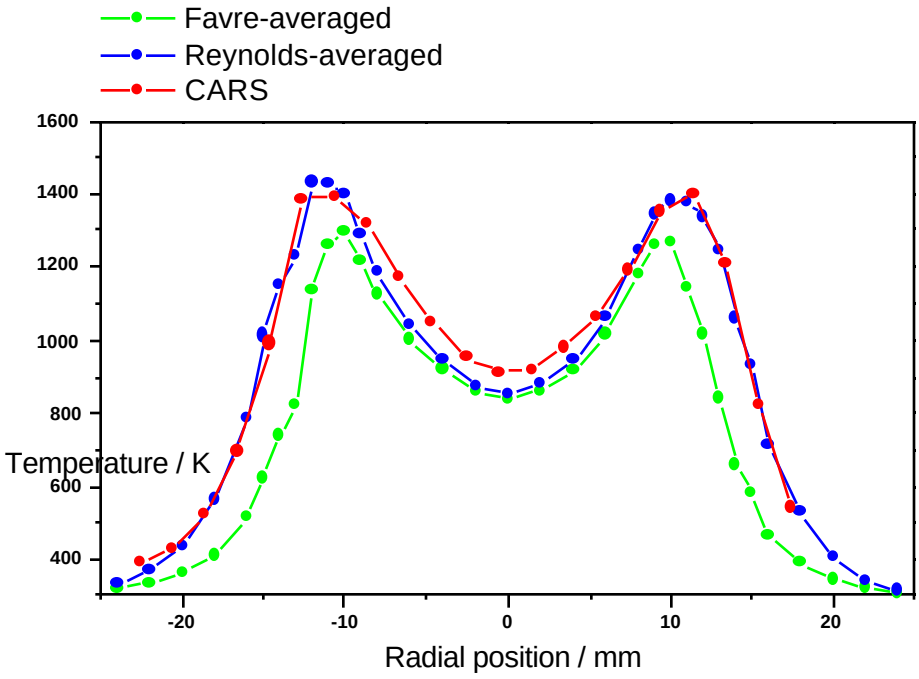

PDF Simulation of a Recirculating Stabilizied Turbulent Nonpremixed Flame

K. Xiao, D. Schmidt, U. Maas
Institut für Technische Verbrennung
Universität Stuttgart
Pfaffenwaldring 12, D-70569 Stuttgart, Germany
e-mail: xiao@itv.uni-stuttgart.de

ABSTRACT

The turbulent nonpremixed CH_4/H_2-air flame [1] stabilized by recirculation behind a bluff-body is studied by a hybrid strategy [3] based on the solution of the transport equation for the joint velocity and composition probability density function (PDF) and a solution of the Reynolds-averaged Navier-Stokes equations using a finite-volume scheme. A Lagrangian particle-tracking Monte-Carlo approach [2] is used to solve the PDF transport equation. The Eulerian mean quantities appearing in this equation such as pressure gradient and the turbulent frequency are supplied by the k-ε turbulence model. The evolution of the reaction progress variables is modeled by a simple interaction by exchage with the mean (IEM) mixing model [5] in combination with the method of intrinsic low-dimensional manifolds (ILDM) [6] which is used to treat finite-rate chemistry. For this purpose a table look-up procedure is implemented to supply the chemical rates of formation for the reaction progress variables, which parametrize the chemical composition.

The calculated distributions of temperature and composition for the recirculating turbulent nonpremixed flame are compared with corresponding measurements made along several radial lines at different axial downstream positions [1]. In general there is good agreement between calculated and measured quantities.

References

[1] http://www.mech.eng.usyd.edu.au/research/energy/#data, Combustion data base, The University of Sydney and The Combustion Research Facility, Sandia National Laboratories.

[2] Pope, S.B., PDF methods for turbulent reactive flows. *Progress in Energy and Combustion Science*, **11**:119–192, 1985.

[3] Correa, S.M. and Pope, S.B., Comparison of a Monte Carlo PDF/finite-volume mean flow model with bluff-body Raman Data. *Twenty-Fourth Symposium (International) on Combustion, The Combustion Institute*, pp 279–285, 1992.

[4] C. G. Speziale, S. Sarkar and T. B. Gatski, Modelling the pressure-strain correlation of turbulence - an invariant dynamical systems approach, *J. Fluid Mech.*, **227**:245, 1991.

[5] C. Dopazo, PDF Approach for a Turbulent Axisymmetric Heated Jet: Centerline Evolution. *Phys. Fluids*, **18**:397, 1975.

[6] U. Maas and S. B. Pope, Simplifying chemical kinetics: Intrinsic low-dimensional manifolds in composition space. *Combustion and Flame*, **88**:239, 1992.

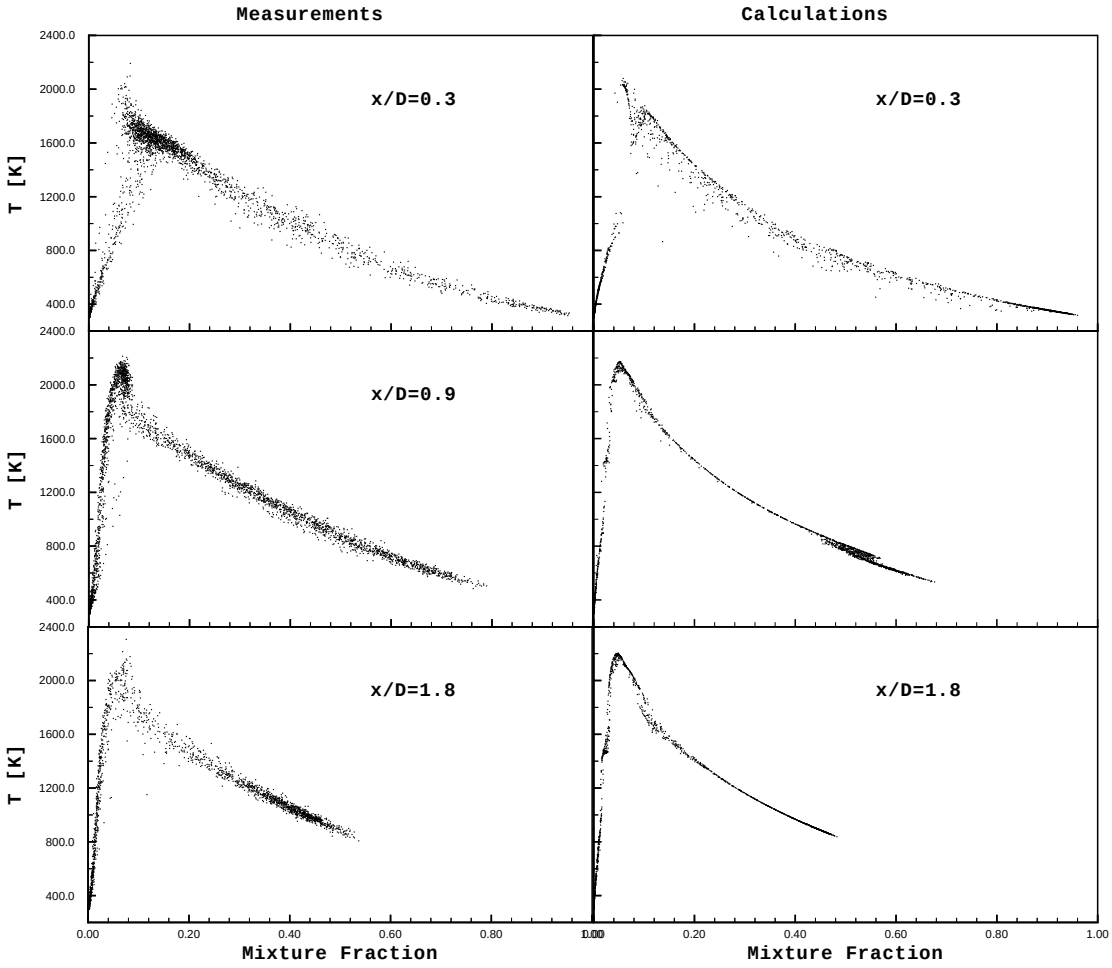

PDF Modelling of Turbulent Non-Premixed Methane Flame: Numerical Aspects

Jun Xu and Stephen B. Pope
Sibley School of Mechanical and Aerospace Engineering
Cornell University
email: xujun@mae.cornell.edu, pope@mae.cornell.edu

In this work, a piloted–jet non-premixed methane flame (Flame L, [1]) is calculated by using a joint velocity–composition–turbulence frequency PDF method in accordance with Monte Carlo approaches. Chemistry is treated a flamelet model. The results, for example the mean velocity and mixture fraction, are in reasonable agreement with the experimental data (Figure 1). However, the purpose is to demonstrate from numerical views that PDF/Monte Carlo methods [2, 3] can give accurate results at a reasonable computational cost. The numerical accuracy is therefore systematically investigated by varying the computational parameters in the calculations.

A PDF/Monte Carlo method has been implemented in the code *PDF2DV* [4] in which a flow is modelled by an ensemble of particles and the particle properties evolve by a set of stochastic differential equations (SDE) that exhibit the same PDF as the modelled PDF transport equation. In a calculation by *PDF2DV*, particles move in physical space and their properties are solved from the SDE's by a time–splitting algorithm [3], while the flow domain is decomposed into a number of cells for the estimation of mean fields, e.g., mean velocity. Usually, the convergence of moments is sought for PDF/Monte Carlo methods. Suppose a calculation is made based on cell particle number N_{pc}, time step Δt and cell size h or total number of cells M^2 ($h \sim M^{-1}$). Then, for the mean of any variable Q, the total error ϵ can be decomposed into discretization error (T_q), bias (B_q) and statistical error (Σ_q)

$$\epsilon \equiv \{Q\}_{\Delta t,h,N_{pc}} - \langle Q \rangle = T_q + B_q + \Sigma_q \vartheta, \tag{1}$$

where $\{Q\}_{\Delta t,h,N_{pc}}$ is an estimator for the expectation $\langle Q \rangle$ and ϑ is a standardized normal distributed random number. First of all, Figure 2 verifies that the stationary solutions are independent of time step Δt. Then, comprehensive computations are conducted to characterize the numerical errors: T_q, B_q and Σ_q. Keeping the time step Δt and cell size h the same, the calculation of mean fields , e.g., the mean velocity with different N_{pc}, shows that the bias scales as N_{pc}^{-1} (Figure 3) and the statistical error indicated by the rms of the stationary solution is convergent at the rate of $N_{pc}^{-1/2}$ (Figure 4). Finally, the second–order accuracy of the spatial error is implied in Figure 5 where the mean velocity is plotted against the grid size for different N_{pc}, especially the extrapolation of an infinite number of particles. To summarize, the total error in the estimate of a mean $\langle Q \rangle$ is expressed by

$$\epsilon = T_q + B_q + \Sigma_q \vartheta = \frac{a}{M^2} + \frac{b}{N_{pc}} + \frac{c}{\sqrt{N_{pc}}}\vartheta, \tag{2}$$

where the error coefficients a, b and c can be estimated from numerical results. Obviously, one can make a calculation as accurate as desired by choosing the computational parameters N_{pc} and M. Based on (2), we also propose an error reduction scheme to make the computation by *PDF2DV* more efficient.

References

[1] A. R. Masri and R. W. Dibble and R. S. Barlow. *Prog. Energy Combust. Sci.*, 22:307, 1996.

[2] S. B. Pope, *Prog. Energy Combust. Sci.*, 11:119, 1985.

[3] S. B. Pope, *J. Comput. Phys.*, 117:332, 1995.

[4] S. B. Pope, *PDF2DV Code (Unpublished)*, Cornell University, 1994.

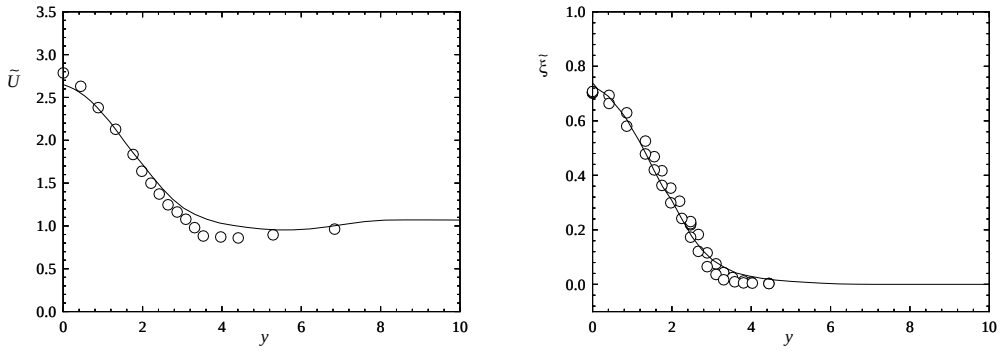

Figure 1: Comparison of mean profiles at $x = 40$. Solid line: PDF calculation with 40×40 cells, $\Delta t = 0.08$ and $N_{pc} = 200$; Symbols: experimental data of Masri et al.

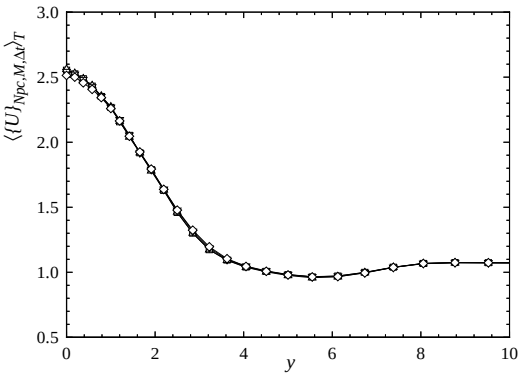

Figure 2: Time step independence of solution (Symbols: different time steps)

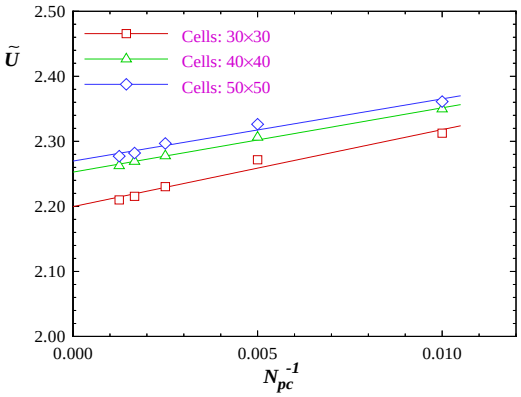

Figure 3: Bias vs. particle number per cell

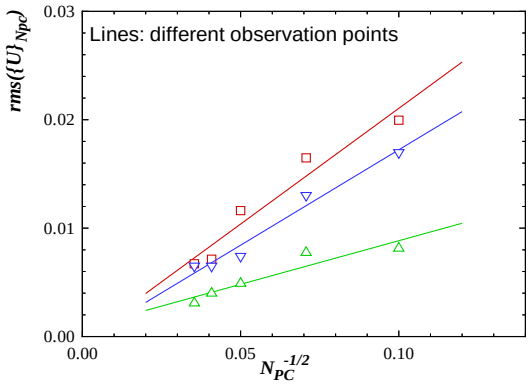

Figure 4: Statistical error vs. particle numer per cell

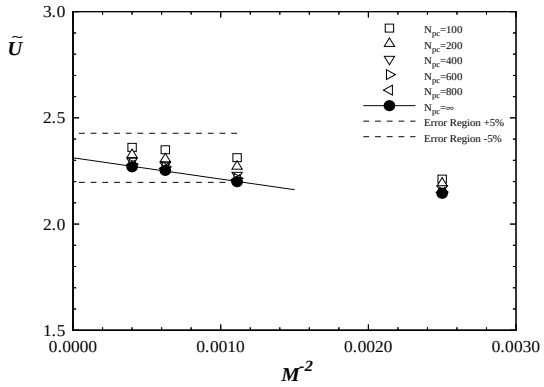

Figure 5: Spatial error vs. cell size

NUMERICAL SIMULATION OF A SWIRL-STABILIZED TURBULENT DIFFUSION FLAME WITH A PRESUMED PROBABILITY DENSITY FUNCTION (PDF) MODEL

B. ZAMUNER*, and F. DUPOIRIEUX

ONERA,
29, avenue de la Division Leclerc, BP 72, 92322 Châtillon Cedex, France

Swirl-stabilized flames are often used in industrial devices since they greatly enhance the mixing process, promote the flow stability, and, eventually, increase the combustion efficiency. Unfortunately, numerical simulation of this type of configuration seems to be a difficult task because the main features of the turbulent flow are poorly predicted with classical turbulence modelling. Indeed, the strong anisotropy resulting from the swirling motion of the fluid cannot be described by a model based on isotropic assumptions, for instance, the two equations k-ε model. Taking into account the turbulent quantities is of great importance since they directly influence the mixing process, and, consequently, the chemical reactions and the production of pollutants. As a matter of fact, this configuration is a good candidate to be a test-case for models which deal with the interaction between turbulence and combustion. Swirl-stabilized turbulent flames have been far less investigated in both numerical and experimental points of view than pilot and bluff-body stabilized flames. However, recent studies [1-3] have shown a growing interest for this topic. Anand *et al.* [4] have performed numerical simulation of the flow in a methane-air step swirl combustor with the help of a joint velocity-scalar probability density function (PDF) method. At ONERA, we decided to calculate the same type of configuration, with slight differences in the injected mass flow rates, but with a stronger swirl effect (Fig. 1).

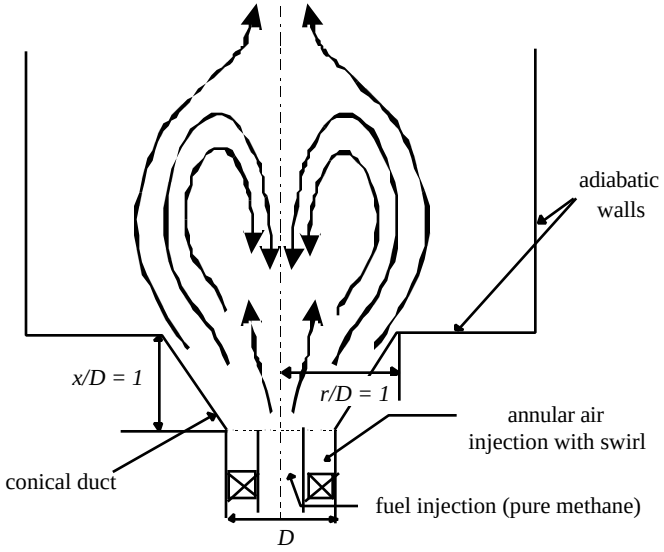

Fig. 1 : Sketch of the experimental configuration

This turbulent air-methane diffusion flame was experimentally studied at CNRS Poitiers, France, with a Gaz de France (GDF) financial support [5]. The main characteristics of the flow in the injector plane, which are kept constant throughout the tests, are presented in table 1. Three swirl numbers (0.1, 0.4 and 0.82) were investigated to show the effects of the rotation intensity. LDV and thermocouple measurements were performed as well as gas analyses with an intrusive sampling probe. Maps of mean temperature, temperature fluctuations, mean concentrations of O_2, CH_4, CO_2 and CO for the different values of the swirl number are also available.

* Corresponding author : zamuner@onera.fr

Air mass flow rate	Fuel mass flow rate	Air inlet velocity	Fuel inlet velocity	Reynolds (based on air inlet)
19 g/s	0.72 g/s	9.2 m/s	2.7 m/s	30,000

Table 1

Due to the high confinement prescribed by the conical duct, a recirculation zone located in a central region is observed for all swirl conditions. However, experimental results clearly show that the flame is shortened and the chemical reactions are enhanced by an increasing swirl intensity

In order to simulate these effects, a turbulent Navier-Stokes solver is used on a axisymmetric 2D 100x100 mesh grid. The two extreme swirl conditions (0.1 and 0.82) are computed with a classical k-ε model and a k-ε-RNG model. A presumed PDF model based on a equilibrium assumption [6] is used to model the turbulent combustion. The β-shaped PDF is fully determined with the local mean mixture fraction $\bar{f}$ and its variance $\overline{f''^2}$ (or g). Unlike k-ε-g model [7], the species balance equations do incorporate production source terms consistent with the Eddy-Break-Up model when $\overline{f''^2}$ tends to zero.

We present results concerning mean velocity components, velocity correlations and mean concentration species. This classical approach seems to give good approximate trends concerning the position of the recirculation zone, but the standard k-ε model underpredicts its size and gives a poor representation of the mixing process (Fig. 2). The k-ε-RNG model with appropriate corrections seems to be a good intermediate way to correctly capture the main features of the flame. Solving the joint composition PDF transport equation with a Monte-Carlo technique [8], in conjunction with a detailed kinetic scheme for methane oxidation, is also planned in a near future to improve CO prediction.

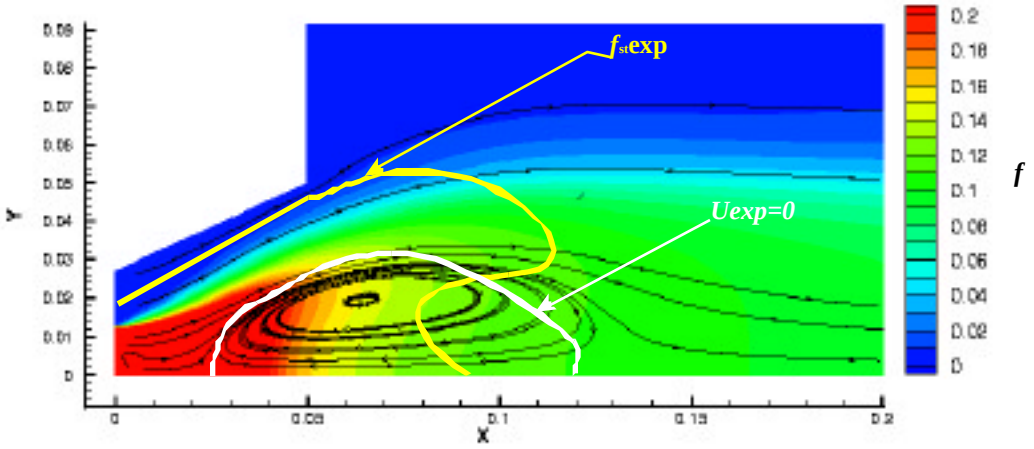

Fig 2.1 : Mixture fraction and streamlines computed with k-ε model (reactive case ; S = 0.82)
Comparisons with experimental results (*white : null velocity line ; yellow : stoichiometric line* f_{st}*=0.055*)

REFERENCES

[1] O. Faltsi-Saravelou, P. Wild, S. S. Sazhin and J. E. Michel, *Combust. Sci. Technol.*, 123:1-22, 1997

[2] L. S. Pedersen, P. Breithaupt, K. D. Lohansen, and R. Weber, *Combust. Sci. Technol.*, 127:251-274, 1997

[3] T. C. Fang, C. M. Megaridis, W. A. Sowa, and G. S. Samuelsen, *Combust. Flame*, 112:312-328, 1998

[4] M. S. Anand, A. T. Hsu, and S. B. Pope, *AIAA Journal*, Vol. 35, No 7, pp 1143-1150, 1997

[5] B. Poireault, *Thèse de l'Université de Poitiers* -ENSMA (in French), 1997

[6] F. Ravet, and L. Vervisch, *AIAA paper* 98-1027, 1998

[7] N. Peters, *21st Symposium (International) on Combustion*, The Combustion Institute, pp. 1231-1250, 1986

[8] R. Borghi, F. Dupoirieux, B. Zamuner, F. Galzin, T. Mantel, *4th World Conference on Exp. Heat Transfer, Fluid Mech. and Thermodyn.*, Brussels, 1997